MOVING-BANK MULTIPLE MODEL ADAPTIVE ESTIMATION APPLIED TO FLEXIBLE SPACESTRUCTURE CONTROL

THESIS

Drew A. Karnick
Second Lieutenant, USAF

AFIT/GE/ENG/86D-41

DEPARTMENT OF THE AIR FORCE
AIR UNIVERSITY
AIR FORCE INSTITUTE OF TECHNOLOGY

Wright-Patterson Air Force Base, Ohio

AFIT/GE/ENG/86D

MOVING-BANK MULTIPLE MODEL ADAPTIVE ESTIMATION APPLIED TO FLEXIBLE SPACESTRUCTURE CONTROL

THESIS

Drew A. Karnick
Second Lieutenant, USAF

AFIT/GE/ENG/86D-41

AFIT/GE/ENG/86D-41

MOVING-BANK MULTIPLE MODEL ADAPTIVE ESTIMATION APPLIED TO FLEXIBLE SPACESTRUCTURE CONTROL

THESIS

Presented to the Faculty of the School of Engineering
of the Air Force Institute of Technology
Air University
In Partial Fulfillment of the
Requirements for the Degree of
Master of Science in Electrical Engineering

Drew A. Karnick, B.S.E.E.
Second Lieutenant, USAF

December 1986

Preface

The purpose of this thesis is to demonstrate the feasibility of the moving-bank multiple model adaptive estimation algorithms as applied to flexible spacestructure control. Moving-bank multiple model adaptive estimation/control is an attempt to reduce the computational loading associated with the implementation of a full-scale multiple model adaptive estimator/controller. The results of this thesis indicate that although the use of a moving bank may provide increased state estimation performance, similar performance can be obtained from a fixed bank estimator with a discretization that covers the range of parameter variation.

I wish to express deep thanks to my thesis advisor, Professor Peter S. Maybeck, for the personal and professional commitment he has shown to me. I also wish to thank Dr. V. B. Venkayya and V. A. Tischler for their assistance during the development of the mathematical model of the flexible space structure. Finally, I wish to thank my wife [redacted] for her support and understanding and for being there when I need her.

— Drew A. Karnick

Table of Contents

List of Figures

List of Tables

Abstract

This investigation focuses on the use of moving-bank multiple model adaptive estimation and control (MMAE). Moving-bank MMAE reduces the computational burden of MMAE by implementing only a subset of the Kalman filters (9 filters versus 100 in this research) that are necessary to mathematically describe the system to be estimated/controlled. Important to the development of the moving-bank MMAE are the decision logics governing the selection of the subset of filters. The decision logics cover three situations: initial acquisition of unknown parameter values; tracking unknown parameter values; and reacquisition of the unknown parameters following a "jump" change in these parameter values.

The thesis applies moving-bank MMAE to a rotating two bay truss model of a flexible spacestructure. The rotating two bay truss approximates a space structure that has a hub with appendages extending from the structure. The mass of the hub is large relative to the mass of the appendage. The hub is then rotated to point the appendage in a commanded direction. The mathematical model is developed using finite element analysis, transformed into modal formulation, and reduced using a method referred to

as singular perturbations. Multiple models are developed by assuming that variation occurs in the mass and stiffness of the structure. Ambiguity function analysis and Monte Carlo analysis of individual filters are used to determine if the assumed parameter variation warrants the application of adaptive control/estimation techniques.

Results indicate that the assumed parameter variation is sufficient to require adaptive control and that the use of a moving bank may provide increased state estimation performance; however, the increase in performance is due primarily to multiple model adaptive estimation. Similar performance can be obtained from a fixed bank estimator with a discretization that covers the range of parameter variation.

MOVING-BANK MULTIPLE MODEL ADAPTIVE ESTIMATION APPLIED TO FLEXIBLE SPACESTRUCTURE CONTROL

I. Introduction

A significant problem in estimation and control is the uncertainty of parameters in the mathematical model used in the design of controllers and/or estimators. These parameters may be unknown, varying slowly, or changing abruptly due to a failure in the physical system. These changes in parameters often necessitate the identification of parameters within the mathematical model and changing the mathematical model during a real-time control problem. This is often referred to as adaptive control and/or estimation. This thesis investigates methods of adaptive control implementing a moving-bank multiple model adaptive estimator.

I.1. Background

Multiple Model Adaptive Estimation (MMAE) involves forming a bank of Kalman filters (3; 6; 7; 12; 13; 17; 18; 20:129-135). The Kalman filter is a recursive data processing algorithm (19:4) and is the optimal estimator for a known linear system with dynamics and measurement noises modeled as white and Gaussian. Each Kalman filter is

associated with a possible value of an uncertain parameter vector. It is assumed that the uncertain parameters can take on only discrete values; either this is reasonable physically or discrete values are chosen from the continuous parameter variation range. The output of each filter is then weighted by the a posteriori probability of that filter being correct, conditioned on the observed time history of measurements. These weighted outputs are summed to form an estimate of the system states. The equations for the MMAE algorithms, as well as convergence properties, are fully developed in Chapter II.

MMAE has been successfully implemented in several estimation and control problems. The application of MMAE to the tracking of airborne targets has been researched (9; 15; 27). The control method has also been used in controlling fuel tank fires (33), addressing terrain correlation (28), and generating estimators for problems in which large initial uncertainties cause non-adaptive extended Kalman filters to diverge (26).

An inherent problem of MMAE is the number of filters required. For example, if there are two uncertain parameters and each can assume one of 10 possible discrete values, then $10^2 = 100$ separate filters are required. Problems requiring larger numbers of uncertain parameters and/or finer parameter discretization quickly become impractical for implementation (3; 6).

Several approaches have been used to alleviate the computational burden of MMAE (3:5). One method uses Markov processes to model the parameter variation (1; 23). A process is considered Markov if its present parameter value depends only on the previous parameter value (1:418). Other methods include: using "pruning" and/or "merging" of "decision tress" of the possible parameter time history (22; 23), hierarchically structuring the algorithms to reduce the number of filters (4), and a method in which the filter is initialized with a coarse parameter space discretization, but after the filter converges to the "nearest" parameter, the filter is rediscretized using a simplex directed method (14).

A method proposed by Maybeck and Hentz (6; 18) is to implement a small number of estimators in a "moving-bank." For instance, one might take the current best estimate of the uncertain parameters, and implement only those estimators (and controllers) that most "closely" surround the estimated value in parameter space. For the case of two uncertain parameters requiring 100 separate filters, the three discrete values of each parameter that most closely surround the estimated value can be selected, only requiring only $3^2 = 9$ separate filters instead of 100; see Figure I-1. As the parameter estimate changes, the choice of filters could change, resulting in a "move" of the bank

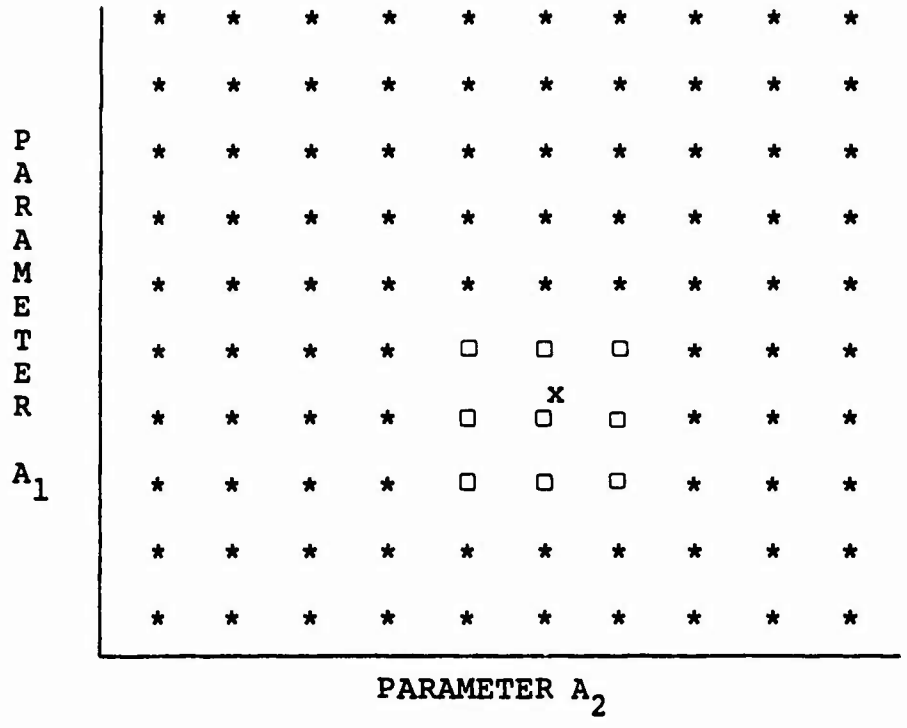

□ used Kalman filter
* unused Kalman filter
x current best estimate of the true parameter value

Fig. I-1. Moving-bank Multiple Model Adaptive Estimator

of 9 filters. Equations for the moving-bank MMAE are developed in Chapter II.

Hentz (6) applied the moving-bank MMAE to a simple but physically motivated two-state system model and was able to demonstrate performance equivalent to the full-bank MMAE algorithm (and also equivalent to a benchmark of an estimator or controller artificially given knowledge of the true parameters), with an order of magnitude less computational loading.

Filios (3) applied the same type of algorithms to a reduced order model of a large flexible spacecraft. The particular problem was such that adaptivity was not required for the range of parameter variations that made physical sense for this application; robust control laws without adaptivity could in fact meet performance specifications. Research had been previously accomplished on the same model which indicated that adaptivity might be needed if very high angular rates were achieved during a maneuver (29).

I.2. Problem

The use of a full scale (full-bank) Multiple Model Adaptive Estimator (MMAE) presents a computational burden that is too large for most applications (3; 6; 18). The moving-bank MMAE was evaluated for a physically motivated but simple system and shown to be feasible (6; 18); however, the moving-bank MMAE has yet to be successfully applied to a more complex space structure application, requiring adaptive estimation/control. This research is directed towards applying the moving-bank MMAE to a system requiring adaptivity and to assess its potential as an estimator and/or controller.

I.3. Scope

The moving-bank multiple model adaptive algorithms are applied to a physical model representative of problems associated with large space structures. The model is a two-bay truss attached to a hub; see Figure I-2. The two-bay

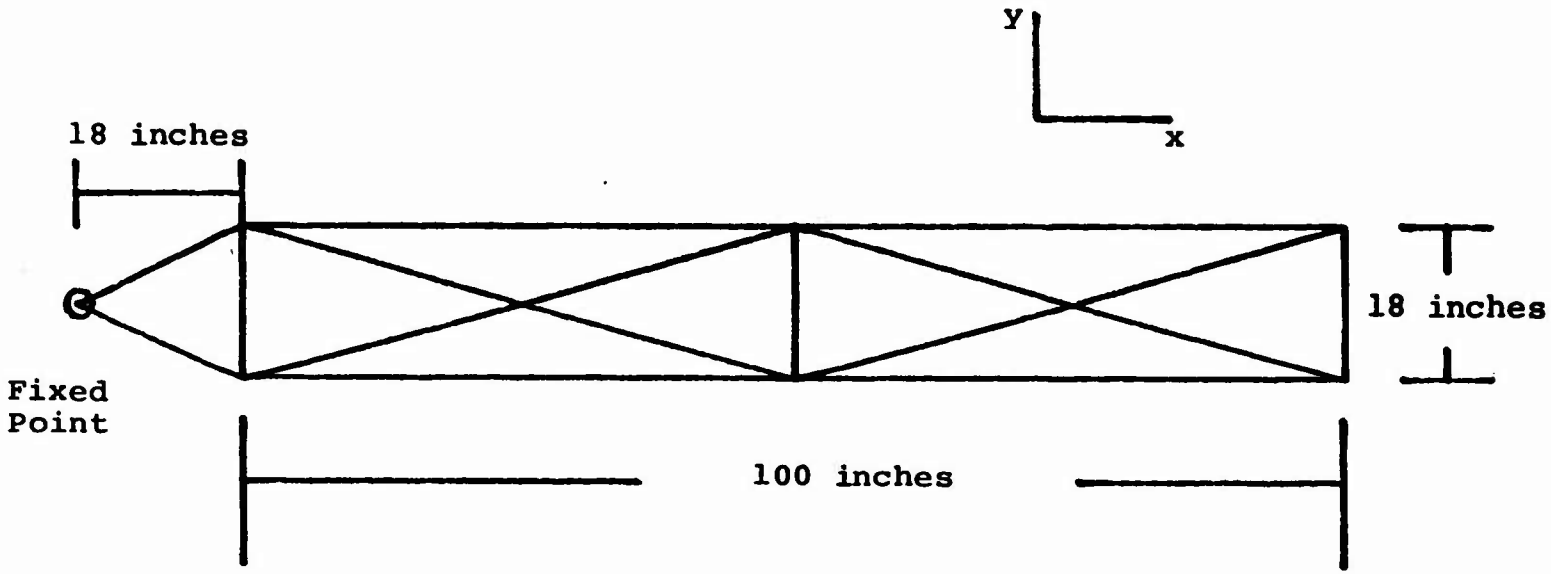

Fig. I-2. Rotating Two-bay Truss Model

truss is 100 inches long and 18 inches high. Only two degrees of freedom (x-y plane) are allowed and translational motion is not permitted. Non-structural masses are added to the structure and have two purposes. First, they can be associated with fuel tanks or some mass on a structure that can be expected to vary in time. Secondly, the non-structural masses are large relative to the structural mass in order to attain the low frequency structural model associated with large space structures (16). The model is described in terms of mass and stiffness matrices obtained from a finite-element analysis. The model is fully developed in Chapter III.

Two uncertain parameters are investigated: the non-structural mass and the stiffness matrix. The uncertain parameters are discretized into 10 points yielding a 10 by 10 (100 point) parameter space. It is assumed that the non-structural masses vary -50 percent to +40 percent from the nominal value in discrete steps of 10 percent. The entire stiffness matrix is allowed to vary 20 percent to -16 percent from the nominal value in discrete steps of 4 percent. The dynamics and measurement noise characteristics are assumed known and modeled as white Gaussian processes.

I.4. Approach

The research is divided into three phases: sensitivity analysis, a parameter and state estimation study,

and a controller study. The sensitivity analysis of non-adaptive algorithms is conducted using ambiguity functions (20:97-99); it will provide information about the performance to be expected from an estimator (20:97) and is used to assess the need for adaptivity and also to provide insight into the discretization of the parameter space. The estimator and controller studies will evaluate the potential of the moving-bank multiple model adaptive algorithm to provide good state estimation and system control performance.

I.4.1. Ambiguity Functions Analysis. A sensitivity analysis is conducted using ambiguity functions (3:33-34; 6:332-333; 20:97-99). The sensitivity analysis is done on non-adaptive estimators based on a representative sample of parameter sets to determine what parameters can and should be estimated. Relatively low sensitivity to a parameter change makes identification of parameter values difficult and removes the need for parameter estimation, since all filters within the parameter variation range will do a good job of state estimation (3:70).

The ambiguity analysis also lends valuable insight into the discretization of the parameter space (3:91). High-sensitivity ambiguity functions illustrate the need for a tightly discretized parameter range. Less sensitive ambiguity functions show that fewer parameter points are needed to span a given parameter variation range.

I.4.2. Parameter and State Estimation Study. The parameter and state estimation study investigate the performance of various decision logics for moving or changing the size of the bank, with respect to initial acquisition of the true parameter values, and also identification of when a change in this true parameter value has occurred. The primary performance criteria is the accuracy of the state estimates and secondarily the accuracy of the parameter estimates. The decision logics that are studied include Residual Monitoring, Parameter Position Estimate Monitoring, Parameter Position and Velocity Estimate Monitoring, and Probability Monitoring (3; 6; 18). These are developed in Chapter II.

Two benchmark estimators will provide standards for state estimate evaluation: a single estimator with artificial knowledge of the true parameter set and a robust, single fixed-gain estimator. The former will indicate the best state estimation performance that could hope to be achieved using adaptive control while the latter estimator will provide information on the performance that can be attained with a non-adaptive estimator.

The parameter and state estimation study is accomplished through Monte Carlo Analysis. A Monte Carlo Analysis involves obtaining a statistically valid number of samples of an error process through simulation and then using this data to compute sample statistics as an

approximation to the true process statistics (19:329). The process statistics provide information on the performance of the estimator or controller being investigated. The simulation is conducted for the following cases:

a. The true parameter set is constant and equal to one of the discretized parameter sets. There are two possible initial conditions:

1. The true parameter set is within the initial discretization chosen for the moving-bank.

2. The true parameter set is outside the initial discretization chosen for the moving-bank.

b. The true parameter set is constant but not equal to one of the discretized parameter sets. This better represents a real world problem since the true parameter set, with probability 1, will not be perfectly matched to a filter in the full bank. Only the condition where the true parameter set is within the initial conditions chosen for the moving-bank is investigated, since similar transient results would be obtained for part 2 of a.

c. The true parameter set is varying. Two effects can be considered:

1. The true parameter set is varying and moves continuously away from the parameter position upon which the bank has previously locked. This could be the result of a slow failure of some part of the system model or

perhaps due to the depletion of fuel or redistribution of weight within a space structure.

2. The true parameter set undergoes a jump change to some other parameter set, perhaps due to an abrupt failure in the system.

I.4.3. Controller Evaluation. The State and Parameter Estimation Study is used to determine the "best" parameter estimation method. This method is used as the basis for a sliding bank multiple model adaptive controller. A Monte Carlo Analysis is performed on this controller, a multiple model adaptive controller, and a controller designed on a nominal value of the parameter vector but using the moving-bank model as a state estimator. The controller algorithms will be more fully developed in Chapter II.

Two benchmark controllers will provide standards for controller evaluation: a single controller with artificial knowledge of the true parameter set and a robust, single fixed-gain controller. The former will indicate the best performance that could hope to be achieved using adaptive control while the latter controller will provide information on the performance that can be attained with a non-adaptive controller.

I.5. Overview

Chapter II develops the detailed algorithms for the moving-bank MMAE and associated controllers and estimators. Chapter III discusses the two-way truss model. Chapter IV presents the ambiguity functions analysis and the simulation used to evaluate the moving-bank MMAE. Chapter V contains analysis of the proposed algorithms and Chapter VI provides conclusions and recommendations.

II. Algorithm Development

II.1. Introduction

This chapter develops the algorithms for the full-scale and moving-bank Bayesian Multiple Model Adaptive Estimator. First, the full-scale model is developed. This is then modified for the moving bank case. The Ambiguity Functions analysis is also developed.

II.2. Bayesian Estimation Algorithm Development

Development of the full-scale Bayesian Multiple model Adaptive Estimation algorithms is presented in this section. For a more rigorous development, the reader is directed to reference (20:129-136).

Let the system under consideration be discrete and described by (3; 6; 19):

$$\underset{\sim}{x}(t_{i+1}) = \Phi(t_{i+1},t_i)\underset{\sim}{x}(t_i) + B_d(t_i)\underline{u}(t_i) + G_d(t_i)\underset{\sim}{w}_d(t_i)$$

$$\underset{\sim}{z}(t_i) = H(t_i)\underset{\sim}{x}(t_i) + \underset{\sim}{v}(t_i) \qquad \text{(II-1)}$$

where "$\underset{\sim}{\ }$" denotes a vector stochastic random process and:

$\underset{\sim}{x}(t_i)$: n-dimensional state vector,

$\Phi(t_{i+1}, t_i)$: state transition matrix,

$\underline{u}(t_i)$: r-dimensional known input vector,

$B_d(t_i)$: control input matrix,

$\underset{\sim}{w}_d(t_i)$: s-dimensional white Gaussian dynamics noise vector,

$G_d(t_i)$: noise input matrix,

$\underset{\sim}{z}(t_i)$: m-dimensional measurement vector,

$H(t_i)$: measurement matrix,

$\underset{\sim}{v}(t_i)$: m-dimensional white Gaussian measurement noise vector,

and the following statistics apply:

$$E\{\underset{\sim}{w}_d(t_i)\} = \underline{0},$$

$$E\{\underset{\sim}{w}_d(t_i)\underset{\sim}{w}_d^T(t_j)\} = Q_d(t_i)\delta_{ij},$$

$$E\{\underset{\sim}{v}(t_i)\} = \underline{0},$$

$$E\{\underset{\sim}{v}(t_i)\underset{\sim}{v}^T(t_j)\} = R(t_i)\delta_{ij},$$

where δ_{ij} is the Kronecker delta function. It is also assumed that $\underset{\sim}{x}(t_o)$, $\underset{\sim}{w}_d(t_i)$, and $\underset{\sim}{v}(t_i)$ are independent for all t_i.

Let $\underset{\sim}{a}$ be the uncertain p-dimensional parameter vector which is an element of A, where A is a subset of R^P. This parameter vector may be uncertain but constant, slowly varying, or it may undergo jump changes. The parameter vector $\underset{\sim}{a}$ can affect any or all of the following within Equation (II-1): Φ, B_d, G_d, Q_d, H, and R. The Bayesian estimator conceptually computes the following conditional density function:

$$f_{\underset{\sim}{x}(t_i),\underset{\sim}{a}|\underset{\sim}{Z}(t_i)}(\underline{x},\underline{a}|\underline{Z}_i) = f_{\underset{\sim}{x}(t_i)|\underset{\sim}{a},\underset{\sim}{Z}(t_i)}(\underline{x}|\underline{a},\underline{Z}_i)$$

$$\cdot f_{\underset{\sim}{a}|\underset{\sim}{Z}(t_i)}(\underline{a}|\underline{Z}_i) \qquad \text{(II-2)}$$

where $\underset{\sim}{Z}(t_i)$ is the vector of measurements from t_o to t_i,

$$\underset{\sim}{Z}(t_i) = [\underset{\sim}{z}^T(t_i),\underset{\sim}{z}^T(t_{i-1}),\ldots,\underset{\sim}{z}^T(t_o)]^T$$

The second term on the right side of Equation (II-2) can be further evaluated:

$$f_{\underset{\sim}{a}|\underset{\sim}{Z}(t_i)}(\underline{a}|\underline{Z}_i) = f_{\underset{\sim}{a}|\underset{\sim}{z}(t_i),\underset{\sim}{Z}(t_{i-1})}(\underline{a}|\underline{z}_i,\underline{Z}_{i-1})$$

$$= \frac{f_{\underset{\sim}{a},\underset{\sim}{z}(t_i)|\underset{\sim}{Z}(t_{i-1})}(\underline{a},\underline{z}_i|\underline{Z}_{i-1})}{f_{\underset{\sim}{z}(t_i)|\underset{\sim}{Z}(t_{i-1})}(\underline{z}_i|\underline{Z}_{i-1})}$$

$$= \frac{f_{\underset{\sim}{z}(t_i)|\underset{\sim}{a},\underset{\sim}{Z}(t_{i-1})}(\underline{z}_i|\underline{a},\underline{Z}_{i-1}) f_{\underset{\sim}{a}|\underset{\sim}{Z}(t_{i-1})}(\underline{a}|\underline{Z}_{i-1})}{\int_A f_{\underset{\sim}{z}(t_i)|\underset{\sim}{a},\underset{\sim}{Z}(t_{i-1})}(\underline{z}_1|\underline{a},\underline{Z}_{i-1}) f_{\underset{\sim}{a}|\underset{\sim}{Z}(t_{i-1})}(\underline{a}|\underline{Z}_{i-1})\underline{da}} \qquad \text{(II-3)}$$

Conceptually, Equation (II-3) can be solved recursively, starting from an a priori probability density function of $f_{\underset{\sim}{a}}(\underline{a})$, since $f_{\underset{\sim}{z}(t_i)|\underset{\sim}{a},\underset{\sim}{Z}(t_{i-1})}(\underline{z}_i|\underline{a},\underline{Z}_{i-1})$ is Gaussian with a mean of $H(t_i)\hat{\underline{x}}(t_i^-)$ and covariance $[H(t_i)P(t_i^-)H^T(t_i) + R(t_i)]$, where $\hat{\underline{x}}(t_i^-)$ and $P(t_i^-)$ are the conditional mean and covariance respectively of $\underset{\sim}{x}(t_i)$ just prior to the measure at t_i, assuming a particular realization $\underline{a}$ of $\underset{\sim}{a}$.

Using the conditional mean, the estimate of $\underset{\sim}{x}(t_i)$ becomes:

$$E\{\underset{\sim}{x}(t_i) \,|\, \underset{\sim}{Z}(t_i) = \underset{\sim}{Z}_i\} = \int_{-\infty}^{\infty} \underset{\sim}{x} \cdot f_{\underset{\sim}{x}(t_i)\,|\,\underset{\sim}{Z}(t_i)}(\underset{\sim}{x}|\underset{\sim}{Z}_i)\,\underset{\sim}{dx}$$

$$= \int_{-\infty}^{\infty} \underset{\sim}{x} \cdot \left[\int_A f_{\underset{\sim}{x}(t_i),\underset{\sim}{a}\,|\,\underset{\sim}{Z}(t_i)}(\underset{\sim}{x},\underset{\sim}{a}|\underset{\sim}{Z}_i)\,\underset{\sim}{da}\right]\underset{\sim}{dx} \tag{II-4}$$

$$E\{\underset{\sim}{x}(t_i)|\,\underset{\sim}{Z}(t_i) = \underset{\sim}{Z}_i\} = \int_{-\infty}^{\infty} \underset{\sim}{x} \cdot \left[\int_A f_{\underset{\sim}{x}(t_i)\,|\,\underset{\sim}{a},\underset{\sim}{Z}(t_i)}(\underset{\sim}{x}|\underset{\sim}{a},\underset{\sim}{Z}_i) \cdot f_{\underset{\sim}{a}\,|\,\underset{\sim}{Z}(t_i)}(\underset{\sim}{a}|\underset{\sim}{Z}_i)\,\underset{\sim}{da}\right]\underset{\sim}{dx}$$

$$= \int_A \left[\int_{-\infty}^{\infty} \underset{\sim}{x} \cdot f_{\underset{\sim}{x}(t_i)\,|\,\underset{\sim}{a},\underset{\sim}{Z}(t_i)}(\underset{\sim}{x}|\underset{\sim}{a},\underset{\sim}{Z}_i)\,\underset{\sim}{dx}\right] f_{\underset{\sim}{a}\,|\,\underset{\sim}{Z}(t_i)}(\underset{\sim}{a}|\underset{\sim}{Z}_i)\,\underset{\sim}{da} \tag{II-5}$$

where the term in brackets is the estimate of $\underset{\sim}{x}(t_i)$ based on a particular value of the parameter vector. This would be the output of the Kalman filter based on a realization of the parameter vector. When $\underset{\sim}{a}$ is continuous over A, this would require an infinite number of filters in the bank. To reduce the number of filters, the parameter space is usually discretized, yielding a finite number of filters. The integrals over A in Equations (II-4) and (II-5) then become summations. Defining $p_k(t_i)$ as the probability that the k^{th} elemental filter is correct, conditioned on the measurement history, it can be shown by a method analogous to the development for Equation (II-3) that $p_k(t_i)$ satisfies:

$$p_k(t_i) = \frac{f_{\underset{\sim}{z}(t_i)|\underset{\sim}{a},\underset{\sim}{Z}(t_{i-1})}(\underline{z}_i|\underline{a}_k,\underline{Z}_{i-1}) \cdot p_k(t_{i-1})}{\sum_{j=1}^{K} f_{\underset{\sim}{z}(t_i)|\underset{\sim}{a},\underset{\sim}{Z}(t_{i-1})}(\underline{z}_i|\underline{a}_j,\underline{Z}_{i-1}) p_j(t_{i-1})} \qquad \text{(II-6)}$$

$$\hat{\underline{x}}(t_i^+) = E\{\underline{x}(t_i)|\underline{Z}(t_i) = \underline{Z}_i\} = \sum_{k=1}^{K} \hat{\underline{x}}_k(t_i^+) \cdot p_k(t_i) \qquad \text{(II-7)}$$

where $\underline{a} \in [\underline{a}_1, \underline{a}_2, \ldots \underline{a}_K]$ and $\underline{x}_K(t_i^+)$ is the mean of $\underline{x}(t_i)$ conditioned on $\underline{a} = \underline{a}_k$ and $\underline{Z}(t_i) = \underline{Z}_i$, i.e. the output of the k^{th} Kalman filter in the bank, based on the assumption $\underline{a} = \underline{a}_k$. Pictorially, the algorithm appears as in Figure II-1.

The probability weighting factors for each Kalman filter are calculated from Equation (II-6), where

$$f_{\underset{\sim}{z}(t_i)|\underset{\sim}{a},\underset{\sim}{Z}(t_{i-1})}(\underline{z}_i|\underline{a}_k,\underline{Z}_{i-1})$$

$$= \frac{1}{(2\pi)^{m/2}|A_k(t_i)|^{1/2}} \exp\left[-(1/2)\underline{r}_k^T(t_i)A_k^{-1}(t_i)\underline{r}_k(t_i)\right] \qquad \text{(II-8)}$$

and

$$A_k(t_i) = H_k(t_i)P_k(t_i^-)H_k^T(t_i) + R_k(t_i)$$

$$\underline{r}_k(t_i) = \underline{z}_i - H_k(t_i)\hat{\underline{x}}_k(t_i^-)$$

m = number of measurements

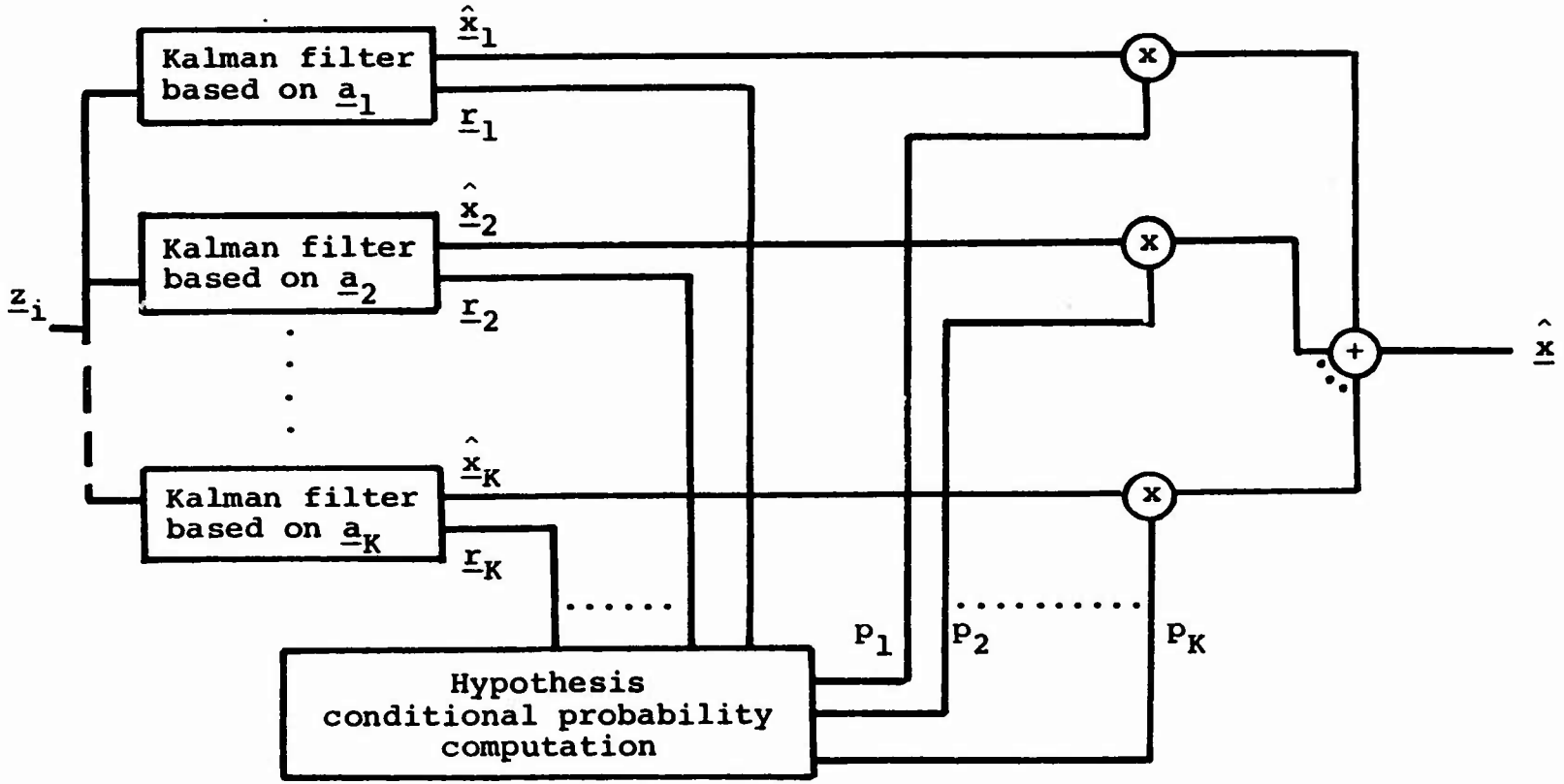

Fig. II-1. Multiple Model Filtering Algorithm

Both the residual covariance $A_k(t_i)$ and the residual $r_k(t_i)$ itself are readily available from the k^{th} elemental filter. The estimate of the parameter and the covariance of the parameter are given by:

$$\hat{\underset{\sim}{a}}(t_i) \triangleq E\{\underset{\sim}{a} | \underset{\sim}{Z}(t_i) = \underset{\sim}{Z}_i\} = \int_{-\infty}^{\infty} \underset{\sim}{a} \cdot f_{\underset{\sim}{a}|\underset{\sim}{Z}(t_i)}(\underset{\sim}{a}|\underset{\sim}{Z}_i)\,d\underset{\sim}{a}$$

$$= \int_{-\infty}^{\infty} \underset{\sim}{a} \left[\sum_{k=1}^{K} p_k(t_i)\,\delta(\underset{\sim}{a} - \underset{\sim}{a}_k)\right] d\underset{\sim}{a}$$

$$= \sum_{k=1}^{K} \underset{\sim}{a}_k p_k(t_i) \qquad \text{(II-9)}$$

and

$$E\{[\underset{\sim}{a} - \hat{\underset{\sim}{a}}(t_i)][\underset{\sim}{a} - \hat{\underset{\sim}{a}}(t_i)]^T | \underset{\sim}{Z}(t_i) = \underset{\sim}{Z}_i\}$$

$$= \sum_{k=1}^{K} [\underset{\sim}{a}_k - \hat{\underset{\sim}{a}}(t_i)][\underset{\sim}{a}_k - \hat{\underset{\sim}{a}}(t_i)]^T \cdot p_k(t_i) \qquad \text{(II-10)}$$

The covariance of the state estimate is given by:

$$P(t_i^+) = E\{[\underset{\sim}{x}(t_i) - \hat{\underset{\sim}{x}}(t_i^+)][\underset{\sim}{x}(t_i) - \hat{\underset{\sim}{x}}(t_i^+)]^T | \underset{\sim}{Z}(t_i) = \underset{\sim}{Z}_i\}$$

$$= \int_{-\infty}^{\infty} [\underset{\sim}{x} - \hat{\underset{\sim}{x}}(t_i^+)][\underset{\sim}{x} - \hat{\underset{\sim}{x}}(t_i^+)]^T f_{\underset{\sim}{x}(t_i)|\underset{\sim}{Z}(t_i)}(\underset{\sim}{x}|\underset{\sim}{Z}_i)\,d\underset{\sim}{x}$$

$$= \sum_{k=1}^{K} p_k(t_i) \int_{-\infty}^{\infty} [\underline{x} - \hat{\underline{x}}(t_i^+)][\underline{x} - \hat{\underline{x}}(t_i^+)]^T$$

$$\cdot f_{\underset{\sim}{x}(t_i)|\underset{\sim}{a},\underset{\sim}{Z}(t_i)}(\underline{x}|\underline{a},\underline{Z}_i)\,d\underline{x}$$

$$= \sum_{k=1}^{K} p_k(t_i)\{p_k(t_i^+) + [\hat{\underline{x}}_k(t_i^+) - \hat{\underline{x}}(t_i^+)]$$

$$\cdot [\hat{\underline{x}}_k(t_i^+) - \hat{\underline{x}}(t_i^+)]^T\} \qquad \text{(II-11)}$$

where $P_k(t_i^+)$ is the covariance of the state estimate of the k^{th} elemental filter.

II.2.1. Filter Convergence. The Bayesian Multiple Model Adaptive Estimator has been shown to be optimal and to converge if the true value of the parameter is nonvarying (5). Convergence for this case occurs when the probability associated with one elemental filter is essentially one and the probability associated with all other elemental filters is essentially zero. The MMAE will converge to the elemental filter with parameter value equal to, or most closely representing, the true parameter set, as defined in (5).

There are no theoretical results available for varying parameters (3:18; 6:8). The fact that the filter can converge to one filter for a non-varying true parameter value, does give reason for some concern. For example, if the true parameter value is varying very slowly, the

algorithm may assume one filter is correct with probability essentially equal to one. However, the true parameter value may eventually become significantly different from the value estimated by the filter (6:9), resulting in filter divergence.

Another possibility is that the algorithm may converge and lock onto the "wrong" filter. The filter is, to some degree, always based on an erroneous model and may converge to the wrong parameter point, especially when operated for a long period when noises are assumed small (20:23). Dasgupta and Westphal investigated the case of unknown biases in the measurement processes and showed that the algorithm may converge to a parameter point that is not close to the true value of the parameter space (3:17; 6:8).

One method of preventing divergence is to add pseudonoise to the assumed model (20:25) in each elemental filter; however, too much pseudonoise addition tends to "mask" the difference between the "correct" and "incorrect" filters. The performance of the MMAE is dependent upon significant differences between the residual characteristics of the "correct" versus "incorrect" elemental filters. If the residuals are consistently in the same magnitude, Equations (II-6) and (II-8) show that the filter with the smallest $|A_k|$, will experience an increase in its probability weighting; however, $|A_k|$ is independent of the residuals as well as the "correctness" of the k^{th} model (20:133).

Hentz and Filios (3; 6) prevented the "lock on" problem discussed previously by fixing the lower bound of the probabilities associated with the implemented filters (1; 20:27). If the computed value of any probability fell below a threshold, it was reset to some minimum value determined by performance analysis.

II.3. Moving Bank Algorithm Development (3:22-33)

The Multiple Model Adaptive Estimator presents a computation burden that is too large for most practical applications (3; 7; 18). Maybeck and Hentz demonstrated that the full bank of filters could be replaced by a subset of filters based on discrete parameter values "closest" to the current estimate of the parameter vector. The probability associated with non-implemented filters is set to 0 while the probability weightings are distributed among the implemented filters. As the parameter set estimate changes, filters that are "closer" to the new parameter estimate are implemented while those "furthest" away are removed. Maybeck and Hentz also investigated changing the discretization levels of the moving bank model. During the acquisition stage, the implemented filters are set to a coarse discretization, then changed to finer discretizations as the parameter estimate improves. Therefore, the implemented filters would not necessarily occupy adjacent discrete

points in the parameter space, as would be used in the full bank MMAE.

II.3.1. Weighted Average (3; 6). The outputs of each elemental filter of the moving bank estimator, are weighted and summed in the same manner as Equations (II-6) and (II-7); however, only the implemented filters in the moving bank are summed. If J filters are implemented, Equation (II-7) becomes:

$$\hat{\underline{x}}(t_i^+) = \sum_{j=1}^{J} \hat{\underline{x}}_j(t_i^+) p_j(t_i) \qquad \text{(II-12)}$$

Similarly, Equation (II-6) describing the $p_k(t_i)$'s become:

$$p_j(t_i) = \frac{f_j(\underline{z}(t_i)) p_j(t_{i-1})}{\sum_{k=1}^{J} f_k(\underline{z}(t_i)) p_k(t_{i-1})} \qquad \text{(II-13)}$$

and Equation (II-8) similarly is:

$$f_j(\underline{z}(t_i)) = \frac{1}{(2\pi)^{m/2} |A_j(t_i)|^{\frac{1}{2}}} \exp[-(1/2)\underline{r}_j^T(t_i) A_j^{-1}(t_i) \underline{r}_j(t_i)] \qquad \text{(II-14)}$$

and

$$A_j(t_i) = H_j(t_i) P_j(t_i^-) H_j^T(t_i) + R_j(t_i)$$

$$\underline{r}_j(t_i) = \underline{z}_i - H_j(t_i) \hat{\underline{x}}_j(t_i^-)$$

m is the dimension of $\underline{z}$ (number of measurements)

R_j is the measurement noise strength in the j^{th} elemental filter.

II.3.2. Sliding the Moving Bank (3:25). The decision logic for moving the "bank" is a critical area of interest. The moving bank MMAE is a smaller version of the full bank MMAE, with the moving bank centered around a parameter estimate. Typically, the moving bank is not initially centered on the true parameter point or the true parameter point may change. This necessitates decision logic for moving the "bank." Several algorithms have previously been investigated including Residual Monitoring, Parameter Position Estimate Monitoring, Parameter Position and Velocity Estimate Monitoring, and Probability Monitoring (3; 7; 18).

II.3.2.1. Residual Monitoring. Let a likelihood quotient for each elemental filter, $L_j(t_i)$, be defined as the quadratic form appearing in Equation (II-8):

$$L_j(t_i) = \underline{r}_j^T(t_i) A_j^{-1}(t_i) \underline{r}_j(t_i) \qquad \text{(II-15)}$$

The decision is made to move the bank if at time t_i:

$$\min[L_1(t_i), L_2(t_i), \ldots, L_J(t_i)] \geq T \qquad \text{(II-16)}$$

where T is a threshold level with a numerical value that is determined during performance evaluations. The bank is

moved in the direction of the filter with the smallest L_j, as that filter would be expected to be nearest to the true parameter set. If the true parameter vector value is outside the moving bank, it would be expected that all the likelihood quotients exceed the threshold. This method should respond quickly to a real need to move the bank but also give erroneous results for a single instance of large residuals possibly due to noise corruption.

II.3.2.2. Probability Monitoring. This method is similar to residual monitoring except that the conditional hypothesis probabilities, generated by Equation (II-6), are monitored. If the conditional hypothesis probability associated with an elemental filter is larger than a previously determined threshold, the bank is centered on that filter. Maybeck and Hentz found this decision logic, as well as parameter position monitoring, to provide the best performance. However, probability monitoring required fewer computations than parameter position monitoring (7:93-99).

II.3.2.3. Parameter Position Estimate Monitoring. This method centers the bank around the current estimate of the true parameter set, which is given by:

$$\underline{a}(t_i) = \sum_{j=1}^{J} \underline{a}_j p_j(t_i) \qquad \text{(II-17)}$$

where J is the number of filters implemented in the moving bank. Movement is initiated when the bank is not centered on the point closest to the current true parameter set estimate (3:26).

II.3.2.4. Parameter Position and Velocity Estimate Monitoring. This method estimates the velocity of the parameter position using the history of parameter position estimates. The velocity estimate is used to estimate the position of the parameter set at the next sample time. The bank is centered at this estimate of the future parameter point, thereby adding "lead" into the positioning of the bank (22). Maybeck and Hentz found this decision logic performed worse than parameter position estimate monitoring or probability monitoring (6:85; 18:23), not providing much desired lead but causing reduced stability in the bank location.

II.3.3. Bank Contraction and Expansion. The filters in the moving bank model do not necessarily need to be at adjacent discretized parameter values; see Figure II-2. This may decrease the accuracy of the initial estimate but it will increase the probability that the true parameter set lies within the bank.

Maybeck and Hentz found that parameter acquisition performance can be improved by starting the moving bank with a coarse discretization so that the entire parameter

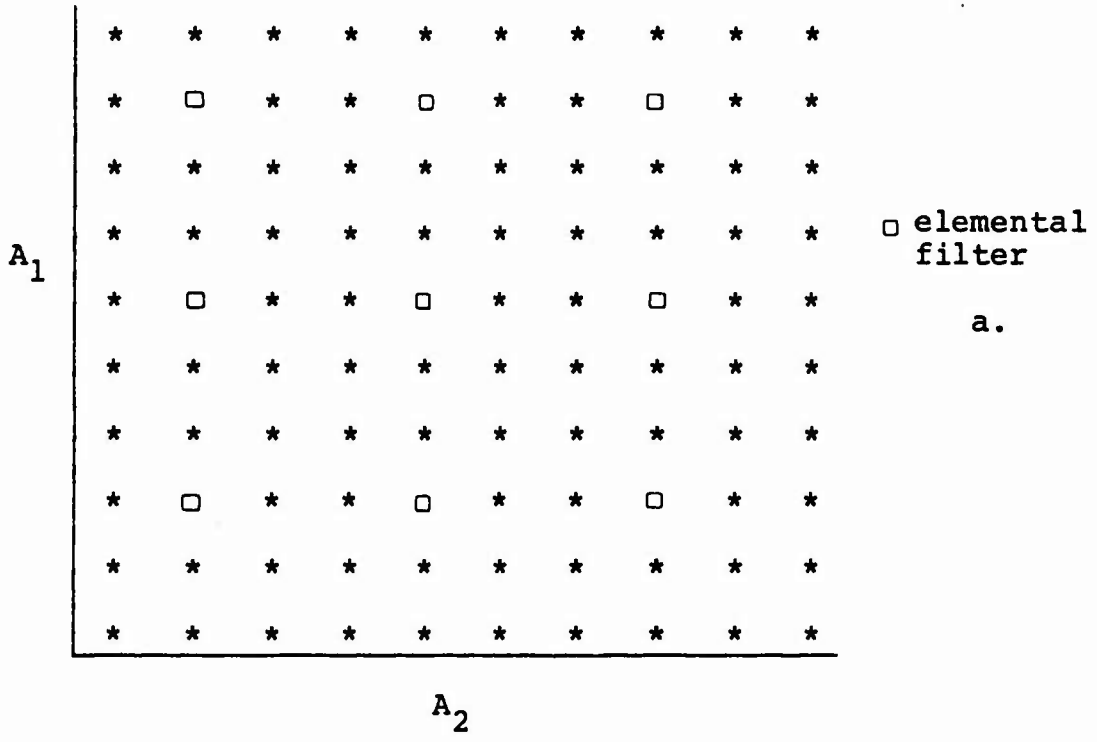

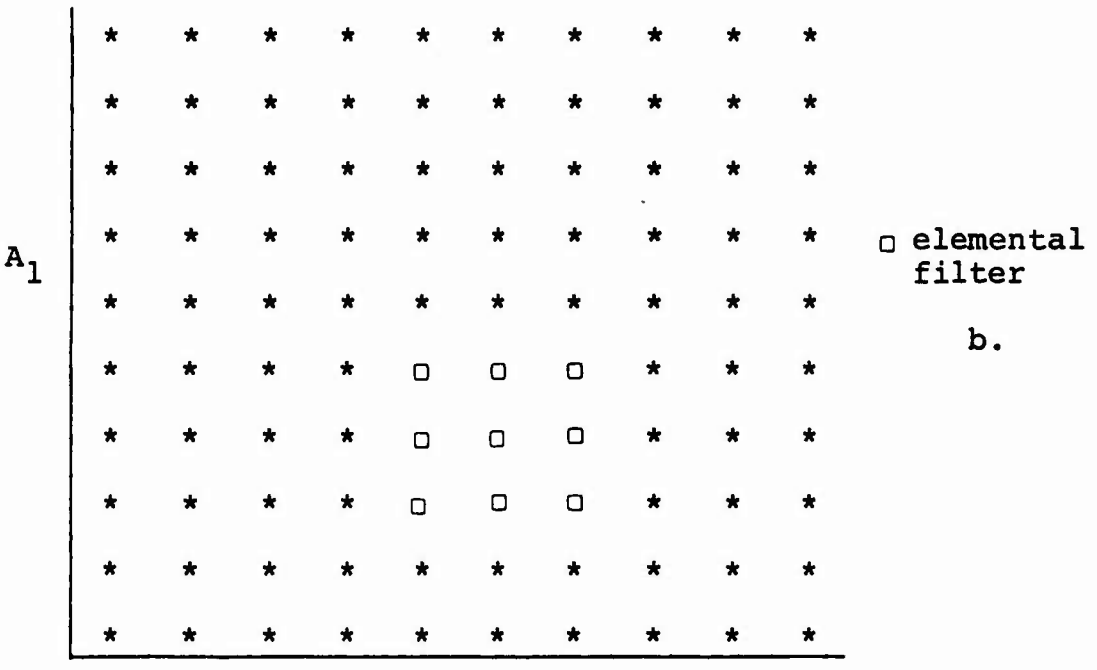

Fig. II-2. Bank Discretizations: a. coarse, b. fine

value range lies within the bank and then contracting the bank into a finer discretization when the parameter covariance (Equation (II-10)) drops below some selected threshold (3:28; 6:26; 18:25).

Another method that may improve acquisition is to monitor the probability associated with a "side" of the bank; see Figure II-3. The probability associated with each side would be calculated as:

$$p_{side}(t_i) = \frac{\sum_{side} f_j(\underline{z}(t_i))}{\sum_{4\ sides} f_j(\underline{z}(t_i))} \qquad \text{(II-18)}$$

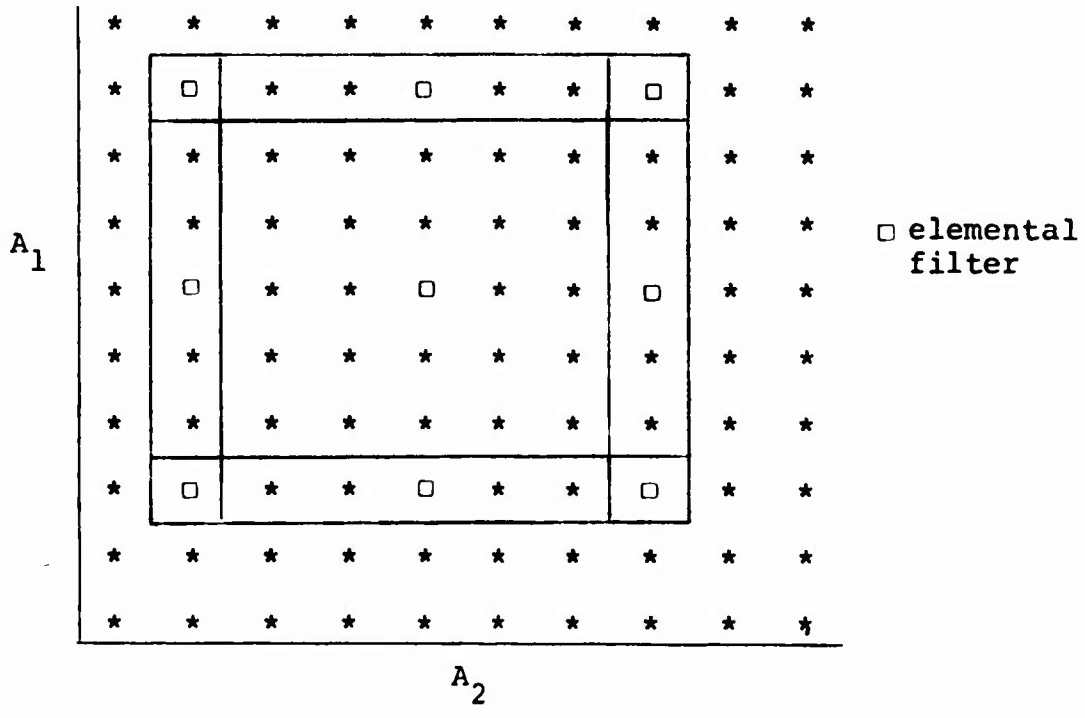

Fig. II-3. Probability Weighting of Sides

Several possibilities exist for threshold logic. If the probability associated with a side falls below a certain threshold, it can be "moved in." Conversely, if the probability associated with a side rises above some threshold, the remaining three sides are "moved in." A third possibility is moving in all four sides if the summed probability of all the "side" filters are below some threshold.

The bank may also need to be expanded if the true parameter value undergoes a jump change to a point outside the range covered by the bank. The jump change could be detected by residual or probability monitoring. For residual monitoring, the likelihood ratios for all the implemented filters are expected to be large and to exceed some threshold. For probability monitoring, it is expected that the conditional hypothesis probabilities be "close" in magnitude. The subsequent bank contraction is accomplished in the same manner as discussed in the previous paragraphs.

II.3.4. Initialization of New Elemental Filters (3:29-31; 6:26-30). When the decision is made to move, expand, or contract the bank, new filters must be brought on line and "incorrect filters" discarded. New filters require new values for Φ, B_d, K (Kalman gain matrix), H, $\underline{x}_j(t_i)$, and $p_j(t_i)$. Except for the last two terms, these are predetermined values associated with the particular filter being implemented.

The current moving bank estimate of $\underline{x}(t_i)$ is an appropriate choice for $\underline{x}_j(t_i)$ for a new elemental filter. The value for $p_j(t_i)$ is dependent on the number of new filters being implemented. If the bank "slides," as shown in Figure II-4a, this involves either three or five new filters. The probability weighting of the discarded filters is redistributed among the new filters. This can be done equally amongst the new filters or in a manner that indicates the estimated "correctness" of the new filter. Hentz suggested the following (7:29):

$$p_{jch}(t_i) = \frac{f_j(\underline{z}(t_i))\left(1 - \sum_{unch} p_k(t_i)\right)}{\sum f_k(\underline{z}(t_i))}$$

where ch = changed, unch = unchanged, and where $f_j(\underline{z}(t_i))$ is defined in Equation (II-14) but with the residual replaced by:

$$\underline{r}_j(t_i) = \underline{z}_i - H_j\hat{\underline{x}}_j(t_i^+)$$

However, this requires additional computations and has demonstrated no significant performance improvement over dividing the probability weighting equally among the changed filters (6:104).

A bank expansion or contraction can result in the resetting of all the filters in the bank as shown in Figure II-4b. Dividing the probability weighting equally

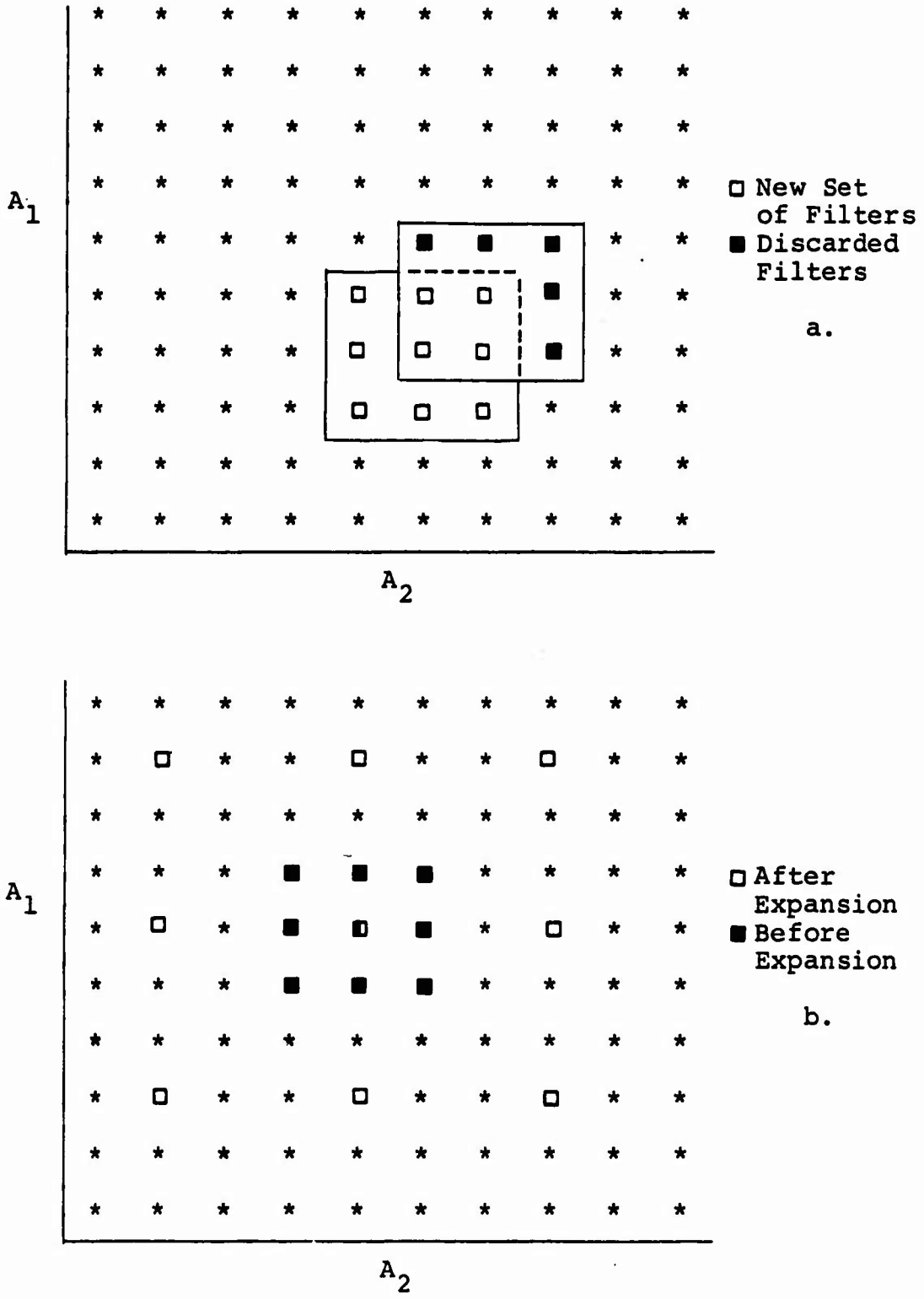

Fig. II-4. Bank Changes: a. move, b. expansion

among the new filters is appropriate since the old probability weightings may no longer be valid.

II.4. Controller and Estimator Design (3:18-22; 6:33-43)

Several controller and estimator designs are appropriate for implementation in the moving bank or full-bank MMAE. All designs considered use the "assumed certainty equivalence design" technique (21:241), which consists of developing an estimator cascaded with a deterministic full-state feedback optimal controller. This method assumes independence between controller and estimator design and is the optimal stochastic controller design for a linear system driven by white Gaussian noise with quadratic performance criterion (21:17).

The moving bank MMAE is the estimator used in this thesis. Each elemental estimator within the full bank is a constant gain Kalman filter whose design is associated with a particular point in the parameter space. Each design assumes a time invariant system with stationary noise. Propagation of the elemental filter estimate, $\hat{\underline{x}}_k(t)$, is given by:

$$\hat{\underline{x}}_k(t_i^-) = \Phi_k \hat{\underline{x}}_k(t_{i-1}^+) + B_{dk}\underline{u}(t_{i-1}) \qquad \text{(II-19)}$$

and the estimate is updated by:

$$\hat{\underline{x}}_k(t_i^+) = \hat{\underline{x}}_k(t_i^-) + K_k[\underline{z}(t_i) - H_k\hat{\underline{x}}_k(t_i^-)] \qquad \text{(II-20)}$$

where, the subscript "K" indicates association with a particular point in the parameter space.

The design of each controller is similar. Each is a linear, quadratic cost, (LQ) full-state feedback optimal deterministic controller, based on an error state space formulation (19:297). The controller is steady-state constant-gain, with gains dependent upon the particular value of the parameter set used in the design. The LQ controller is developed fully in Appendix A.

Three estimator/controller combinations are considered. First, the estimator provides only a state vector estimate to a fixed-gain controller which is designed around a nominal value of the uncertain parameter set. The controller algorithm is of the form:

$$\underline{u}(t_i) = -G_c^*[\underline{a}_{nom}]\hat{\underline{x}}(t_i^+) \qquad \text{(II-21)}$$

The second design method is for the estimator to provide parameter and state vector estimates to a controller with gains that are dependent on the parameter estimate:

$$\underline{u}(t_i) = -G_c^*[\hat{\underline{a}}(t_i^-)]\hat{\underline{x}}(t_i^+) \qquad \text{(II-22)}$$

where the parameter estimate generated at the previous sample time is used in order to reduce computational delay.

A third approach is to form an elemental controller for each of the elemental filters of the sliding bank. The

control outputs are probabilistically weighted, similar to Equation (II-12), to form:

$$\underline{u}(t_i) = \sum_{j=1}^{J} p_j(t_i)\underline{u}_j(t_i) \qquad \text{(II-23)}$$

where,

$$\underline{u}_j(t_i) = -G_c^*[\underline{a}_j]\hat{\underline{x}}_j(t_i^+) \qquad \text{(II-24)}$$

This is usually referred to as a multiple model adaptive controller (MMAC) (21:253).

Two benchmark controllers are also investigated: a single controller with artificial knowledge of the true parameter set and a robust, single fixed-gain controller. The former represents the "best" that can be achieved through adaptive control. The robust controller will represent the "best" control that can be achieved using non-adaptive control.

II.5. Ambiguity Function Analysis (3; 6; 20:97-99)

Ambiguity function analysis can provide information about the performance of an estimator. The generalized ambiguity function is given by:

$$A_i(\underline{a},\underline{a}_t) \triangleq \int_{-\infty}^{\infty} \cdots \int_{-\infty}^{\infty} L[\underline{a},\underline{Z}_i] \cdot f_{\underline{\underline{Z}}(t_i)|\underline{\underline{a}}(t_i)}(\underline{Z}_i|\underline{a}_t)\, d\underline{Z}_i$$

where $\underline{a}$ is the parameter vector, $\underline{a}_t$ is the true parameter vector, and $L[\underline{a},\underline{Z}_i]$ is a likelihood function upon which a

parameter estimate would be based via maximum likelihood techniques. For a given value of $\underline{a}_t$, the curvature of the function of $\underline{a}$, at the value of $\underline{a}_t$, provides information on the ability of the filter to estimate that parameter: the sharper the curvature, the greater the precision. This curvature is inversely related to the Cramér-Rao lower bound on the estimate error covariance matrix by

$$E\{[\underline{a} - \underline{a}_t][\underline{a} - \underline{a}_t]^T\} \geq [-(\partial^2/\partial \underline{a}^2)\ A_i(\underline{a},\underline{a}_t)|_{\underline{a}=\underline{a}_t}]^{-1}$$

The ambiguity function value $A_i(\underline{a},\underline{a}_t)$ for any $\underline{a}$ and $\underline{a}_t$ can be calculated from the output of a conventional nonadaptive Kalman filter sensitivity analysis (20:97-99) in which the "truth model" is identical to the model upon which the Kalman filter is based, except that they are based on $\underline{a}_t$ and $\underline{a}$, respectively. The ambiguity function is then given by

$$\begin{aligned} A_i(\underline{a},\underline{a}_t) = \sum_{j=i-N+1}^{i} & [m/2\ \ln(2\pi) - 1/2\ \ln[|A(t_j;\underline{a}|] \\ & - 1/2\ \mathrm{tr}\{A^{-1}(t_j;\underline{a})[H(t_j)P_e(t_j^-;\underline{a}_t,\underline{a})H^T(t_j)+R(t_j)]\}] \\ & - n/2\ \ln(2\pi) - 1/2\ \ln[|P(t_i^+;\underline{a}|] \\ & - 1/2\ \mathrm{tr}[P^{-1}(t_i^+;\underline{a})P_e(t_i^+;\underline{a}_t,\underline{a})] \end{aligned} \qquad \text{(II-25)}$$

where,

$$A(t_i;\underline{a}) = [H(t_i)P(t_i^-;\underline{a})H^T(t_i) + R(t_i)]^{-1}$$

for the Kalman filter based on $\underline{a}$,

and $P_e(t_i^{\pm};\underline{a}_t,\underline{a})$ is the covariance matrix of the error between the state estimate of the Kalman filter based on $\underline{a}$ and the states of the true system based on $\underline{a}_t$, where "-" or "+" denotes before or after incorporation of the i^{th} measurement.

"m" is the number of measurements.

"n" is the number of states.

The terms are summed over the most recent N sample times (20:98); however, here N is set equal to one. This reduces the size of the fluctuations in the value of $A_i(\underline{a},\underline{a}_t)$. Consequently, this flattens the surface of the plot of the ambiguity function plotted as a function of the parameter $\underline{a}$. The main benefit of setting N = 1 is that this significantly reduces the number of computations.

Filios encountered numerical difficulties while evaluating the ambiguity function (3:64). The covariance matrix at time t_i^+ was ill conditioned. Therefore, it was impossible to compute the ambiguity function as described in Equation (II-25). The numerical difficulties were overcome by approximating the expressions for the probability weighting factors (Equation II-14)) and the ambiguity function (Equation II-25)). Equation (II-14) is approximated as

$$f_j(\underline{z}(t_i)) = \exp[-(1/2)\underline{r}_j^T(t_i)A_j^{-1}(t_i)\underline{r}(t_i)]$$

This is no longer a true density function because the scale factor is incorrect; however, because of the denominator in Equation (II-13), the probability weightings are still correct in the sense that they add to one (3:65). If the determinants of the A matrices of the elemental filters are expected to be approximately equal in magnitude, in the absence of numerical problems, the relative magnitudes of the value of the ambiguity functions will not be significantly altered (3:65). Equation (II-25) was approximated by removing the terms containing the determinants of $P(t_i^+)$ and A. Equation (II-25) becomes

$$A_i(\underline{a},\underline{a}_t) = m/2\ \ln(2\pi) - n/2\ \ln(2\pi)$$

$$- 1/2\ tr\{A^{-1}(t_i;\underline{a})[H(t_i)P_e(t_i^-;\underline{a}_t,\underline{a})H^T(t_i)+R(t_i)]\}$$

$$- 1/2\ tr\{P^{-1}(t_i^+;\underline{a})P_e(t_i^+;\underline{a}_t,\underline{a})\} \qquad \text{(II-26)}$$

This is a reasonable approximation since the determinants of $P(t_i^+)$ and A will have a minimal effect on the ambiguity function, since its primary sensitivity is in the functions that are being preserved (3:66). It was not known whether numerical difficulties will be encountered with the model being used in this thesis effort. However, since the approximation would not significantly alter the outcome of the ambiguity function analysis, the decision was made to incorporate it to take advantage of the smaller computational load.

II.6. Summary

This chapter developed algorithms necessary for implementation of the full-scale and moving bank multiple model adaptive estimator and appropriate adaptive controller based on this type of estimation. The moving bank MMAE is expected to yield significant computation savings over the full-scale MMAE. The ambiguity functions analysis was also developed. Ambiguity functions are expected to give insight into the parameters that need adaptive estimation and into the appropriate levels of discretization of the parameter space to perform such estimation.

III. Rotating Two-bay Truss Model

III.1. Introduction

This chapter develops the system equations for the rotating two-bay truss model of a flexible space structure. The structure consists of a truss that rotates around a fixed point, thereby incorporating both rigid body rotation and bending mode dynamics. The differential equations describing the equations of motions are developed and then transformed into modal coordinates. The actual physical structure of the two-bay truss is discussed, as is the finite element analysis used to obtain the mass and stiffness matrices which describe the rotating two-bay truss. The need for order reduction and the order reduction technique employed in this thesis is also developed.

III.2. Second Order and State Space Form Models

The general second-order differential equations which describe the forced vibration of a large space structure with active controls and n frequency modes can be written as (16; 30):

$$M\ddot{\underline{r}}(t) = C\dot{\underline{r}}(t) + K\underline{r}(t) = \underline{F}_1(u,t) + \underline{F}_2(t) \qquad \text{(III-1)}$$

where,

M - constant nxn mass matrix

C - constant nxn damping matrix

K - constant nxn stiffness matrix

$\underline{r}(t)$ - vector representing structure's physical coordinates

$\underline{F}_1(u,t)$ - control input

$\underline{F}_2(t)$ - disturbances and unmodeled control inputs

The control system is assumed to consist of a set of discrete actuators. The external disturbances and unmodeled control inputs are represented by white noise, thus producing:

$$M\underset{\sim}{\ddot{r}}(t) + C\underset{\sim}{\dot{r}}(t) + K\underset{\sim}{r}(t) = -b\underline{u}(t) - g\underset{\sim}{w} \qquad \text{(III-2)}$$

where "$\underset{\sim}{\ }$" denotes a vector stochastic random process and:

$\underline{u}(t)$ - vector of length m representing actuator input,

b - nxm matrix identifying position and relationship between actuators and controlled variables (16),

$\underset{\sim}{w}$ - vector of length r representing dynamic driving noise, where r is the number of noise inputs,

g - nxr matrix identifying position and relationships between dynamic driving noise and controlled variables.

The state representation of Equation (III-2) can be written as:

$$\underset{\sim}{\dot{x}} = A\underset{\sim}{x} + B\underline{u} + G\underset{\sim}{w} \qquad \text{(III-3)}$$

where,

$$\underset{\sim}{x} = \begin{bmatrix} \underset{\sim}{r} \\ \underset{\sim}{\dot{r}} \end{bmatrix}_{2nx1} \qquad \dot{\underset{\sim}{x}} = \begin{bmatrix} \underset{\sim}{\dot{r}} \\ \underset{\sim}{\ddot{r}} \end{bmatrix}_{2nx1} \tag{III-4}$$

and the open-loop plant matrix A, the control matrix B, and the noise matrix G are given by:

$$A = \begin{bmatrix} 0 & I \\ -M^{-1}K & -M^{-1}C \end{bmatrix}_{2nx2n} \qquad B = \begin{bmatrix} 0 \\ -M^{-1}b \end{bmatrix}_{2nxm}$$

$$G = \begin{bmatrix} 0 \\ -M^{-1}g \end{bmatrix}_{2nxm} \tag{III-5}$$

It is assumed that the noise can be represented as inputs that enter the system at the same place as the actuators (b matrix = g matrix). Measurements are assumed available from position and velocity sensors which are co-located for simplicity. Accelerometer measurements are not used because this would increase the number of states in the model and it is not clear that this additional complexity would aid in evaluating the moving-bank MMAE. It is assumed that the measurements are noise corrupted due either to deficiencies in the model of the sensor or some actual external measurement noise. The measurements are modeled as:

$$\underset{\sim}{z} = \begin{bmatrix} H & 0 \\ 0 & H' \end{bmatrix}_{px2n} \underset{\sim}{x} + \underset{\sim}{v} \qquad \text{(III-6)}$$

where p is the number of measurements, $\underset{\sim}{v}$ is an uncertain measurement disturbance of dimension p and modeled as a white noise (19:114), H is the position measurement matrix, and H' is the velocity measurement matrix. The velocity and position measurement matrices are identical because of co-location of the velocity and position sensors; therefore, both measurement matrices will be referred to as the H matrix.

III.3. Modal Analysis

Modal analysis is used to transform the system into a set of independent equations by transforming the system from physical coordinates to modal coordinates. In order to achieve decoupling, the damping matrix must be assumed to be a linear combination of the mass and stiffness matrices (16):

$$C = \alpha K + \beta M \qquad \text{(III-7)}$$

The modal coordinates are related to the physical coordinates by

$$\underline{r} = T\ \underline{\Omega} \qquad \text{(III-8)}$$

where $\underline{r}$ is as defined previously and $\underline{\Omega}$ represents the modal coordinates. T is an nxn matrix of eigenvectors and is the solution to (16; 25; 30; 31):

$$w^2MT = KT \tag{III-9}$$

The values of w which solve Equation (III-9) are natural or modal frequencies (8:66). Substituting Equation (III-8) into Equation (III-3) gives

$$\underset{\sim}{\dot{x}}' = A'\underset{\sim}{x}' + B'\underline{u} + G'\underset{\sim}{w} \tag{III-10}$$

where $\underline{x}'$ is now defined as:

$$\underset{\sim}{x}' = \begin{bmatrix} \underset{\sim}{\Omega} \\ \underset{\sim}{\dot{\Omega}} \end{bmatrix}_{2nx1} \qquad \underset{\sim}{\dot{x}}' = \begin{bmatrix} \underset{\sim}{\dot{\Omega}} \\ \underset{\sim}{\ddot{\Omega}} \end{bmatrix}_{2nx1} \tag{III-11}$$

and the open loop plant matrix A', the control matrix B', and the noise matrix G' are:

$$A' = \begin{bmatrix} 0 & I \\ -T^{-1}M^{-1}K_T & -T^{-1}M^{-1}C_T \end{bmatrix}_{2nx2n}$$

$$B' = \begin{bmatrix} 0 \\ -T^{-1}M^{-1}b \end{bmatrix} \qquad G' = \begin{bmatrix} 0 \\ -T^{-1}M^{-1}b \end{bmatrix} \tag{III-12}$$

The A' matrix is also of the form (30; 31):

$$A' = \begin{bmatrix} O & I \\ [-w_i^2] & [-2\zeta_i w_i] \end{bmatrix}_{2nx2n} \qquad \text{(III-13)}$$

where each of the four partitions are nxn dimensional and diagonal. The measurements become:

$$\underset{\sim}{z} = \begin{bmatrix} HT & O \\ O & HT \end{bmatrix} \underline{x}' + \underset{\sim}{v}$$

The formulation of the system in modal coordinates allows some assumptions concerning structural damping (16). It is assumed that uniform damping exists throughout the structure. The level of structural damping is determined by selecting a value for the damping coefficients (ζ_i) and substituting this value into Equation (III-13). The particular value of the damping coefficient has no effect on the calculation of w_i since it is the natural or modal frequency. The assumption simplifies the determination of structural damping and allows a better physical insight into formulating the problem than does the selection of values for α and β as shown in Equation (III-7). The damping coefficient of $\zeta = 0.005$ is chosen for implementation because it is characteristic of damping associated with large space structures (16; 22).

III.4. Two-bay Truss

III.4.1. Introduction. This section describes the physical structure of the two-bay truss rotating about a fixed point. The physical dimensions of the model, analysis used to develop the two-bay truss model, sensors and actuators, and the physical parameter variations of the model are discussed.

III.4.2. Background. A fixed two-bay truss was originally developed to study the effects of structural optimization on optimal control design (30); see Figure III-1. A similar model was used to research active control laws for vibration damping (16). The model was modified to lower the structural frequencies, thereby making the problem more like a large space structure (16). This was done by adding non-structural masses at nodes 1-4. The model was further modified for this research by adding rigid body motion; see Figure III-2. The rotating two-bay truss approximates a space structure that has a hub with appendages extending from the structure. The mass of the hub is large relative to the mass of the appendage. The hub is then rotated to point the appendage in a commanded direction.

The rigid body motion is established by adding a point (node 7) that remains fixed while the two-bay truss is free to rotate about this point in the x-y plane; see

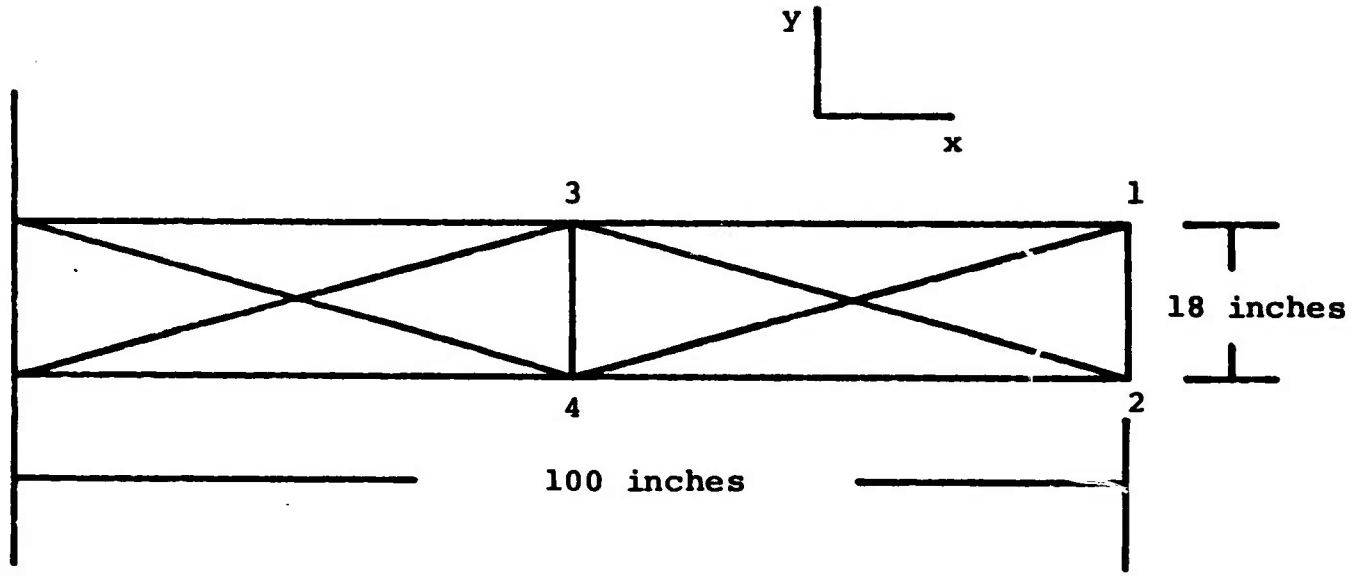

Fig. III-1. Two-bay Truss Model

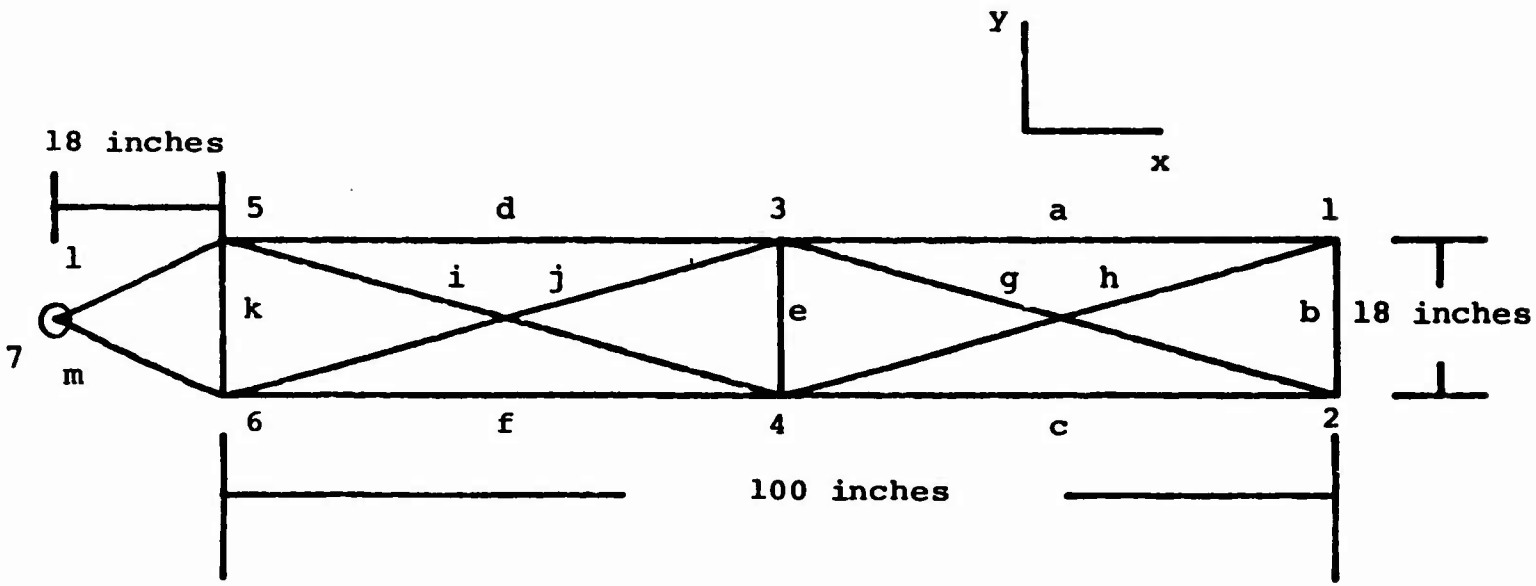

Fig. III-2. Rotating Two-bay Truss Model

Figure III-2. The truss is connected to this point using rods having radii that are large relative to the rods used to construct the two-bay truss. Making the rods large makes a very "stiff" link between the truss and node 7. This introduces high frequency modes into the structure but keeps the lower modal frequencies similar to the case where the truss is fixed.

III.4.3. Two-bay Truss Construction. The structure consists of 13 rods which are assumed to be constructed of aluminum, having a modulus of elasticity of 10^7 psi and weight density of .1 lb/in^3 (30). The cross-sectional areas of each member shown in Figure III-2 are given in Table III-1.

TABLE III-1

STRUCTURAL MEMBER'S CROSS-SECTIONAL AREAS

Member	Area (in^2)	Member	Area (in^2)
a	.00321	h	.00328
b	.00100	i	.00439
c	.00321	j	.00439
d	.01049	k	.20000
e	.00100	l	.20000
f	.01049	m	.20000
g	.00328	-	-

The cross-sectional areas of rods a-j were calculated by optimizing the weight of the structure shown in Figure III-1. First, a non-optimal structure was constructed with all rods having identical cross-sectional areas. A second structure

was then calculated with its weight minimized with respect to the constraint that the fundamental frequency remain unchanged. Rods k-m are used to make the "stiff" link between node 7 and the two-bay truss. The area was arbitrarily selected to be large relative to the area of other rods in order to achieve this stiffness.

Non-structural masses with a mass of 1.294 lb-sec^2/in, are located at positions 1, 2, 3 and 4 as shown in Figure III-2. The non-structural mass is very large compared to the structural mass but this is necessary to achieve the low frequencies associated with large space structures (16). The actual value of the non-structural mass was selected using an optimization technique (31) which found the mass necessary to attain a frequency of 0.5 Hz in the lowest mode for the fixed two-bay truss (16).

The mass and stiffness matrices, describing the system model, were obtained using finite element analysis (31). Finite element analysis models a structure as consisting of a finite number of nodes connected by elements. The program has the capability to use a number of different elements, but this research uses rods which are described by cross-sectional area, modulus of elasticity, and weight density. The finite element program produces mass and stiffness matrices with dimension equal to the number of degrees of freedom (DOF) associated with the model. Each row of the mass and stiffness matrix is associated with a

specific node and DOF. For the two-bay truss shown in Figure III-2, row 1 of each mass and stiffness matrix is associated with the x-axis DOF of node 1. Each node has three translational DOF. Only planar motion is being considered; therefore, the nodes are modeled with only two DOF. For this problem, node 7 was fixed. Therefore, all three DOF associated with this node are eliminated, thereby reducing the dimensionality of the mass and stiffness matrices to 12 states and thus eventually yielding a 24-state model. The mass and stiffness matrices for the specifications previously discussed, are listed in Appendix B. These are the nominal matrices from which parameter variations are considered.

III.4.4. Sensors and Actuators. Velocity and position sensors are assumed co-located at nodes 1 and 2 as shown in Figure III-2. Two additional sensors for angular displacement and velocity are co-located on the hub (node 7) of the two-bay truss. Actuators are placed at nodes 1 and 2 as shown in Figure III-2. An additional actuator is located on the hub.

The states corresponding to velocity and position are directly available in physical variable formulation (Equations III-3, III-4, III-5) while the states corresponding to angular displacement and velocity are directly available in modal formulation (Equations III-10, III-11,

III-12, III-14). The H and b matrices are constructed by calculating separate matrices in the different state space formulations. These matrices are augmented after the physical variable formulations have been transformed into modal coordinates.

III.4.5. Physical System Parameter Uncertainty. The purpose of this thesis is to test the moving-bank multiple model adaptive estimation and control algorithms. Therefore, the model must have parameter uncertainty which allows adaptive estimation to be applied. A 10 by 10 point parameter space is created by considering two physically motivated parameter variations. First it is assumed that the four non-structural masses vary -50 percent to +40 percent from the nominal value in discrete steps of 10 percent. The variation is assymmetric simply to allow the 10 point parameter variation. This weight variation can be physically related to fuel being expended from or added to a tank or weight being shifted to a different section (other than the two-bay truss) of the space structure. Secondly, the entire stiffness matrix is allowed to vary -20 percent to +16 percent from the nominal value in discrete steps of 4 percent. This can be associated with structural fatigue in the rods or a failure of a member within the structure itself. The realism of the magnitude of these parameter variations has not been rigorously investigated;

however, the variation is necessary to produce the changes in the system model of a magnitude as to require adaptive estimation and control. Both the mass and stiffness variation is uniform as there is no strong evidence that introducing a nonlinear variation scale will improve moving-bank MMAE performance.

III.5. State Reduction

III.5.1. Introduction. The mass and stiffness matrices were previously shown to be of dimension 12. This produces a system model that has 24 states, which is much larger than desired for this thesis effort and for a practical control application. This section develops a method of order reduction referred to as singular perturbations (9; 10; 16; 21:219). The method of singular perturbations assumes that faster modes reach steady state essentially instantaneously. This section develops the method of singular perturbations and then discusses the magnitude of the order reduction.

III.5.2. Development. The deterministic system is reformulated as follows:

$$\begin{bmatrix} \dot{\underline{x}}_1 \\ \dot{\underline{x}}_2 \end{bmatrix} = \begin{bmatrix} A_{11} & A_{12} \\ A_{21} & A_{22} \end{bmatrix} \begin{bmatrix} \underline{x}_1 \\ \underline{x}_2 \end{bmatrix} + \begin{bmatrix} B_1 \\ B_2 \end{bmatrix} \underline{u} \qquad \text{(III-15)}$$

$$\underline{z} = [H_1 \quad H_2] \, \underline{x} \qquad \text{(III-16)}$$

The $\underline{x}_1$ states are to be retained and A_{11} and A_{22} are square matrices. If only high frequency modes are eliminated, steady state is assumed to be reached instantaneously in these modes ($\dot{\underline{x}}_2 = \underline{0}$). The $\underline{x}_2$ states are then expressed in terms of the $\underline{x}_1$ states:

$$\dot{\underline{x}}_2 = \underline{0} = A_{21}\underline{x}_1 + A_{22}\underline{x}_2 + B_2\underline{u} \qquad \text{(III-17)}$$

$$\underline{x}_2 = -A_{22}^{-1}(A_{21}\underline{x}_1 + B_2\underline{u}) \qquad \text{(III-18)}$$

Substituting for $\underline{x}_2$ gives

$$\dot{\underline{x}}_1 = A_r\underline{x}_1 + B_r\underline{u} \qquad \underline{z} = H_r\underline{x}_1 + D_r\underline{u} \qquad \text{(III-19)}$$

where:

$$A_r = (A_{11} - A_{12}A_{22}^{-1}A_{21}) \qquad \text{(III-19a)}$$

$$B_r = (B_1 - A_{12}A_{22}^{-1}B_2) \qquad \text{(III-19b)}$$

$$H_r = (H_1 - H_2A_{22}^{-1}A_{21}) \qquad \text{(III-19c)}$$

$$D_r = (-H_2A_{22}^{-1}B_2) \qquad \text{(III-19d)}$$

Note that the D_r matrix did not exist before order reduction. It is a direct-feed term which was not in the unreduced system (16).

This order reduction technique is now applied to a system of the form of Equation (III-10). Reordering

Equation (III-13) into the reduced-order form produces Equation (III-20), where the upper partition contains the modes to be retained while the lower partition contains those assumed to reach steady state instantaneously.

$$A = \left[\begin{array}{cc|cc} 0 & I & \multicolumn{2}{c}{\multirow{2}{*}{O}} \\ [-w_1^2] & [-2\zeta_1 w_1] & & \\ \hline \multicolumn{2}{c|}{\multirow{2}{*}{O}} & 0 & I \\ & & [-w_2^2] & [-2\zeta_2 w_2] \end{array}\right]_{2nx2n} \qquad \text{(III-20)}$$

Comparing Equation (III-20) to Equation (III-15) shows that the partitions A_{12} and A_{21} are zero. Substituting this result into Equation (III-19) yields:

$$A_r = A_{11} \qquad \text{(III-21a)}$$

$$B_r = B_1 \qquad \text{(III-21b)}$$

$$H_r = H_1 \qquad \text{(III-21c)}$$

$$D_r = (-H_2 A_{22}^{-1} B_2) \qquad \text{(III-21d)}$$

D_r is the only term in Equation (III-19) that is dependent upon terms associated with the states assumed to reach steady state instantaneously. The other reduced-order matrices are calculated simply by truncating those states associated with $\underline{x}_2$.

Calculation of D_r can be greatly simplified by examining the form of Equation (III-21d). H_2 is similar in form to Equation (III-6):

$$H_2 = \begin{bmatrix} H_2 & 0 \\ 0 & H_2' \end{bmatrix} \qquad \text{(III-22)}$$

H_2 represents measurement of the unmodeled position states while H_2' represents measurement of the unmodeled velocity states. In Equation (III-6), it was assumed that the position and velocity measurement matrices were identical because of co-located position and velocity sensors. The same assumption can be made in Equation (III-22); however, the distinction between the velocity and measurement matrices will be retained since it is shown in Equation (III-26) to be important in the general development of the reduced order matrices. As was shown in Equation (III-20), A_{22} is a square matrix of the form:

$$A_{22} = \begin{bmatrix} 0 & I \\ [-w_2^2] & [-2\zeta_2 w_2] \end{bmatrix} \qquad \text{(III-23)}$$

where each of the four partitions is a square, diagonal matrix whose dimension is dependent upon the number of states to be retained. Its inverse is (8):

$$A_{22}^{-1} = \begin{bmatrix} [-w_2^2]^{-1}[2\zeta_2 w_2] & [-w_2^2]^{-1} \\ I & 0 \end{bmatrix} \qquad \text{(III-24)}$$

B_2 is similar in form to the matrix B described in Equation (III-5):

$$B_2 = \begin{bmatrix} 0 \\ b' \end{bmatrix} \qquad \text{(III-25)}$$

where b' represents the rows of the matrix product $-M^{-1}b$ corresponding to the unmodeled states. Evaluation of Equation (III-21d) yields:

$$n_r = \begin{bmatrix} H_2[-w_2^2]^{-1}b' \\ 0 \end{bmatrix}_{pxl} \qquad \text{(III-26)}$$

where p is the number of measurements. Only the position measurements are affected since the lower portion is zero. The D_r matrix is only dependent upon the position portion of the measurement matrix and not the velocity measurement matrix. The inverse of w_{22} is easily calculated since the matrix is diagonal. An example of detailed system matrix development and order reduction is listed in Appendix B.

III.5.3. Order Reduction Selection. The number of modes retained was determined by examination of the eigenvalues and frequencies of the unreduced system (Table III-2). The frequencies can be distinctly divided into several

TABLE III-2

EIGENVALUES AND FREQUENCIES

Mode No.	Eigenvalues*	Frequencies
1	0.0000	0.0000
2	8.8922	1.4152
3	22.5492	3.5888
4	29.5444	4.7021
5	31.1519	4.9580
6	32.8002	5.2203
7	54.3893	8.6563
8	58.1592	9.2563
9	985.9204	156.9141
10	9018.8987	1435.4023
11	11515.9941	1832.8274
12	19956.5072	3176.1768

* The eigenvalues are for an undamped system ($\zeta = 0$).

groups of closely spaced frequencies. For example, modes 4, 5, and 6 are clearly one set of closely spaced frequencies. When reducing the order of system by the method of singular perturbations, it is desirable not to make the reduction at a point which will divide a group of "closely spaced" frequencies (22). At the same time, a sufficient number of frequencies must be retained in order to do an adequate job of estimation and control. An obvious selection of a reduced order model is to retain the first three modes, resulting in a six-state system. Keeping any more modes will result in the requirement to retain the frequency group at modes at 4, 5, and 6, which would result in a much larger 12-state system.

III.6. Summary

This chapter developed the system equations for the two-bay truss with rigid body motion. The mathematical model is dependent upon physical parameters which, in reality, vary from those used in the mathematical model. The moving-bank MMAE will be used to estimate both the reduced order system states and the varying parameters of the physical system.

IV. Simulation (3; 6)

IV.1. Introduction

Evaluation of the performance of the moving-bank multiple model adaptive estimator/controller for this application requires simulating actual space structure movement and estimator/controller operation. The computer simulation provides a Monte Carlo and sensitivity analysis (using ambiguity functions) of the estimator/controller. This chapter provides background on the Monte Carlo simulation, briefly outlines the computer software, and then discusses the simulation plan for analyzing the performance of the estimator design logics and the moving-bank algorithms.

IV.2. Monte Carlo Analysis

It is desired to obtain statistical information on the estimator/controller's performance. One method of generating these statistics is through the use of a Monte Carlo study. This involves obtaining many samples of the error process through simulation and then using this data to approximate the process statistics (19:329).

The true system model under consideration can be described by a linear time-invariant difference equation:

$$\underset{\sim}{x}(t_{i+1}) = \Phi(t_{i+1},t_i)\underset{\sim}{x}(t_i) + B_d(t_i)\underline{u}(t_i) + G_d(t_i)\underset{\sim}{w}_d(t_i) \qquad \text{(IV-1)}$$

(See Equation II-1) for a complete definition of terms.) B_d and G_d are the discrete-time equivalents of the B and G matrices given in Equation (III-5). It is assumed that the noise input matrix is identical to the control input matrix, therefore (19:171),

$$B_d = G_d = \int_{t_{i-1}}^{t_i} \Phi(t_i,\tau)B \, d\tau \qquad \text{(IV-2)}$$

Noise corrupted measurements are provided to the estimator in the form of:

$$\underset{\sim}{z}(t_i) = H\underline{x}(t_i) + \underset{\sim}{v}(t_i) \qquad \text{(IV-3)}$$

where H is the measurement matrix and $\underset{\sim}{v}(t_i)$ is a discrete time, zero-mean, white Gaussian measurement noise with covariance matrix R. Matrices Φ, B_d, G_d, and H are functions of the true parameter vector $\underline{a}_t$:

$$\underline{a}_t = [M, K]^T$$

where, M and K are the mass and stiffness parameters, respectively and are discussed in Section III.4.

The simulation is accomplished for a sufficient number of runs so that the computed sample means and variances of the random variables of interest are good approximations to true ensemble averages. The number of simulation runs selected is 10 and this is determined by

observation of the sample statistics as the number of Monte Carlo runs is increased (3:52).

Figure IV-1 illustrates the simulation for obtaining individual samples of the Monte Carlo analysis (3:53). The variables not previously defined are:

$\underset{\sim}{x}_t(t_i)$ = "truth model" states

$\hat{\underset{\sim}{x}}(t_i)$ = estimate of system states

$\hat{\underset{\sim}{a}}(t_i)$ = estimate of uncertain parameter vector

$\underset{\sim}{e}_a(t_i)$ = error in the parameter estimate

$$\underset{\sim}{e}_a(t_i) = \underset{\sim}{a}_t(t_i) - \hat{\underset{\sim}{a}}(t_i)$$

$\underset{\sim}{e}_x(t_i)$ = error in the system state estimate

$$\underset{\sim}{e}_x(t_i) = T\underset{\sim}{x}_t(t_i) - \hat{\underset{\sim}{x}}(t_i)$$

where, T is a n x n_t matrix to make the dimensions compatible since the estimate is typically of lesser dimension than the "truth model" states.

The sample mean of the variables of interest is computed as (3:53; 6:46; 19:129):

$$E[\underset{\sim}{e}_x(t_i)] \simeq \hat{\underset{\sim}{M}}_{ex}(t_i) \overset{\Delta}{=} (1/N) \sum_{k=1}^{N} \underset{\sim}{e}_{xk}(t_i) \qquad \text{(IV-4)}$$

where,

N = total number of simulation runs

$\underset{\sim}{e}_{xk}(t_i)$ = value of $\underset{\sim}{e}_x(t_i)$ during the kth simulation run

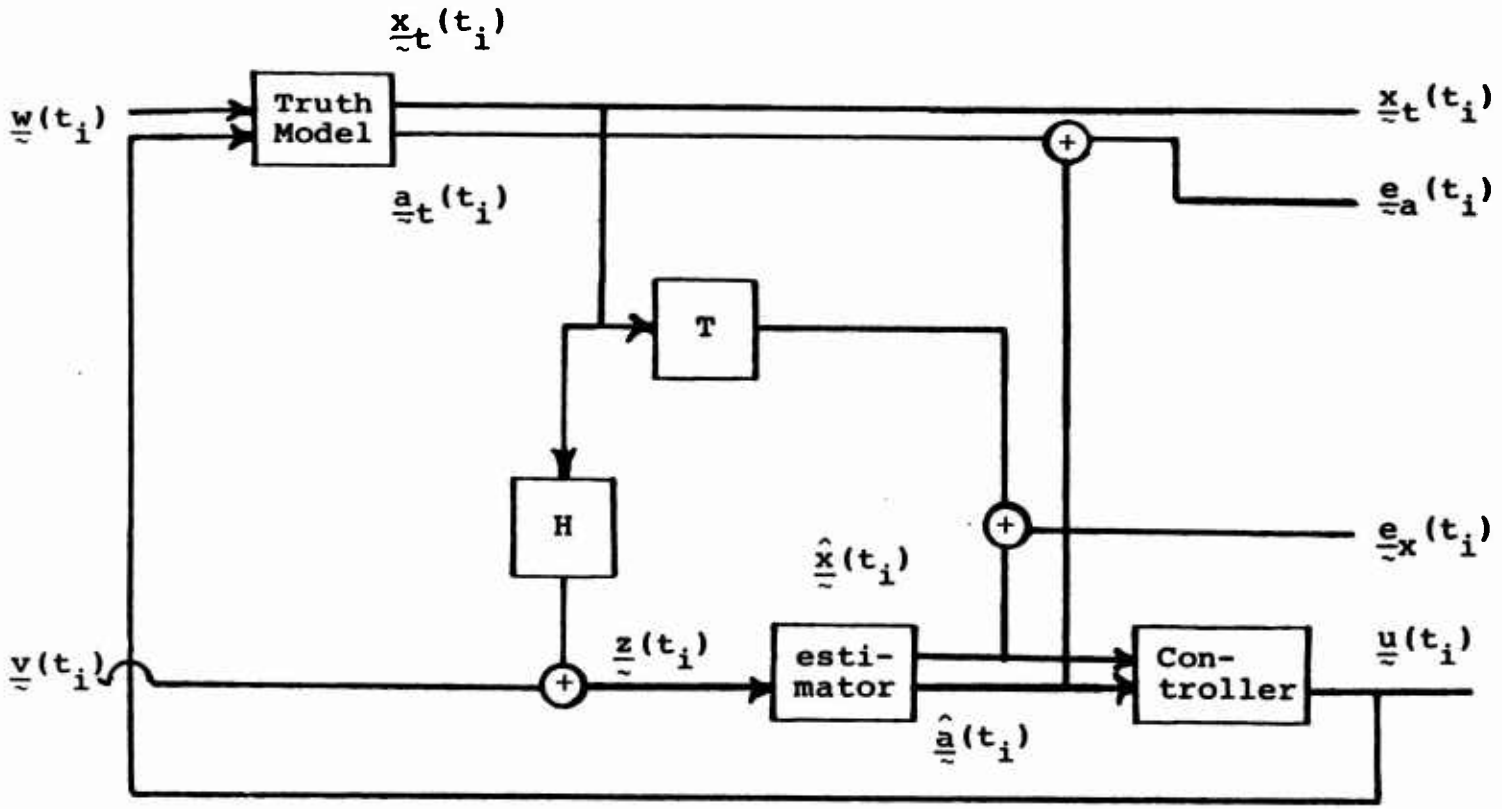

Fig. IV-1. System Estimator, and Controller Simulation

The sample covariance of $\underset{\sim}{e}_x(t_i)$ is computed as (3:54; 6:47; 19:130):

$$E\{[\underset{\sim}{e}_x(t_i) - E\{\underset{\sim}{e}_x(t_i)\}][\underset{\sim}{e}_x(t_i) - E\{\underset{\sim}{e}_x(t_i)\}]^T\} \simeq P_{ex}(t_i) \triangleq$$

$$[1/(N-1)] \sum_{k=1}^{N} \underset{\sim}{e}_{xk}(t_i)\underset{\sim}{e}_{xk}^T(t_i) - [N/(N-1)]\, \hat{M}_{ex}(t_i)\hat{M}_{ex}^T(t_i) \qquad \text{(IV-5)}$$

When evaluating the estimator alone, the feedback controller in Figure IV-1 is replaced by a dither signal with a frequency and amplitude that is determined by trial and error. It has been shown that a dither signal can be used to excite the system model and enhance parameter identification (6:50,58-59; 20:135,136; 21:229).

The error in the state estimate and the error in the parameter estimate are useful in evaluating the performance of the estimator. The error in the state estimate gives the best means of comparing the estimator to other types of estimators while the error in the parameter estimate lends insight into the accuracy of a parameter estimate that may be fed to an adaptive controller and provides a means of evaluating various move, contract, and expand algorithms (3:54).

When evaluating the estimator/controller combination it is more appropriate to examine the statistics of the true state values. In this thesis effort, the control

objective is to quell any oscillations in the two-bay truss structure and to "point" the two-bay truss in a commanded direction. It is important to examine the magnitude of the control inputs in order to detect unreasonable commanded control levels. Lynch (16) in his research with a fixed two-bay truss (see (Section III.4.2) limited the magnitude of the force of an individual actuator to 100 lbs. Although this limit is not implemented in this thesis, it is used as a general guideline as to a reasonable range of actuator activity.

IV.3. Software Description (3:55-59)

IV.3.1. Introduction. The analysis of the moving-bank estimator/controller required the development of four computer programs. Each of these programs is a modification of programs developed by Hentz and Filios (3; 6). For a more detailed description of the following programs, the reader is referred to Filios (3). The first program is a preprocessor which creates a parameter space that is utilized in the Monte Carlo simulation and ambiguity functions analysis (see Section II.5). The second program simulates the moving-bank multiple model adaptive estimator and performs Monte Carol simulation runs and generates data for each run. This program is also modified to produce Monte Carlo runs of individual elemental filters. The third program is a postprocessor that computes the

means and variances of variables of interest and then generates the plots of statistics for the Monte Carlo simulation. The fourth program computes the ambiguity functions and generates their plots.

IV.3.2. Preprocessor. The preprocessor computes the discretized, reduced order, system matrices (Φ, B_d, G_d, H, D_r in Equations (II-1) and (III-19)) for each parameter point within the parameter space, Kalman filter and LQ controller gains, and information needed for the ambiguity functions analysis (see Section II.5). An input file allows the state and control weighting matrices, dynamic driving noise, measurement noise, as well as the time increment for the discrete system to be varied. This input file also contains the mass and stiffness matrices and two vectors which specify the mass and stiffness variation. The mass and stiffness matrices are used to determine a 24-state system (see Equation III-4) which is then reduced to the number of states specified (see Section III.5).

IV.3.3. Primary Processor. The primary processor performs the Monte Carlo simulations. The program consists of an executive subroutine which calls several subroutines. For each sample period, the true system and the filters currently implemented in the moving bank are propagated forward from the most recent sample time. A

noise-corrupted measurement is then made of the true system and the filters of the moving bank are updated. The program then calculates the necessary control inputs and makes decisions on whether to move, expand, or contract the bank. After each sample period is complete, the values of the variables of interest are written to a data file.

The inputs to the primary processor describe the parameter space (obtained from the preprocessor) and true system parameters, and specify the move/contract/expand algorithms to be implemented, the associated thresholds, initial probability weightings for the filters in the moving bank, and initial filter states. The output of the primary processor is a data file for each variable of interest (state estimate, actual state values, control inputs) covering all of the simulation runs, and a more detailed print file covering just the first Monte Carlo run. The print file lists the exact filters implemented in the moving bank and the variables which affect the decision algorithms.

IV.3.4. Postprocessor. The postprocessor takes the variable data files obtained from the primary processor and calculates the sample means and variances from t_o to t_f. Plots are then generated of the time histories of the means of each variable $\pm$ 1σ, where σ is the standard deviation. The postprocessor is run for each data file generated by the primary processor.

IV.3.5. Ambiguity Functions Analysis. The ambiguity functions analysis involves two programs. The first evaluates the ambiguity function for each point in the parameter space (see Chapter II for a full discussion of ambiguity functions) and writes this information (a 10x10 matrix) to a file. A dither signal is used to enhance the difference between filter models. The input file to this program specifies the truth model, number of Monte Carlo runs, as well as the time length of the simulation. The system matrices are obtained from the same file generated by the preprocessor for the primary processor. The second program reads the information from a file and then generates a three-dimensional plot of the ambiguity function values versus location in the parameter space (see Figure V-1).

IV.4. Simulation Plan

IV.4.1. Introduction. The simulation plan involves three phases. First, the ambiguity functions analysis is performed to establish the suitability of the model for adaptive estimation and to lend insight into the appropriate degree of parameter variation of the two-bay truss. The second phase evaluates the performance of only the adaptive estimator. The purpose is to determine which decision logic provides the "best" estimation performance. The final phase incorporates several possible controller

structures in order to evaluate the different adaptive estimation/control algorithms.

The "truth model" for all simulations is of the same dimension as the internal filter model (see Section III.5.3). The system is driven by zero-mean white noise and a dither signal that is determined by trial and error. The strength of this white noise as well as the measurement noise is determined by trial and error with the criteria that the noise add a reasonable amount of uncertainty to the system during a sample period (see Appendix B for more discussion of the selection of noise strengths).

IV.4.2. Ambiguity Functions Analysis. The ambiguity functions analysis is generated for non-adaptive estimators based on a representative sample of parameter sets, to determine what parameters can and should be estimated. Relatively low sensitivity of filter performance to a parameter change makes identification of the parameter difficult and removes need for adaptivity, since all filters within the parameter range can accurately estimate the states (3:70).

Once the model is determined to be appropriate for adaptive estimation, the ambiguity function analysis also lends valuable insight into the proper level of discretization of the parameter space (3:91). Highly sensitive ambiguity functions establish the need for a tightly

discretized parameter range, whereas ambiguity functions that are less highly peaked in certain parameter directions show that fewer parameter points are needed to span that particular parameter range.

IV.4.3. Parameter and State Estimation Study. The estimator is first evaluated using only movement of a bank at the finest level of discretization (see Figure II-2). The decision logics for moving (see Chapter II) are individually implemented in a series of simulation runs and then compared. For these simulations the parameters are forced to (see Section I.4.2):

a. be constant and equal to a discretized point in the parameter space; or

b. be constant but between and not equal to a discretized point in the parameter space; or

c. vary, either continuously or by undergoing a jump value.

The evaluation of these decision logics is based upon the accuracy of the state estimate and the speed with which the decision logic acquires the true point in the parameter space. Although parameter estimation is the primary impetus for implementation of a moving-bank MMAE, state estimation and ultimately controller performance, are the standards by which the moving-bank are judged.

The bank expansion and contraction algorithms are evaluated by using a jump change in the uncertain parameters being estimated. The change places the uncertain parameters outside the current range of the moving bank. The purpose of the expansion algorithm is to allow the bank to respond more quickly to a jump change in the uncertain parameter than would be possible by using the bank movement alone (3:62). Therefore, the expansion algorithms are evaluated by comparing the results to a simulation using a jump change in parameters but not allowing bank expansion.

IV.4.4. Controller Study and Design. The State and Parameter Estimation Study is used to determine the "best" bank motion decision logic method. This method is used as the basis for a controller using the moving bank multiple model adaptive estimator. A Monte Carlo analysis is performed on this controller, a multiple model adaptive controller, and controller designed on a nominal value of the parameter vector but using the moving bank model as a state estimator (see Section III.4). Two benchmark controllers are also investigated through Monte Carlo analysis: a single controller with artificial knowledge of the true parameter set and a robust, single fixed-gain controller (see Section II.4).

IV.5. Summary

The simulations for the moving bank estimator/controller evaluation have been described in this chapter. The Monte Carlo simulation for performance assessment, the associated software, and the simulation plan have been discussed. The results of these simulations are discussed in the following chapter.

V. Results

V.1. Introduction

The results of the ambiguity functions analysis and the Monte Carlo simulations are presented. The goal of the ambiguity functions analysis is to determine the suitability of the two-bay truss for application of the moving-bank multiple model adaptive estimator. This analysis produces no conclusive results, but similar information is in fact obtained from Monte Carlo analysis of individual filters within the parameter space. The Monte Carlo analysis indicates a significant change in estimator performance over the range of the parameter variation, and thus provides insight into the usefulness of adaptation for this application. The purpose of the Monte Carlo analysis of the moving-bank MMAE is to evaluate the move, expand, and contract algorithms developed in Chapter III and to investigate the effectiveness of the moving-bank MMAE as a controller. Results indicate that the moving bank provides an increase in performance over a single filter not given knowledge of the true parameter vector; however, the increase in performance is due more to the performance of the Bayesian multiple model estimation algorithm rather than that of any moving-bank decision logics. It is found that a fixed bank does an excellent job of estimation and

control and performs nearly as well as a filter given artificial knowledge of the true parameter variation.

Please note that this chapter continually refers to parameter points (i.e., parameter point (5,5)). The first number corresponds to variation in the non-structural mass of the rotating two-bay truss while the second number corresponds to variation in the stiffness matrix. See Section III.4.5 for a complete discussion.

V.2. Ambiguity Functions Analysis

The ambiguity functions analysis experiences no apparent numerical problems but does not produce clear results. The analysis is done using both covariance and Monte Carlo analyses to obtain the necessary error covariance matrices (see Chapter II). When Monte Carlo analysis is used, the results indicate a need for adaptive estimation since the ambiguity function values experience relatively large variations (see Figure V-1). This indicates a need for adaptive estimation; however, it was found through repeated ambiguity function evaluation for individual choices of parameter values in the "truth" and "filter" models, that the computation of the ambiguity functions did not converge despite a very large number of Monte Carlo runs. Table V-1 contains the ambiguity function evaluation for five ambiguity function runs for the case of the implemented filter being identical to the truth model. The number of Monte Carlo runs is set at 10

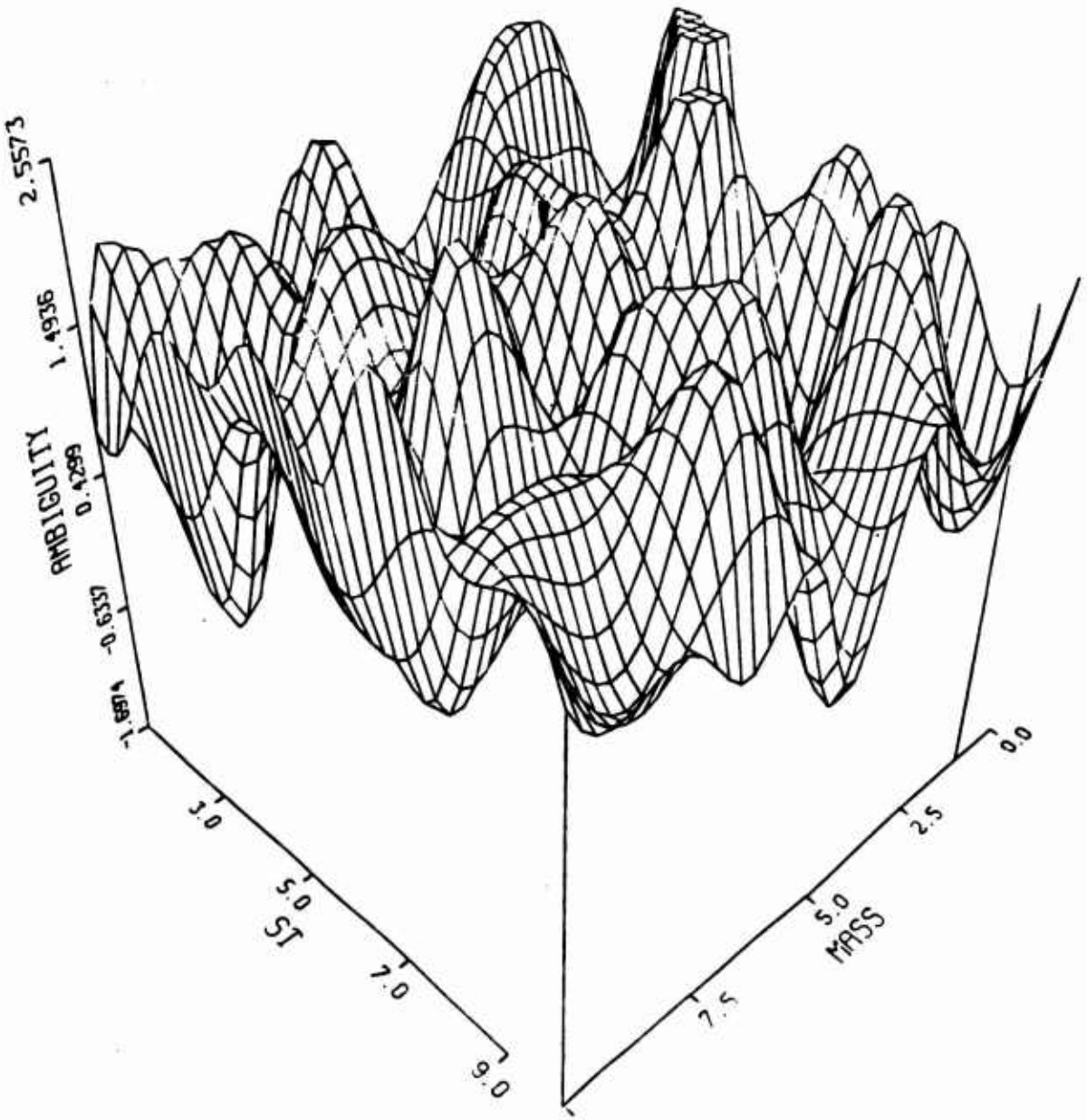

Fig. V-1. Ambiguity Function Plot; Parameter at Mass = 1, Stiffness = 5

TABLE V-1

DIFFERENT AMBIGUITY FUNCTION EVALUATIONS
FOR THE SAME CONDITIONS

0.55126
2.23278
1.68001
1.85798
1.51977

and each of the Monte Carlo runs ran for 10 seconds at a time interval of 0.05 seconds. Figure V-1 plots the ambiguity functions for the true parameter point (indicated by arrow in Figure V-1) being located at (5,5) in the parameter space. The magnitude of the variation of the ambiguity functions in Table V-1 as compared to the magnitude scale in Figure V-1 indicates inconclusive computation of the ambiguity functions. Better results could not be obtained by increasing the number of Monte Carlo runs.

More repeatable results are obtained using covariance analysis, but is is suspected that numerical difficulties do occur. Despite a very large number of propagation cycles, the error variances did not converge and in fact diverged. Through Monte Carlo analysis of the individual filters, it is shown that the filters are stable (see Section V.3). Results can be obtained by arbitrarily limiting the number of sample periods to 50. The ambiguity functions are plotted for several points in the parameter

space and indicated erroneously that all filters in the space would do equally well in obtaining state estimates.

One possible reason for the inconclusive ambiguity function analysis is the set of approximations made in the development of the ambiguity functions (see Section II.5). In Equation (II-25), N was set equal to one. This greatly reduced the number and complexity of computer operations. The result is a reduction in the fluctuation in the ambiguity function, but this may have produced a numerically inaccurate algorithm when implemented on a finite word-length computer.

V.3. Monte Carlo Analysis of Individual Filters

Monte Carlo analysis of individual filters provides the information that is desired from ambiguity functions. It shows a significant performance difference between filters based upon different points in the parameter space. Simulations are conducted for various filters in the parameter space, against a truth model based on some arbitrary point in the parameter space. A dither signal with a magnitude of 5 and frequency of 30 rad/sec is used to excite the system. The magnitude and frequency are determined by trial and error with the criteria that the dither signal cause significant differences in the state estimation performance between elemental filters. Appendix C contains state error statistics plots for the case of the

truth model being based on the parameter point 5,5 (nominal values of non-structural mass and stiffness matrix). Simulation runs are made for filters corresponding to each adjacent point in the parameter space at the finest level of discretization (see Figure II-2b). These plots show a significant degradation in estimation performance when the filter model differed from the truth model. The plots also indicate that the mass variation cause more degradation in performance than did the variation in the stiffness matrices.

The plots also show that different combinations of mass and stiffness variation have varying effects on estimation performance. Figure C-6 is for a filter based on the point (6,6) in the parameter space, which is a 10 percent increase in the non-structural mass and a 4 percent increase in the stiffness matrix (see Section III.4.5). An increase in the non-structural mass lowers the modal frequencies of the filter model, while an increase in the stiffness matrix pushes the filter frequencies higher. One would expect a cancelling effect and estimation performance that is better than parameter points (5,6) and (6,5), yet worse than for the truth model (parameter point (5,5)). Figures C-1, C-2, C-5, and C-6 support this result.

The parameter points (6,4) (increase in non-structural mass and decrease in stiffness matrix) and (4,6) (decrease in non-structural mass and increase in

stiffness matrix) demonstrate the additive effect of the parameter variation. The former decreases the structural frequencies while the latter causes higher structural frequencies. In both cases, one would expect an additive degradation in performance. For example, filter (6,4) should perform worse than filters (6,5) and (5,4). Figures C-4, C-5, and C-9 support this result.

V.4. Moving-Bank MMAE

V.4.1. Introduction. The performance of the moving bank with probability monitoring is discussed with respect to parameter and state estimation. The bank fails to identify a truth model parameter vector although it was able to provide good state estimation. Expansion and contraction of the bank is not considered because of time limitations and the fact that the investigation of moving-bank algorithms did not lead to a logical basis for contracting or expanding the bank.

V.4.2. Parameter Estimation. Investigation of bank movement using probability monitoring is very inconclusive. This is due to the continual movement of the bank because of the varying of Bayesian weightings on the elemental filters. Table V-2 contains the filter weightings and the location (the center filter of the moving-bank) for the first second of a performance evaluation of a moving-bank initialized at its finest discretization

TABLE V-2

FILTER PROBABILITY WEIGHTINGS

Time	Parameter Point	P1	P2	P3	P4	P5	P6	P7	P8	P9
0.05	5,5	.0093	.0093	.0093	.0093	.9259	.0093	.0093	.0093	.0093
0.10	5,5	.0099	.0099	.0099	.0099	.9033	.0099	.0166	.0156	.0151
0.15	5,5	.0094	.0094	.0094	.0094	.0094	.0094	.9004	.0341	.0094
0.20	6,4	.0096	.0096	.0096	.0570	.0880	.0096	.7852	.0219	.0096
0.25	7,3	.0093	.0093	.9258	.0093	.0093	.0093	.0093	.0093	.0093
0.30	6,4	.0098	.0098	.0098	.0148	.6294	.0098	.2116	.0953	.0098
0.35	6,4	.0480	.1237	.2265	.0096	.5324	.0308	.0096	.0096	.0096
0.40	6,4	.0351	.1806	.5735	.0096	.1519	.0204	.0096	.0096	.0096
0.45	5,5	.0093	.0093	.9257	.0093	.0093	.0093	.0093	.0093	.0093
0.50	4,6	.1408	.2772	.5254	.0094	.0094	.0094	.0094	.0094	.0094
0.55	3,7	.0093	.0093	.9259	.0093	.0093	.0093	.0093	.0093	.0093
0.60	2,8	.0093	.0093	.0093	.0093	.0093	.0093	.9190	.0155	.0093
0.65	3,7	.0093	.0093	.0093	.9236	.0110	.0093	.0093	.0093	.0093
0.70	3,6	.0105	.0775	.6592	.0096	.1997	.0146	.0096	.0096	.0096
0.75	2,7	.0095	.0942	.8394	.0095	.0095	.0095	.0095	.0095	.0095
0.80	2,7	.0093	.0093	.9253	.0093	.0093	.0093	.0093	.0093	.0093
0.85	2,7	.0093	.0093	.9259	.0093	.0093	.0093	.0093	.0093	.0093
0.90	2,7	.0093	.0093	.5616	.0093	.0093	.0093	.3729	.0093	.0093
0.95	2,7	.0093	.0093	.0093	.0093	.0093	.0093	.9253	.0093	.0093
1.00	3,6	.0096	.0096	.0108	.0445	.8870	.0096	.0096	.0096	.0096

(see Figure II-2b) and initially centered at parameter point (5,5). The weightings vary between several filters with no clear-cut tendency towards any one filter. The truth model is based upon the internal model of the filter implemented at parameter point (5,5). The bank is using probability monitoring with a bank move threshold of 0.25. The bank move threshold is arbitrarily selected since examination of the probability weightings (see Table V-2) do not indicate a better choice. Hentz (6:62) showed that performance increases as the probability threshold decreases and that the best estimation performance is achieved with thresholds near zero. With thresholds this low, the bank moves anytime the largest filter does not have the largest probability weightings. The magnitude of the dither signal is 100 with a frequency of 30 rad/s. The reasoning for the increase in the magnitude of the dither signal over that of the Monte Carlo analysis of individual filters is presented in Sections V.4 and V.5.

An attempt is made to determine trends in the movement in the bank. This is accomplished by keeping a record of the parameter point about which the moving-bank is centered. The elements of a 10x10 matrix are initialized to zero and then one is added at each sample time to the matrix element corresponding to the current location of the moving bank. Entries are recorded from t = 1.0 to 5.0. Recording is not started at t = 0.0 in an attempt to avoid

transient effects. Figures V-2 and V-3 show the results where the true parameter points are (1,10) and (10,1), respectively. In each of the figures, one point in the 10x10 matrix corresponds to a 3x3 grid on the depicted surface. The arrow points to the parameter location of the truth model. The dither signal applied has a magnitude of 100 and frequency of 30 rad/s. The only information the figures yield is qualitative in nature. Different truth models do affect the movement of the bank. In Figure V-2, it can be seen that the bank tends to center itself in the general area of the true parameter point. In Figure V-3, the true parameter point is changed and this certainty seems to "pull" the bank in the general direction of the new point, though not to the extent of causing the bank to center on the actual point (10,1).

The continual changing of filter weightings may be due to "relatively" similar performance between filters. The weighting of each filter is dependent upon the accuracy of the filter prediction of the current measurement, as shown in Equation (II-6). In the absence of noise, the truth model would predict the next measurement perfectly. With noise dynamically affecting the system, the correct filter will have an incorrect estimate. If the magnitude of the noise is great enough, a filter based upon an incorrect but similar model could produce an estimate that is as good or possibly even better. How often an

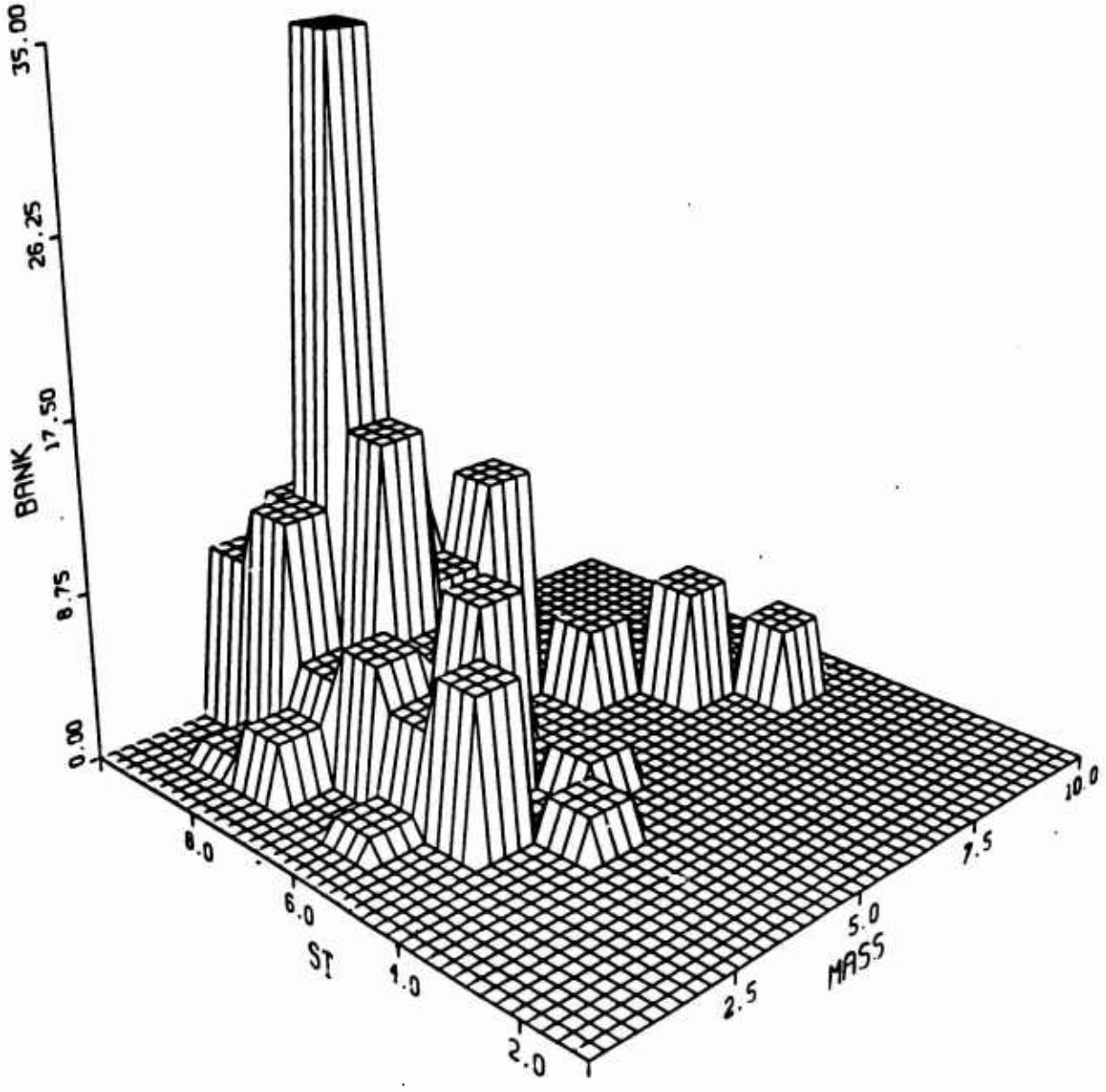

Fig. V-2. Bank Location Time History; True Parameter at Mass = 1, Stiffness = 10

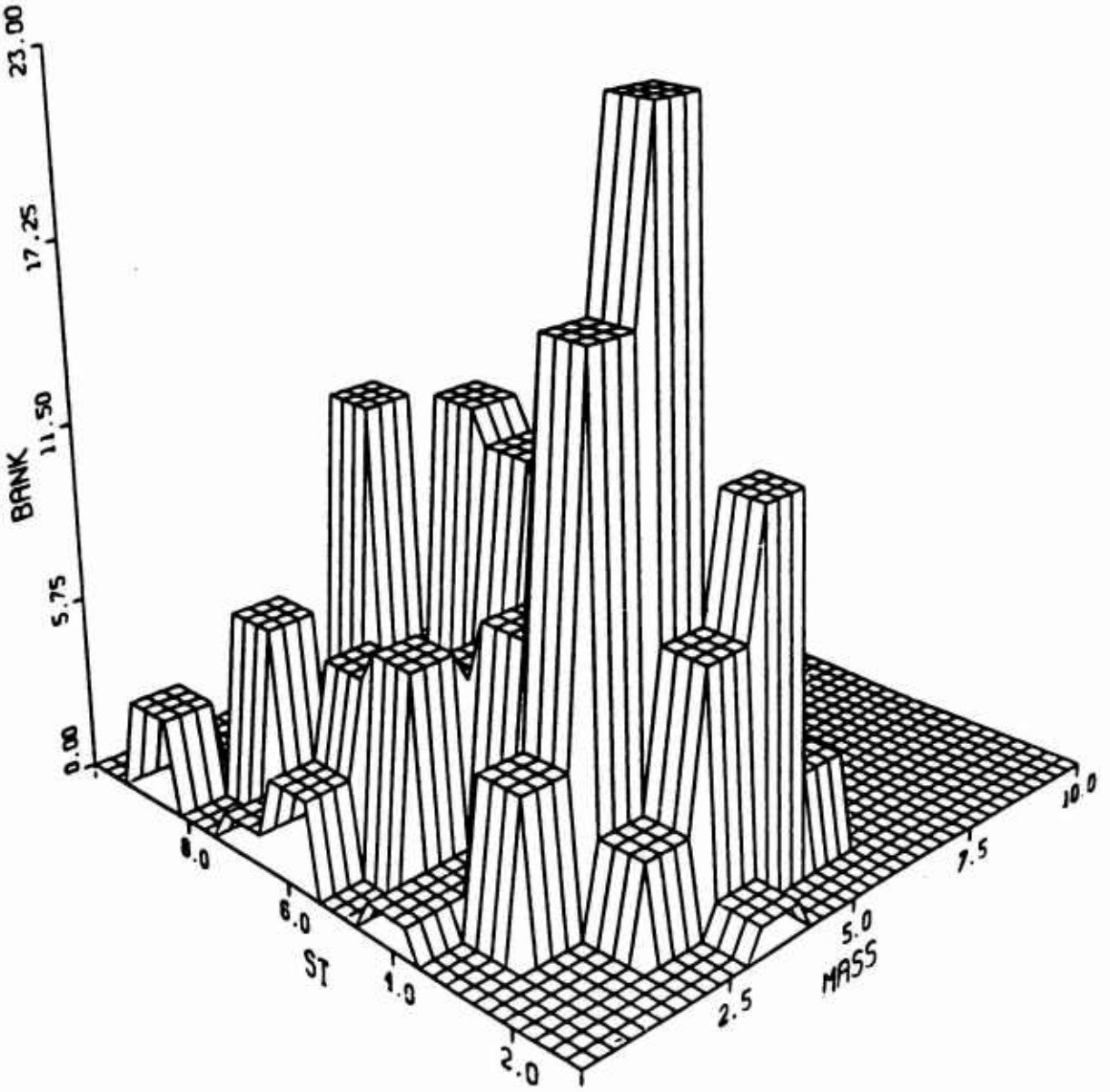

Fig. V-3. Bank Location Time History; True Parameter at Mass = 10, Stiffness = 1

"incorrect" filter suggests an equally or more accurate estimate is dependent upon the magnitude of the dynamics driving noise and measurement noise as compared to the differences between correct and incorrect filters, and upon the statistics of the dynamics driving noise and the measurement noise.

V.4.3. State Estimation. Simulations are run for the case of a truth model being equivalent to the model implemented in one of the elemental filters in the parameter space. First, the case is investigated for feedback control being a dither signal with magnitude of 5 and frequency of 30 rad/sec. This dither signal is used because results of the Monte Carlo analysis of individual filters (see Section V.3) clearly indicate that the rotating two-bay truss requires adaptive estimation when subject to a dither signal of this magnitude and frequency. Results indicate that, although the individual filters vary significantly in performance when matched against a truth model based upon a different point in the parameter space for the conditions, that the Bayesian estimation algorithm produces a very robust state estimation algorithm. This supports the use of a bank, but not necessarily a moving bank. Appendix D contains two sample state estimation plots which illustrate sample state estimation performance using probability monitoring. The benchmark of performance, a single

filter given artificial knowledge of the true parameter is contained in Appendix C (Figure C-1).

V.5. Fixed-Bank MMAE

During the course of the moving-bank simulations, the bank was often "fixed" in order to investigate the trends that occurred in the weightings and to assist in evaluating the moving-bank MMAE. It is found that, even if the bank does not move, a subset of the filters within the bank provided increased performance and robustness over a single filter. At a dither signal with a magnitude of 5 and frequency of 30 rad/sec, the fixed-bank algorithm did a good job estimating at all points in the parameter space as compared to a single filter given artificial knowledge of the true parameter vector. It was previously shown that significant performance degradation occurred for the case of individual filters at a dither signal with a magnitude of 5 and frequency of 30 rad/sec.

The magnitude of the dither signal is increased to 100. The performance of the estimator is still nearly identical to the case of a single filter given artificial knowledge of the parameter. In these initial investigations, the bank is set at its closest discretization and centered at the parameter point (5,5). Figure E-1 is the simulation for a Monte Carlo run against a truth model based on the parameter point (5,5). Figures E-2 through E-5 (in Appendix E) are the simulation plots for Monte Carlo runs

against several truth models which are based on parameter values outside the discretization of the bank. The plots indicate good state estimation performance at all points. A small decrease in performance is indicated at parameter point (3,7). This point corresponds to an additive degradation in filter performance from both parameter variations (see Section V.3); therefore, one would expect to see the most performance degradation from this point.

The fixed-bank MMAE is also investigated at various discretizations. The state estimation performance are compared at discretization levels of 1 (finest discretization), 2 and 4 (coarsest discretization) and at a dither signal of 100 using the parameter point (3,7) as a truth model. Results indicate that the bank at a discretization level of 2 and 4 outperformed the bank at a discretization level of 1; see Figures E-4, E-6, and E-7. This is particularly evident in the error plot corresponding to the velocity of the second bending mode (EX(6)). This indicates that the bank does a better job of encompassing the true parameter value as the discretization becomes coarser.

V.6. Moving-Bank and Fixed-Bank Comparison

The moving-bank and fixed-bank estimator are compared against identical truth models. First, the magnitude of the dither signal is set equal to 100 at a frequency of 30 rad/sec. The truth model is selected at parameter point

(3,7) in order to make use of previous figures. Simulations were conducted for the moving-bank and the fixed-bank at various discretizations. The moving-bank is implemented using probability monitoring with a move threshold = 0.25. The bank move threshold is arbitrarily selected since examination of the probability weightings (see Table V-2) do not indicate a better choice. Figures F-1, E-4, E-6, and E-7 illustrate the results. The plot corresponding to the velocity of the second bending mode (EX(6)) most clearly illustrates differences in performance. Performance is similar for all cases except for the case of a fixed bank with discretization of 1, which indicated a small degradation in performance. In addition, the moving-bank estimator result (Figure F-1) has a "spike" in the estimate of the rigid body position state at approximately t = 4 seconds which probably corresponds to a move in the wrong direction.

Additional Monte Carlo runs are conducted against a truth model based on the parameter point (1,10) and with a dither signal magnitude of 500 and frequency of 30 rad/sec (see Figures G-2, G-3, G-4, and G-5). The parameter point (1,10) and the large dither signal are chosen because it is desired to enhance the identifiability of the system. A significant degradation in performance occurs at all discretizations; however, it shows a clear performance increase in estimation performance with coarser parameter

discretization. The moving bank performance is similar to the simulation with discretization level of 4 (Figures F-2 and F-5, respectively). The moving-bank shows slightly better performance in estimating the velocity of the second bending mode (EX6)) while the discretized fix-bank does a better job of estimating the angular velocity (EX(4)). The reason for this pattern of performance is not obvious.

V.7. Controller Performance

Controller performance (see Section II.4 and Appendix A) is investigated for the case of only the fixed bank, although few results are obtained because of time constaints. A controller using the moving bank is not investigated also because of time constraints. The system is excited with a dither signal of magnitude 500 and frequency of 30 rad/sec for 1 second. This is done to produce a large oscillation in the structure on which the effects of active control would be obvious. Figure H-1 shows the result of the dither signal with no control applied. For subsequent plots, at time = 1 second, a steady-state feedback controller is used to quell the structural oscillations induced by the dither signal and to force the angular position (state 1), to zero. Nominal control gains (see Section II.4 and Appendix A) corresponding to parameter point (5,5) were used. Figure H-2 shows the states and control for the case of truth model being at parameter

point (5,5). The control clearly damps out structural oscillations and also "points" the rotating two-bay truss by bringing the rigid body position state (X(1)) to near zero. The scale of the plots corresponding to the rigid body state is in radians. Obviously, the control of this state needs to be improved. For all control simulations, the control of the rigid body states (X(1) and X(4) are nearly identical. This is expected since the modeling of the rigid body states is not changed by the parameter variation investigated in this thesis (see Appendix B, A matrix).

Figures H-2 and H-3 are for truth models at parameter points (3,7) and (7,3) respectively. States 3 and 6 (corresponding to the highest frequency bending mode position and velocity) are clearly controlled better when the truth model is at parameter point (7,3). Hentz found that when the true natural frequency (of a simple two state system) is greater than the natural frequency upon which the controller is designed, the moving-bank estimator/ fixed-gain controller drove the system unstable (6:105). As compared to parameter point (5,5), the parameter point (7,3) corresponds to an increase in the non-structural mass and decrease in the stiffness matrix (both decrease the natural frequencies) while the parameter point (3,7) corresponds to a decrease in non-structural mass and increase in the stiffness matrix (both increase the natural

frequencies); therefore, it is expected that a steady-state controller designed upon the parameter point (5,5) would do a better job of controlling a truth model based on parameter point (7,3).

Slightly better transient results are obtained for the rigid body motion state (X(1)) when the truth model is at parameter point (7,3) although the control of the rigid body states is nearly identical for all controller simulations (Figures H-2, H-3, H-4). This is expected since the modeling of the rigid body states is identical for all points in the parameter space (see Appendix B, A matrix).

V.8. Summary

The results of the moving-bank Multiple Model Adaptive Estimator as applied to the two-bay truss model of a space structure have been presented. The analysis of moving-bank logics is very inconclusive; however, the use of probability monitoring improves performance over the case of fixed bank of filters corresponding to the finest discretization level in the parameter space. The Multiple Model Adaptive Estimation algorithms provide a substantial increase in performance over the case of a single non-adaptive Kalman filter. As such, the use of a subset of filters of the full bank as well as a full bank is supported, particularly with coarse discretization to allow the true parameter value to be encompassed within the bank

while not requiring an excessive number of elemental filters within the algorithm. Limited investigation into feedback control of the structure shows the ability to quell structural oscillations, but very poor performance in "pointing" the structure.

VI. Conclusions and Recommendations

VI.1. Introduction

The investigation of the moving-bank Multiple Model Adaptive Estimator took an unexpected course in that its results do little to support or argue for a particular decision logic for controlling bank motion. Instead, the results mainly focus on the issue of whether a fixed bank is more appropriate than a moving bank. The results do provide support for implementation of the Multiple Model Adaptive Estimator in either form. The thesis does provide valuable insight into the issue of parameter discretization and generates a model of a space structure on which more research into Multiple Model Adaptive Estimation can be based.

VI.2. Conclusions

The rotating two-bay truss model of a space structure clearly requires adaptive estimation when subjected to the parameter variation investigated in this thesis. Although no conclusions could be drawn from the ambiguity functions analysis, the Monte Carlo analyses of individual filters versus various truth models with dither signal clearly showed that adaptive estimation is appropriate.

The results indicate that a fixed bank with the truth model parameter value within the area of the bank

performs as well as a moving bank in Monte Carlo simulations where the truth model is of the same order as the elemental filter model. When the truth model parameter vector is set at parameter point (1,10) and subjected to a dither signal of magnitude 500 at frequency of 30 rad/sec, a moving bank showed better performance than a fixed bank with discretization levels of 1 and 2, and centered at parameter point (5,5). This indicates that the moving bank may sometimes be appropriate; however, similar performance can be achieved by assuring that the truth model parameter vector lies within the discretization of the bank. Regardless, the use of Multiple Model Adaptive Estimation is strongly supported because of the robustness of the algorithm and because the state estimation performance for a dither signal of magnitudes 5 and 100, is near that of a filter given artificial knowledge of the true parameters.

Although the moving-bank algorithm is sometimes able to estimate the states accurately, it is never able to identify the truth model parameter vector. Hentz (6) was probably able to obtain satisfactory identification; the identification problem is simpler for the two-state system he investigated and because the magnitude of the parameter variation was very large compared to that investigated in this thesis.

VI.3 Recommendations

It is recommended that research continue using the rotating two-bay truss model of a flexible space structure. Parameter variations are available which make adaptive estimation appropriate.

The "truth model" used in all simulations is of the same order as the internal model of the elemental filters. Future research should implement higher order truth models as benchmark performance standards and carefully investigate the effects of purposeful order reduction on estimator/controller performance and robustness.

If continued research is to be accomplished with the rotating two-bay truss model, more realistic dynamics driving noise and measurement strengths must be investigated. As is discussed in Appendix B, the dynamics noise and measurement noise matrices are determined by trial and error with the main goal being that of obtaining a model which needs adaptive estimation. Because of time constraints, examination of the effect of these Q and R matrices ceased once results of the Monte Carlo analysis indicated this goal was accomplished. In addition, the control of the structure should be examined in more detail. All of this should be done using a single filter versus a higher order truth model, before implementing any form of a Multiple Model Adaptive Estimator.

Investigation is needed of the effect of various discretizations of the parameter space. Especially needed is an investigation into the relationship between the dynamics and measurement noise strengths and various discretizations. As is discussed previously, in a Multiple Model Adaptive Estimator, care must be taken not to add too much noise to the system model because this masks the difference between correct and incorrect filters. In addition, the magnitude of the "real world" noise must have similar consideration. Too tight a discretization wastes computational resources with little gain in performance, while a sparse parameter discretization may sacrifice performance for unnecessary robustness.

The rotating two-bay truss model used in this thesis effort used measurements obtained from position and velocity sensors as well as gyros on the hub. A more realistic implementation might be the use of only gyros and accelerometers for sensors; therefore, the mathematical model should implement angular rate and acceleration measurements as well as position measurements.

It may be possible to use fixed-bank Multiple Model Adaptive Estimation Algorithm in conjunction with a single "moving" filter. The bank would be coarsely discretized to assure that the true parameter vector lies within the bank and provide adequate estimation/controller performance while the single filter moved around the parameter space.

The bank would provide a parameter estimate to a single filter which could be used thereafter. In case of a system failure or large parameter variation, a new reacquisition could be accomplished.

VI.4. Summary

This thesis applies the fixed-bank and moving-bank multiple model adaptive estimator to a flexible space-structure. Although the use of a moving bank may provide increased state estimation performance, similar performance can be obtained from a fixed bank estimator with a discretization that covers the range of parameter variation.

Appendix A: LQG Controller Development

Assume that we are given the following stochastic system (3:20-22; 6:33-35):

$$\underset{\sim}{\dot{x}}(t) = F\underset{\sim}{x}(t) + B\underset{\sim}{u} + G\underset{\sim}{w}(t) \tag{A-1}$$

where

$$E\{\underset{\sim}{w}(t)\} = \underline{0} \quad \text{and} \quad E\{\underset{\sim}{w}(t)\underset{\sim}{w}^T(t+\tau)\} = Q\delta(\tau)$$

and the quadratic cost function to be minimized is:

$$J = E\{\int_0^\infty (1/2)[\underset{\sim}{x}^T(t)W_x\underset{\sim}{x}(t) + \underset{\sim}{u}^T(t)W_u\underset{\sim}{u}(t)]dt\} \tag{A-2}$$

where W_x and W_u are weighting matrices to be chosen (iteratively) to yield a controller with desirable performance characteristics. The optimal discrete linear feedback control law, assuming full-state access, is given by:

$$\underline{u}(t_i) = -G_c^* \underline{x}(t_i) \tag{A-3}$$

where the constant gains, G_c^*, that minimize J, are given by (21:68,122):

$$G_c^* = [U + B_d^T K_c B_d]^{-1}[B_d^T K_c \Phi + S^T] \tag{A-4}$$

where K_c satisfies the algebraic Riccati equation

$$K_c = X + \Phi^T K_c \Phi - [B_d^T K_c \Phi + S^T]^T G_c^* \tag{A-5}$$

and

$$X = \int_{t_i}^{t_{i+1}} \Phi^T(\tau,t_i)W_x\Phi(\tau,t_i)d\tau$$

$$U = \int_{t_i}^{t_{i+1}} [\bar{B}^T(\tau,t_i)W_x\bar{B}(\tau,t_i) + W_u]d\tau$$

$$S = \int_{t_i}^{t_{i+1}} \Phi^T(\tau,t_i)W_x\bar{B}(\tau,t_i)d\tau$$

$$\bar{B}(t,t_i) \triangleq \int_{t_i}^{t} \Phi(t,\tau)Bd\tau$$

$$B_d = \bar{B}(t_{i+1},t_i)$$

$\Phi(t_2,t_1)$ is the state transition matrix from t_1 to t_2 and:

$$\Phi = \Phi(t_{i+1},t_i)$$

It should be noted that Equation (A-3) is also the solution for the deterministic LQ optimal control problem with no driving noise $\underset{\sim}{w}(t)$. If full state access is replaced by noise-corrupted measurements, $\underset{\sim}{x}(t_i)$ in Equation (A-3) is replaced by the state estimate $\hat{\underset{\sim}{x}}(t_i^+)$, which is generated by a Kalman filter. This type of controller is often described as having the "certainty equivalence" property (19:17).

Appendix B: Rotating Two-Bay Truss System Matrices

This appendix lists and discusses example system matrices for the rotating two-bay truss. The reduced order matrices are developed from the mass and stiffness matrices (see Sections III.2 and III.4.3). The system is in modal formulation (see Section III.3.) and is composed of 6 states with 6 measurements and 3 control inputs.

Appendix B

System Matrices

Stiffness Matrix

ROW 1	1.188E+3	1.966E+2	.000E+0	.000E+0
	-6.424E+2	.000E+0	-5.461E+2	-1.966E+2
	.000E+0	.000E+0	.000E+0	.000E+0
ROW 2	1.966E+2	6.263E+2	.000E+0	-5.556E+2
	.000E+0	.000E+0	-1.966E+2	-7.077E+1
	.000E+0	.000E+0	.000E+0	.000E+0
ROW 3	.000E+0	.000E+0	1.188E+3	-1.966E+2
	-5.461E+2	1.966E+2	-6.424E+2	.000E+0
	.000E+0	.000E+0	.000E+0	.000E+0
ROW 4	.000E+0	-5.556E+2	-1.966E+2	6.263E+2
	1.966E+2	-7.077E+1	.000E+0	.000E+0
	.000E+0	.000E+0	.000E+0	.000E+0
ROW 5	-6.424E+2	.000E+0	-5.461E+2	1.966E+2
	4.019E+3	6.693E+1	.000E+0	.000E+0
	-2.099E+3	.000E+0	-7.320E+2	-2.635E+2
ROW 6	.000E+0	.000E+0	1.966E+2	-7.077E+1
	6.693E+1	7.212E+2	.000E+0	-5.556E+2
	.000E+0	.000E+0	-2.635E+2	-9.487E+1
ROW 7	-5.461E+2	-1.966E+2	-6.424E+2	.000E+0
	.000E+0	.000E+0	4.019E+3	-6.693E+1
	-7.320E+2	2.635E+2	-2.099E+3	.000E+0
ROW 8	-1.966E+2	-7.077E+1	.000E+0	.000E+0
	.000E+0	-5.556E+2	-6.693E+1	7.212E+2
	2.635E+2	-9.487E+1	.000E+0	.000E+0
ROW 9	.000E+0	.000E+0	.000E+0	.000E+0
	-2.099E+3	.000E+0	-7.320E+2	2.635E+2
	8.618E+4	4.788E+4	.000E+0	.000E+0
ROW 10	.000E+0	.000E+0	.000E+0	.000E+0
	.000E+0	.000E+0	2.635E+2	-9.487E+1
	4.788E+4	1.390E+5	.000E+0	-1.111E+5
ROW 11	.000E+0	.000E+0	.000E+0	.000E+0
	-7.320E+2	-2.635E+2	-2.099E+3	.000E+0
	.000E+0	.000E+0	8.618E+4	-4.788E+4
ROW 12	.000E+0	.000E+0	.000E+0	.000E+0
	-2.635E+2	-9.487E+1	.000E+0	.000E+0
	.000E+0	-1.111E+5	-4.788E+4	1.390E+5

Mass Matrix

Note that the first 8 diagonal elements are essentially the values of the non-structural mass because the non-structural mass is large compared to the structural mass.

ROW 1	1.294E+0	-2.395E-6	.000E+0	.000E+0
	6.927E-6	.000E+0	6.652E-6	2.395E-6
	.000E+0	.000E+0	.000E+0	.000E+0
ROW 2	-2.395E-6	1.294E+0	.000E+0	7.764E-7
	.000E+0	.000E+0	2.395E-6	8.621E-7
	.000E+0	.000E+0	.000E+0	.000E+0
ROW 3	.000E+0	.000E+0	1.294E+0	2.395E-6
	6.652E-6	-2.395E-6	6.927E-6	.000E+0
	.000E+0	.000E+0	.000E+0	.000E+0
ROW 4	.000E+0	7.764E-7	2.395E-6	1.294E+0
	-2.395E-6	8.621E-7	.000E+0	.000E+0
	.000E+0	.000E+0	.000E+0	.000E+0
ROW 5	6.927E-6	.000E+0	6.652E-6	-2.395E-6
	1.294E+0	-8.152E-7	.000E+0	.000E+0
	2.263E-5	.000E+0	8.916E-6	3.210E-6
ROW 6	.000E+0	.000E+0	-2.395E-6	8.621E-7
	-8.152E-7	1.294E+0	.000E+0	7.764E-7
	.000E+0	.000E+0	3.210E-6	1.156E-6
ROW 7	6.652E-6	2.395E-6	6.927E-6	.000E+0
	.000E+0	.000E+0	1.294E+0	8.152E-7
	8.916E-6	-3.210E-6	2.263E-5	.000E+0
ROW 8	2.395E-6	8.621E-7	.000E+0	.000E+0
	.000E+0	7.764E-7	8.152E-7	1.294E+0
	-3.210E-6	1.156E-6	.000E+0	.000E+0
ROW 9	.000E+0	.000E+0	.000E+0	.000E+0
	2.263E-5	.000E+0	8.916E-6	-3.210E-6
	8.817E-4	-6.402E-5	.000E+0	.000E+0
ROW 10	.000E+0	.000E+0	.000E+0	.000E+0
	.000E+0	.000E+0	-3.210E-6	1.156E-6
	-6.402E-5	8.343E-4	.000E+0	1.553E-4
ROW 11	.000E+0	.000E+0	.000E+0	.000E+0
	8.916E-6	3.210E-6	2.263E-5	.000E+0
	.000E+0	.000E+0	8.817E-4	6.402E-5

ROW 12	.000E+0	.000E+0	.000E+0	.000E+0
	3.210E-6	1.156E-6	.000E+0	.000E+0
	.000E+0	1.553E-4	6.402E-5	8.343E-4

A Matrix

.000E+0	.000E+0	.000E+0	1.000E+0	.000E+0	.000E+0
.000E+0	.000E+0	.000E+0	.000E+0	1.000E+0	.000E+0
.000E+0	.000E+0	.000E+0	.000E+0	.000E+0	1.000E+0
.000E+0	.000E+0	.000E+0	.000E+0	.000E+0	.000E+0
.000E+0	-7.918E+1	.000E+0	.000E+0	-8.898E-2	.000E+0
.000E+0	.000E+0	-5.085E+2	.000E+0	.000E+0	-2.255E-1

Rows 1 and 4 correspond to the rigid body angular position and velocity, respectively. Rows 2 and 3 correspond to the position of the first and second bending modes, respectively, while rows 5 and 6 represent the velocity of these bending modes, respectively.

B Matrix

.000E+0	.000E+0	.000E+0
.000E+0	.000E+0	.000E+0
.000E+0	.000E+0	.000E+0
-4.773E-1	-2.711E-1	1.000E+0
2.589E-1	14.736E-1	.000E+0
9.488E-2	1.590E-1	.000E+0

The first two columns represent inputs from actuators located on the truss while the third column is due to an actuator located on the hub (see Section III.4.4.). The non-zero portion of the first two columns was designed in physical coordinates in the unreduced system as

$$\begin{matrix} 0\ 1\ 0\ 0\ 0\ 0\ 0\ 0\ 0\ 0\ 0\ 0 \\ 0\ 0\ 0\ 0\ 0\ 1\ 0\ 0\ 0\ 0\ 0\ 0 \end{matrix}^{T} \qquad \text{(B-1)}$$

and then transformed into modal coordinates where the angular input actuator was then added by augmenting a column and

entering a 1.00 in the row corresponding to the angular velocity state.

H Matrix

6.066E-1	-3.239E-1	-1.228E-1	.000E+0	.000E+0	.000E+0
3.444E-1	5.925E-1	-2.057E-1	.000E+0	.000E+0	.000E+0
.000E+0	.000E+0	.000E+0	6.066E-1	-3.239E-1	-1.228E-1
.000E+0	.000E+0	.000E+0	3.444E-1	5.925E-1	-2.057E-1
1.000E+0	.000E+0	.000E+0	.000E+0	.000E+0	.000E+0
.000E+0	.000E+0	.000E+0	1.000E+0	.000E+0	.000E+0

The first four rows represent measurements from the position and velocity sensors located on the two bay truss while the last two rows represent measurements of the angular velocity and position of the hub (see Section III.4.4.). The position and velocity portion of the matrix were calculated in physical coordinates and then transformed into modal coordinates (see Section III.3.) where the angular measurements were augmented. Note that the entries in rows 1 and 2 are identical to those in rows 3 and 4 because of co-location of velocity and position sensors. Rows 1 and 2 were designed in physical coordinates in the unreduced system as:

$$\begin{matrix} 0\ 1\ 0\ 0\ 0\ 0\ 0\ 0\ 0\ 0\ 0\ 0 \\ 0\ 0\ 0\ 0\ 0\ 1\ 0\ 0\ 0\ 0\ 0\ 0 \end{matrix} \qquad \text{(B-2)}$$

Only the first twelve columns are listed because the remaining columns are zero.

Controller State Weighting Matrix

The state weighting matrices (see Appendix A) were also determined by trial and error; however, a first cut at the 6 state weighting matrix was obtained using the following weightings[1]:

Angular Position	$0.5Iw_{BW}^2$
Angular Velocity	$0.5I$
Bending Mode Position	$0.5MK_{nat}$
Bending Mode Velocity	$0.5M$

(B-3)

where I is the moment of inertia, BW denotes the bandwidth of the controlled system, K_{nat} is the natural frequency of the mode, and M is the mass of the structure. Note that 0.5M can be factored out of each term, which accounts for the identity elements in the state weighting matrix listed below. A limited amount of trial and error was used in order to improve the controller performance. The goal was to quell oscillations as well as force the rigid body angular po-si-tion to zero, in order to simulate pointing a structure. The following state weighting matrix was implemented:

7.627E+3	.000E+0	.000E+0	.000E+0	.000E+0	.000E+0
.000E+0	7.9178E+1	.000E+0	.000E+0	.000E+0	.000E+0
.000E+0	.000E+0	5.085E+2	.000E+0	.000E+0	.000E+0
.000E+0	.000E+0	.000E+0	1.500E+2	.000E+0	.000E+0
.000E+0	.000E+0	.000E+0	.000E+0	1.000E+0	.000E+0
.000E+0	.000E+0	.000E+0	.000E+0	.000E+0	1.000E+0

---

[1]Maybeck, Peter S., "Improved Controller Performance Through Estimation of Uncertain Parameters," Spacecraft Autopilot Development Memo #17-68, Massachusetts Institute of Technology, Instrumentation Laboratory, Cambridge, Massachusetts (October 17, 1968).

Control Weighting Matrix

The control weighting matrices (see Appendix A) were determined basically by trial and error in conjunction with a method used by Venkayya[2]. Lynch [16] in his research with a fixed two bay truss (see Section III.4.2.) limited the magnitude of the force of an individual actuator to 100 lbs. Although this limit was not implemented in this thesis, it was used as a general guideline as to a reasonable range of actuator activity.

$$\begin{bmatrix} 300 & 0 & 0 \\ 0 & 300 & 0 \\ 0 & 0 & 900 \end{bmatrix}$$

D_r Matrix

The D_r matrix (see Section III.5) is used in a method of order reduction referred to as singular perturbations. This thesis used reduced order models; however, this method was not implemented because truth models were of the same order.

-4.253E-4	6.396E-5	0.000E-0
6.396E-5	-3.583E-4	0.000E-0
0.000E-0	0.000E-0	0.000E-0
0.000E-0	0.000E-0	0.000E-0
0.000E-0	0.000E-0	0.000E-0
0.000E-0	0.000E-0	0.000E-0

[2]Venkayya, V.B., Tischler, V.A., Khot, Narenndra, S., "Dynamics and Control of Space Structures, "26th Structures, Structural Dyanamics, and Materials Conference, Orlando, Florida, April 1985 (AIAA No. -85-0629-CP).

Noise Matrices

A viable estimation system depends upon information from both the measurements and the mathematical model of that system. Making the R matrix too small (which corresponds to very accurate measurements) results in the filter essentially using only the measurement information and discarding the information propagated from the previous sample period, while assuming very inaccurate measurements causes the filter to depend only upon its internal model. The former would make implementation of the moving-bank multiple model adaptive estimator difficult and pointless since differences in the internal filter models would have little effect on estimation accuracy.

The covariance update for a discrete time system is calcualated as [19:275]:

$$P(t_i^+) = P(t_i^-) - K(t_i^-)H(t_i)P(t_i^-) \qquad \text{(B-4)}$$

where,

$$K(t_i) = P(t_i)H^T(t_i i)H(t_i)P(t_i^-)H^T(t_i)$$

$$P(t_i) = (t_i,t_{i-1})P(t_{i-1}^+)\ ^T(t_i,t_{i-1}) + \int_{t_{i-1}}^{t_i} \phi(t_i,\tau)G(\tau)Q(\tau)G^T(\tau)\ \phi^T(t_i,\tau)d\tau$$

The Q and R matrix were selected to satisfy two basic criteria. First, the Q matrix must be large enough to excite the system reasonably, over a single propagation cycle. Secondly, the R matrix must be on the same order of magnitude as the $H(t_i)P(t_i^-)H^T(t_i)$ term so that the filter will use both the measurements and internal model informa-

tion. The Q matrix was selected by purely trial and error starting with an identity atrix. The initial R matrix was selected by arbitrarily determining levels of errors for measurments of the velocity, position, and angular states. These initial attempts produced a system which essentially believed only the internal dynamics model. Another R matrix was implemented by simply calculating $H(t_i)P(t_i^-)H^T(t_i)$. Inspection of the $P(t_i^-)$ and $P(t_i^+)$ matrices indicated that the design goals had been achieved. The values in the Q matrix were reduced slightly in the final design in order to produce a system which weighted internal information more than measurements although within the criteria discussed previously. The Q and R matrices are:

Q Matrix

10	0	0
0	10	0
0	0	1

R MATRIX

2.700E-3	-3.700E-3	7.000E-4	-1.000E-4	7.000E-4	7.000E-4
-3.700E-3	7.600E-3	-6.000E-4	1.400E-3	4.000E-4	4.000E-4
7.000E-4	-6.000E-4	4.303E+0	3.058E-1	7.000E-4	5.423E+0
-1.000E-4	1.400E-3	3.058E-1	4.267E+0	4.000E-4	3.057E+0
7.000E-4	4.000E-4	7.000E-4	4.000E-4	1.200E-3	1.200E-3
7.000E-4	4.000E-4	5.423E+0	3.057E+0	1.200E-3	8.550E+0

Appendix C: Monte Carlo Simulations of Elemental Filters

Appendix C contains the Monte Carlo runs of elemental filters versus a truth model. The title of each figure indicates the parameter point upon which the filter model is designed. The truth model for all simulations is based upon the internal model of the filter at parameter point (5,5). The magnitude of the dither signal is equal to 5 at a frequency of 30 rad/sec.

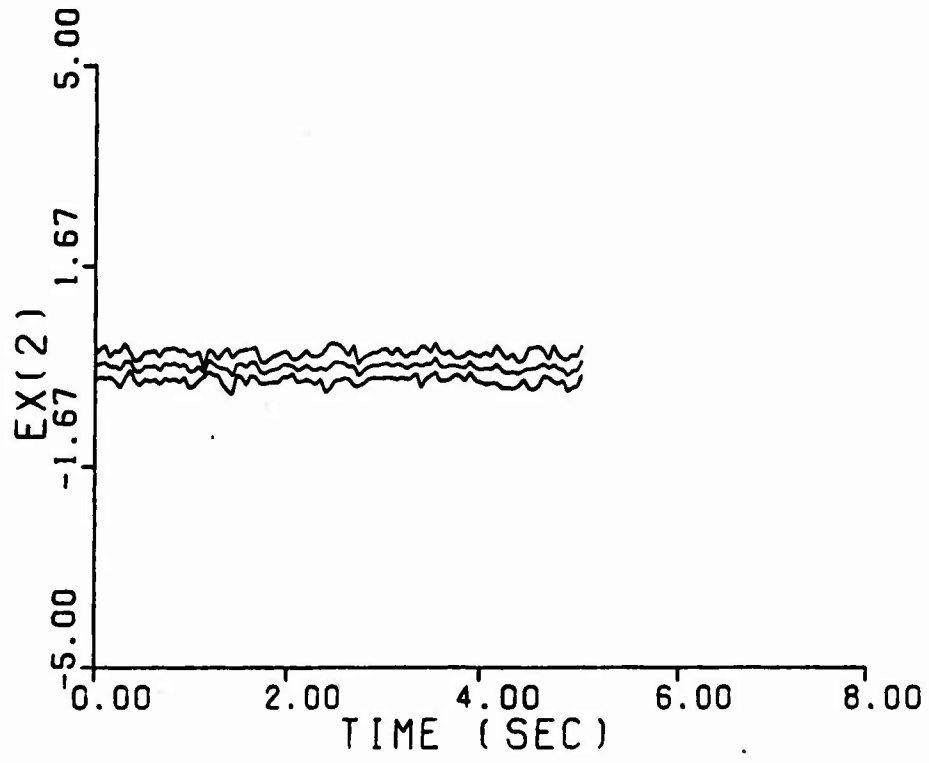

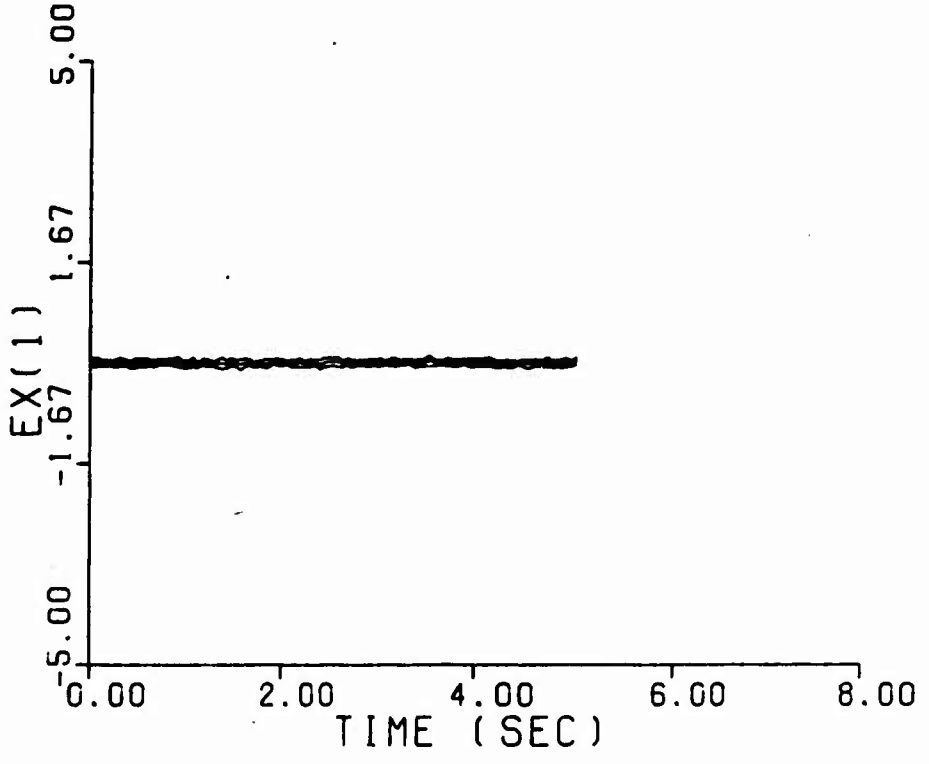

Fig. C-1. Parameter Point 5,5

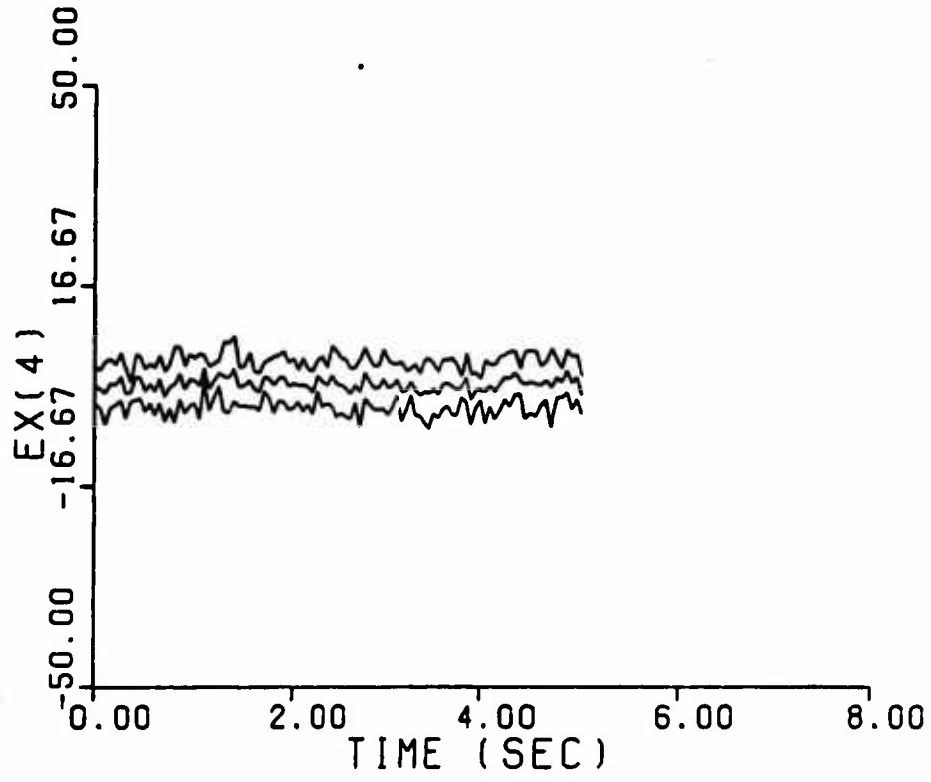

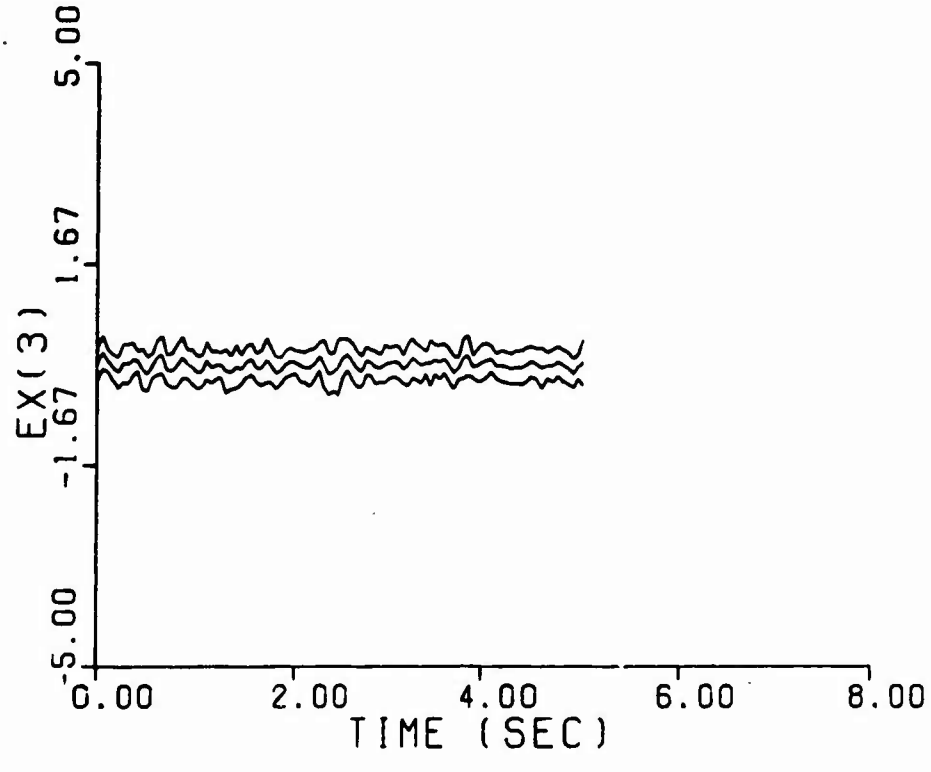

Fig. C-1--Continued

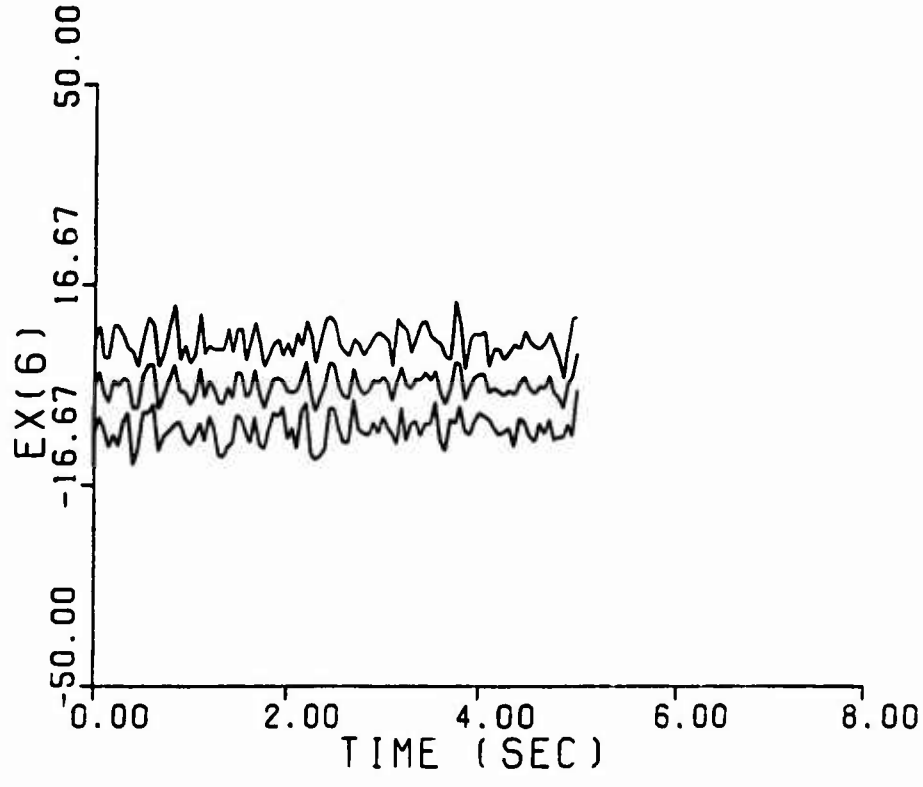

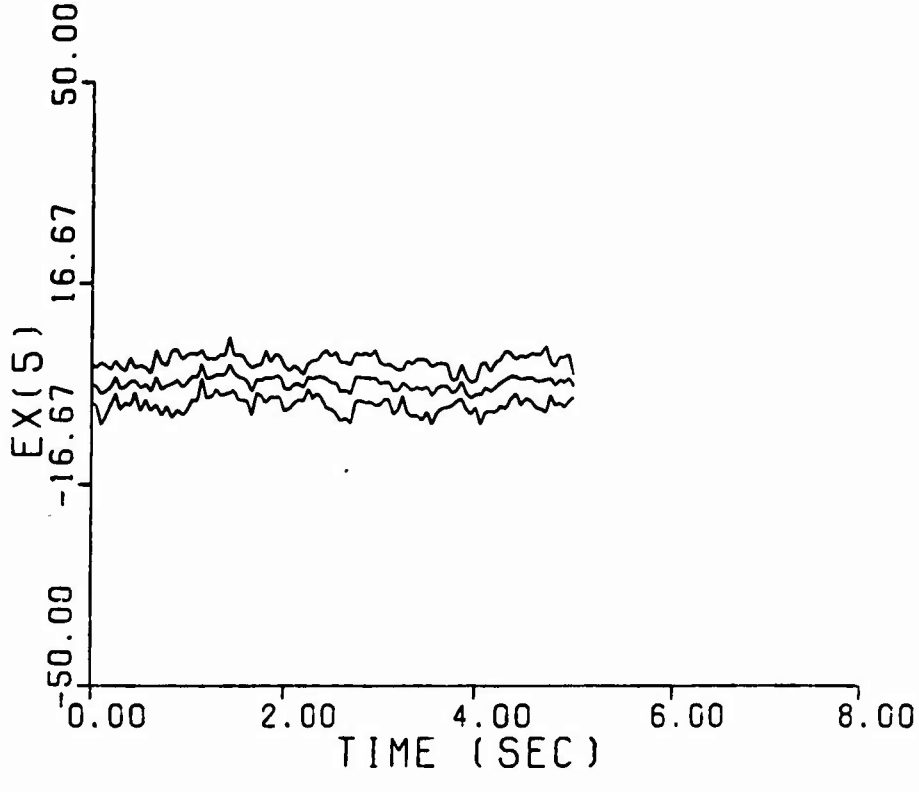

Fig. C-1--Continued

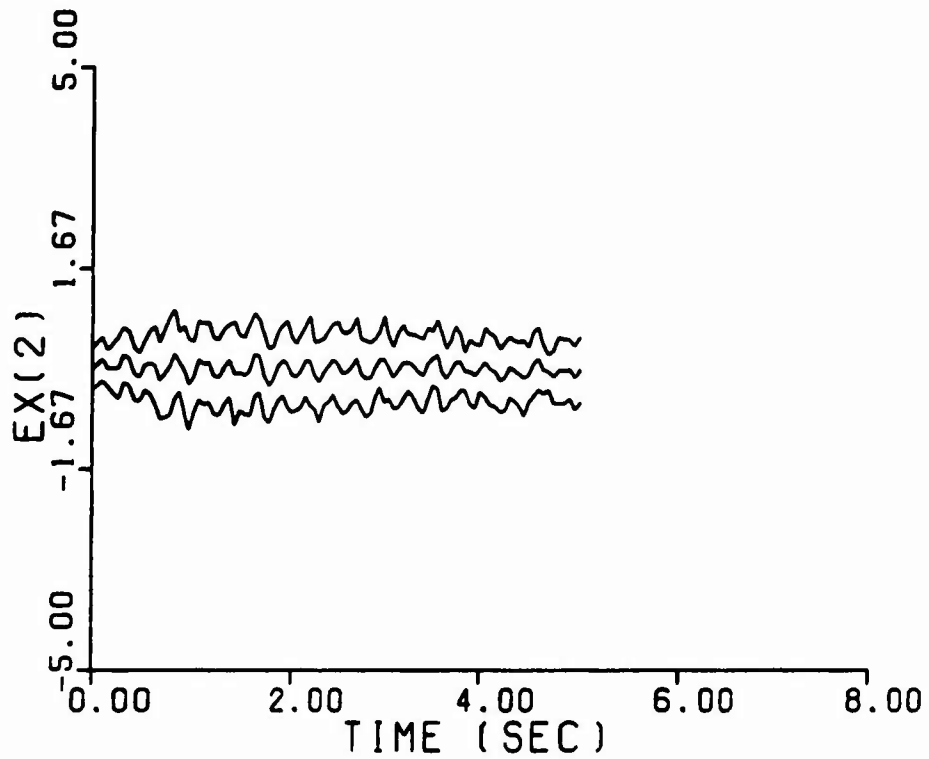

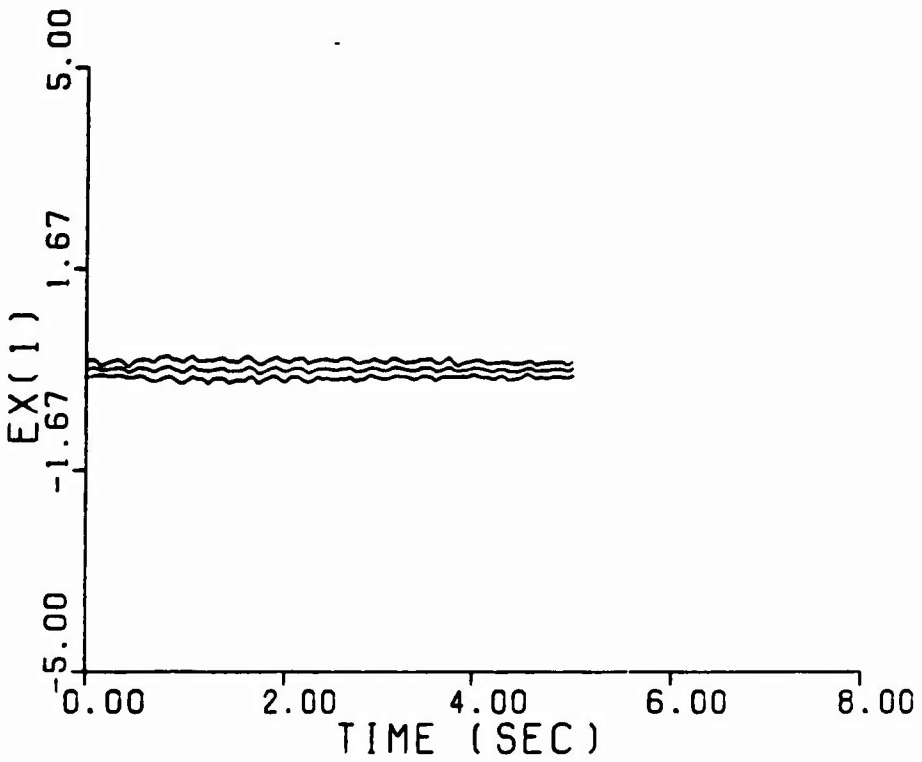

Fig. C-2. Parameter Point 5,6

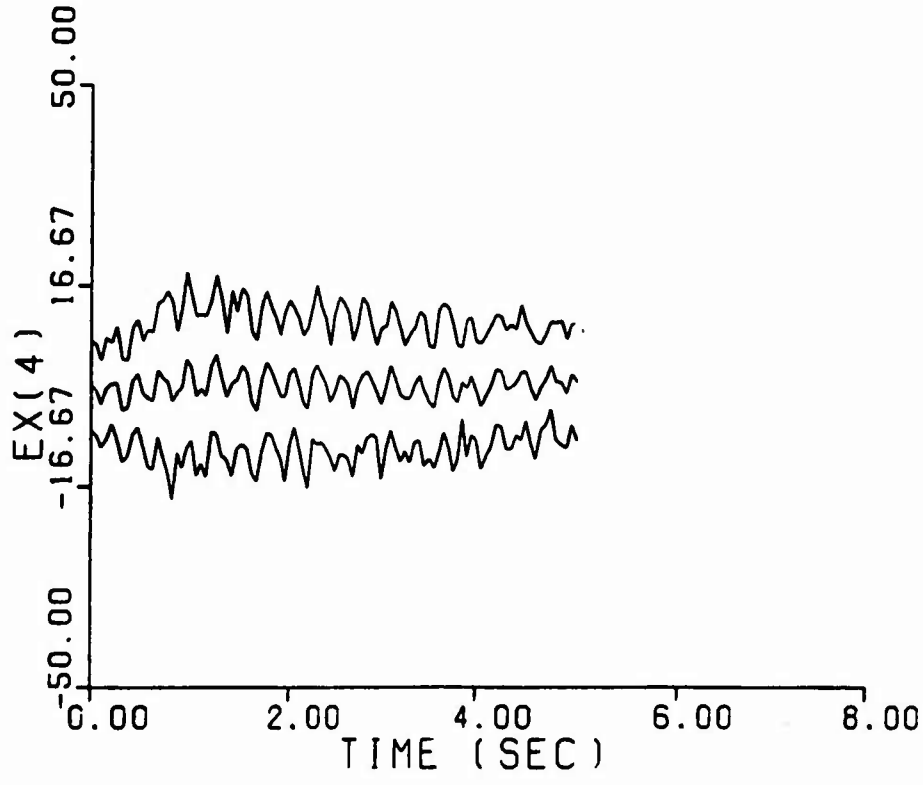

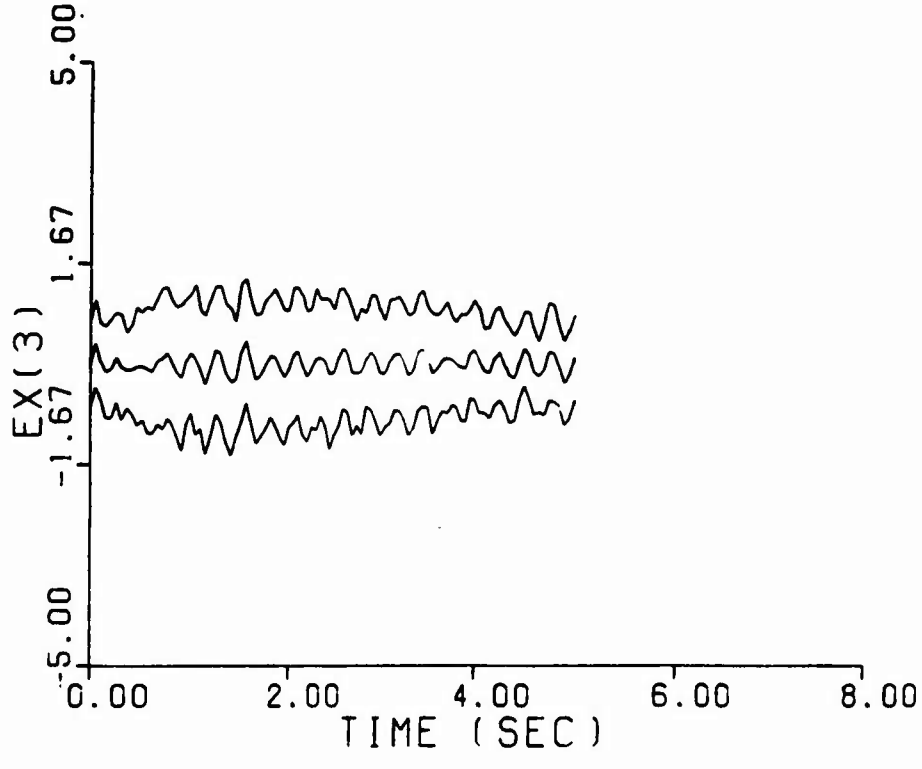

Fig. C-2--Continued

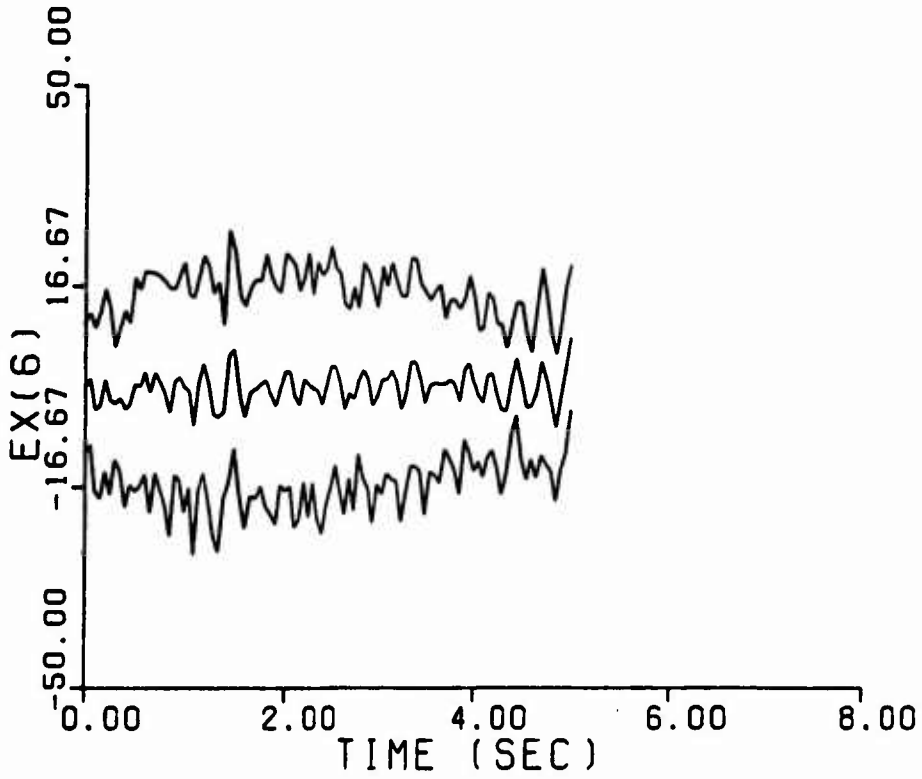

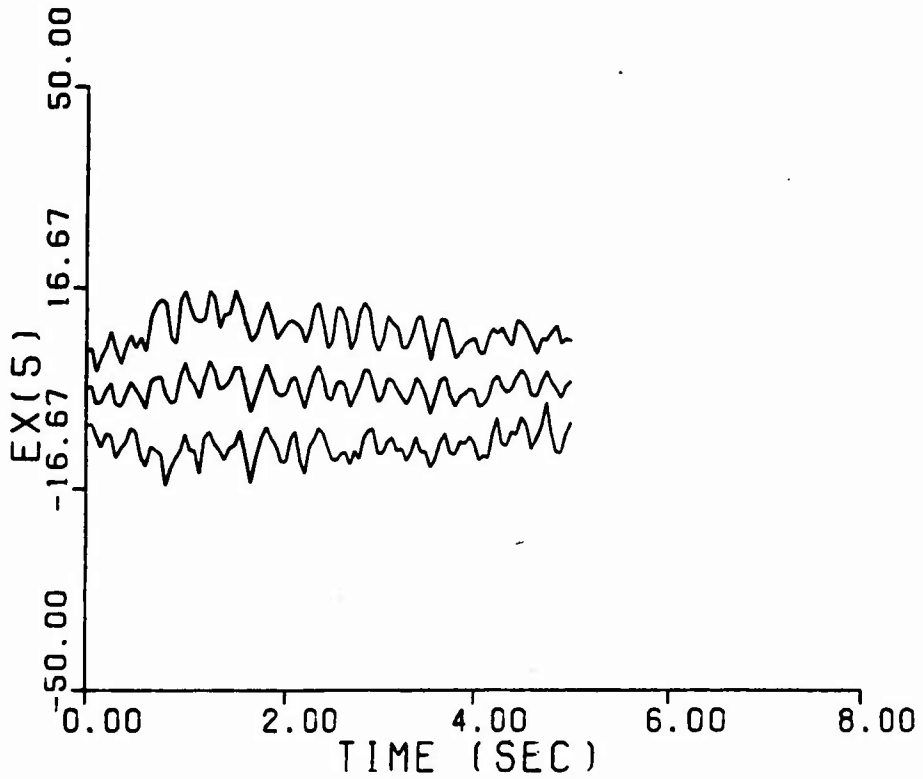

Fig. C-2--Continued

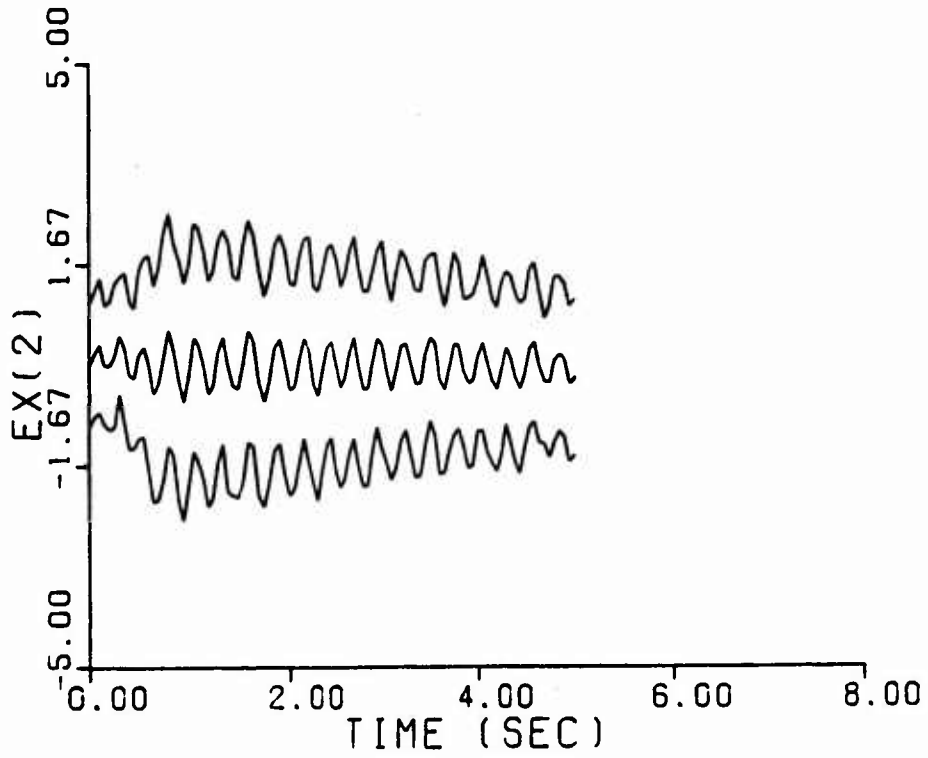

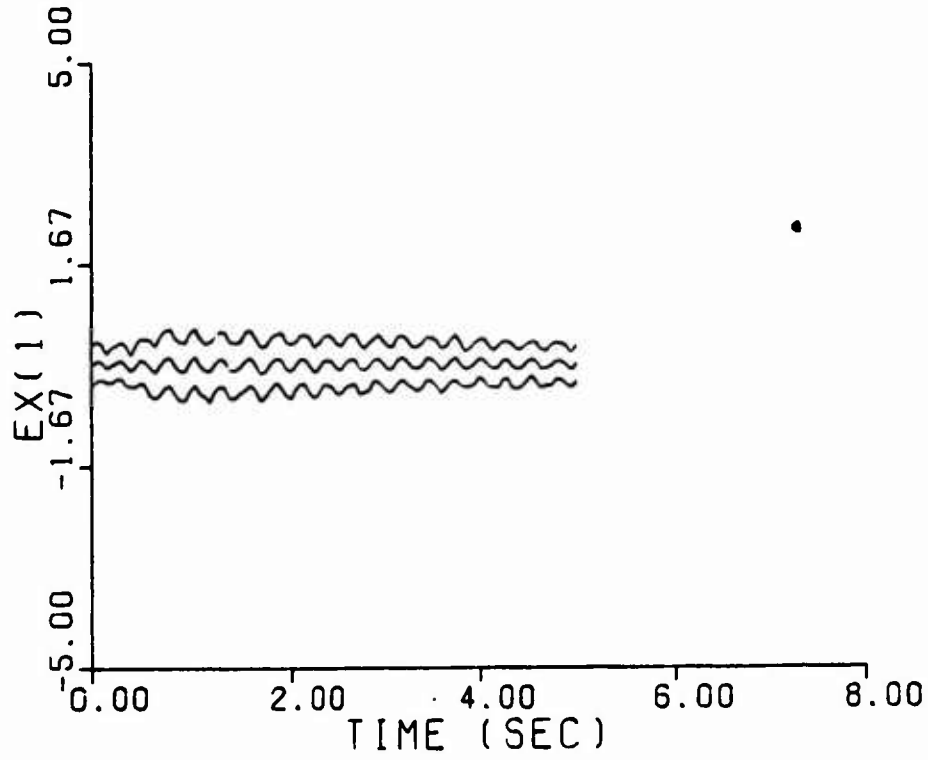

Fig. C-3. Parameter Point 4,5

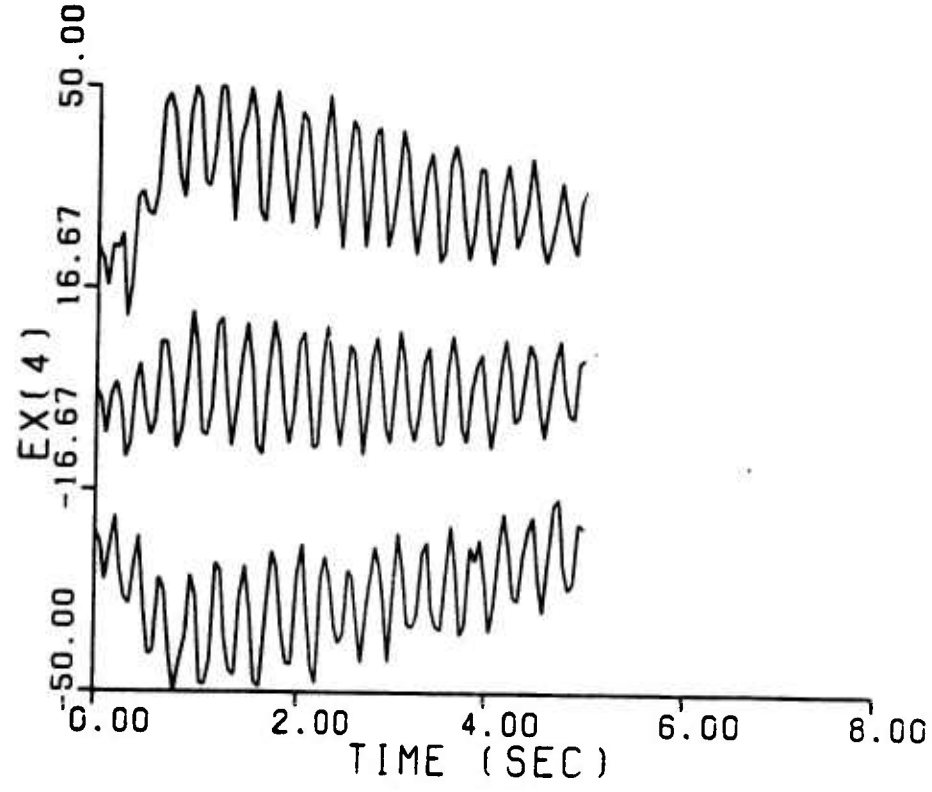

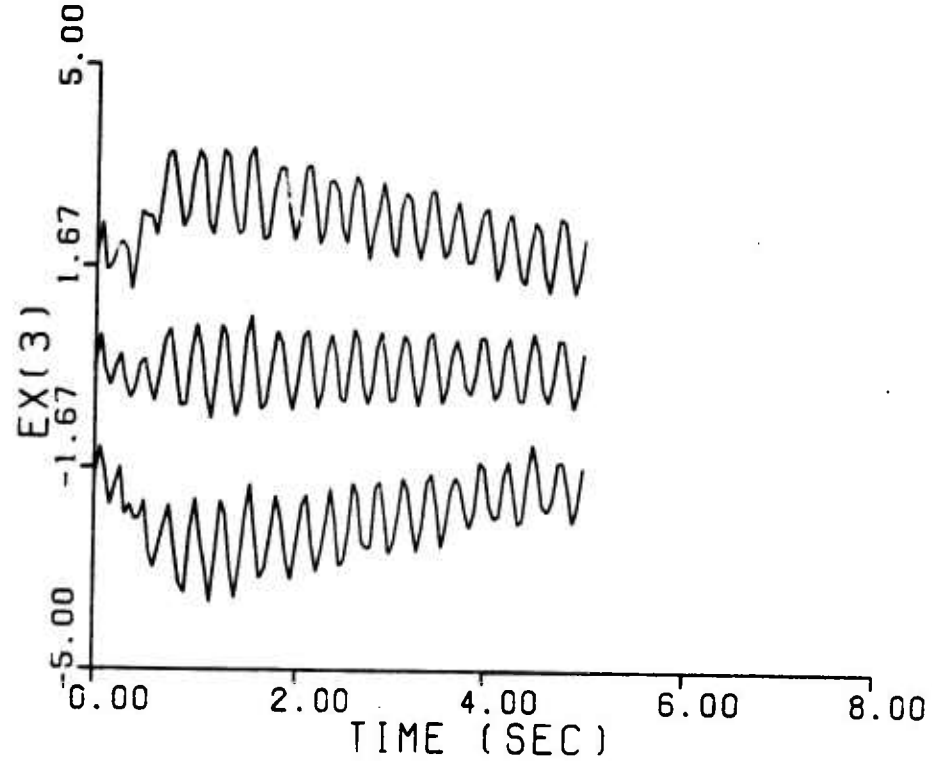

Fig. C-3--Continued

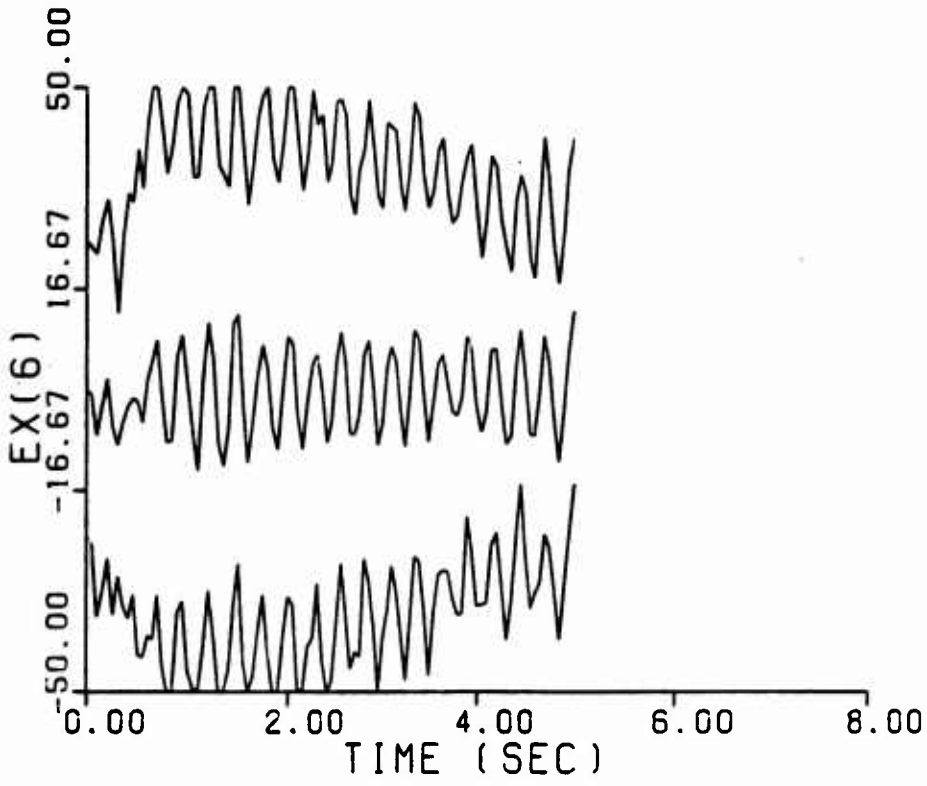

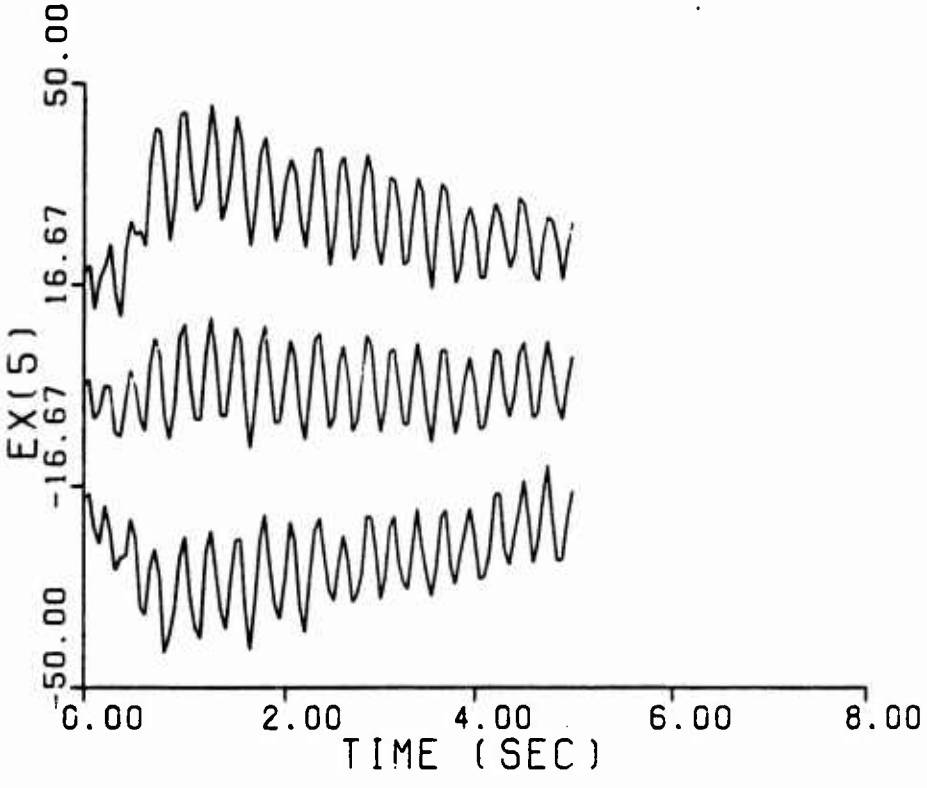

Fig. C-3--Continued

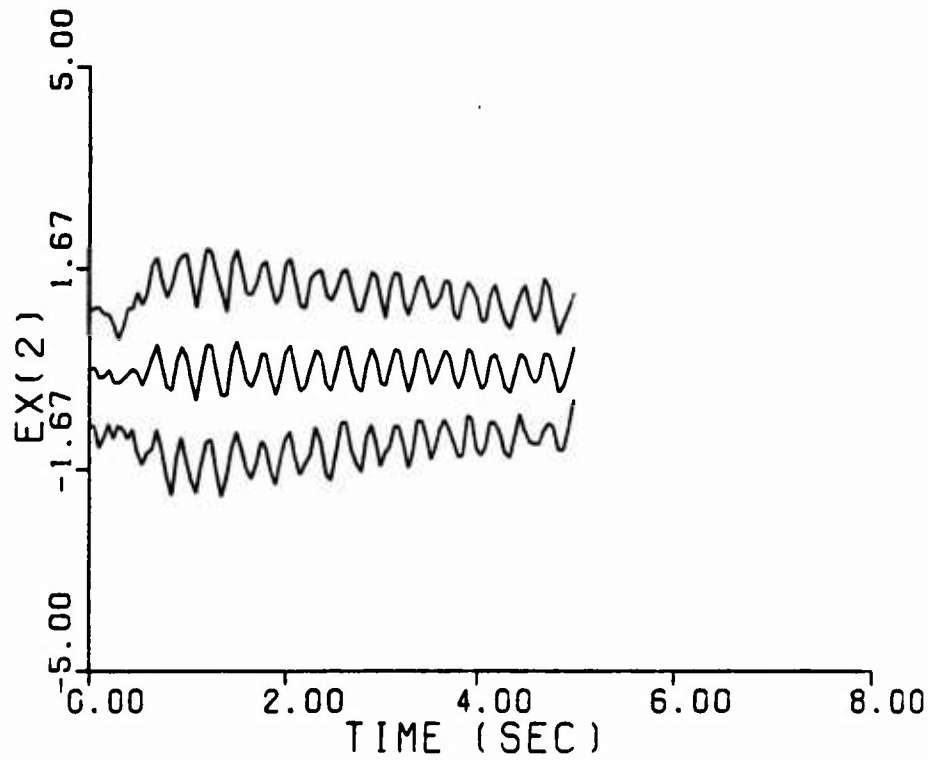

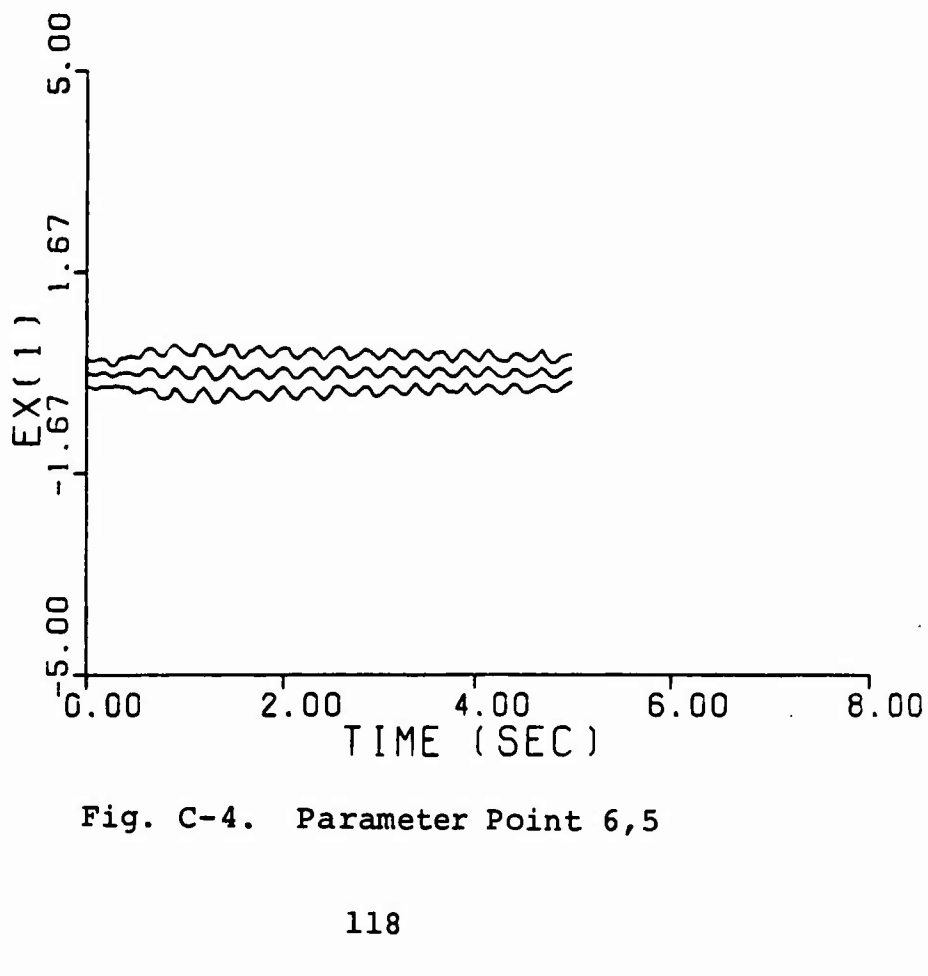

Fig. C-4. Parameter Point 6,5

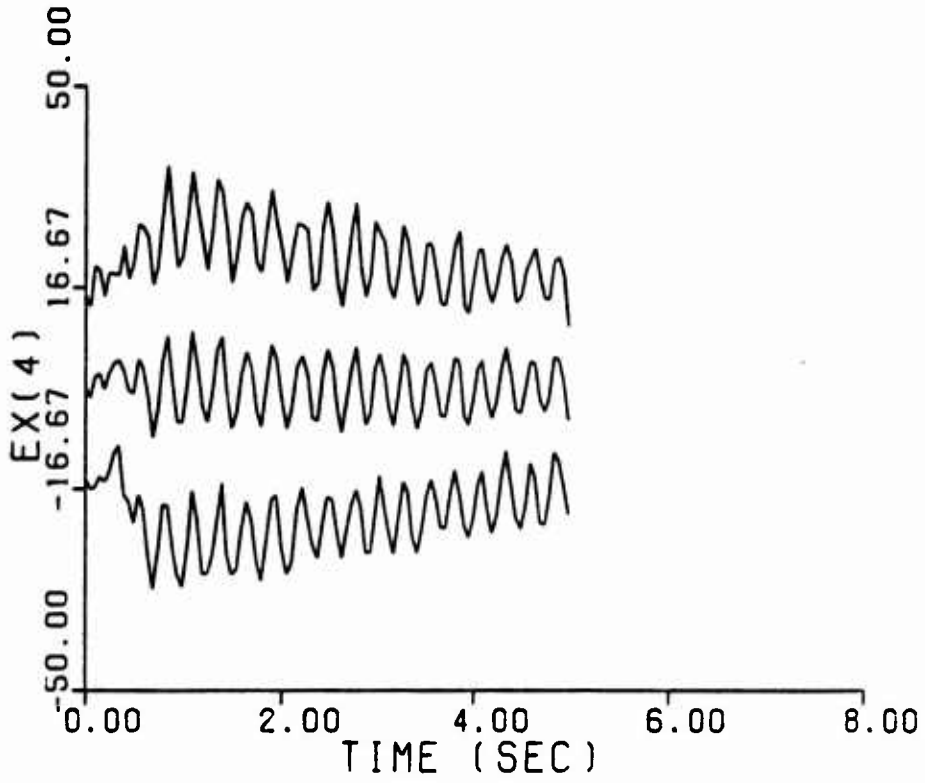

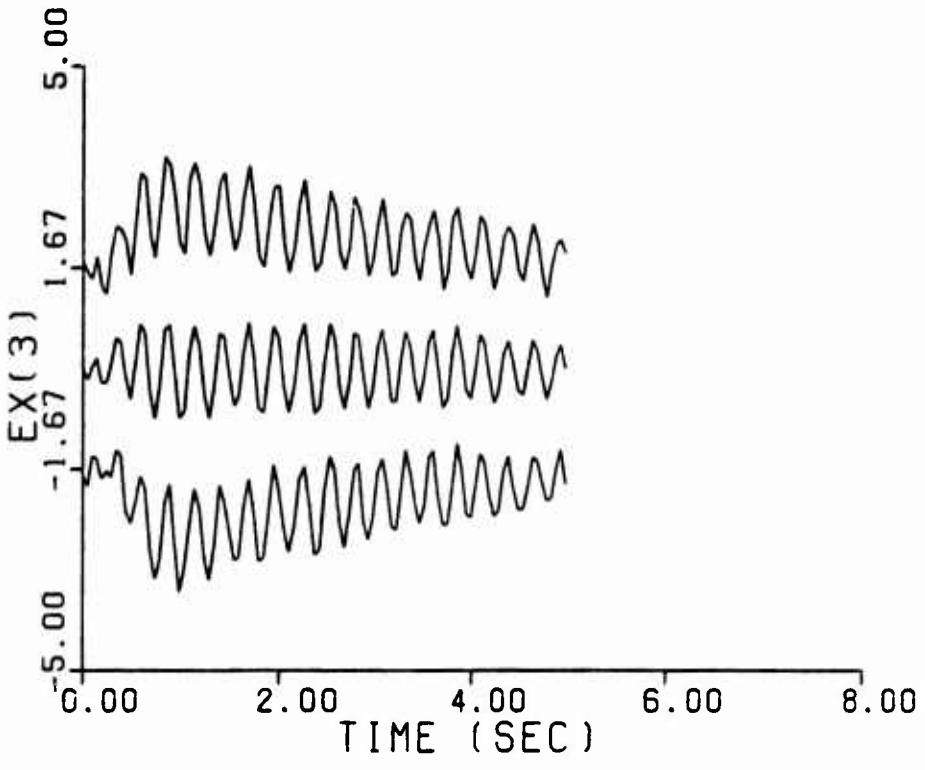

Fig. C-4--Continued

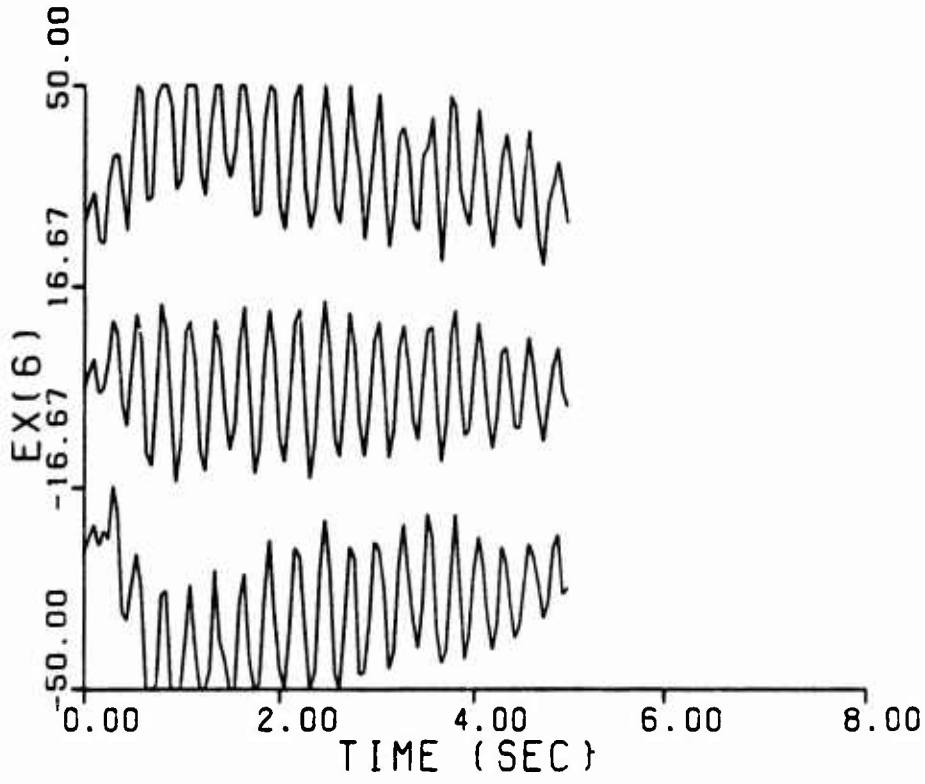

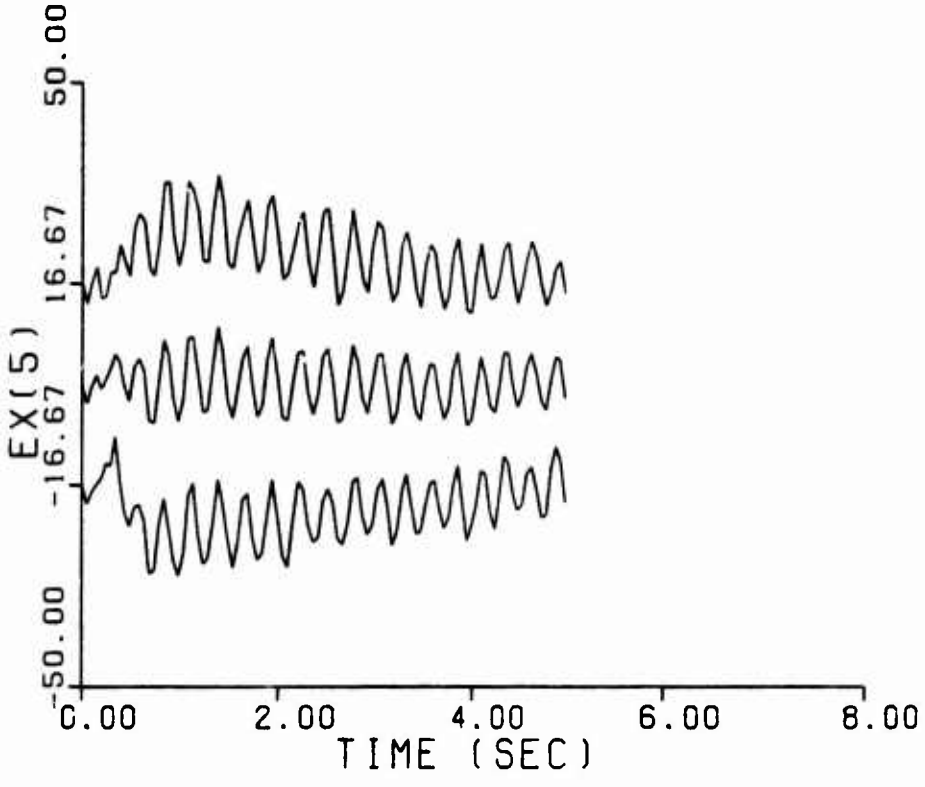

Fig. C-4--Continued

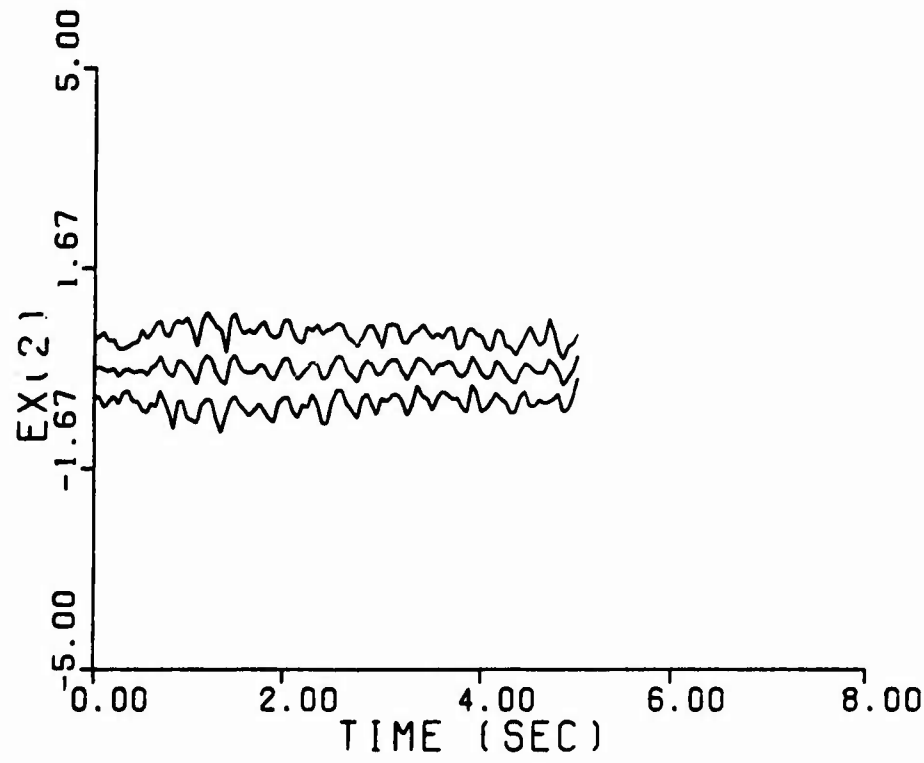

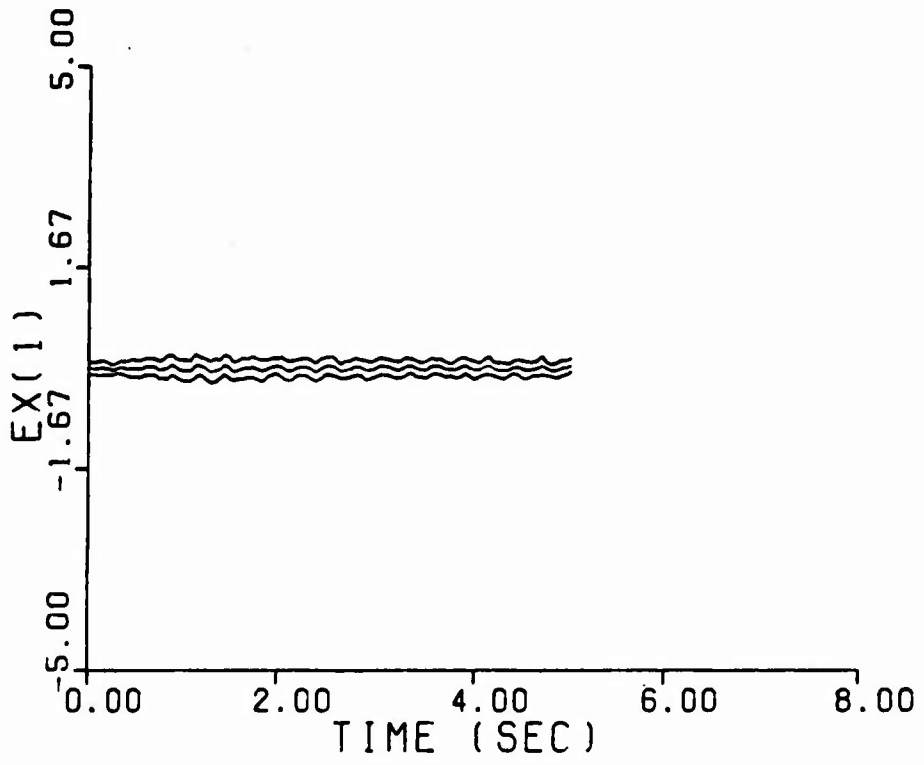

Fig. C-5. Parameter Point 5,4

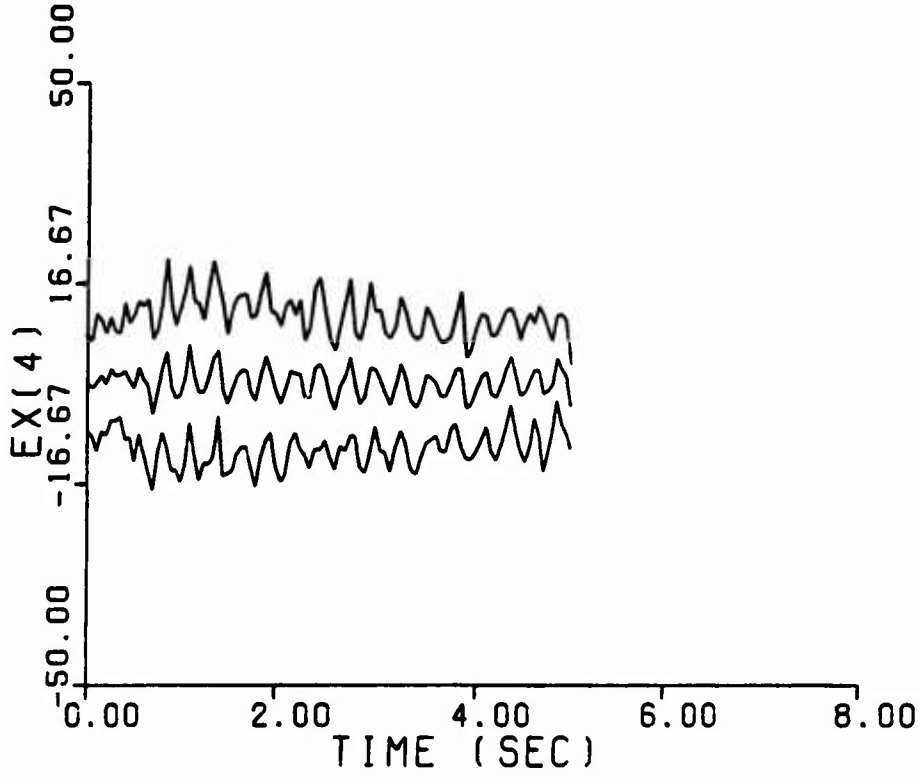

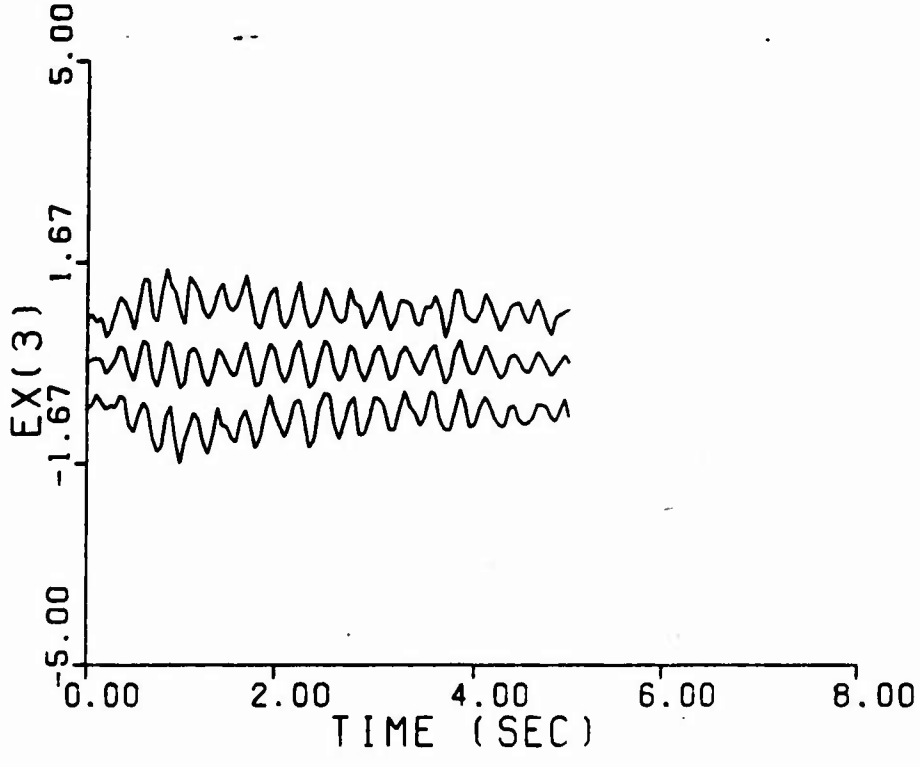

Fig. C-5--Continued

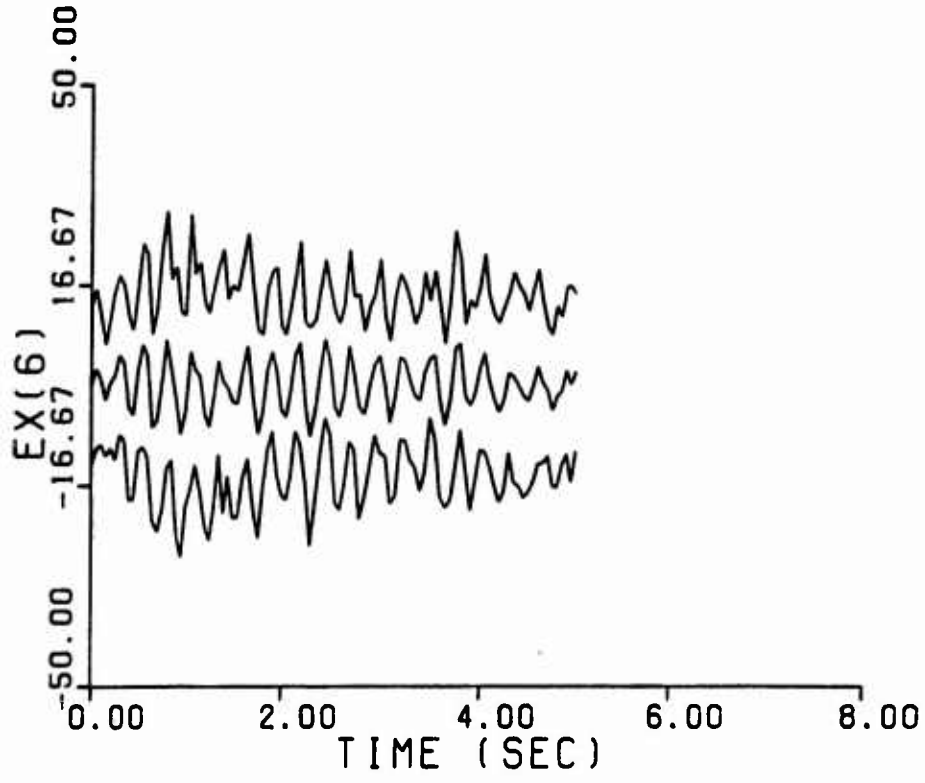

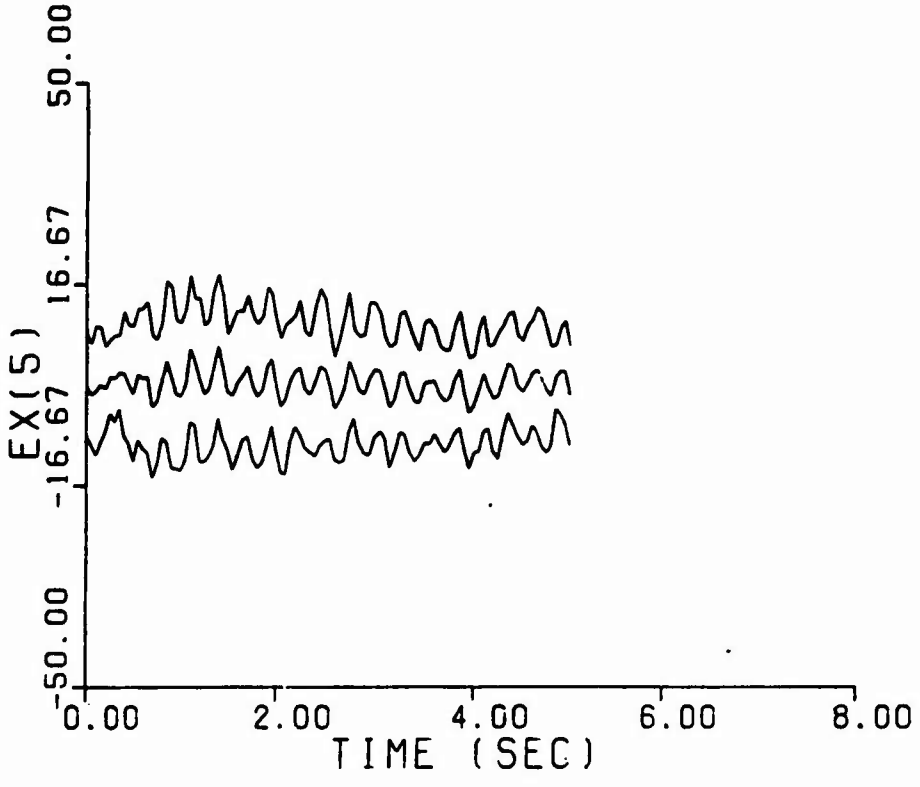

Fig. C-5--Continued

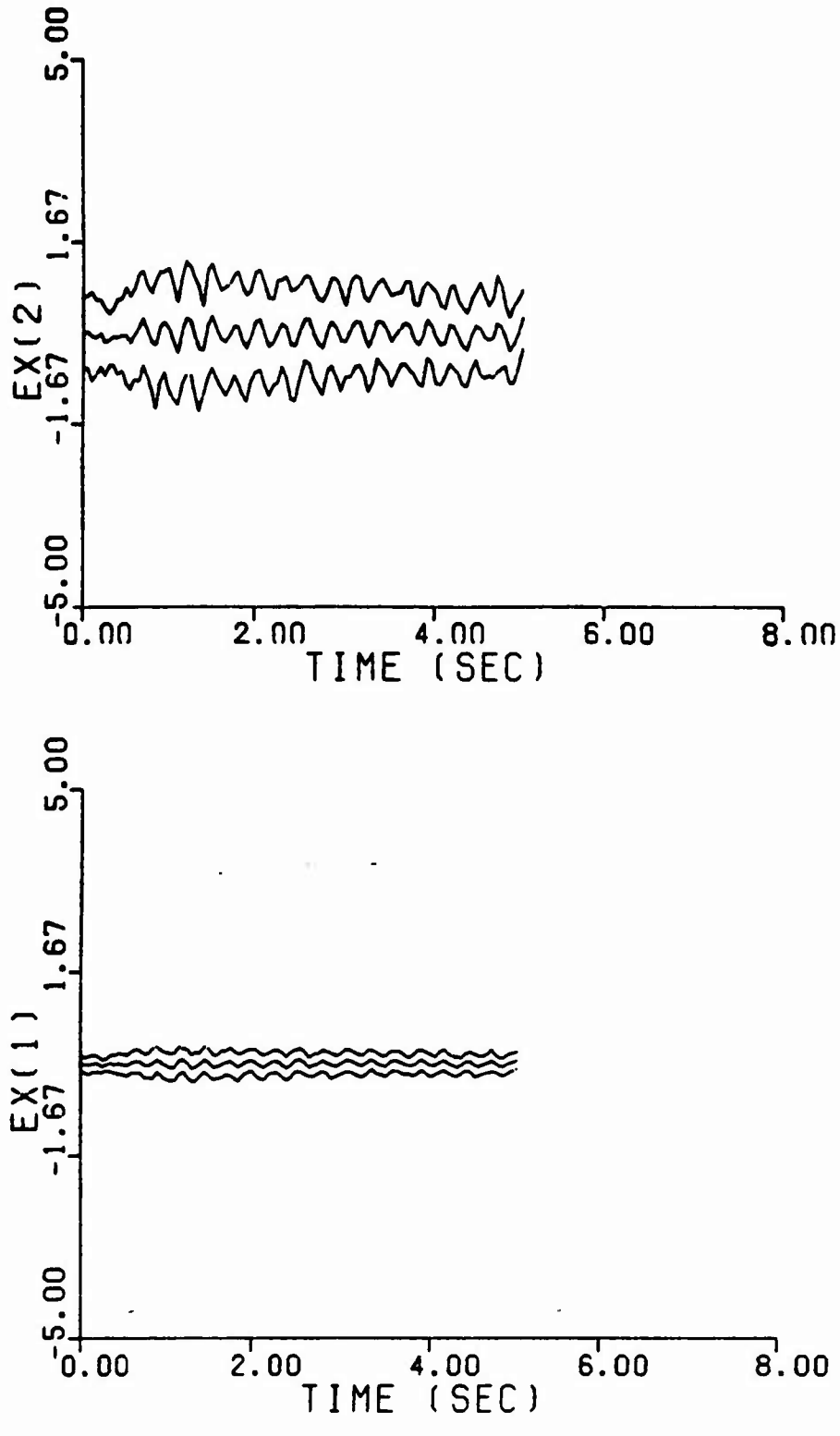

Fig. C-6. Parameter Point 6,6

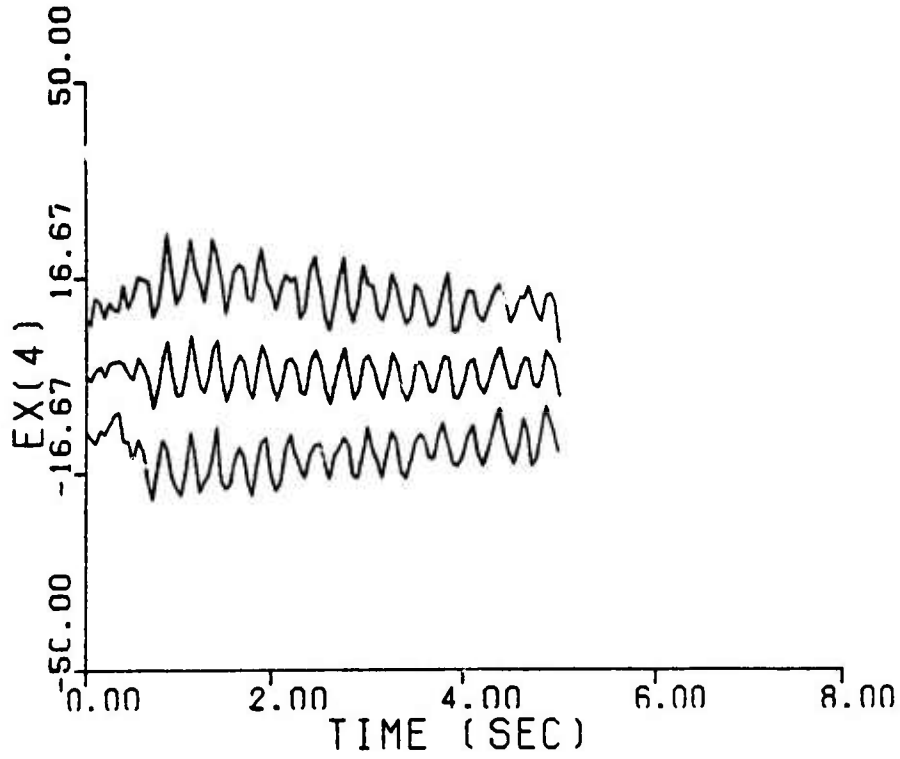

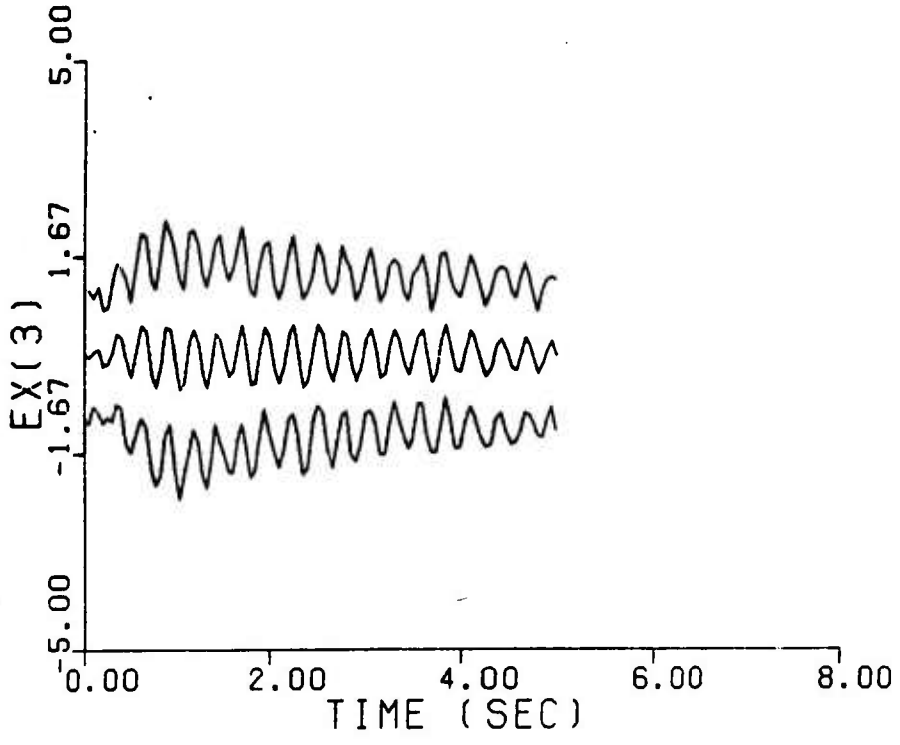

Fig. C-6--Continued

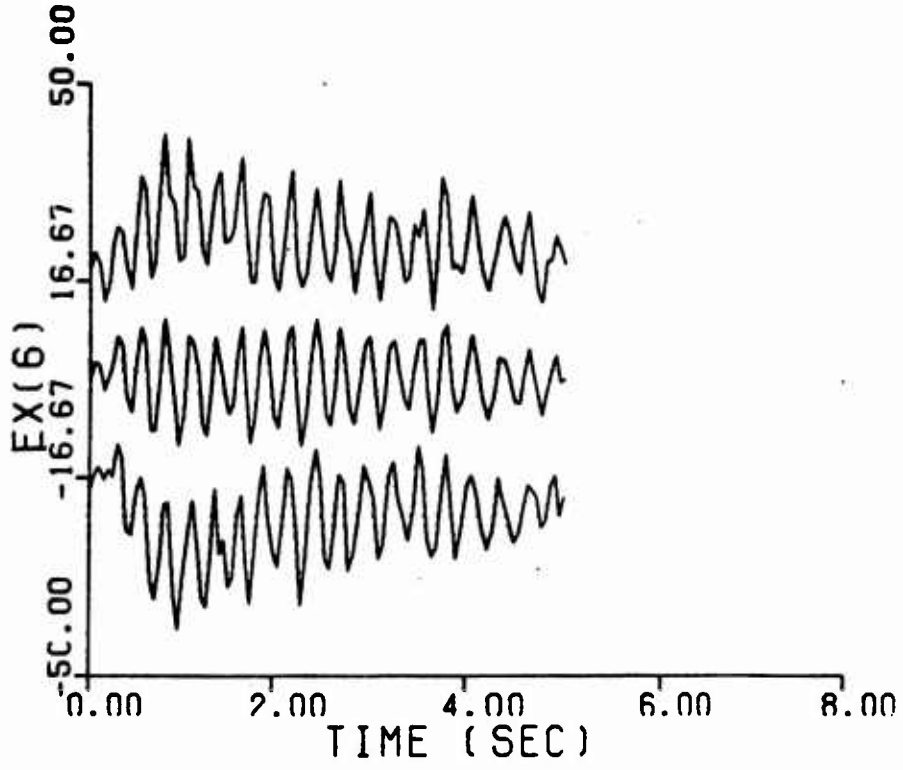

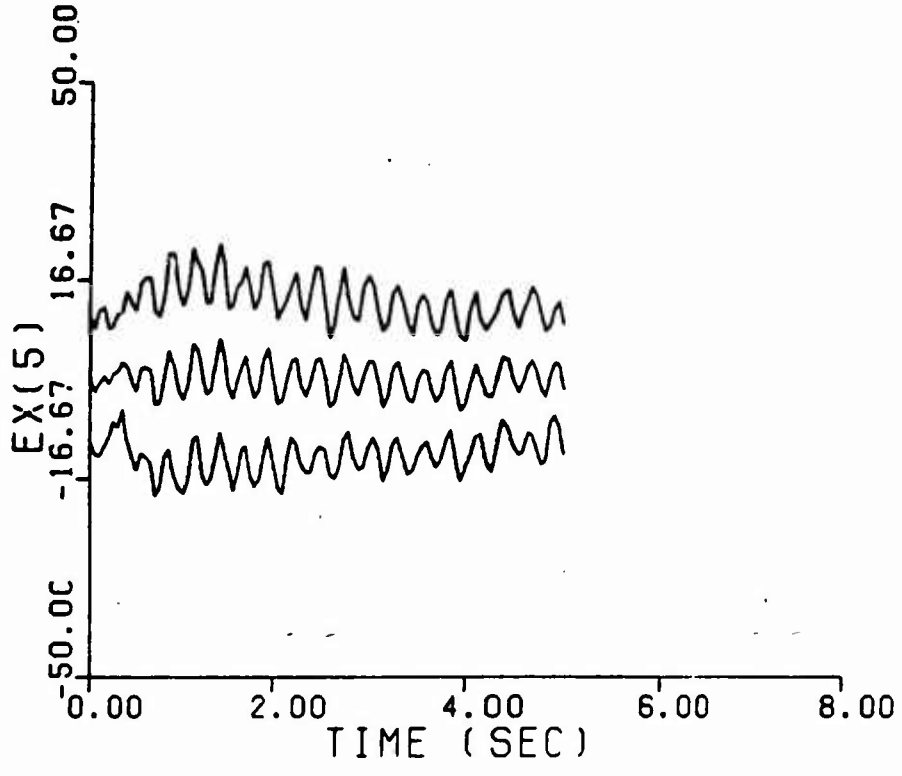

Fig. C-6--Continued

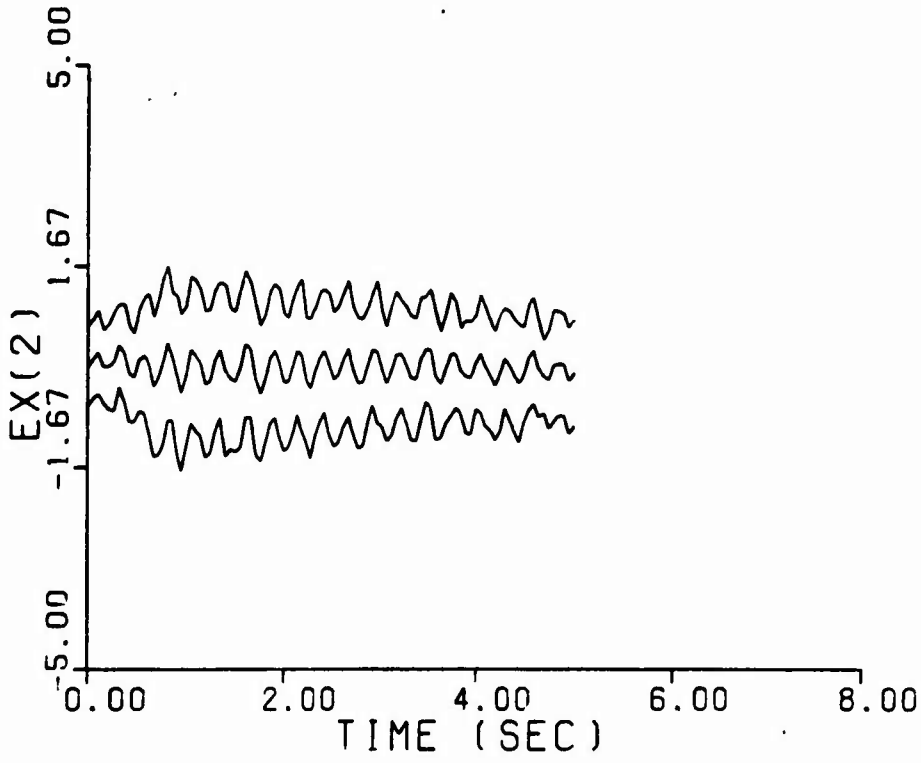

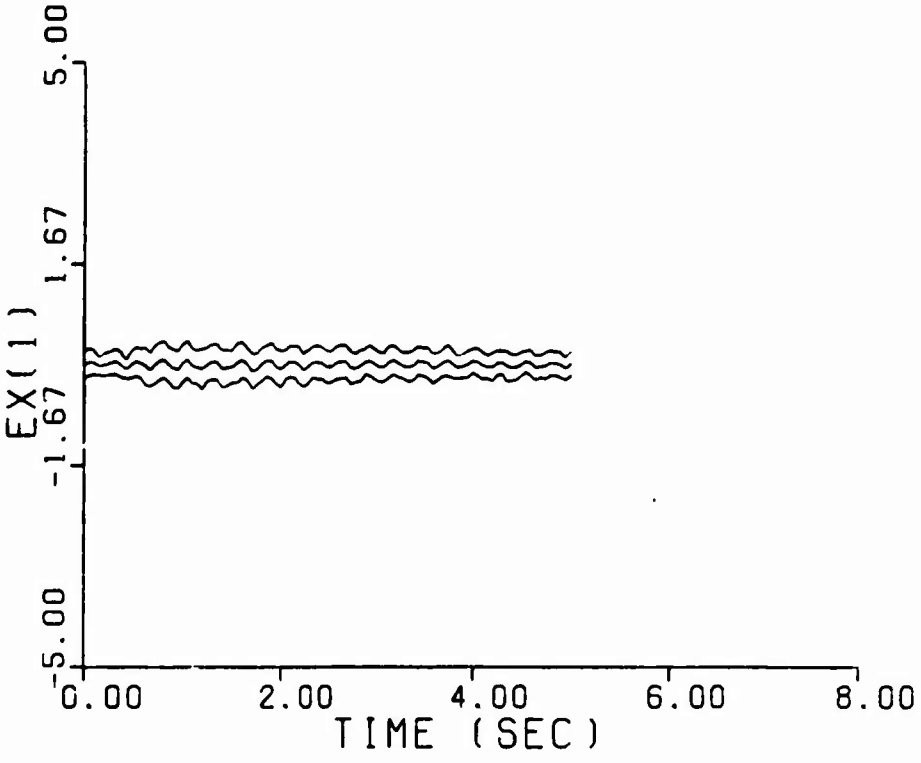

Fig. C-7. Parameter Point 4,4

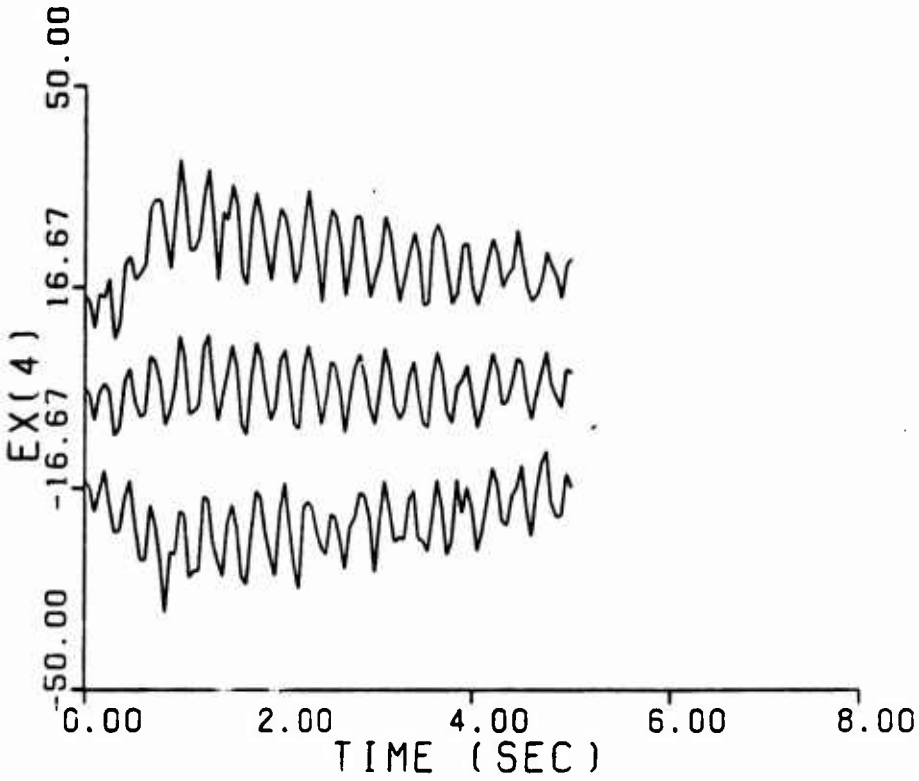

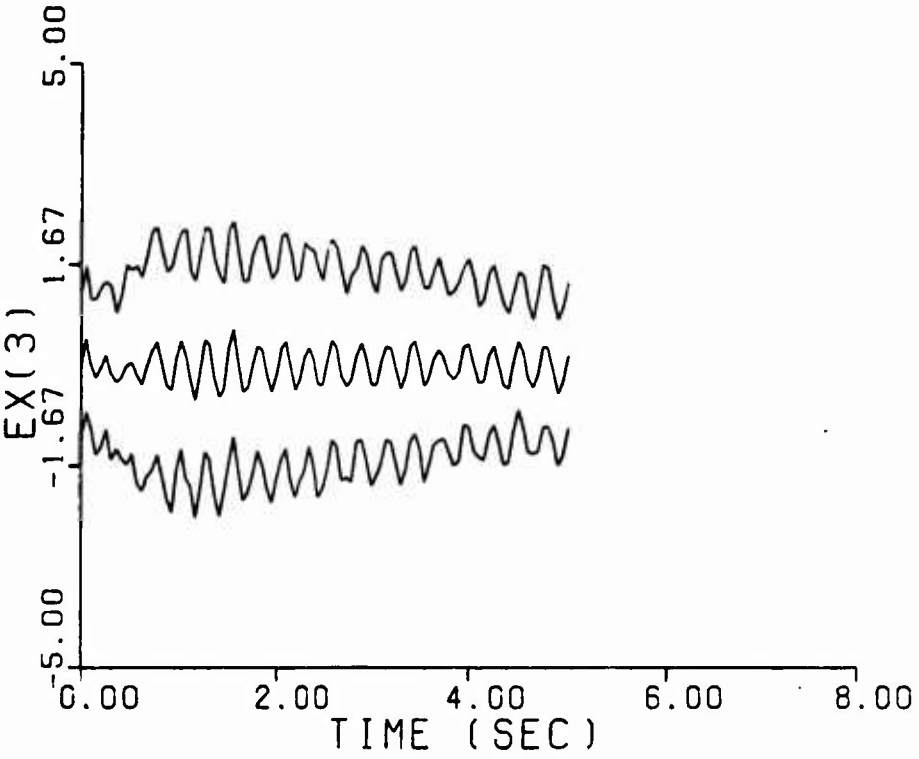

Fig. C-7--Continued

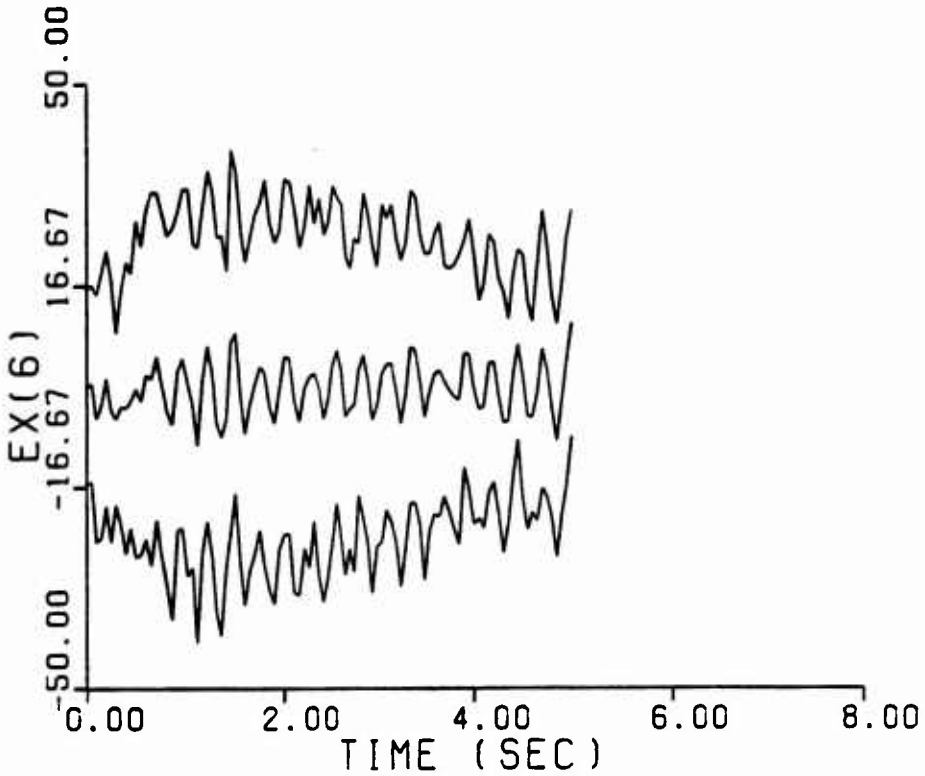

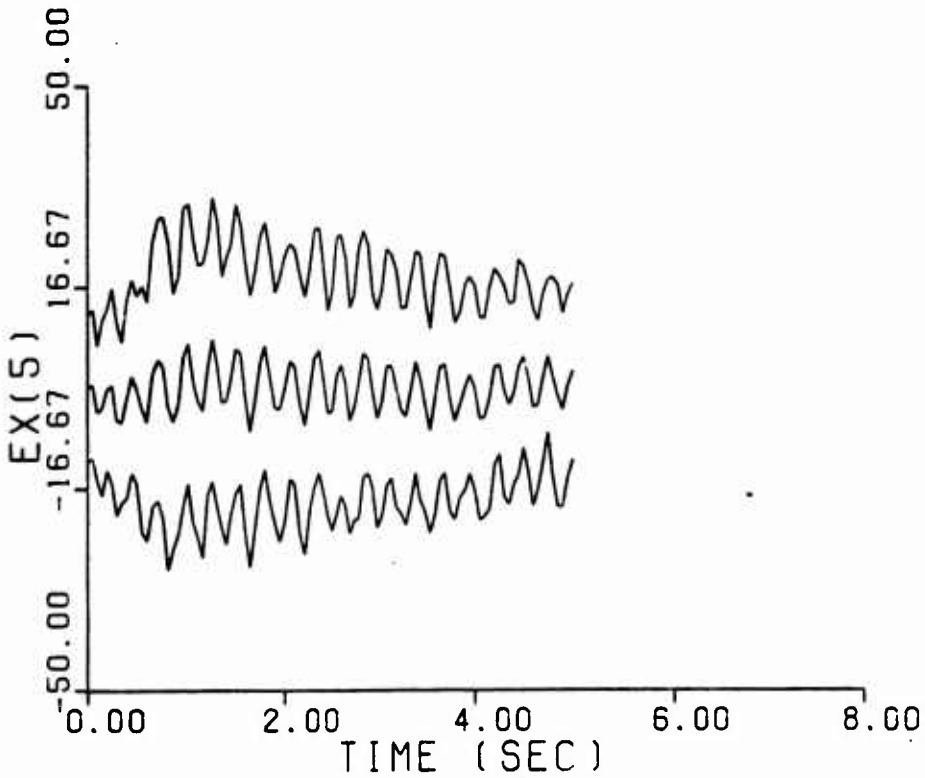

Fig. C-7--Continued

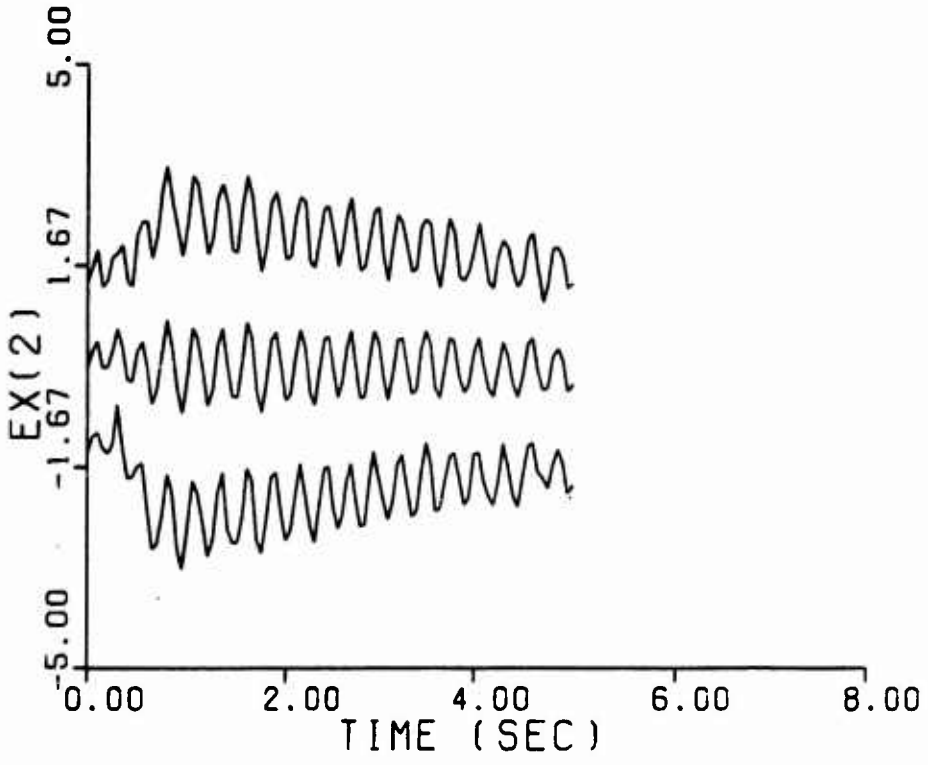

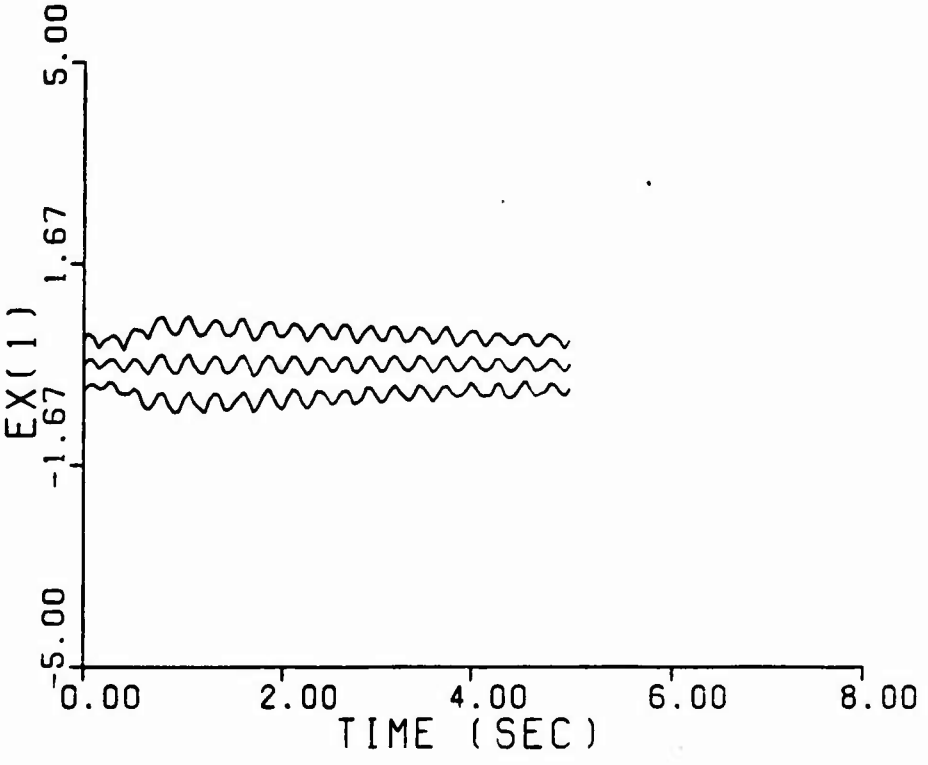

Fig. C-8. Parameter Point 4,6

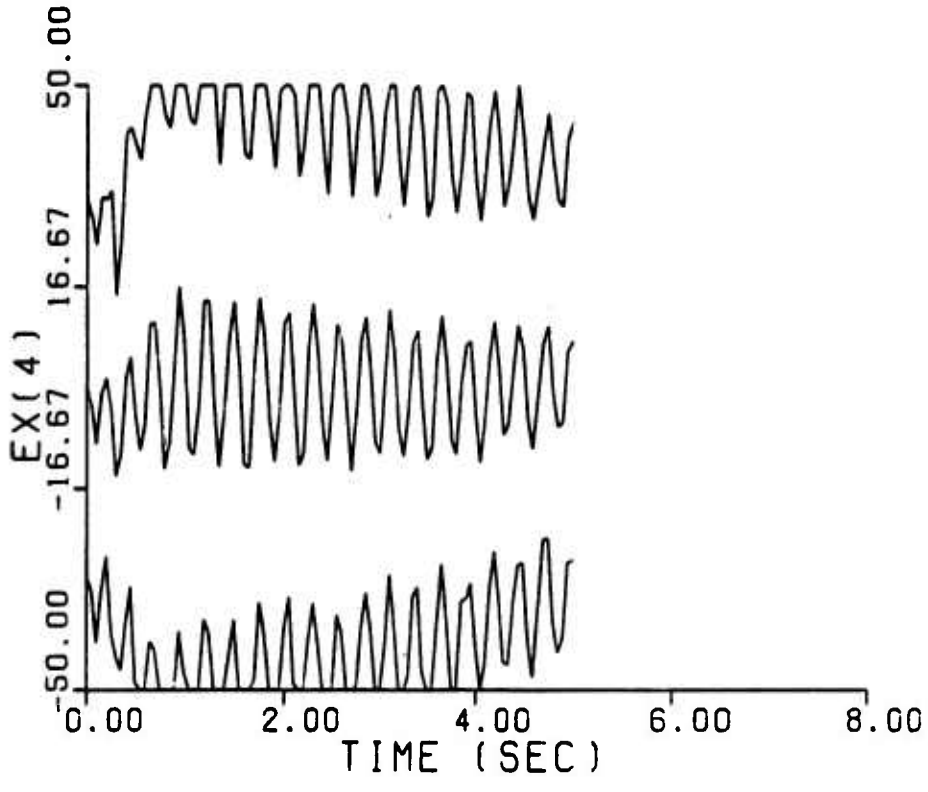

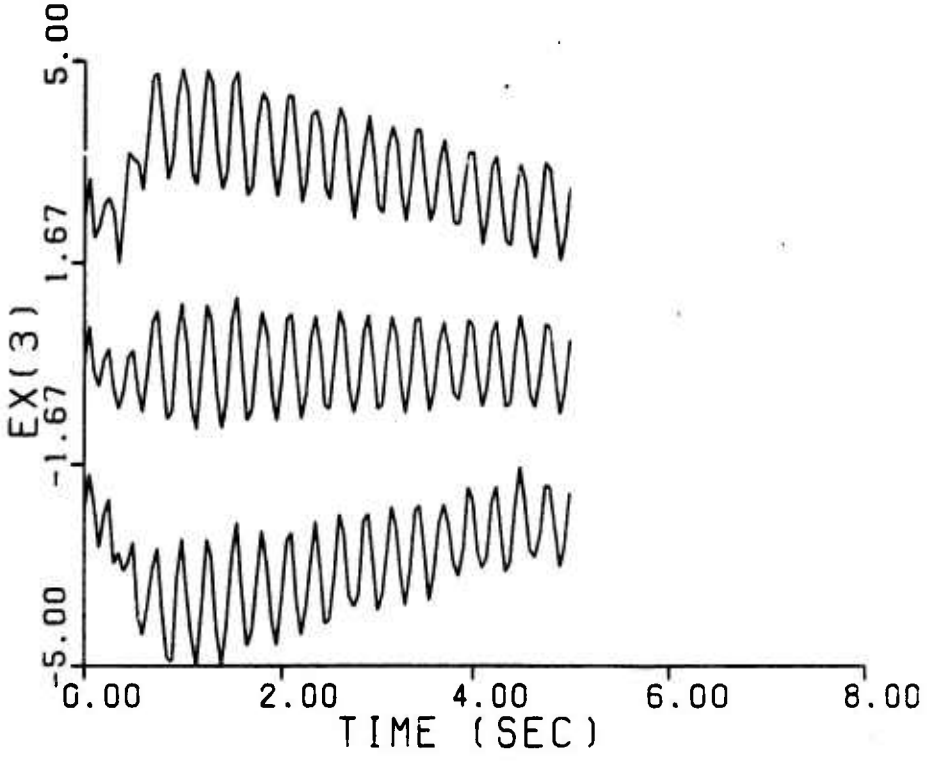

Fig. C-8--Continued

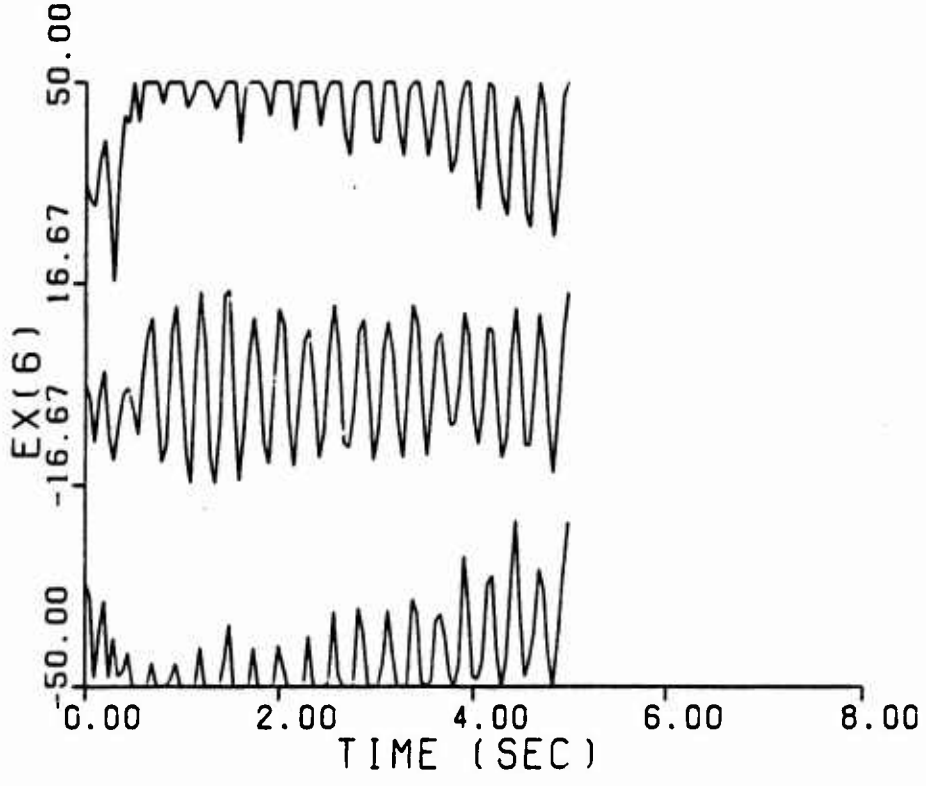

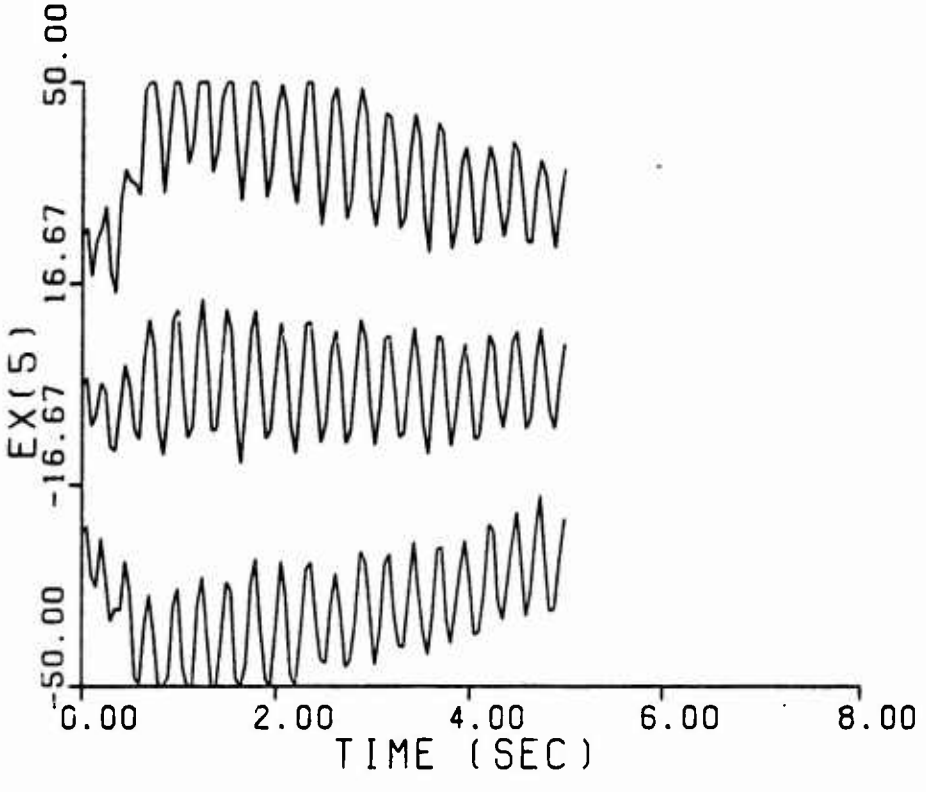

Fig. C-8--Continued

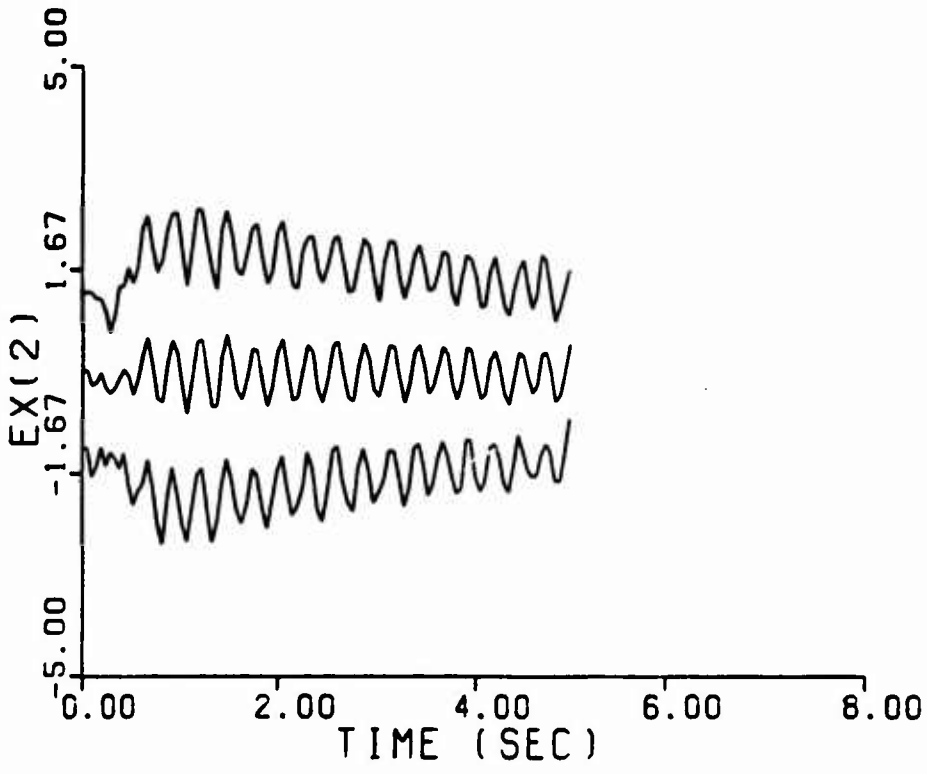

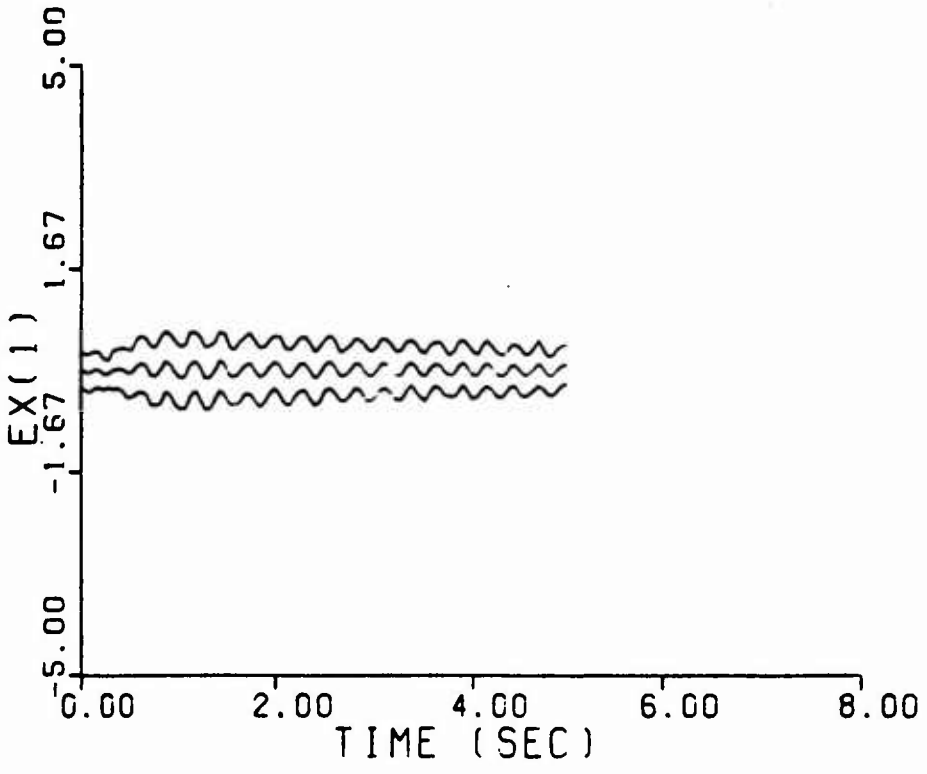

Fig. C-9. Parameter Point 6,4

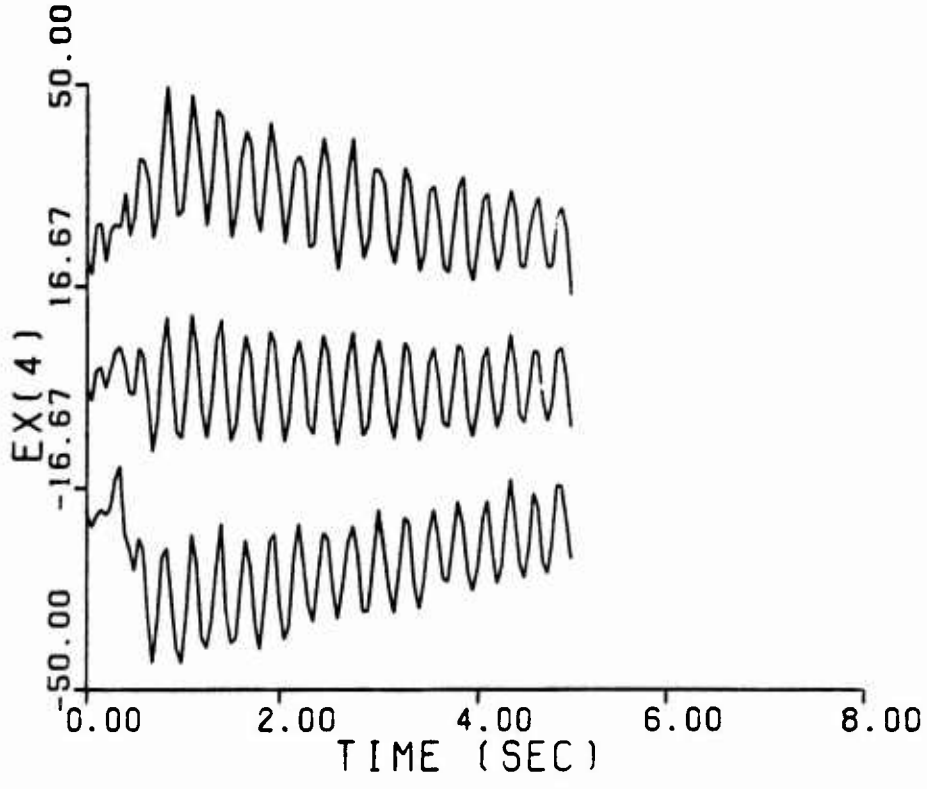

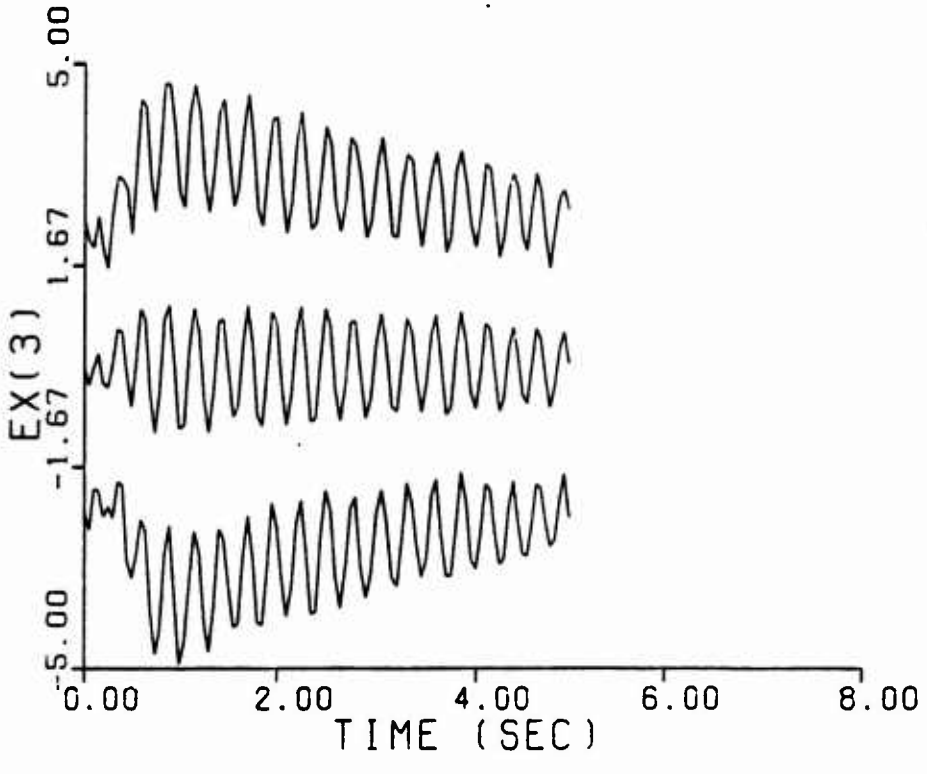

Fig. C-9--Continued

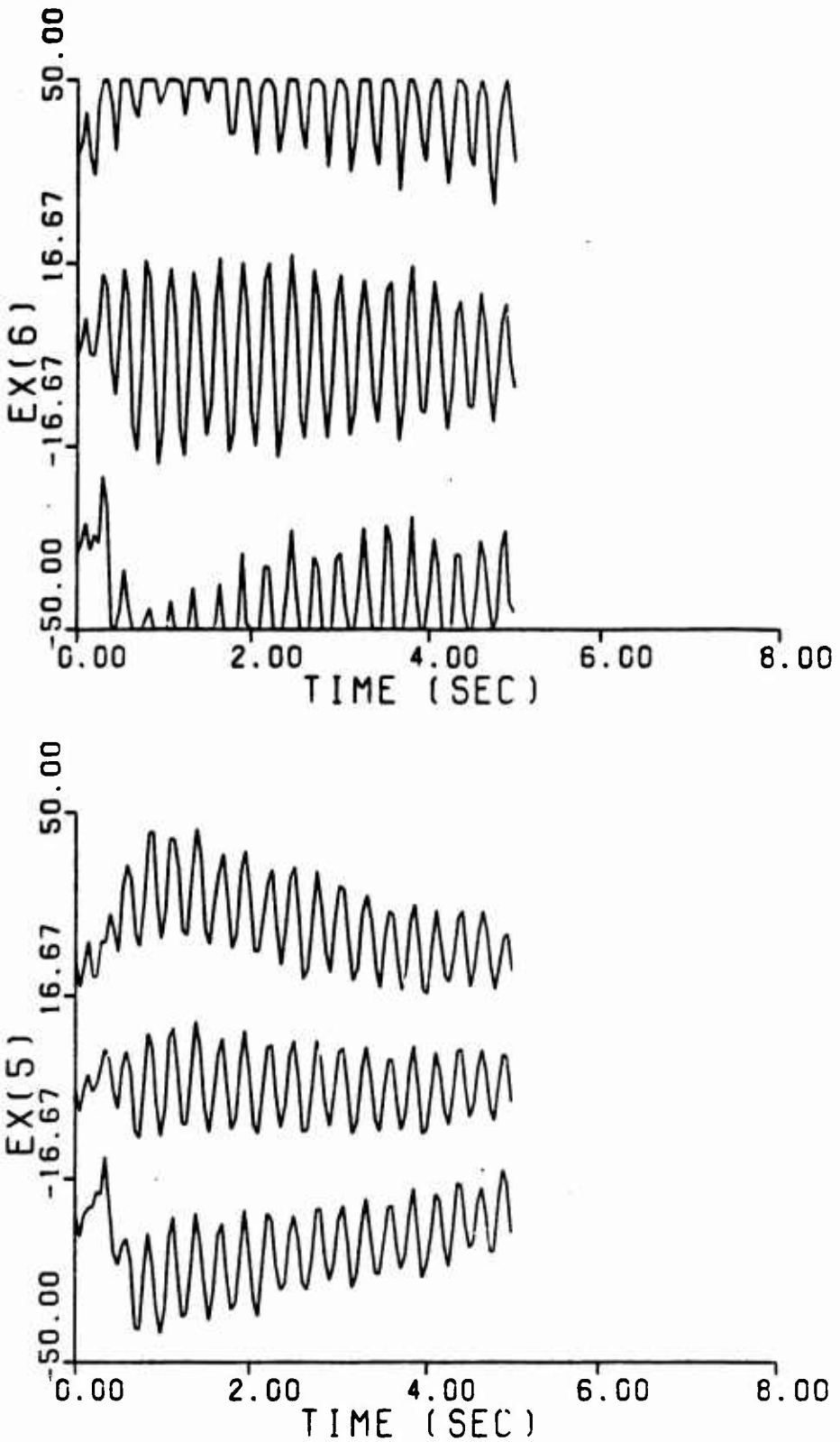

Fig. C-9--Continued

Appendix D: Monte Carlo Simulation Plots of the Moving-Bank Multiple Model Adaptive Estimator

Appendix D contains sample plots reflecting the performance of the moving bank multiple model adaptive estimator at its finest discretization, using probability monitoring. The bank is initially centered at the parameter point (5,5). The magnitude of the dither signal is equal to 5 at a frequency of 30 rad/sec. The title of each figure indicates the parameter point upon which the truth model is based.

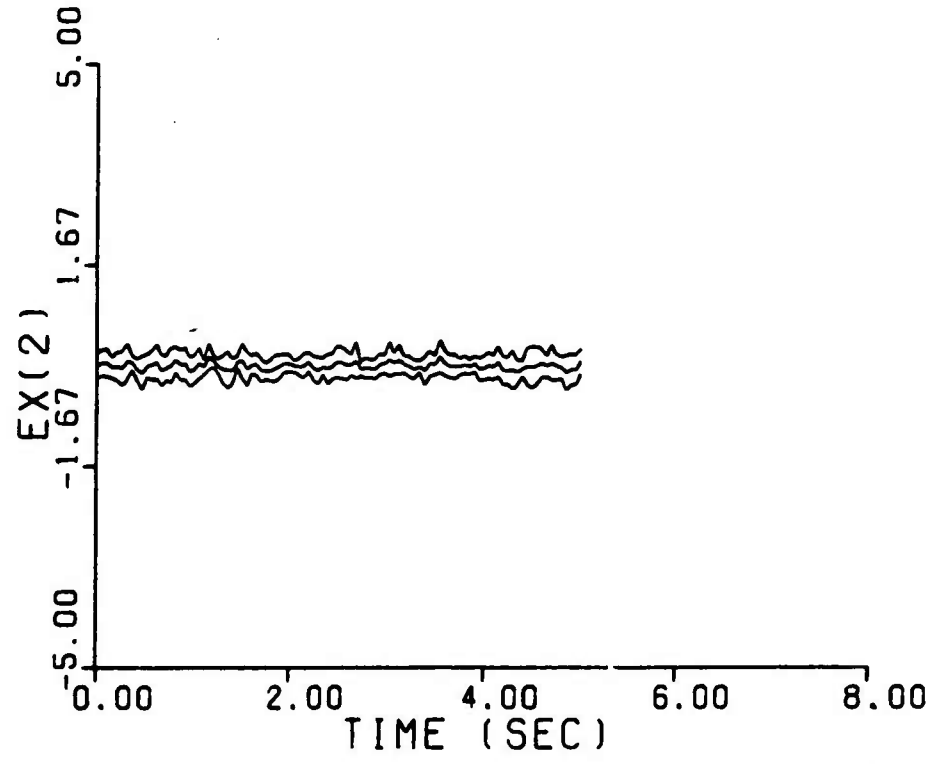

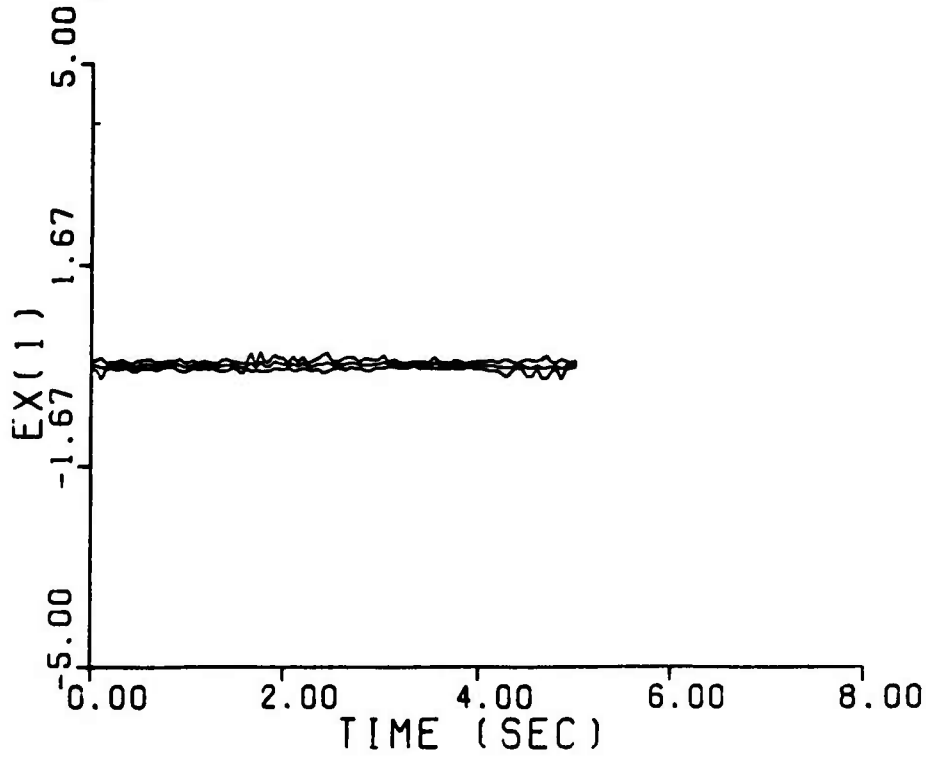

Fig. D-1. Truth Model 1,10

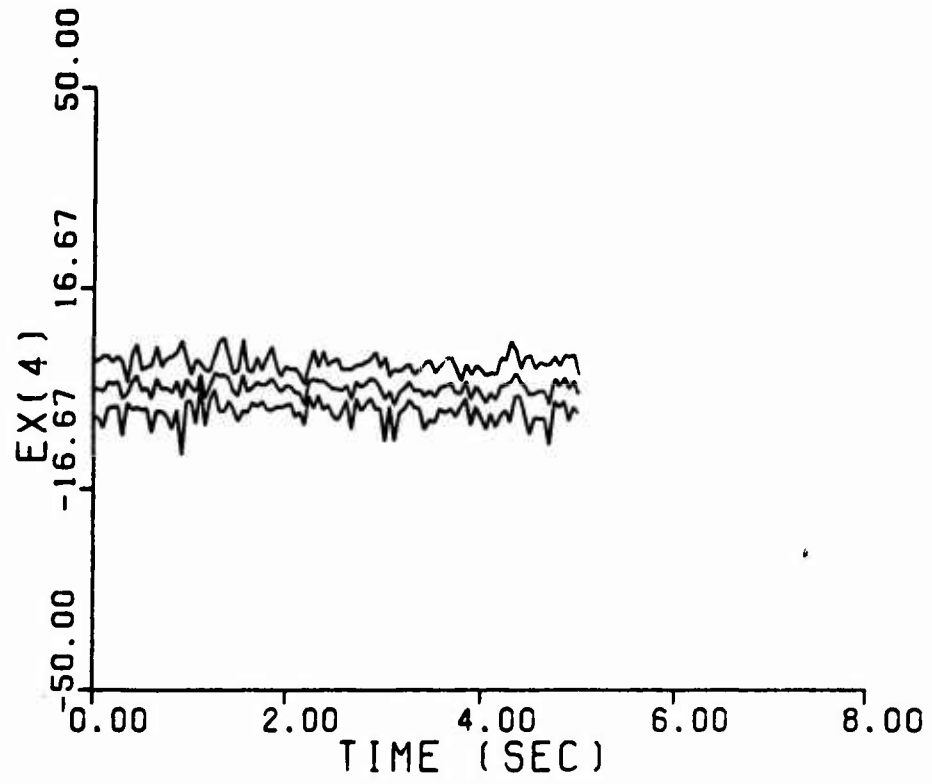

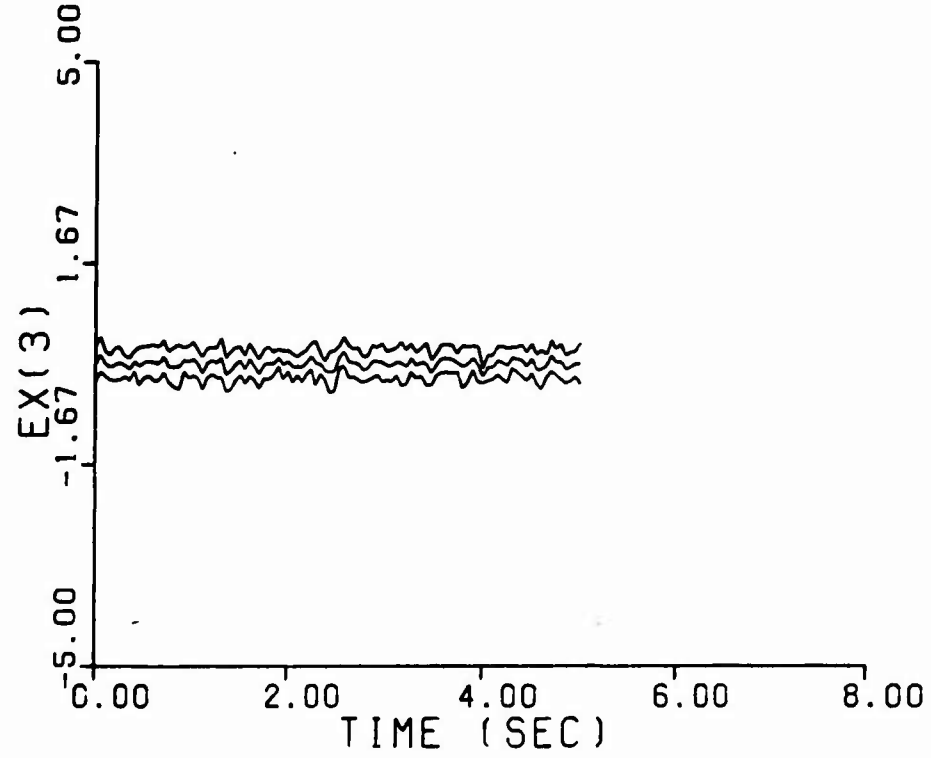

Fig. D-1--Continued

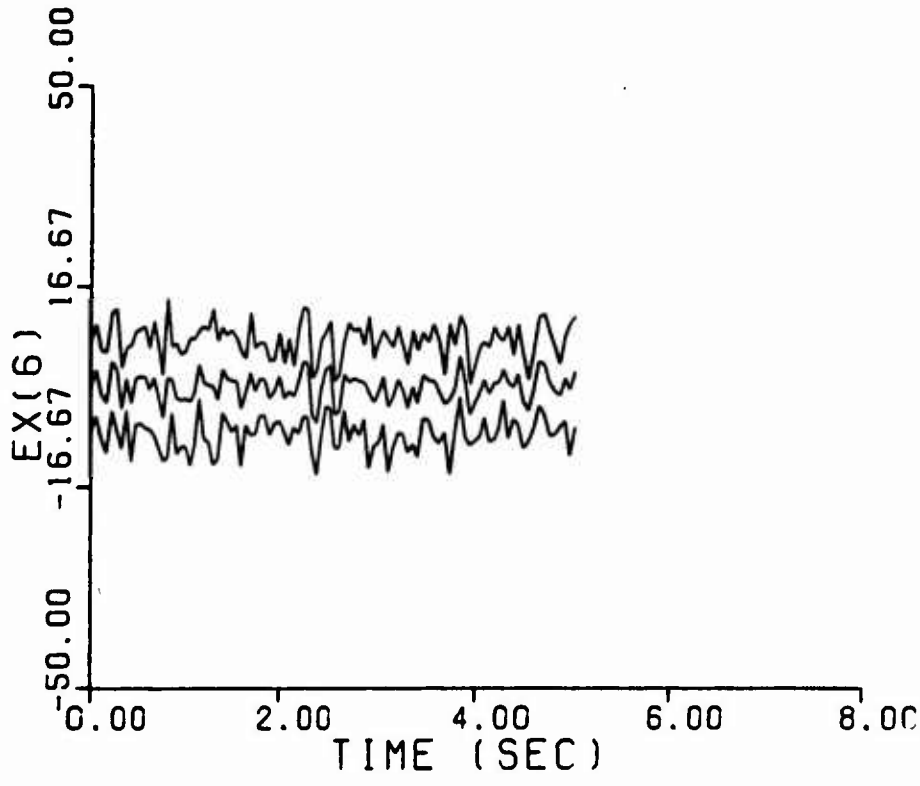

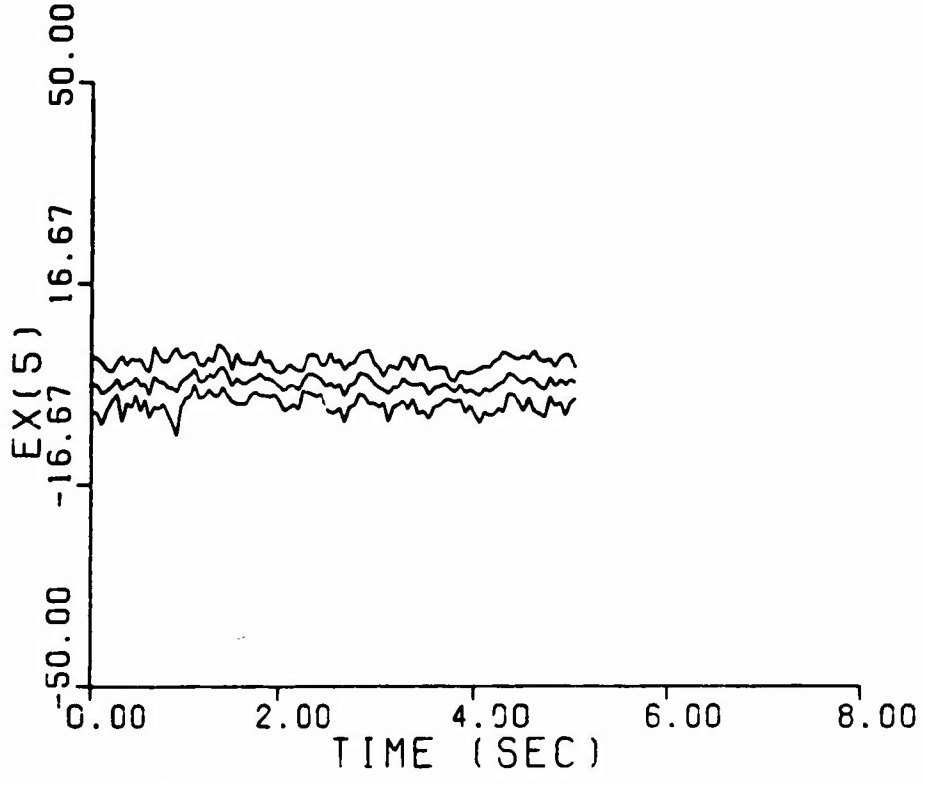

Fig. D-1--Continued

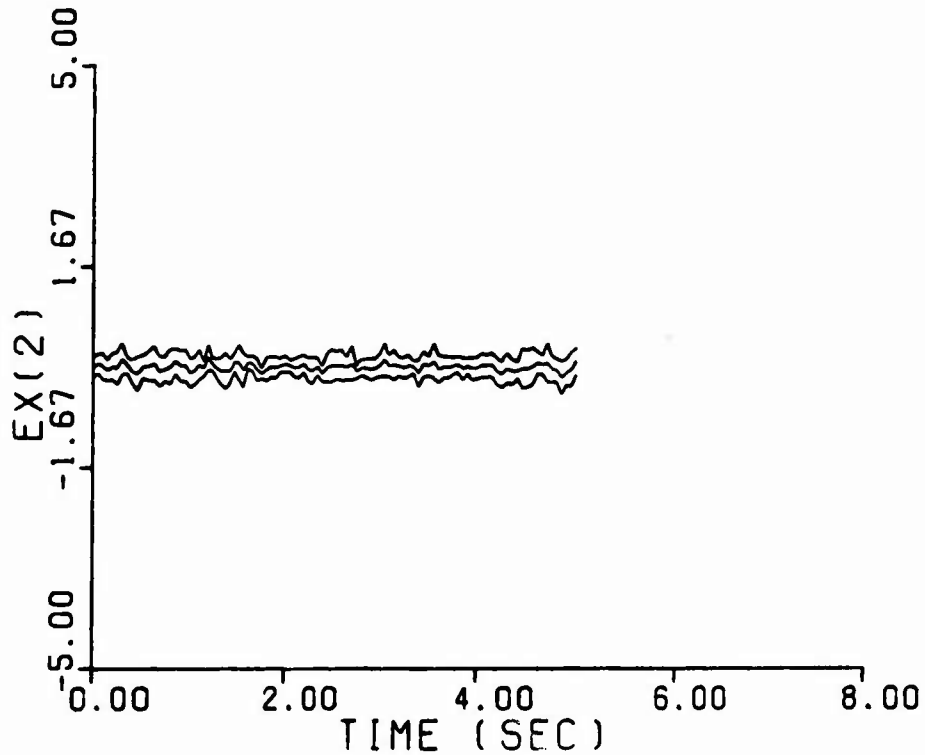

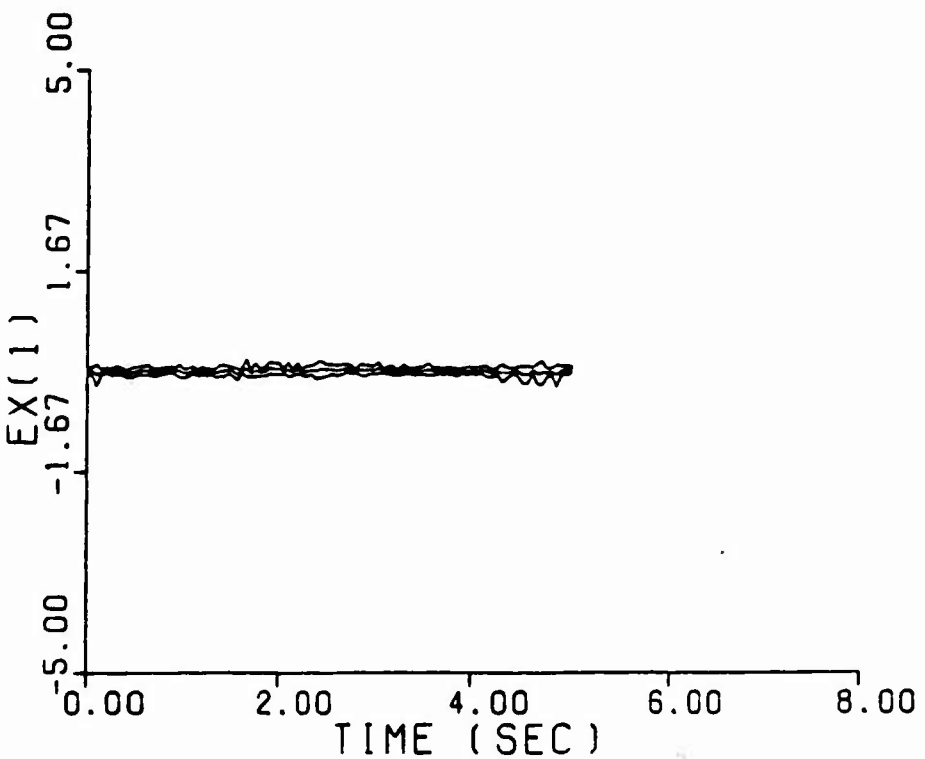

Fig. D-2. Truth Model 7,8

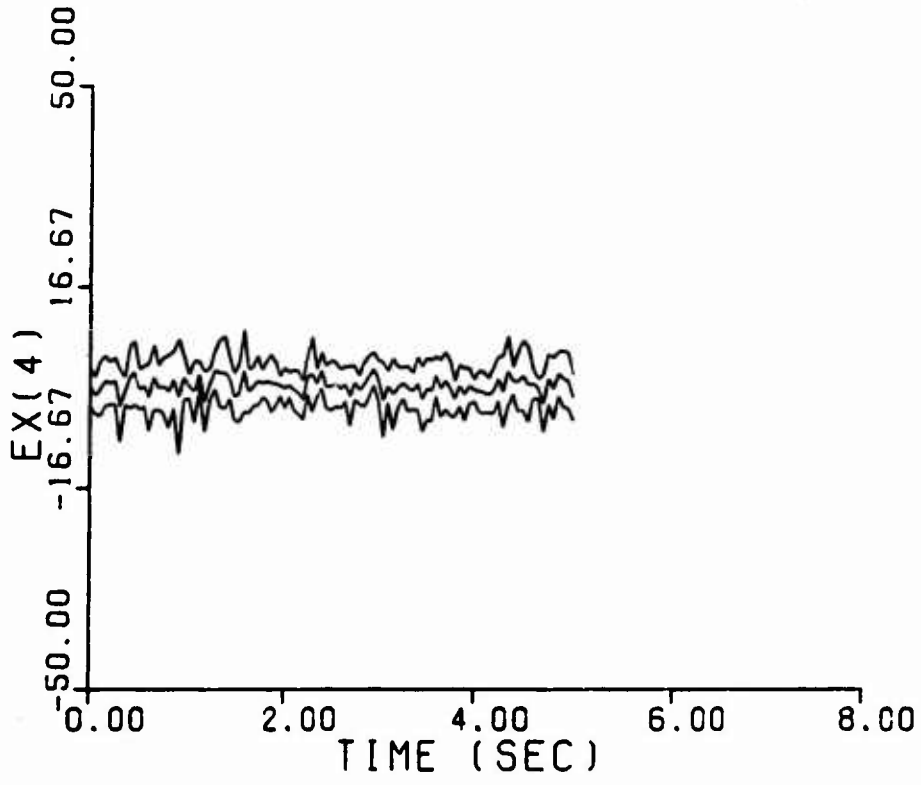

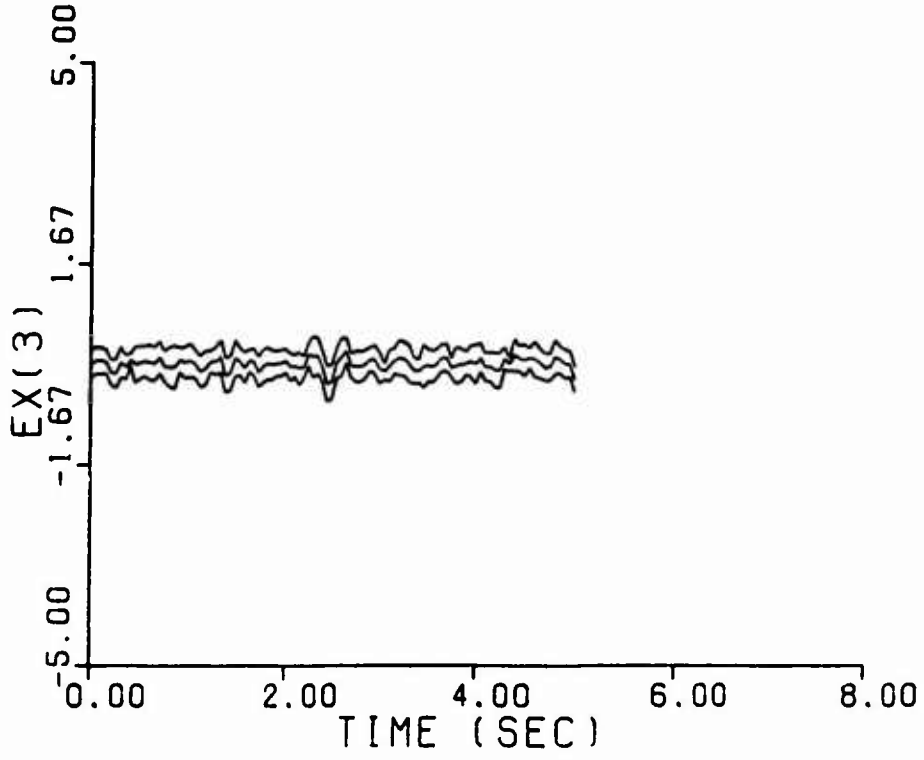

Fig. D-2--Continued

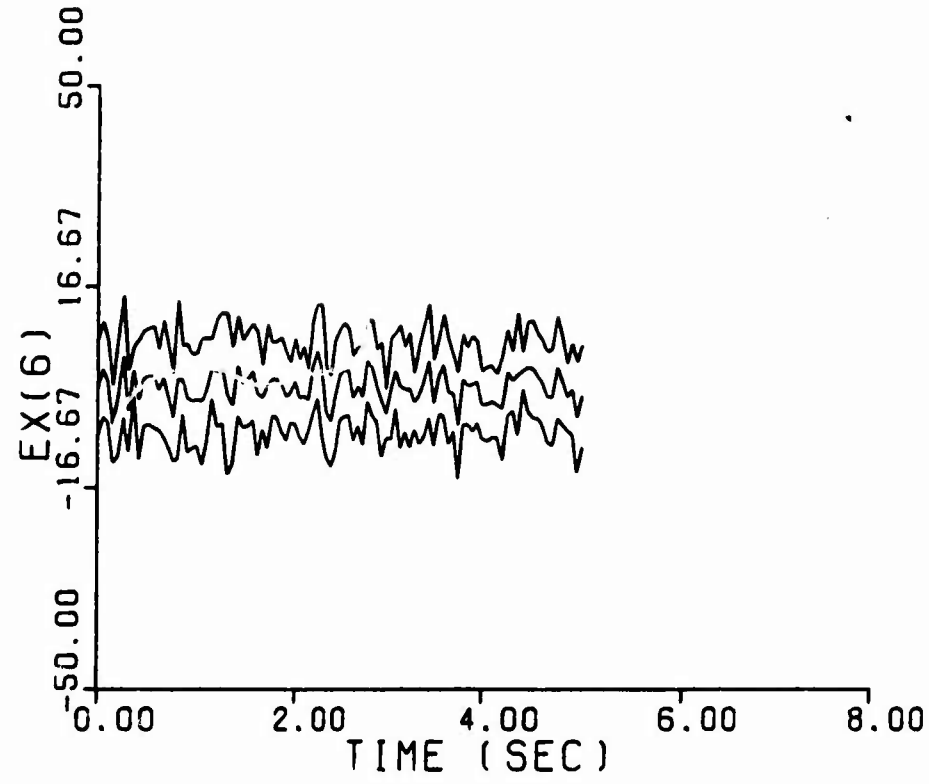

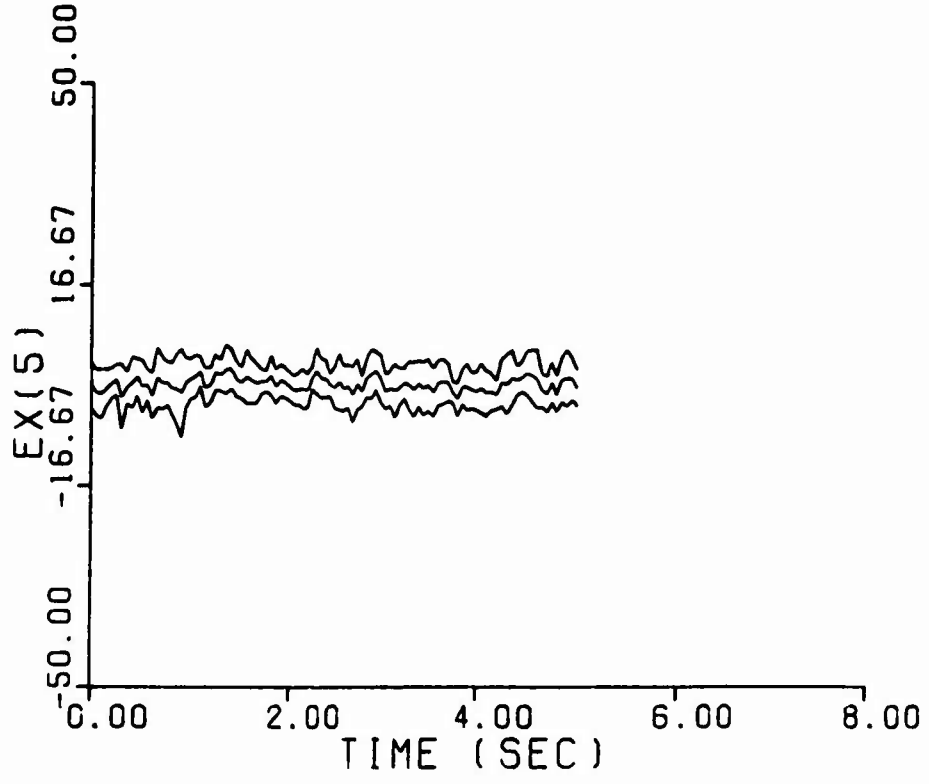

Fig. D-2- ontinued

Appendix E: Monte Carlo Simulation Plots of Fixed-Bank Multiple Model Adaptive Estimator

Appendix E contains plots reflecting the performance of the fixed-bank estimator at various discretizations and against various truth models. The magnitude of the dither signal is equal to 100 at a frequency of 30 rad/sec. The title of each figure indicates the parameter vector upon which the truth model is based.

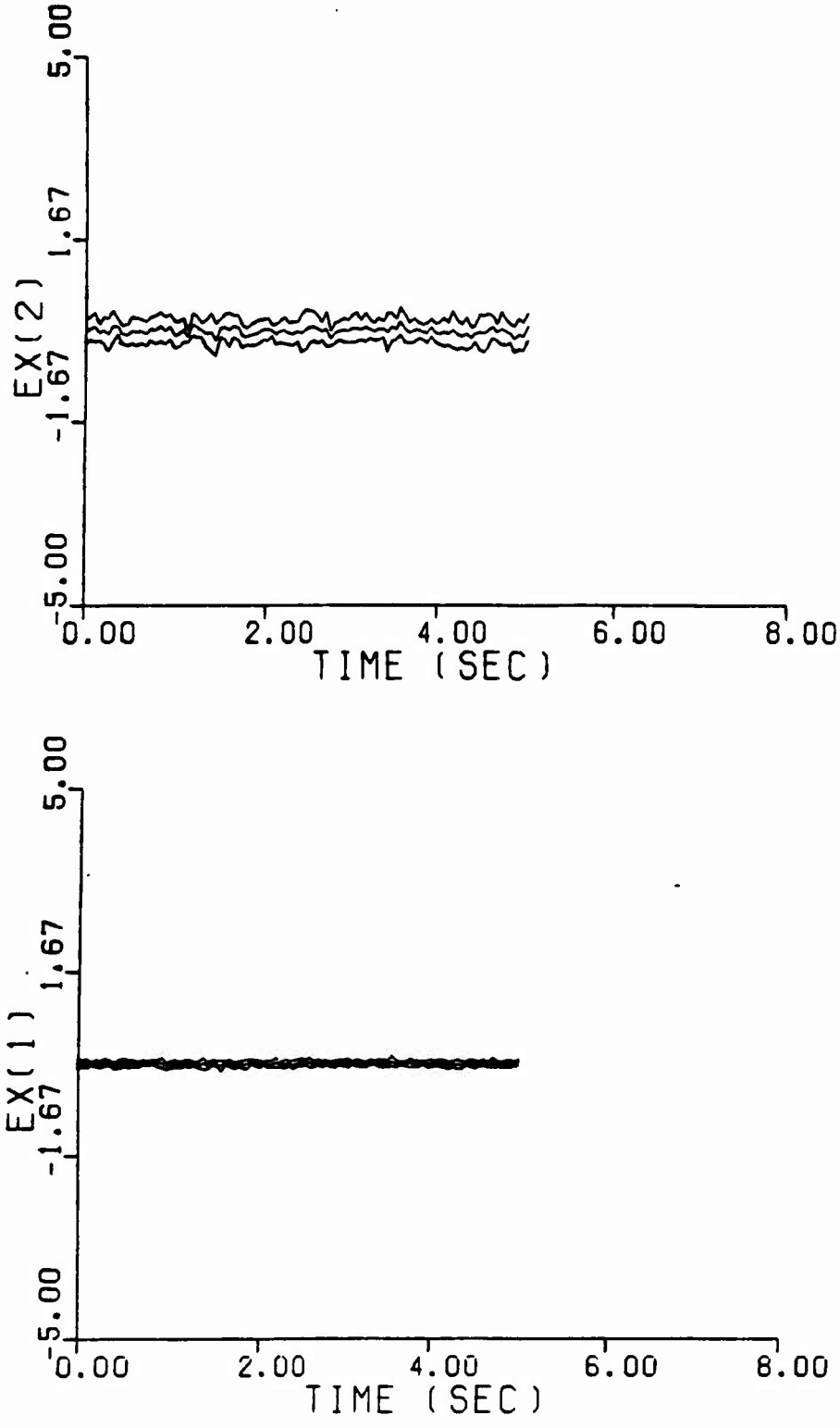

Fig. E-1. Discretization = 1, Truth = 5,5

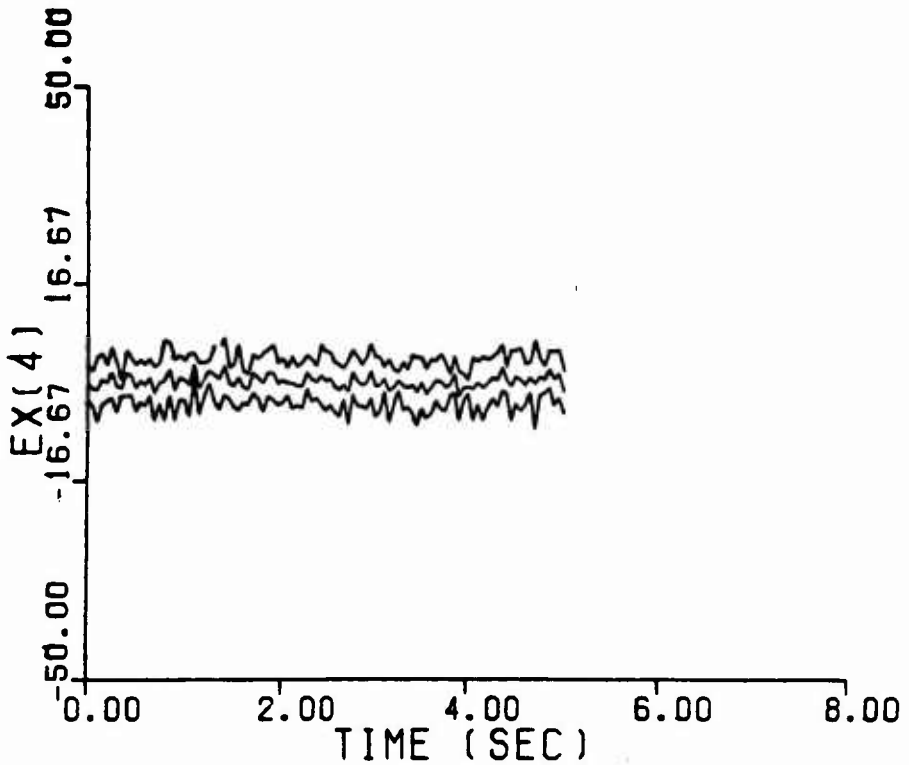

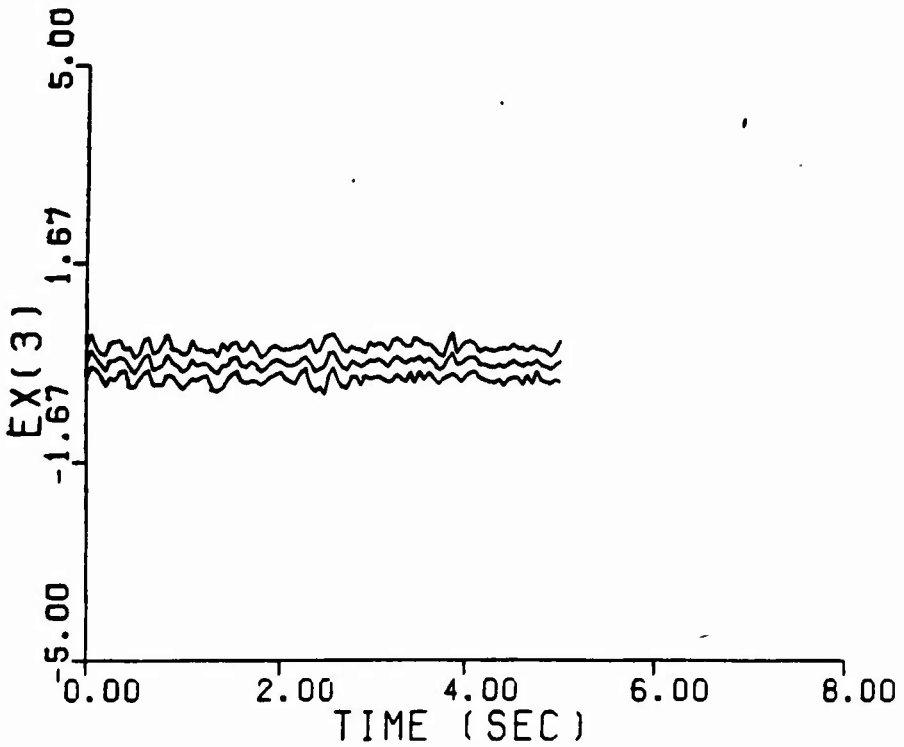

Fig. E-1--Continued

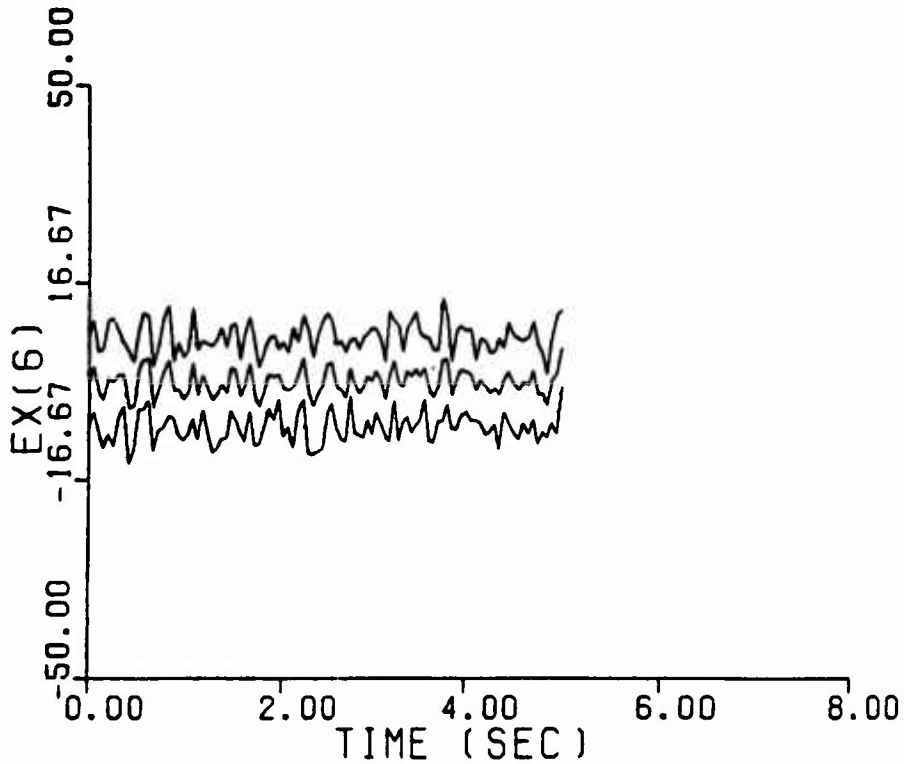

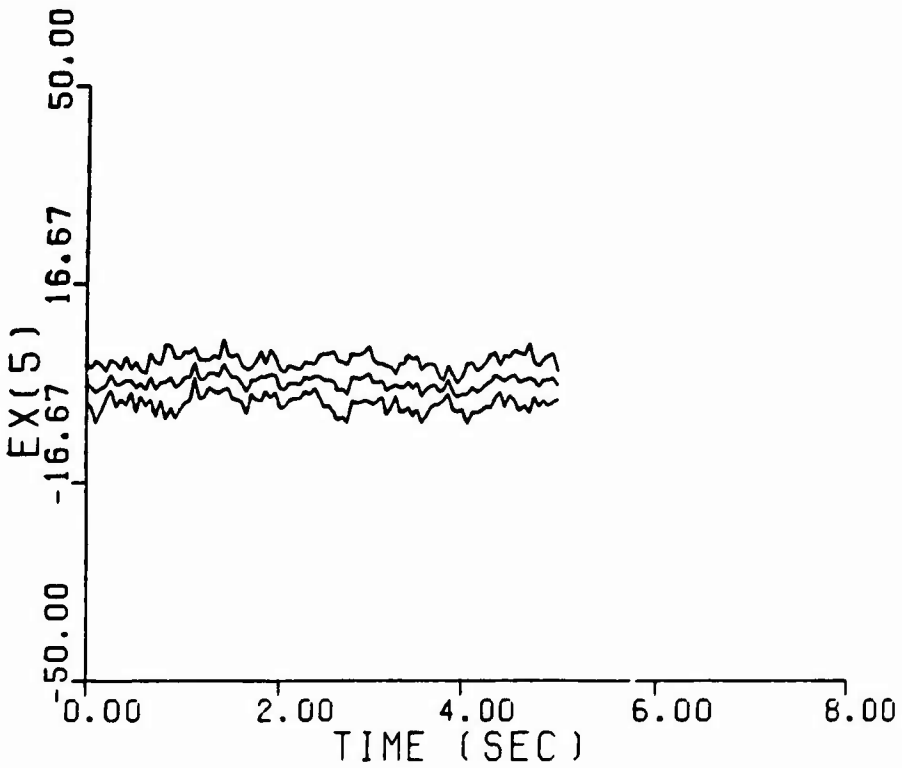

Fig. E-1--Continued

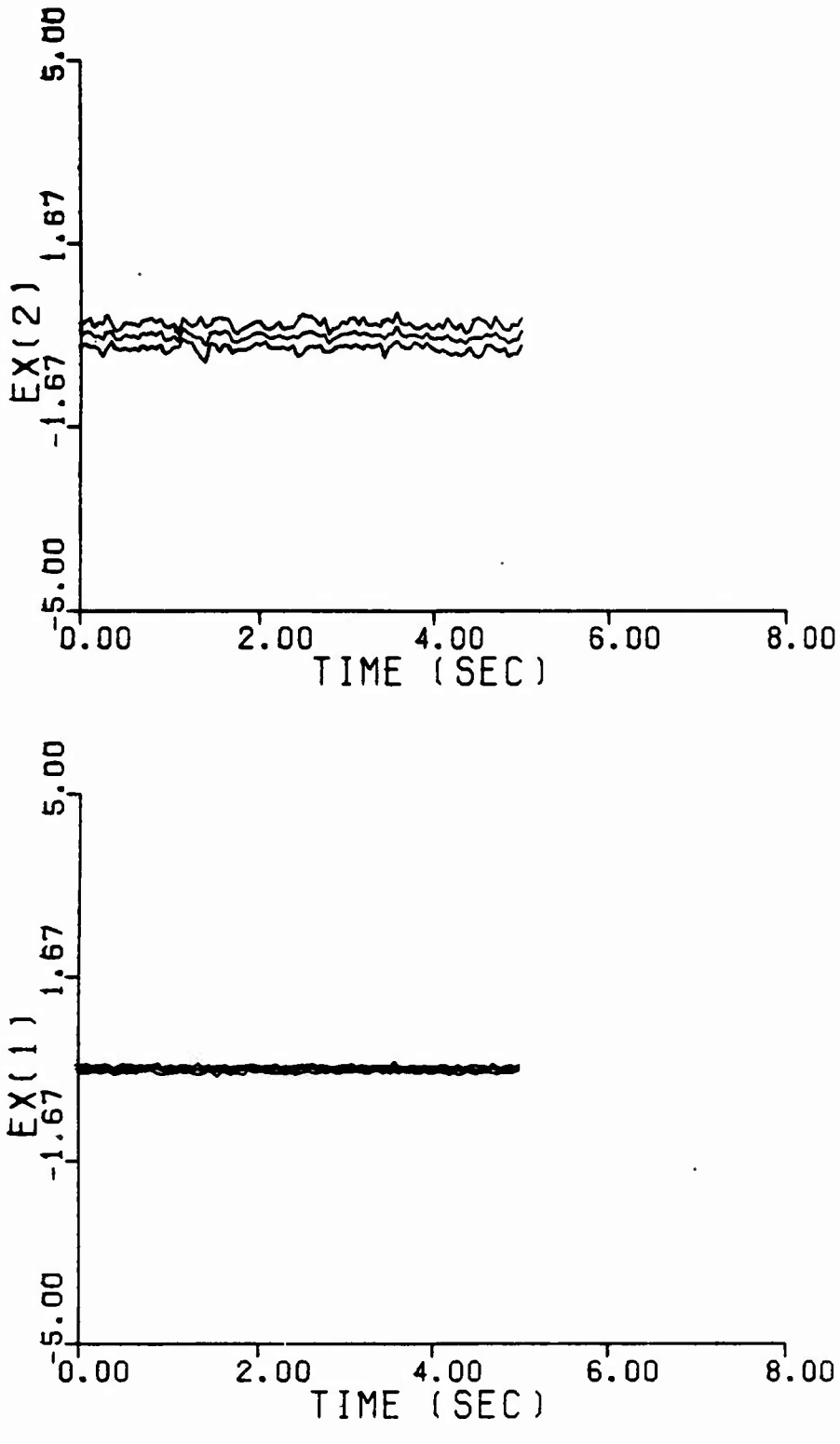

Fig. E-2. Discretization = 1, Truth = 3,3

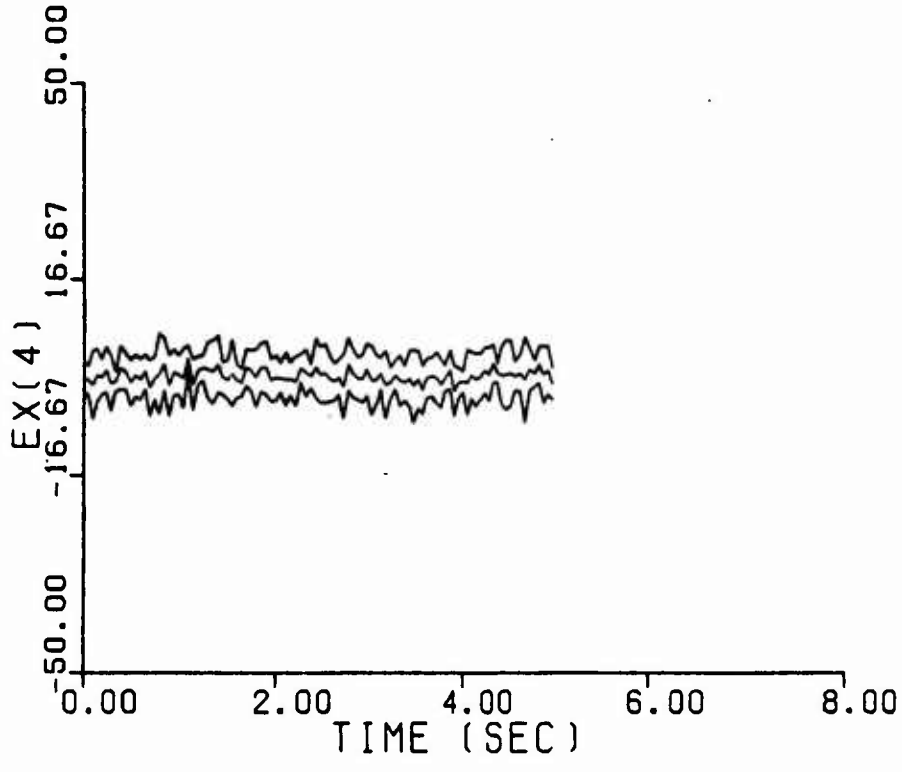

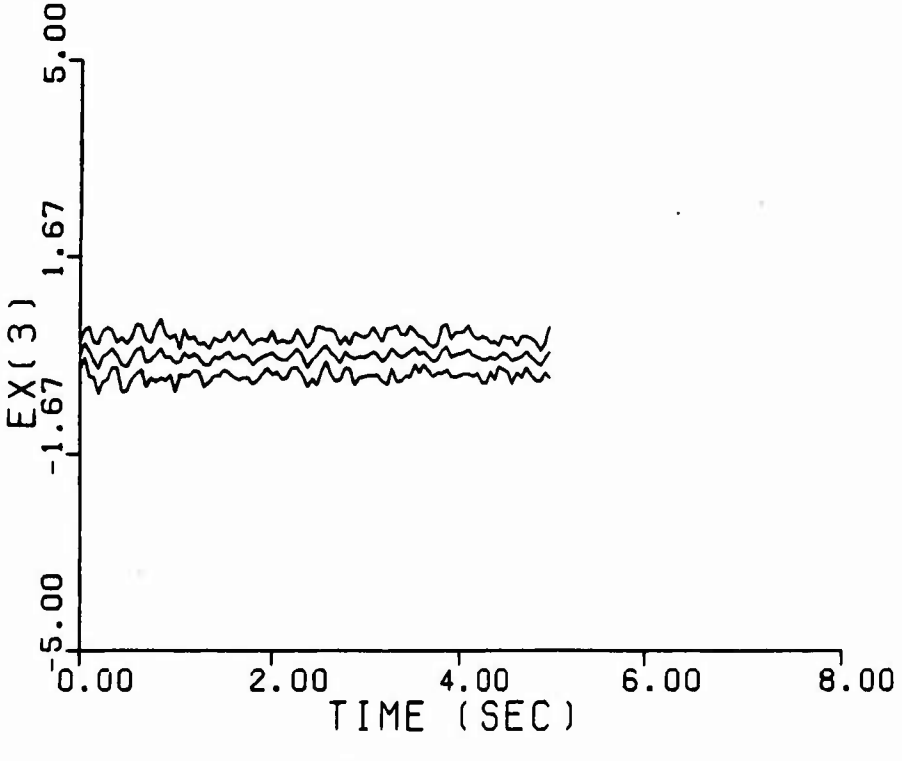

Fig. E-2--Continued

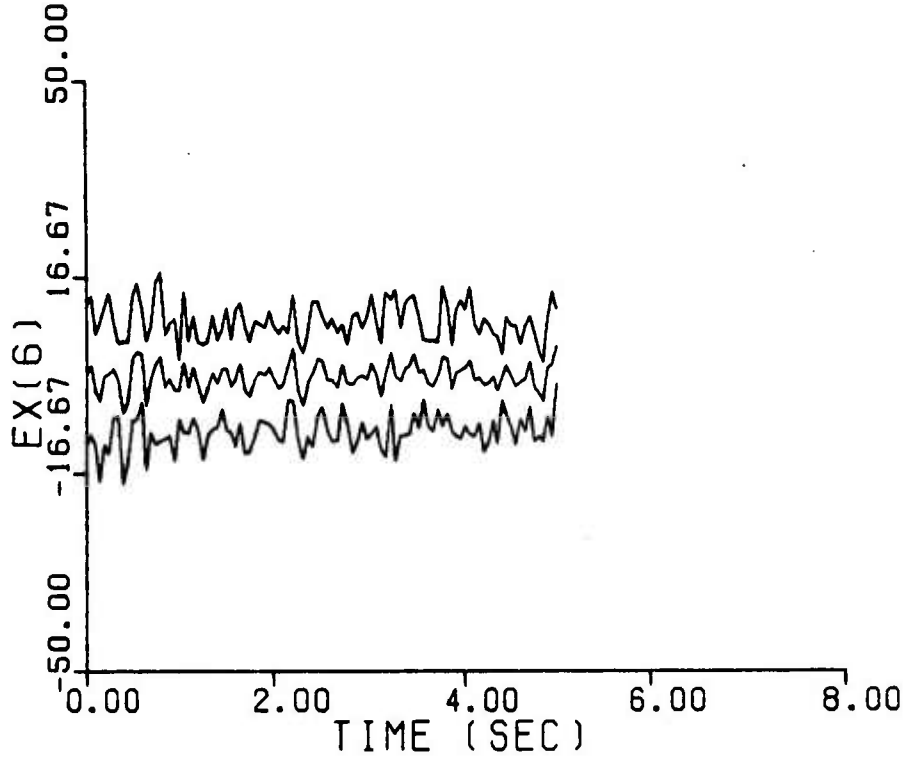

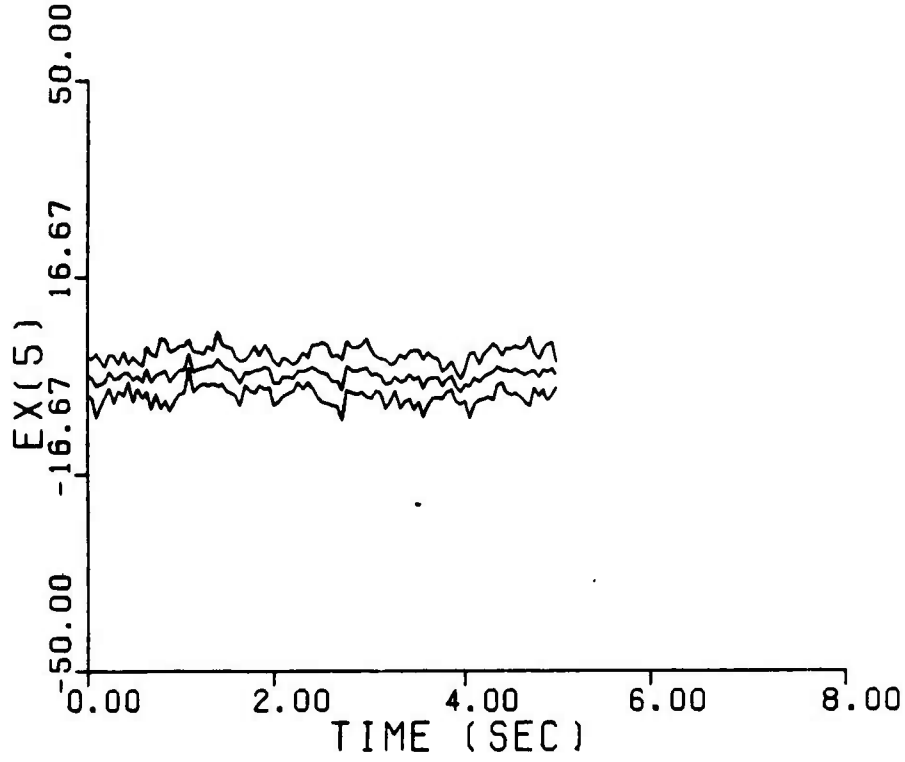

Fig. E-2--Continued

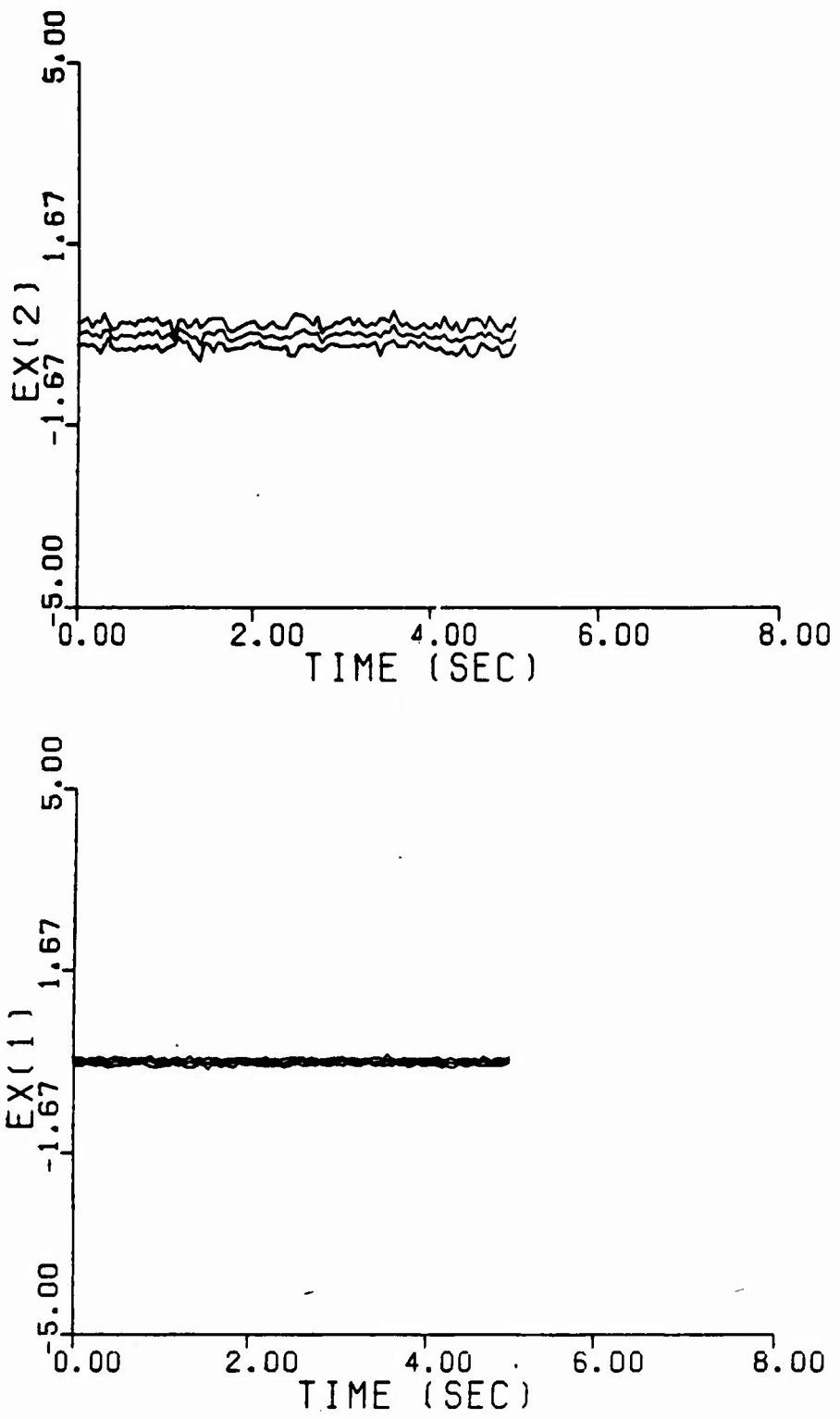

Fig. E-3. Discretization = 1, Truth = 7,3

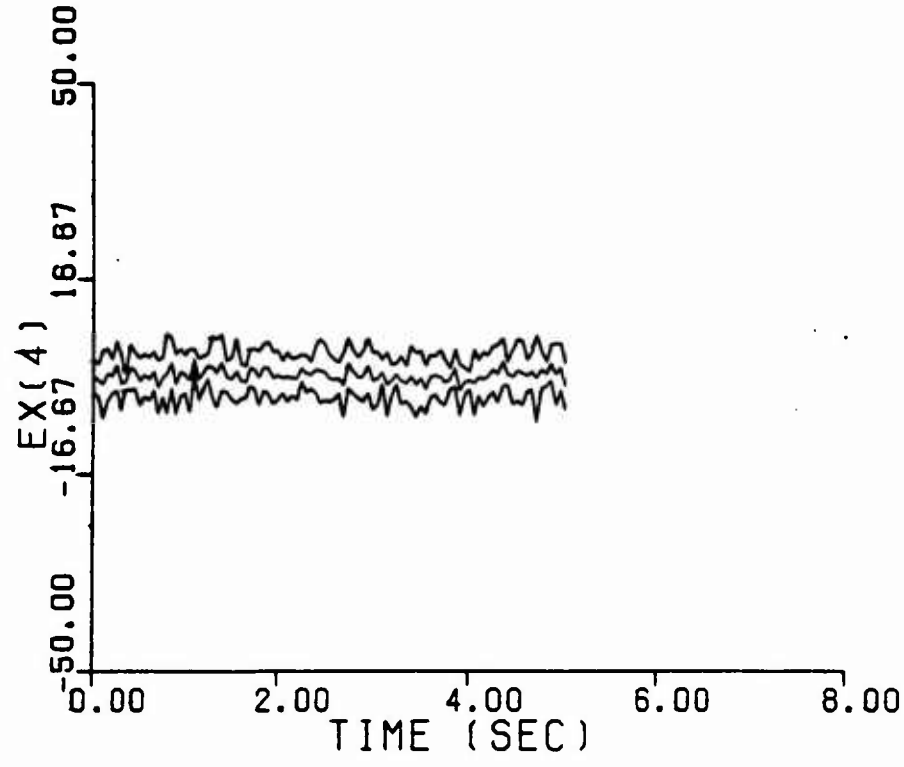

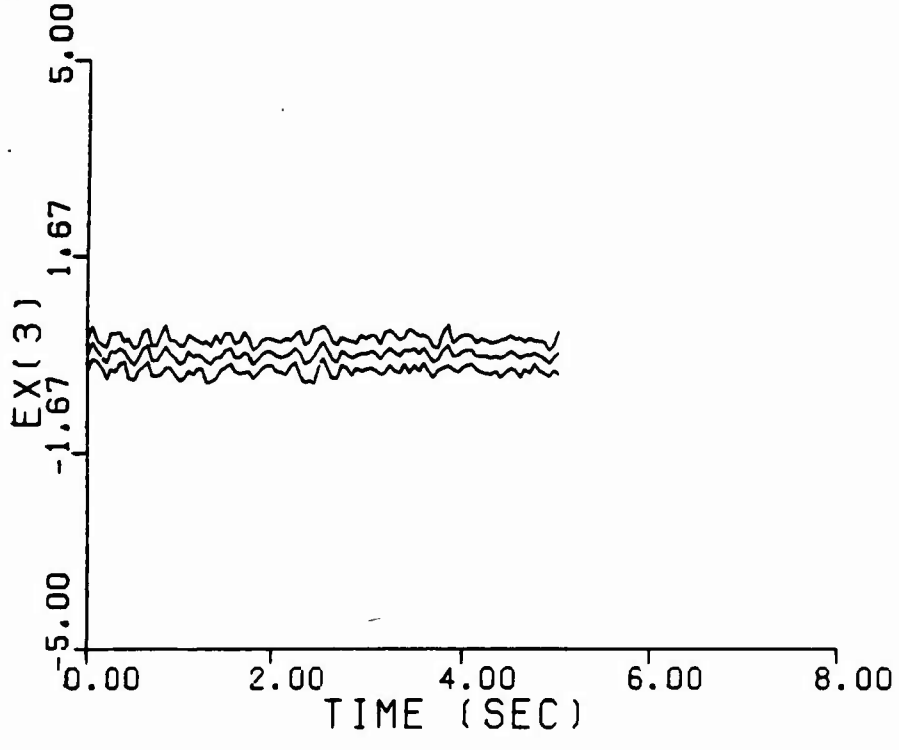

Fig. E-3--Continued

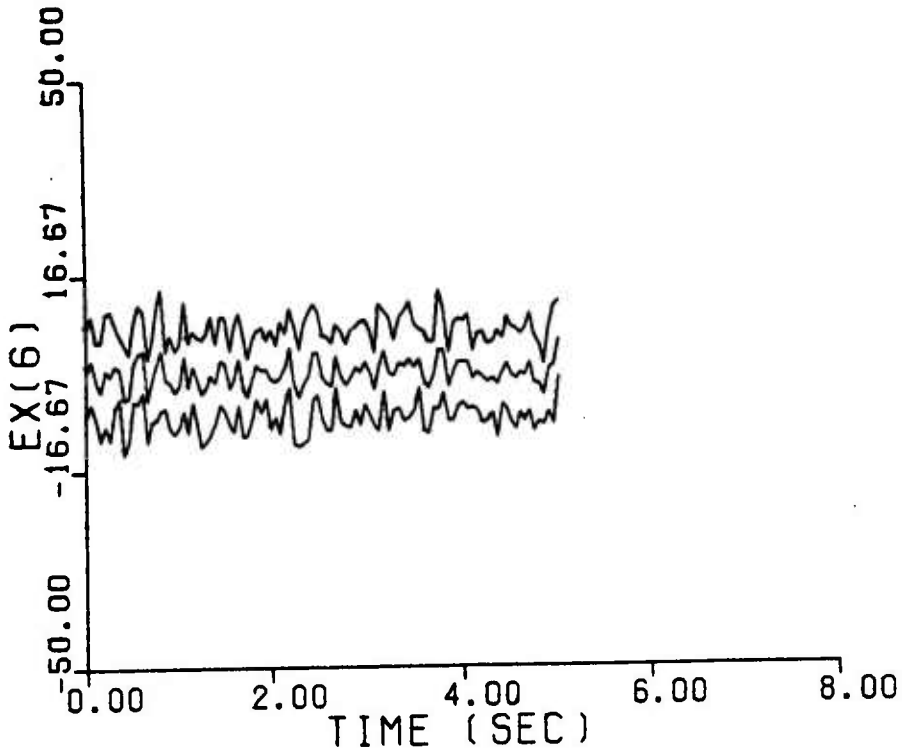

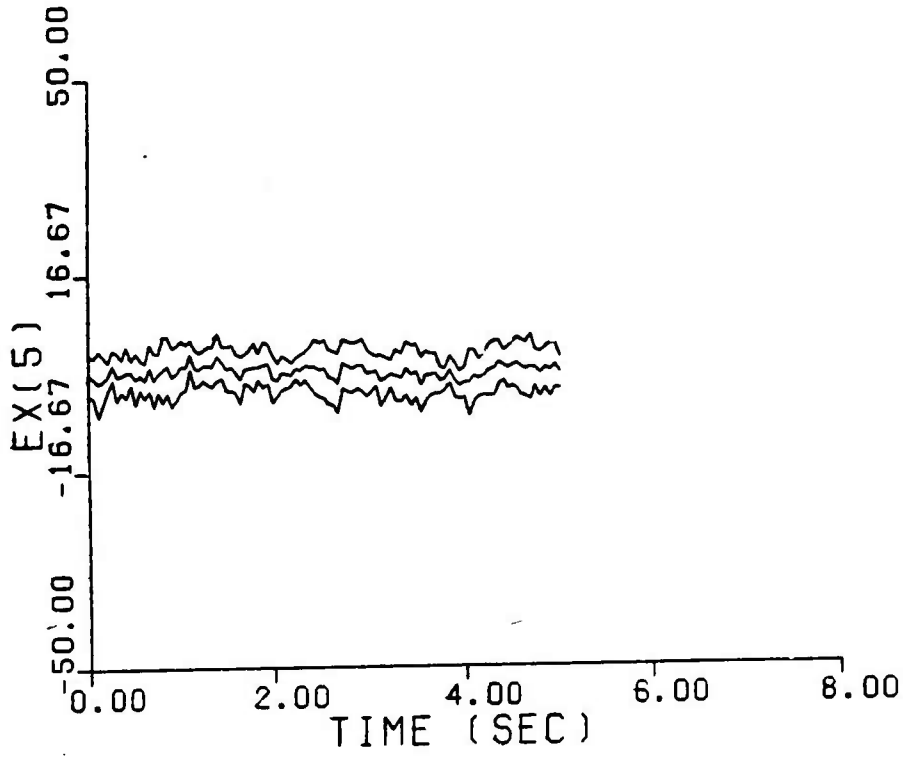

Fig. E-3--Continued

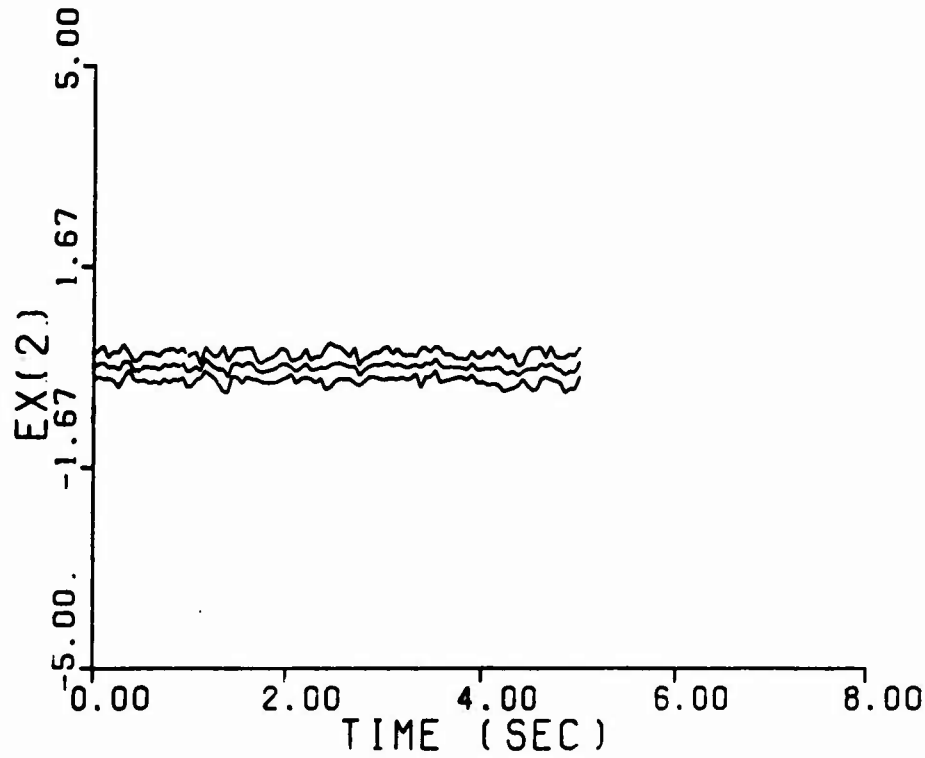

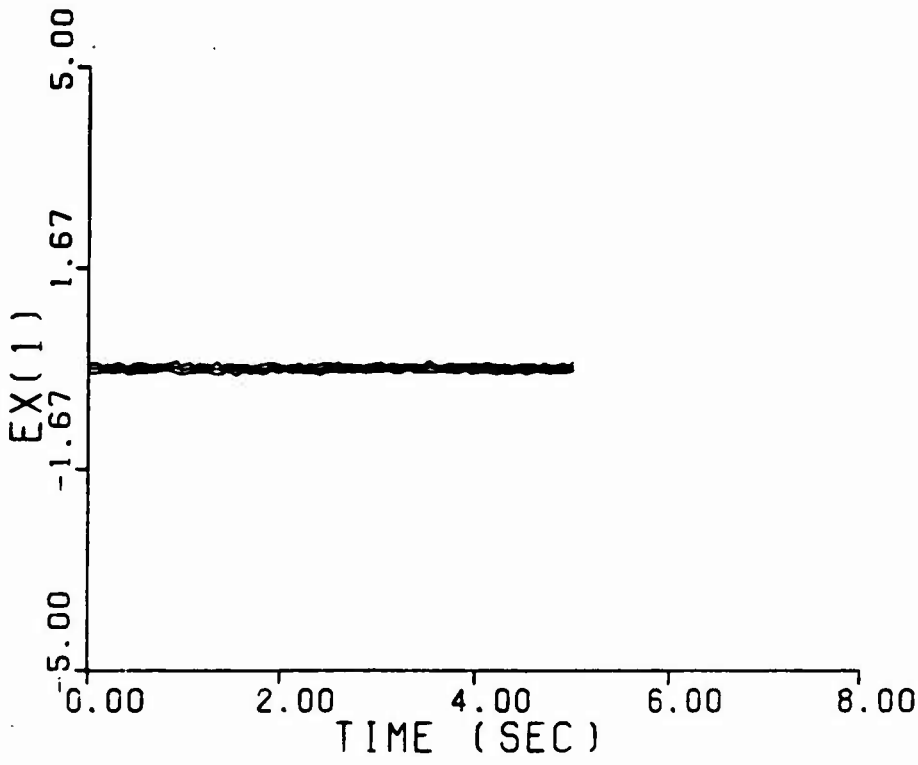

Fig. E-4. Discretization = 1, Truth = 3,7

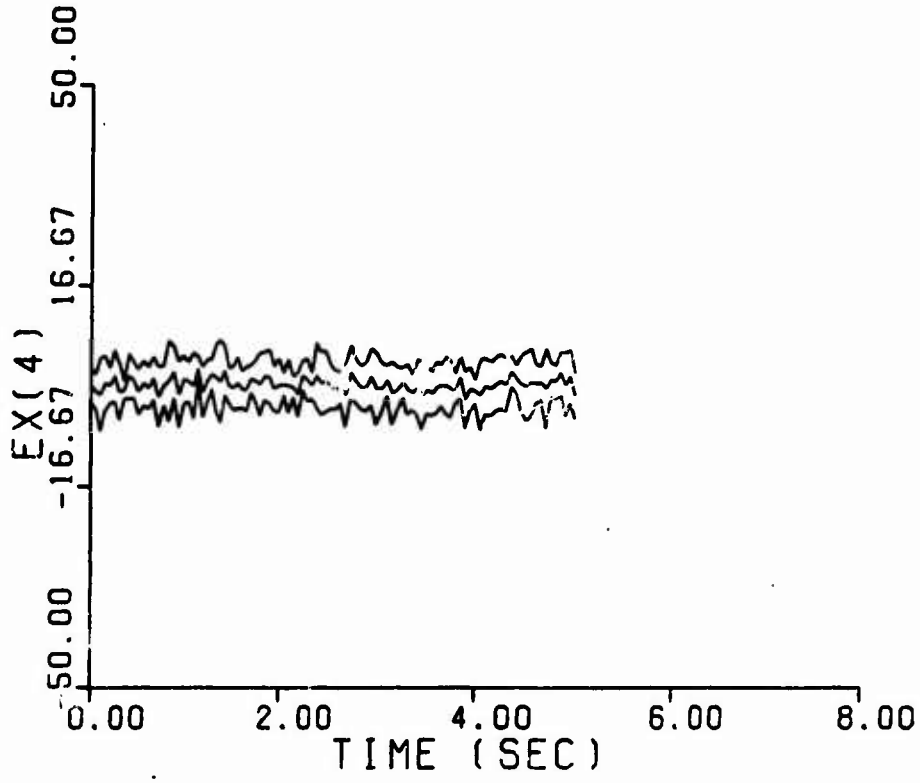

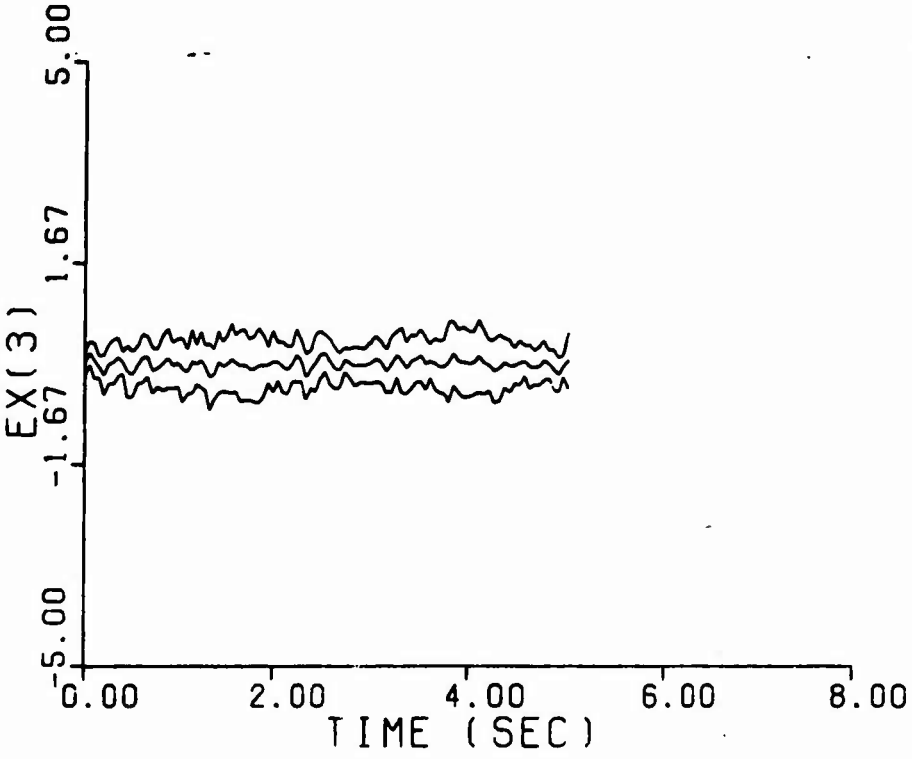

Fig. E-4--Continued

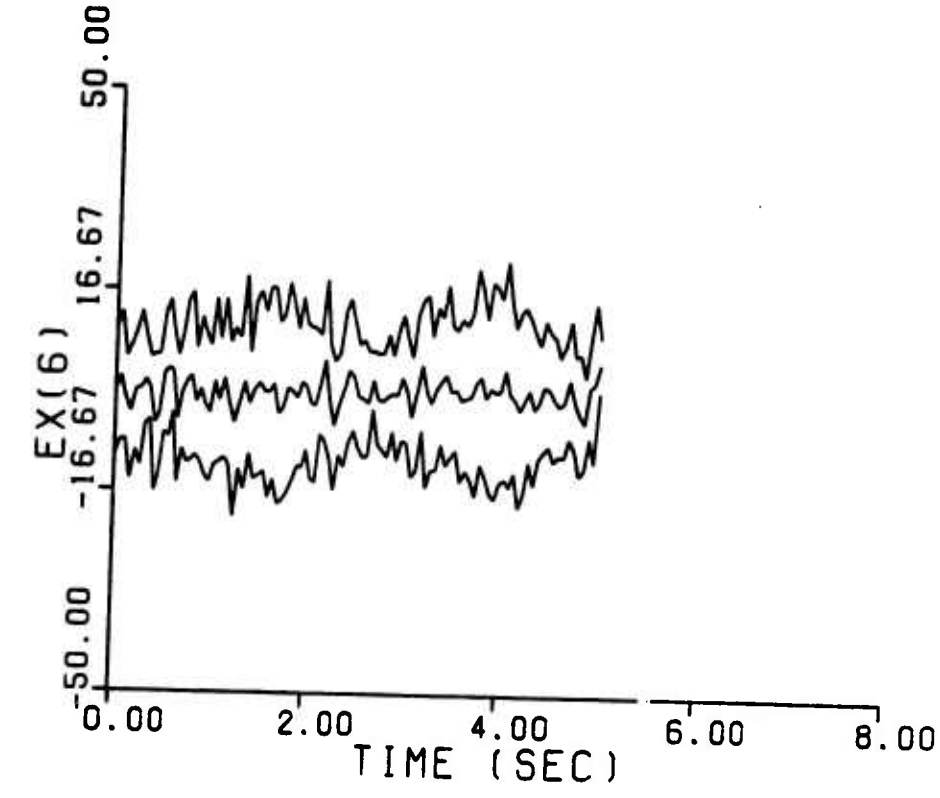

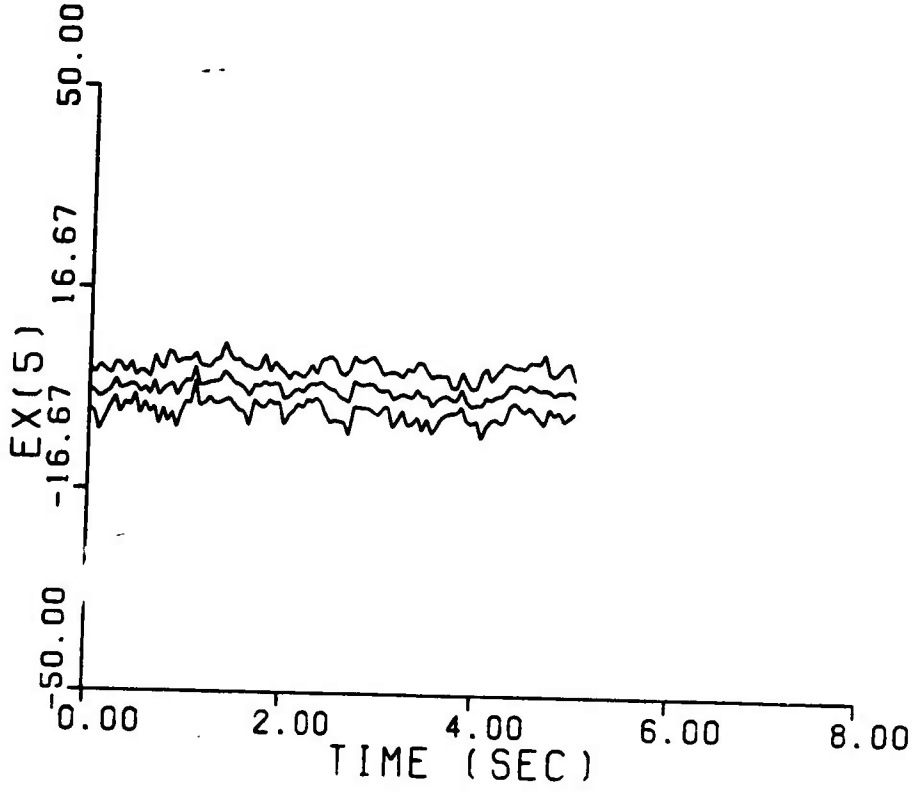

Fig. E-4--Continued

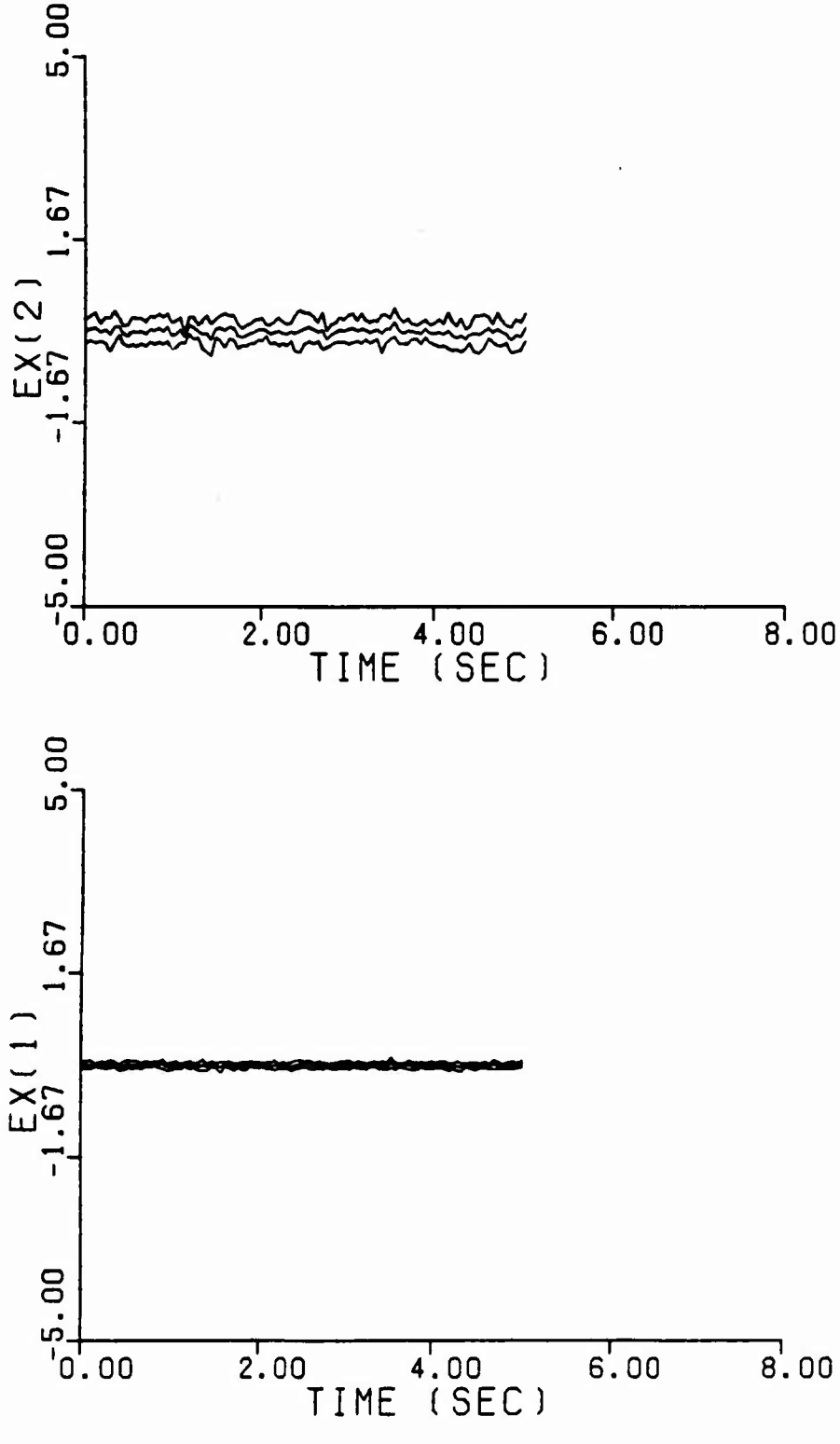

Fig. E-5. Discretization = 1, Truth = 7,7

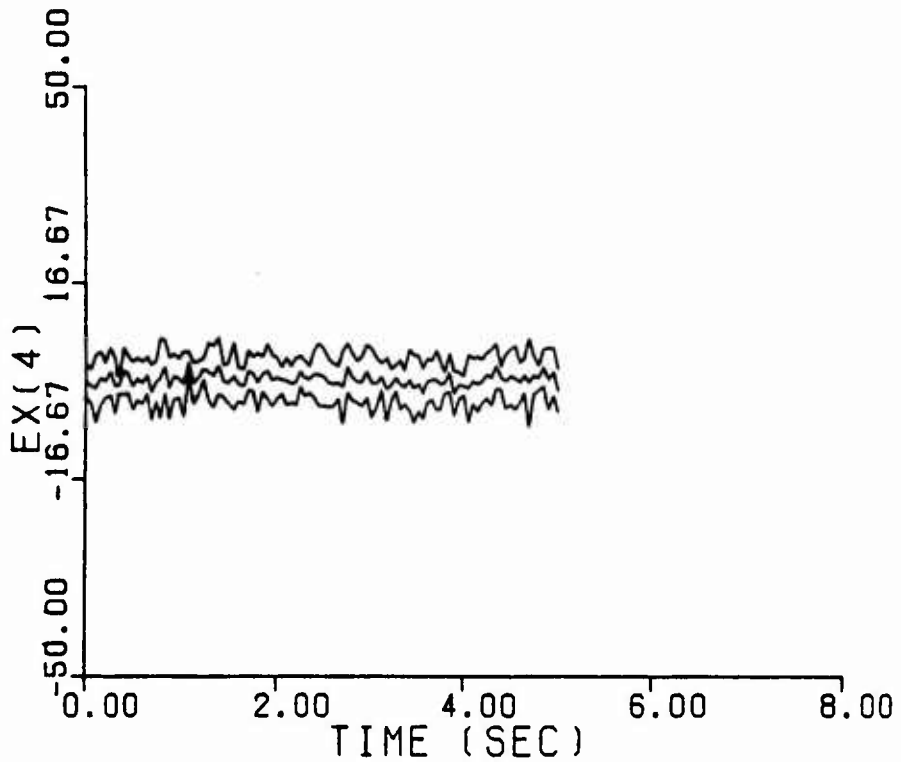

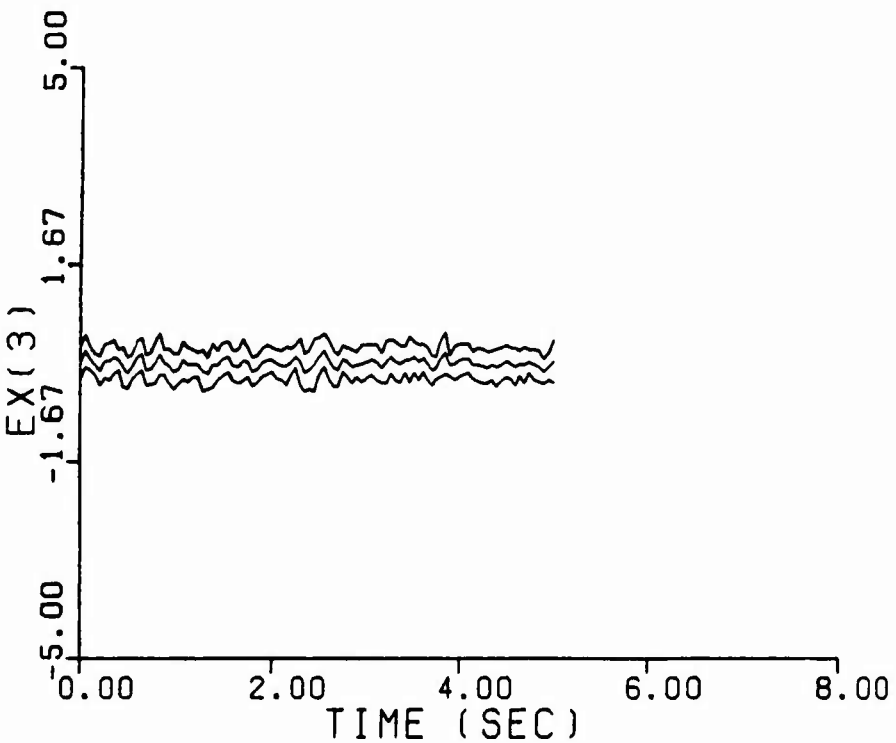

Fig. E-5--Continued

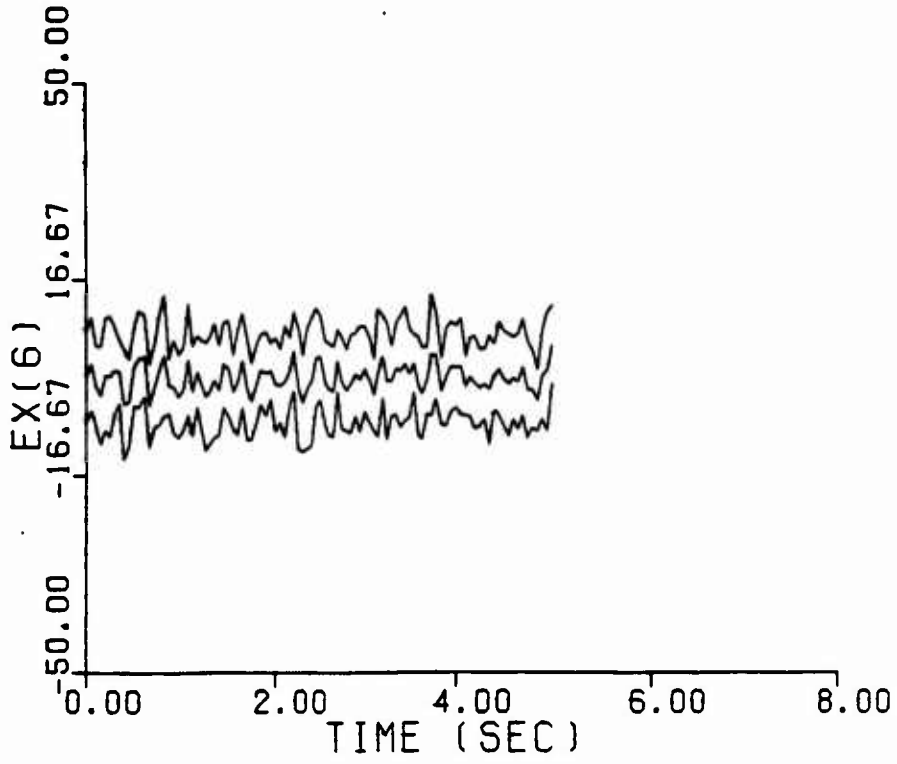

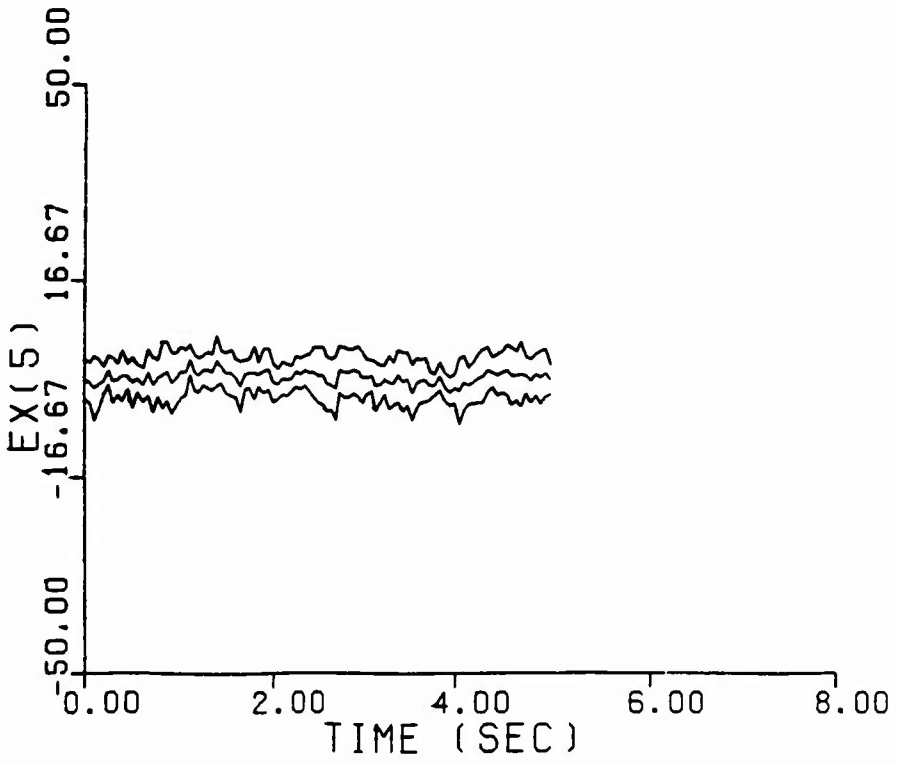

Fig. E-5--Continued

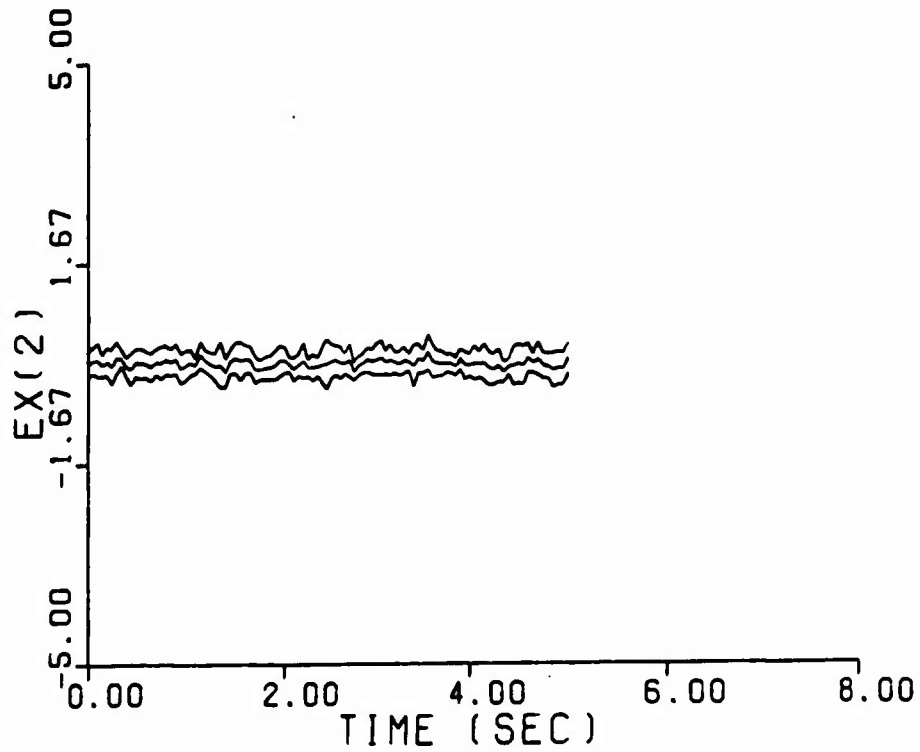

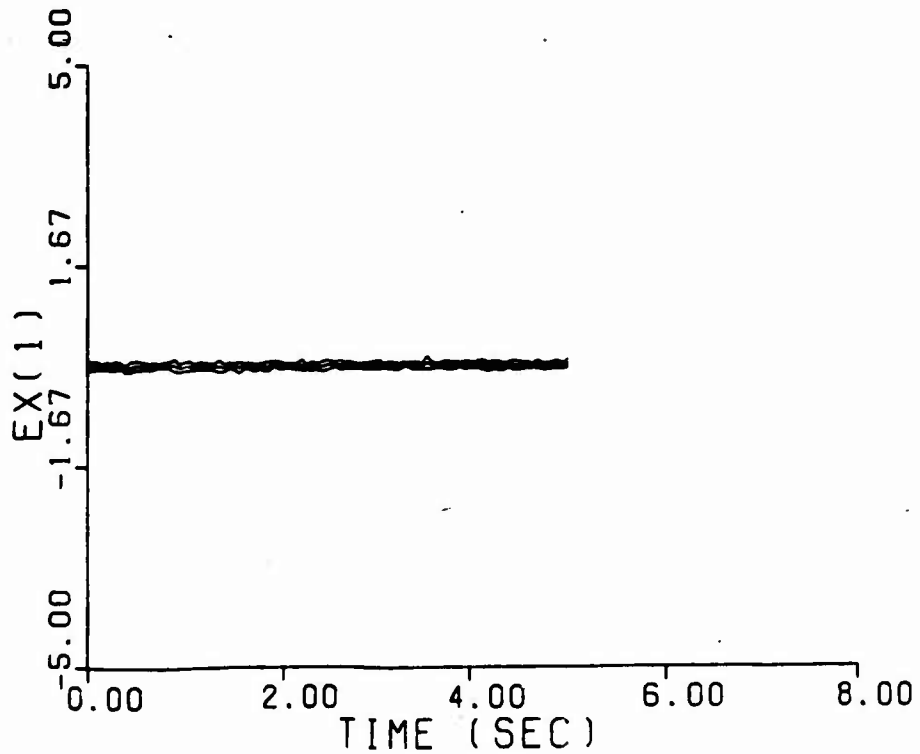

Fig. E-6. Discretization = 2, Truth = 3,7

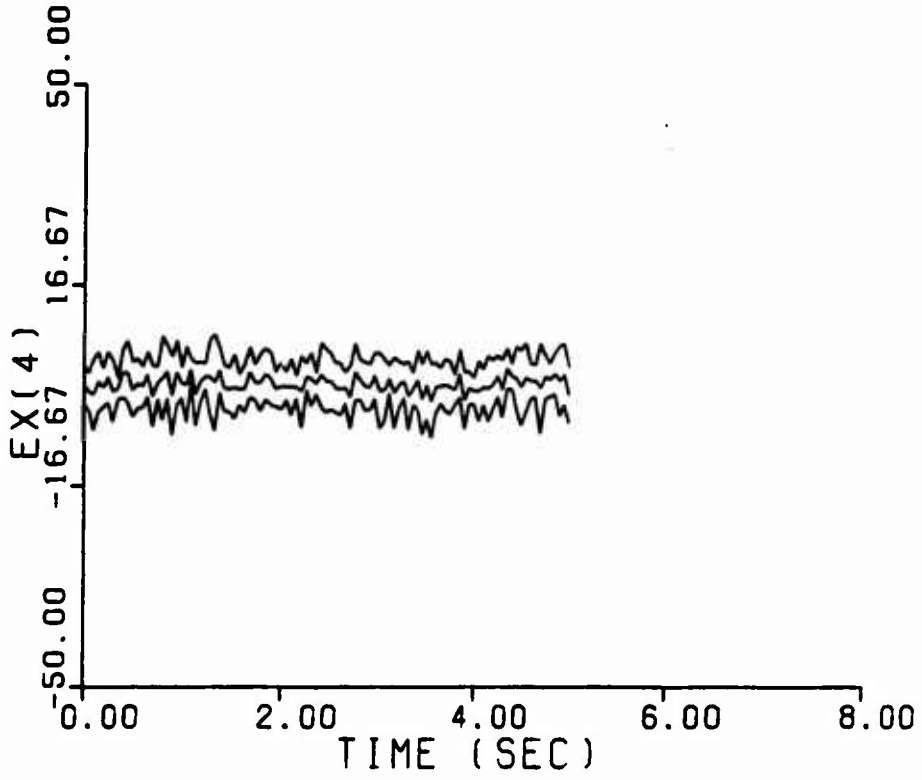

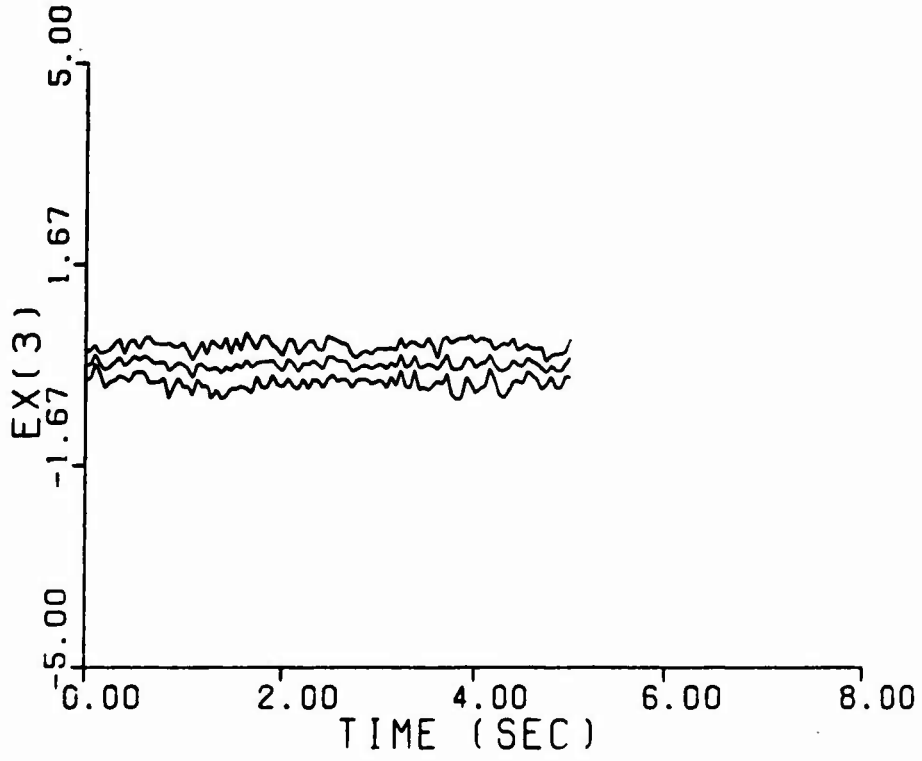

Fig. E-6--Continued

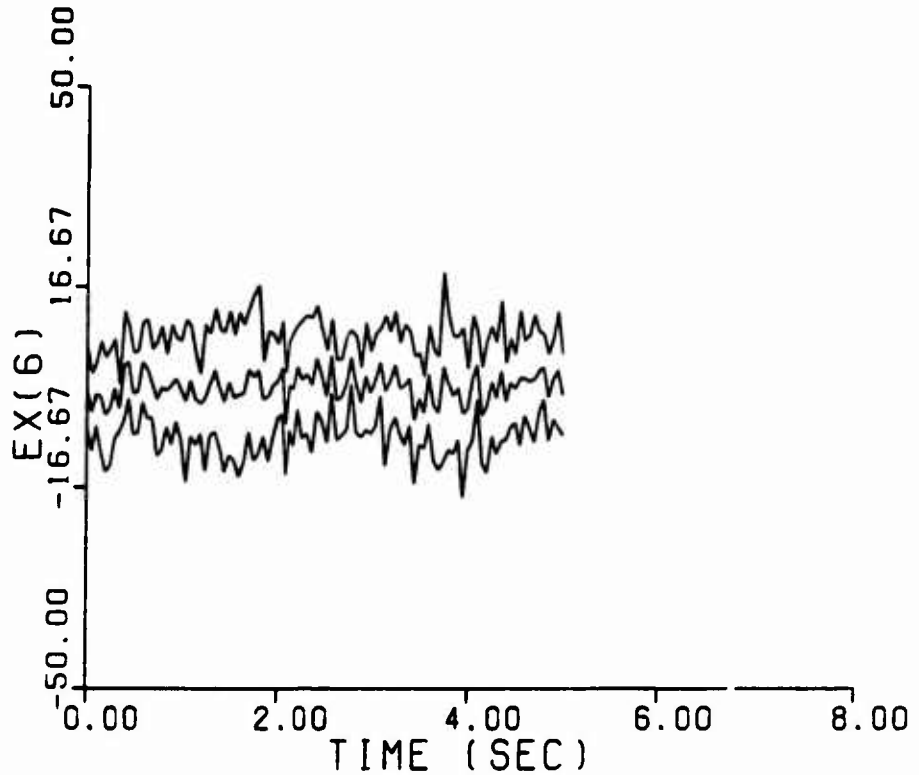

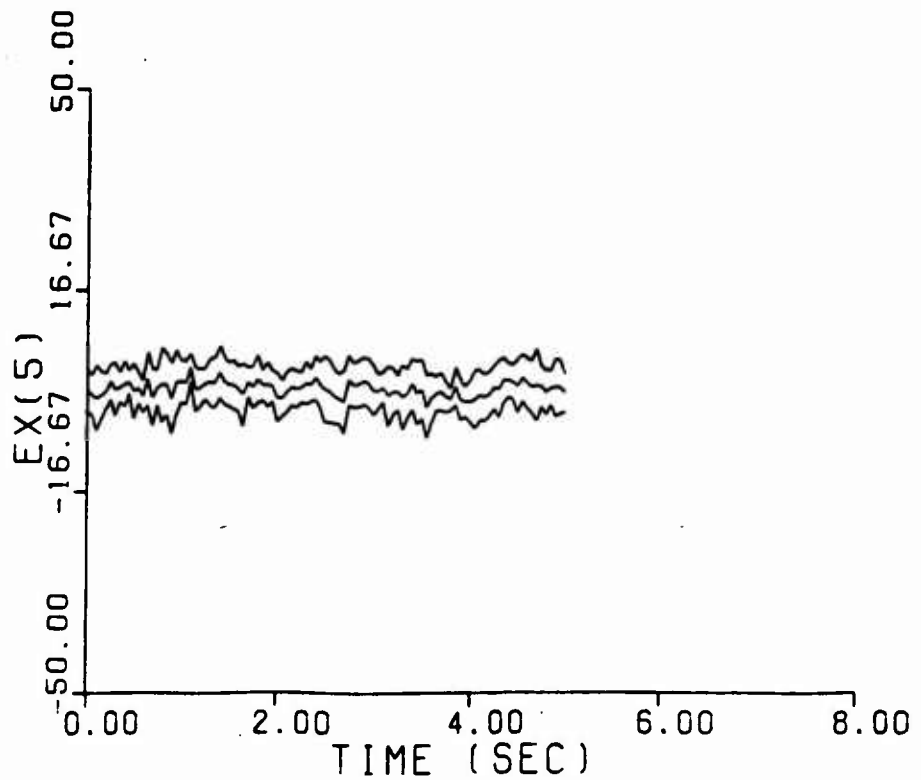

Fig. E-6--Continued

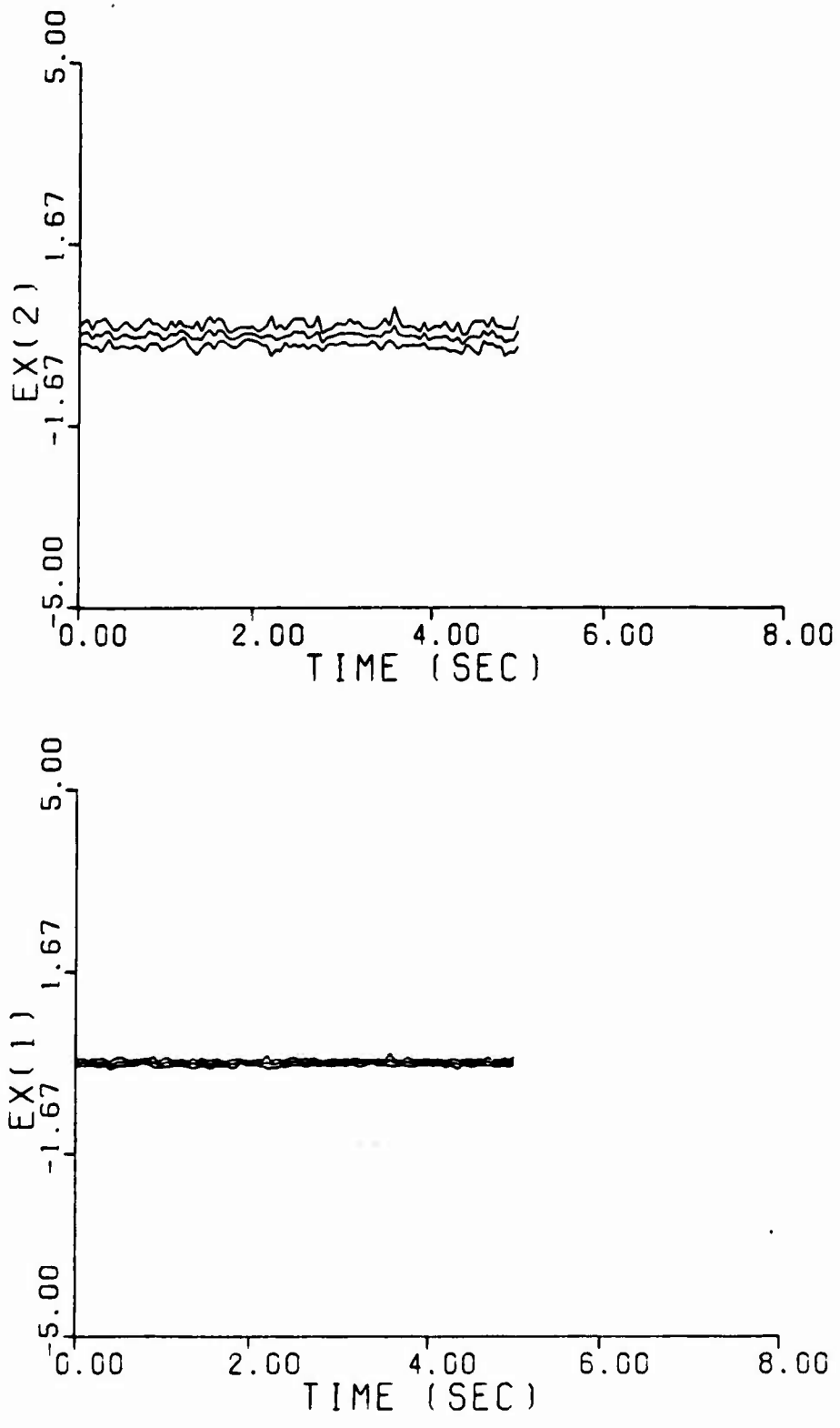

Fig. E-7. Discretization = 4, Truth = 5,5

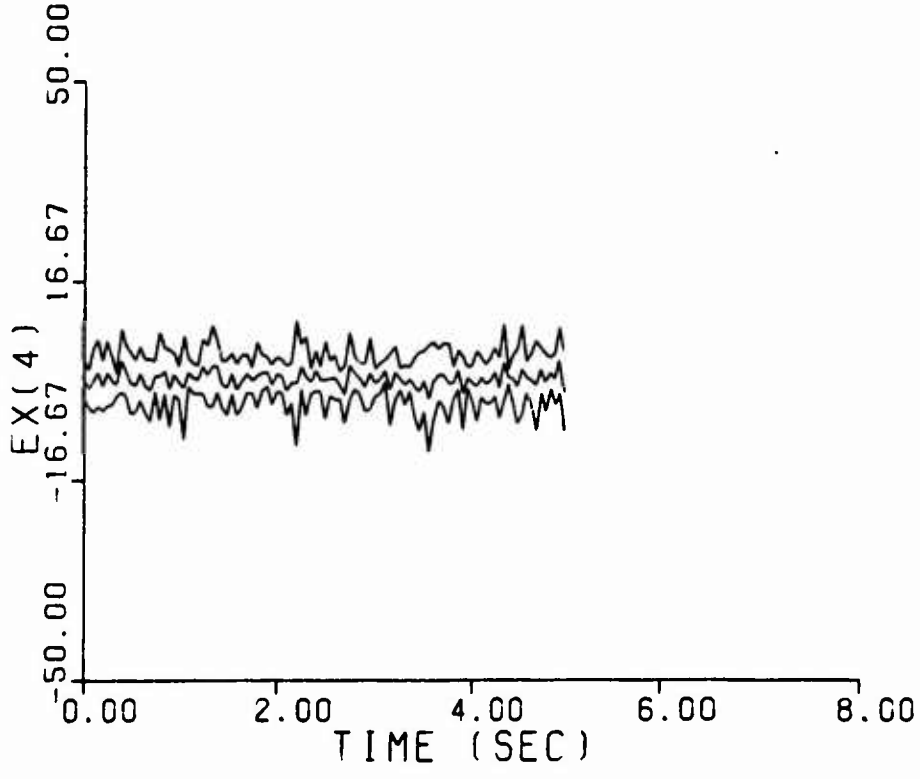

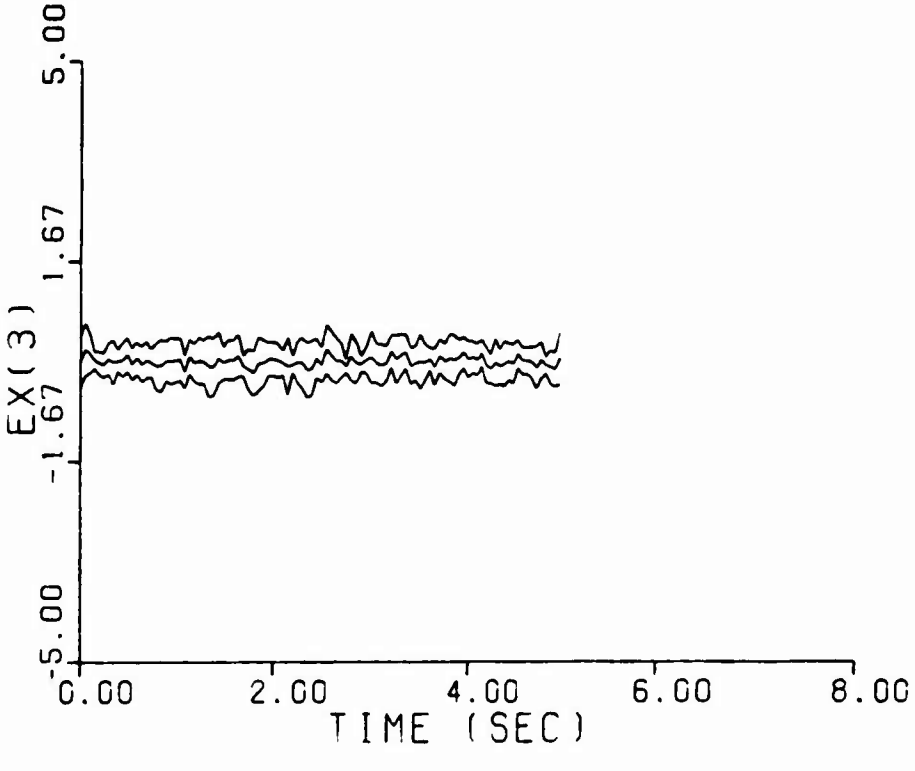

Fig. E-7--Continued

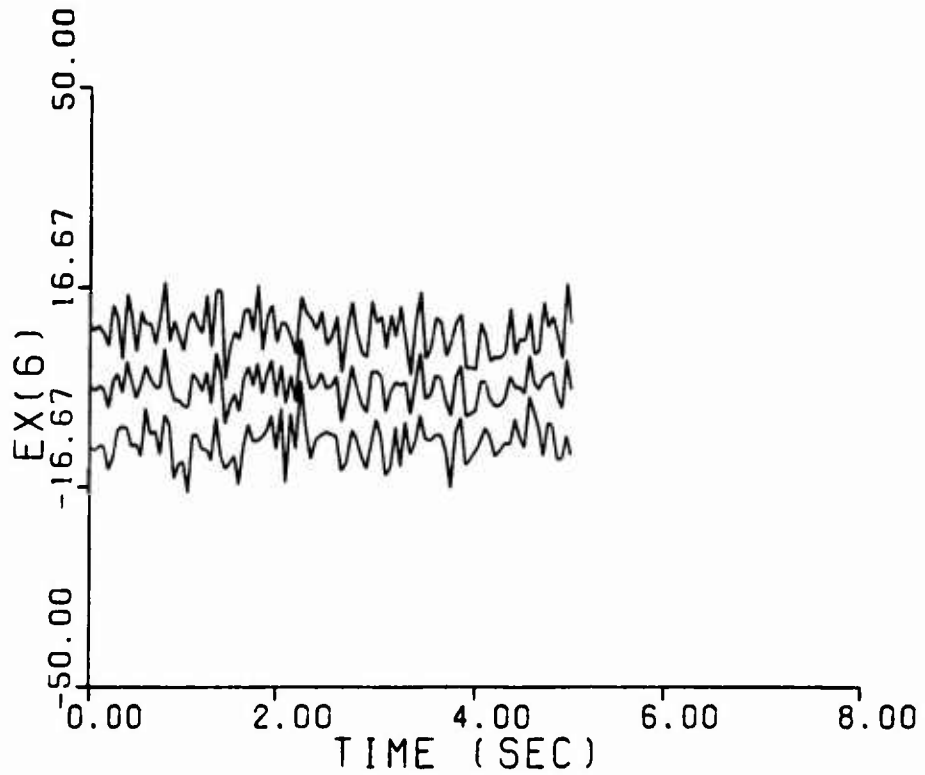

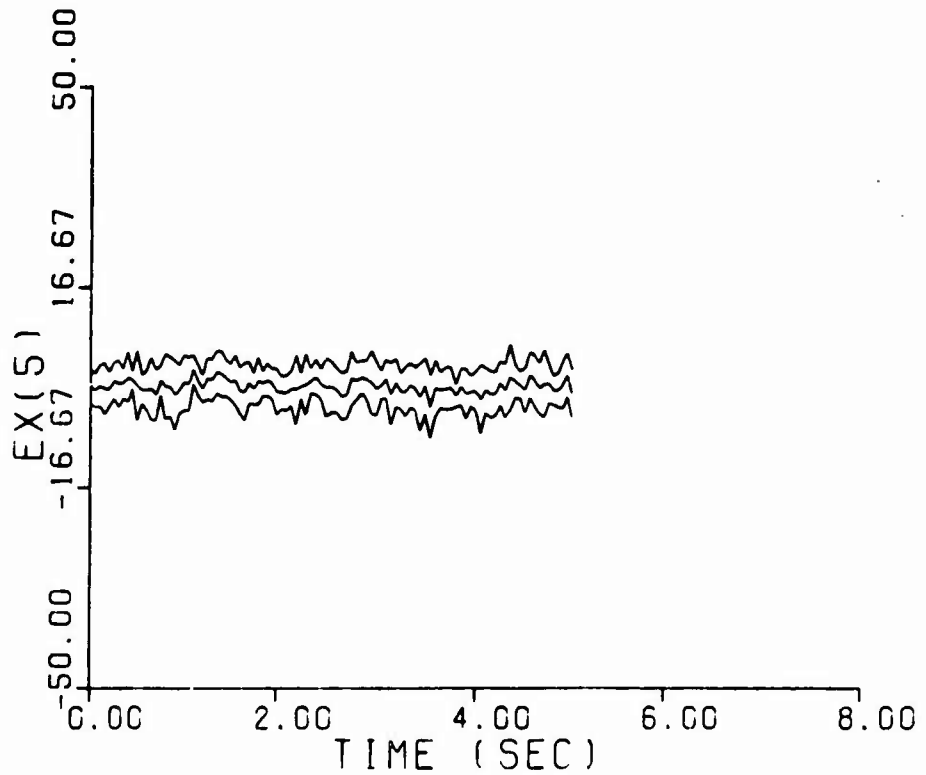

Fig. E-7--Continued

Appendix F: Fixed-Bank and Moving-Bank Comparison with Dither Signal = 100

This appendix contains a plot used in comparing the performance of a fixed-bank to a moving-bank estimator. Probability monitoring is implemented with a bank move threshold of 0.25. The bank is at its finest discretization with a dither signal of magnitude = 100 and frequency of 30 rad/sec. The truth model is based on the parameter vector (3,7).

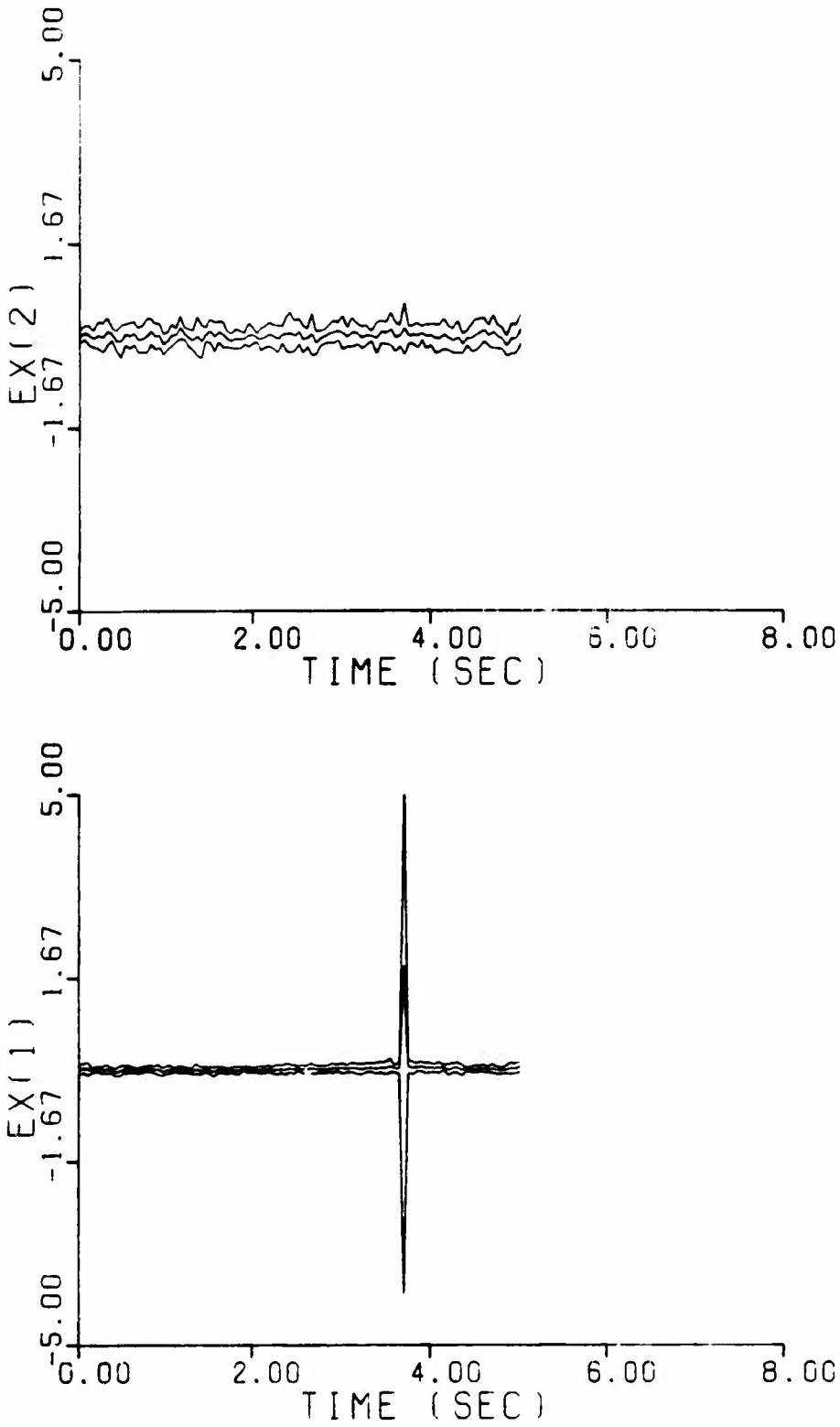

Fig. F-1. Moving-Bank Comparison, Dither Signal = 100

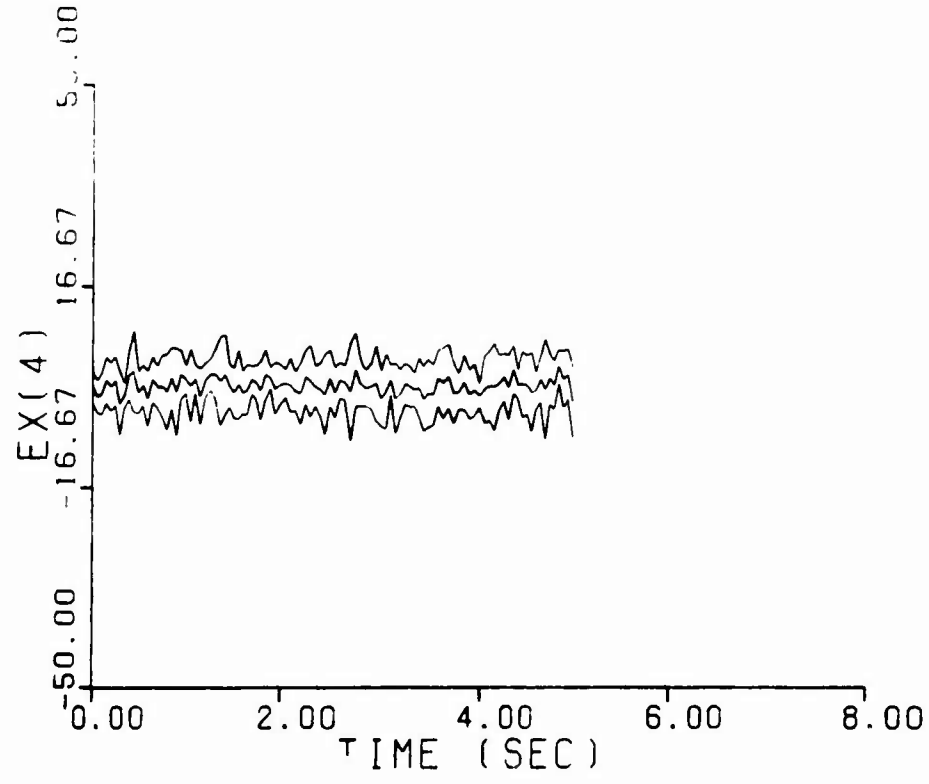

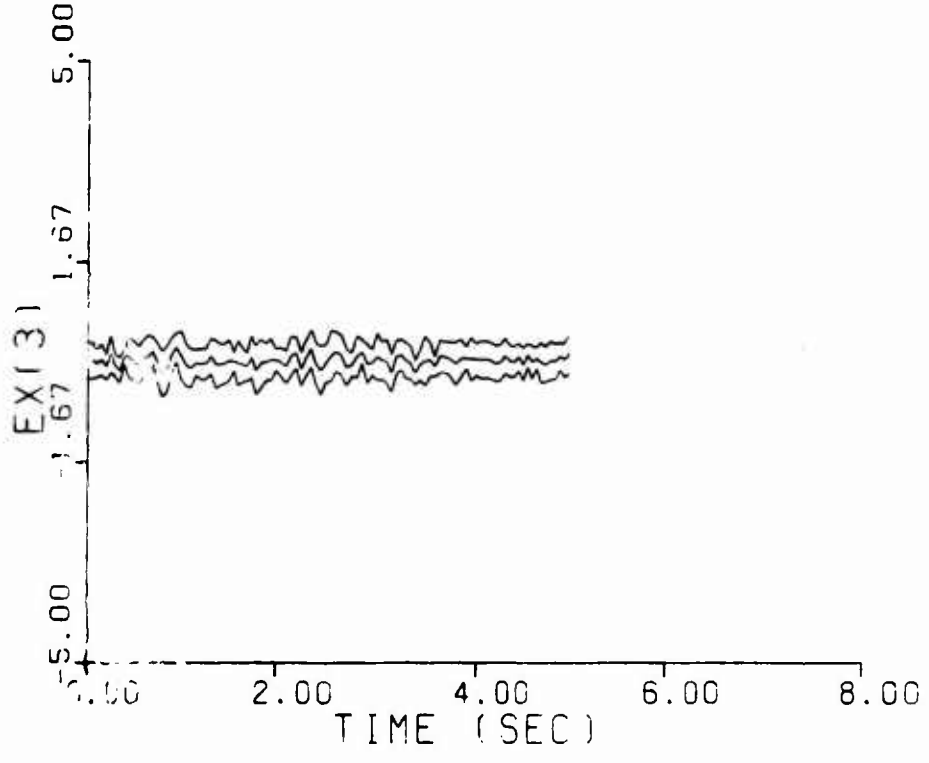

Fig. F-1--Continued

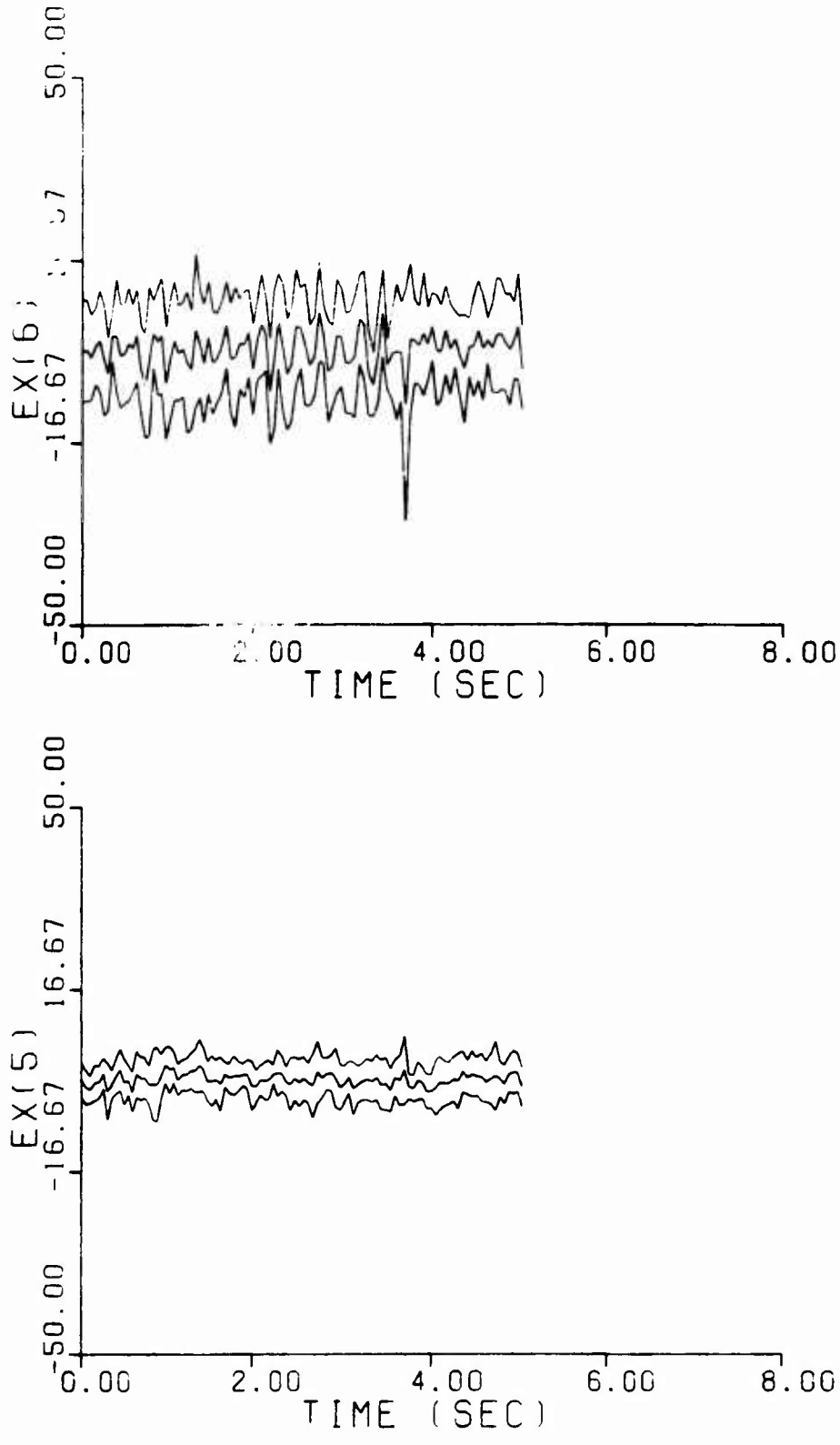

Fig. F-1--Continued

Appendix G: Fixed-Bank and Moving-Bank Comparison with Dither Signal = 500

This appendix contains plots used in comparing the performance of a fixed-bank to a moving-bank estimator. The dither signal is of magnitude = 100 and frequency = 30 rad/sec. The truth model is based upon the parameter point (1,10). Figure G-1 implements a moving bank that is initially centered on the parameter point (5,5) while the remaining figures are from simulations incorporating a fixed-bank. The title indicates the discretization of the filter as well as the bank move threshold for the case of the moving-bank.

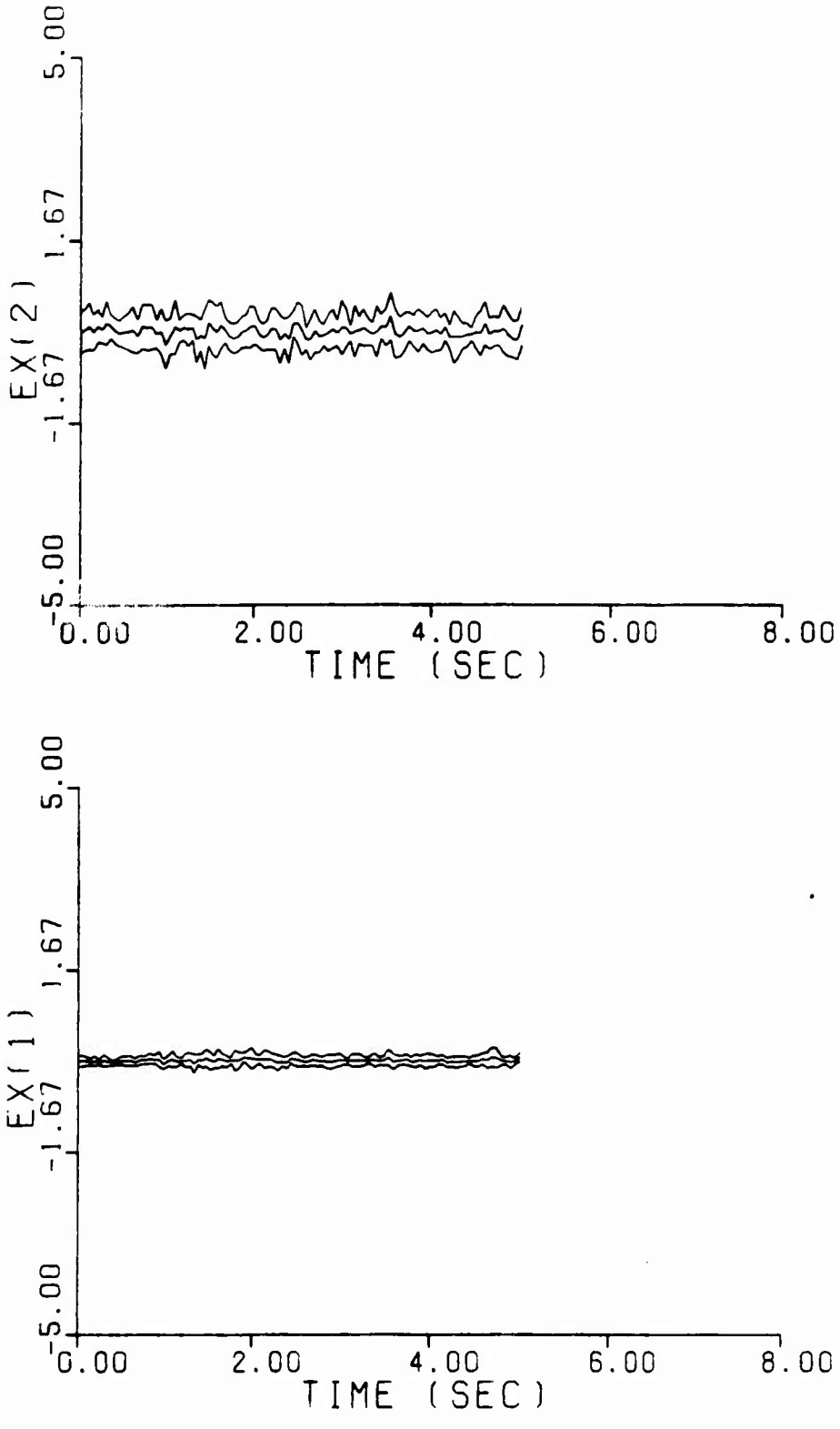

Fig. G-1. Discretization = 1, Bank Move Threshold = 0.25

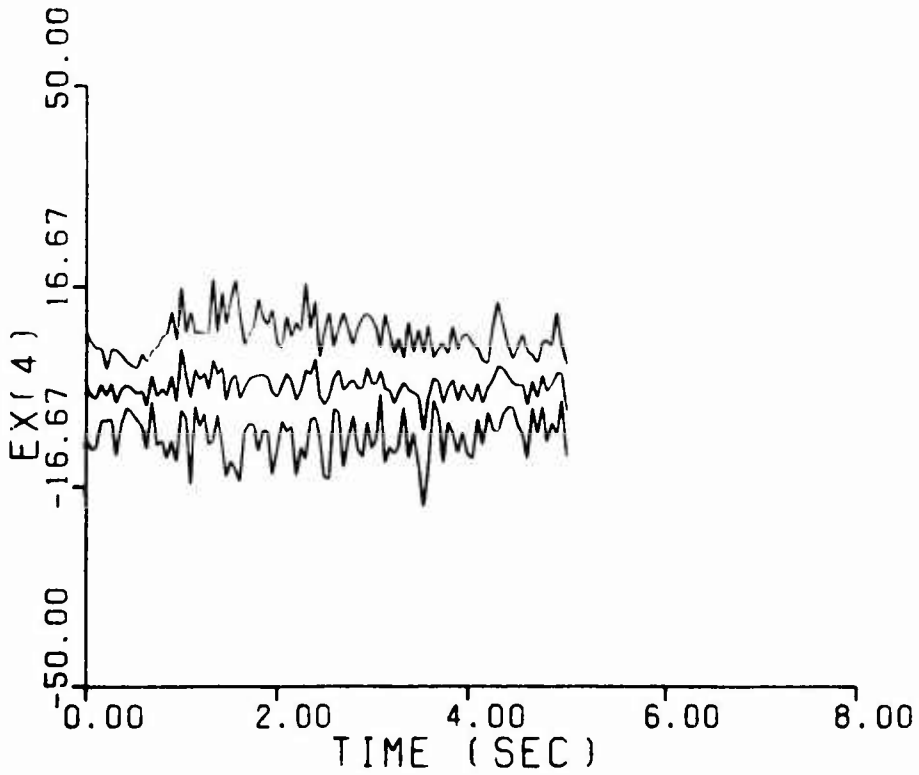

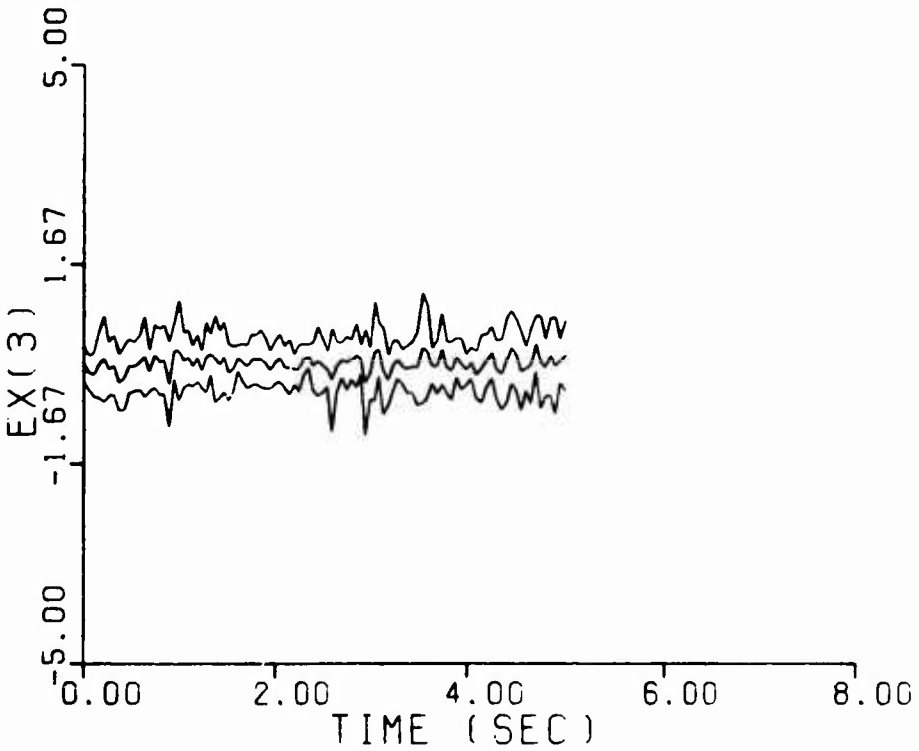

Fig. G-1--Continued

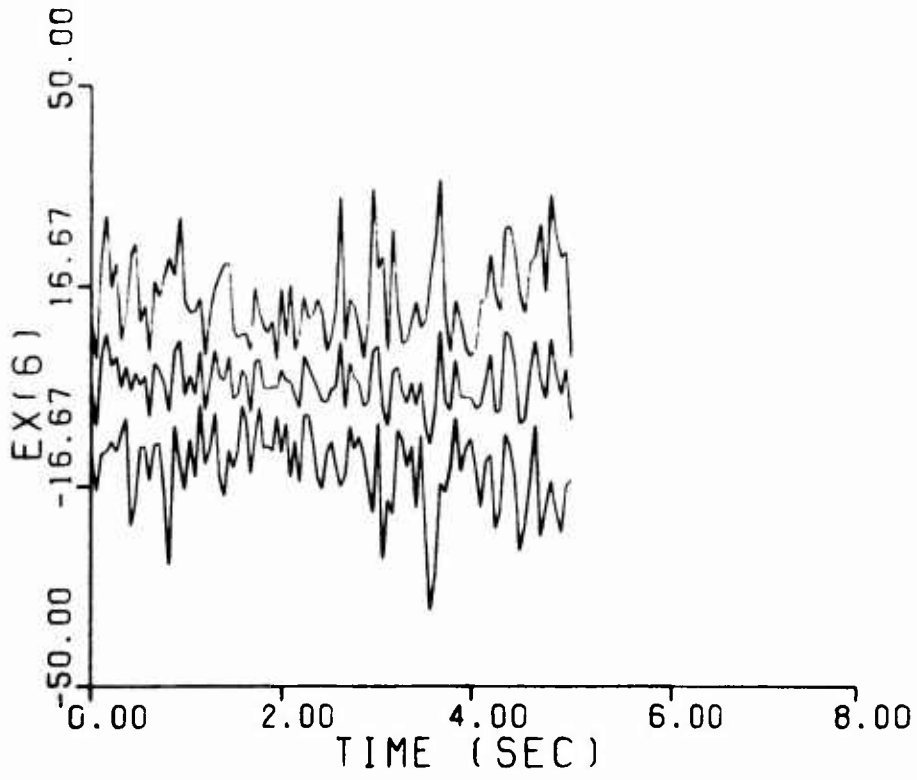

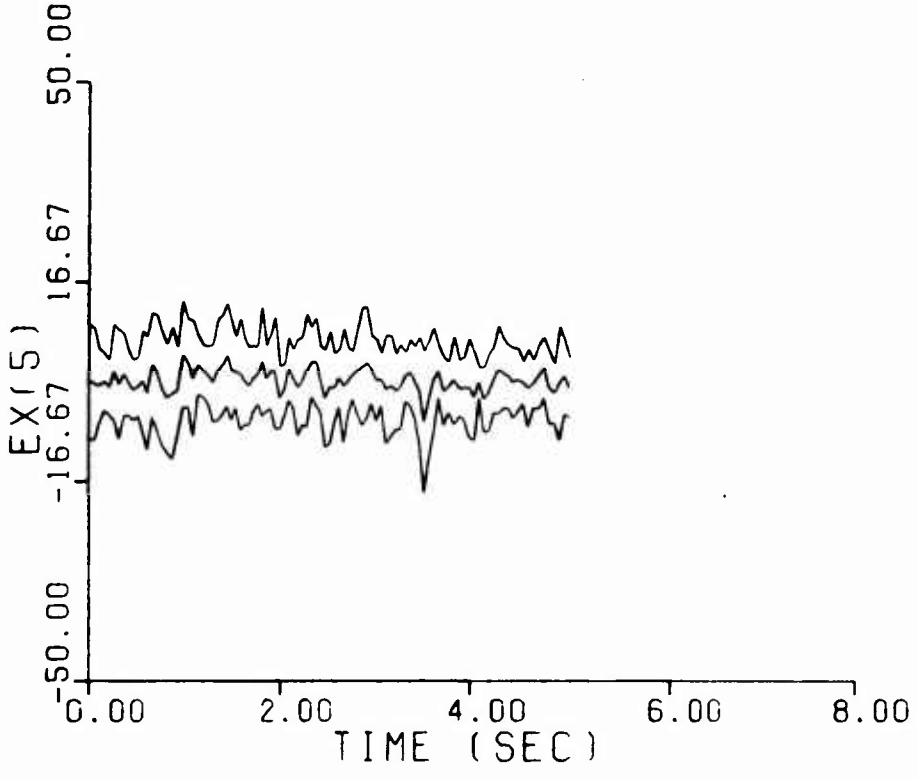

Fig. G-1--Continued

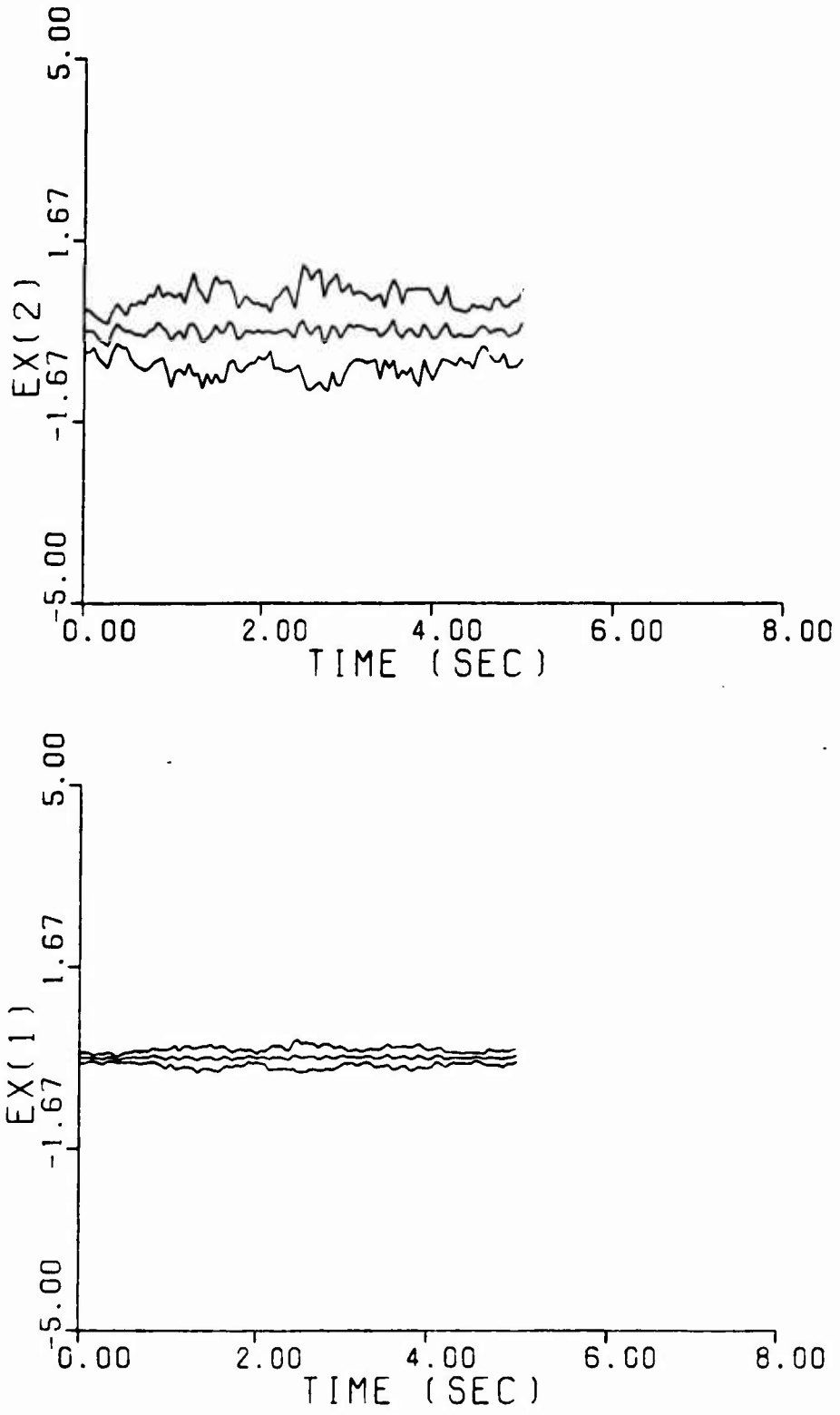

Fig. G-2. Discretization = 1

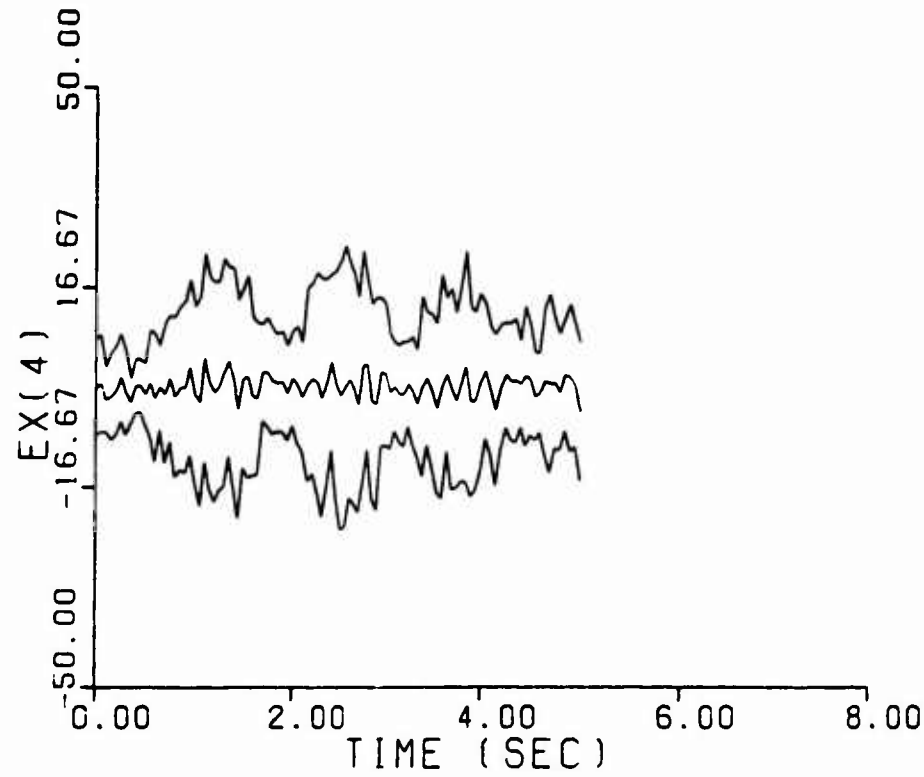

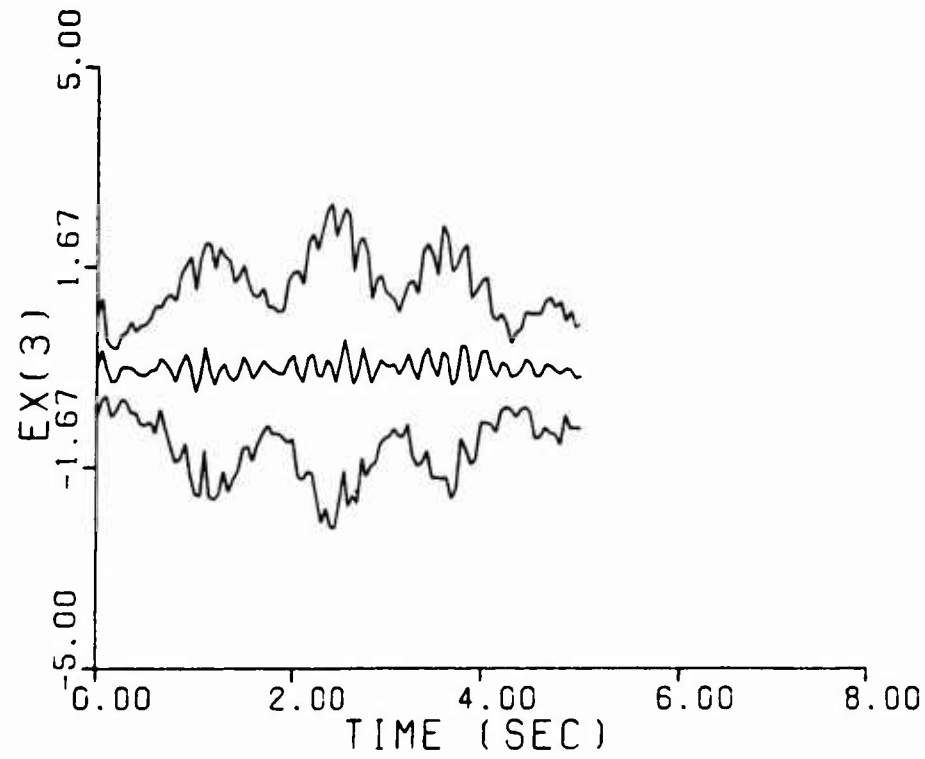

Fig. G-2--Continued

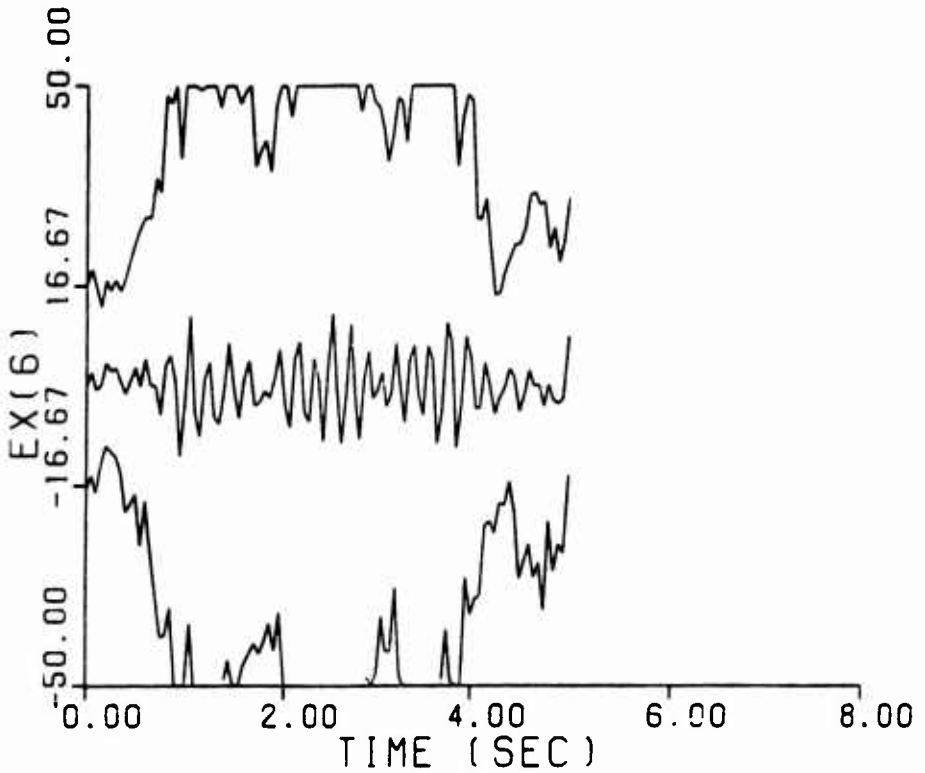

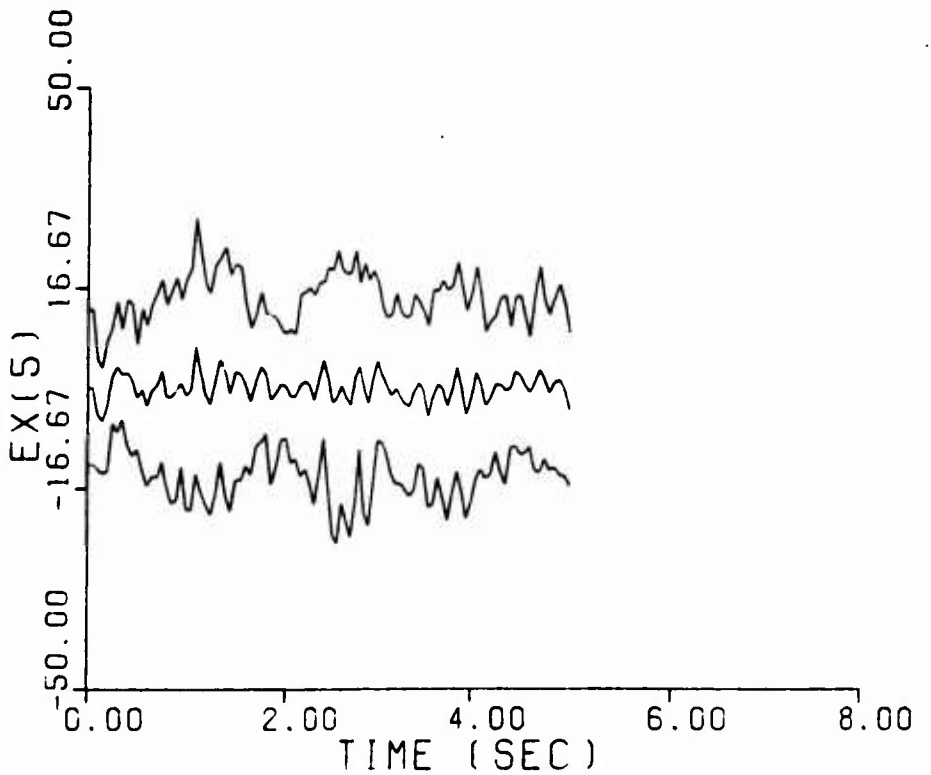

Fig. G-2--Continued

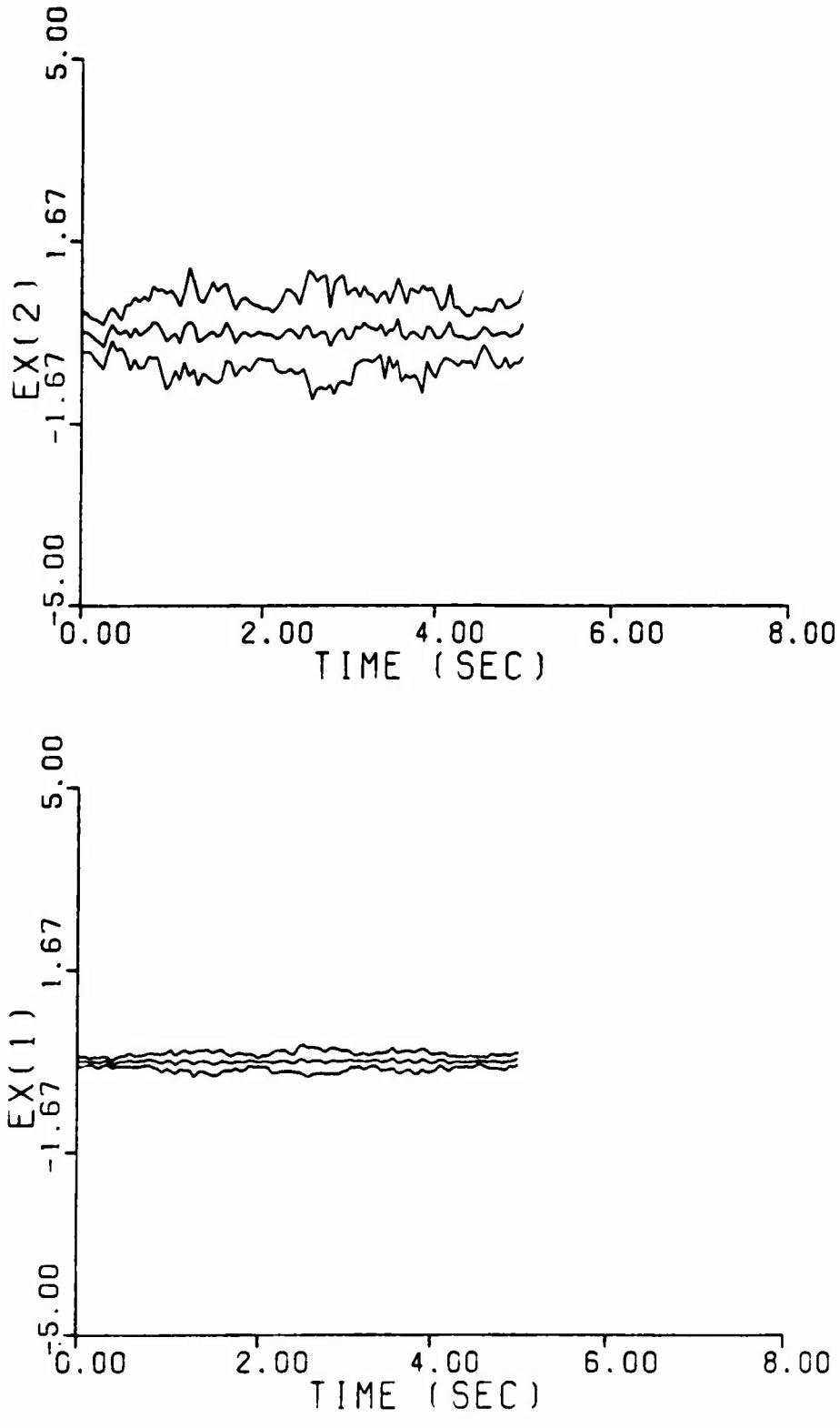

Fig. G-3. Discretization = 2

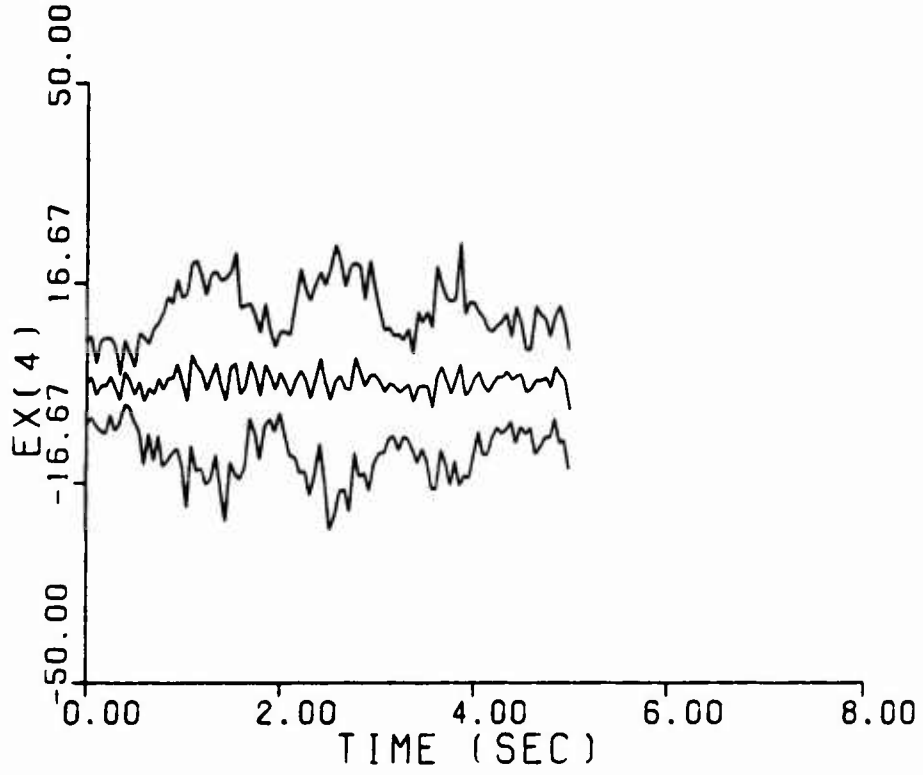

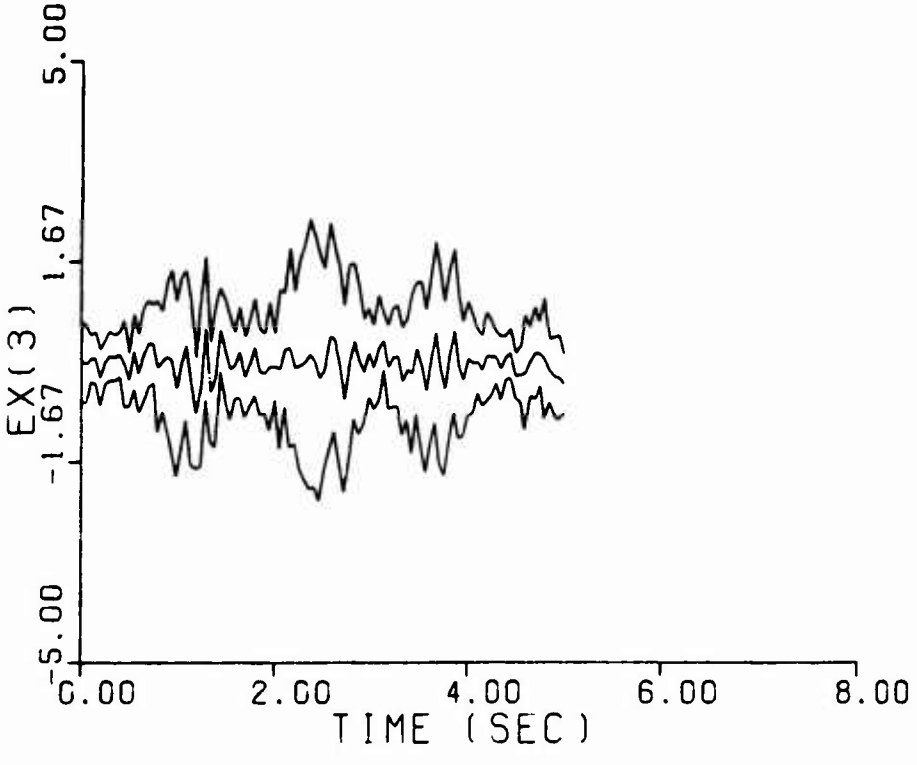

Fig. G-3--Continued

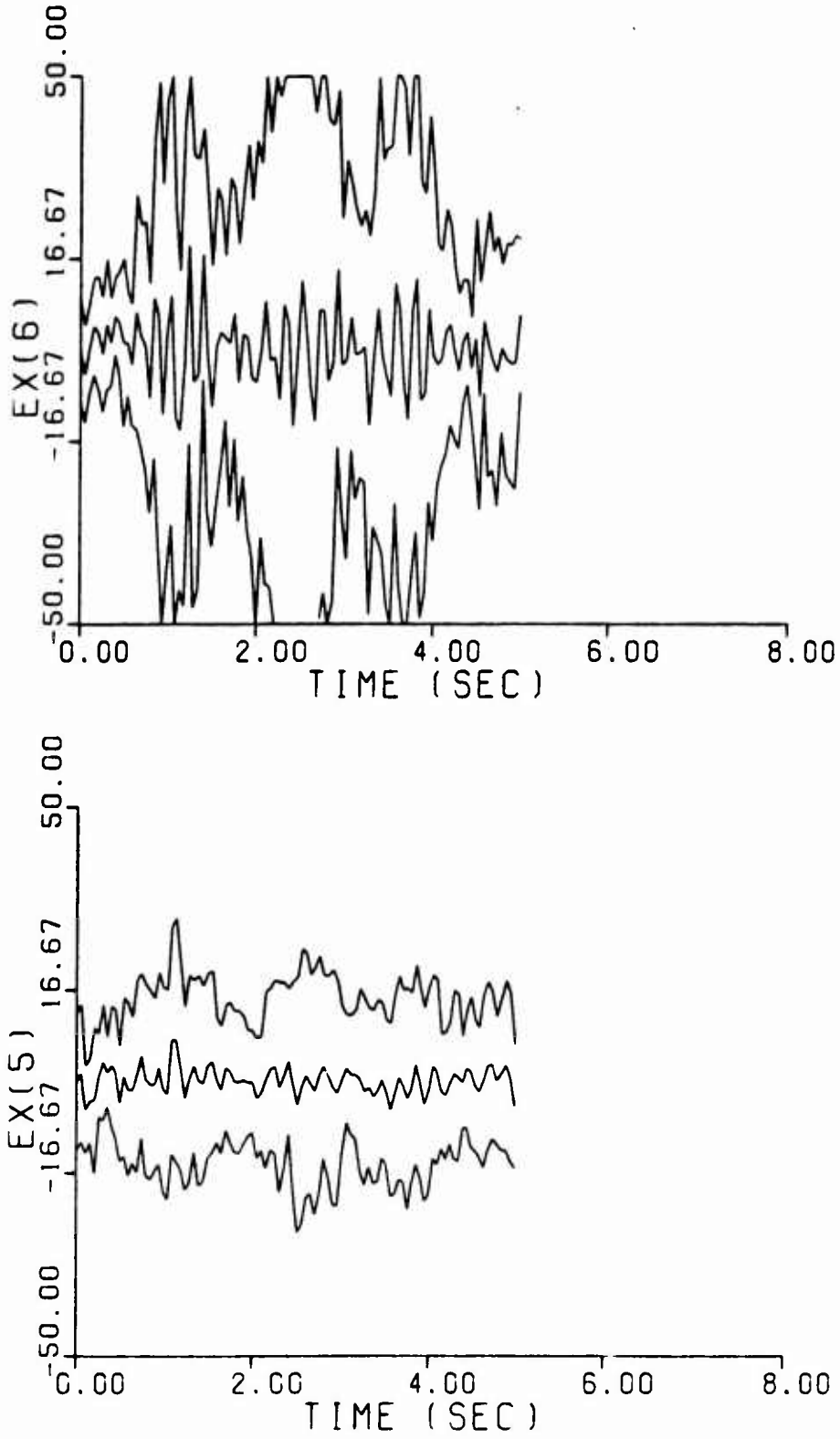

Fig. G-3--Continued

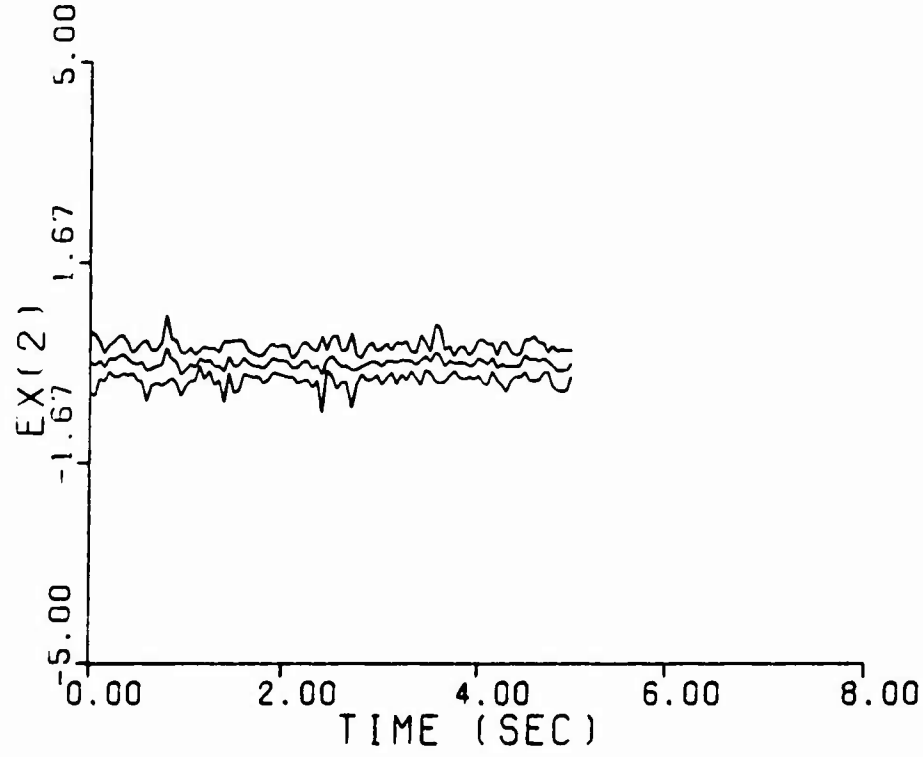

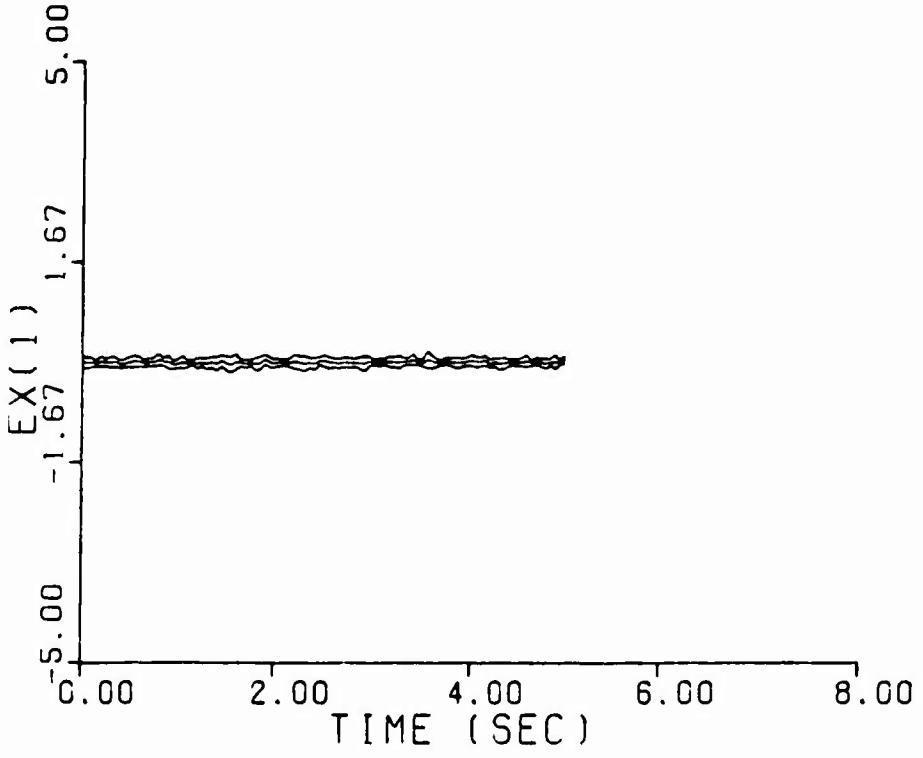

Fig. G-4. Discretization = 4

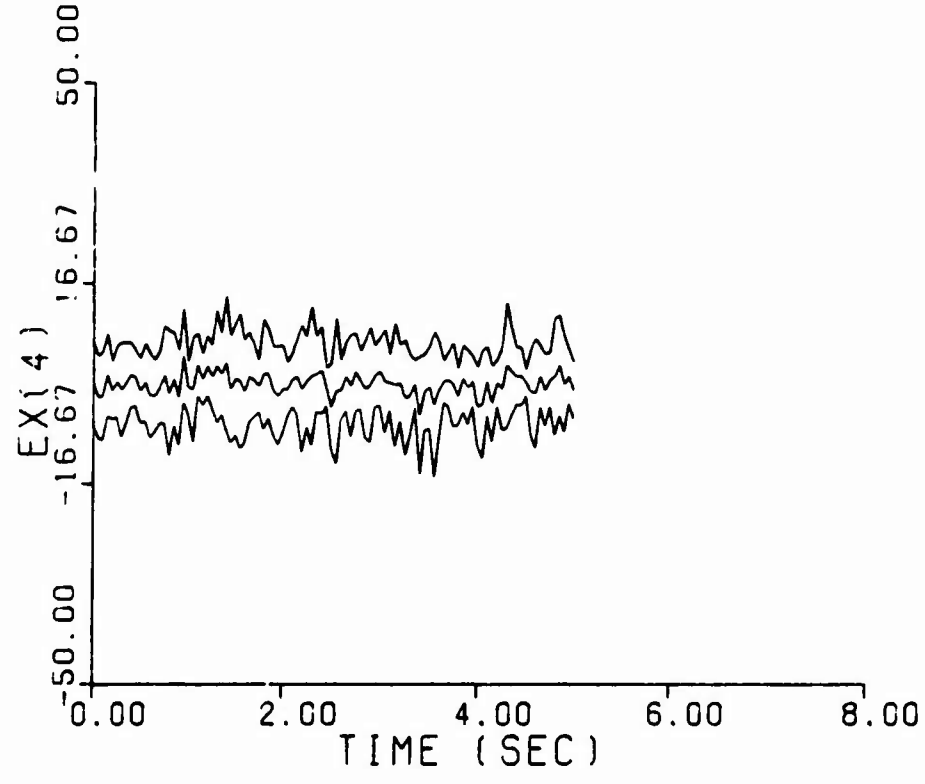

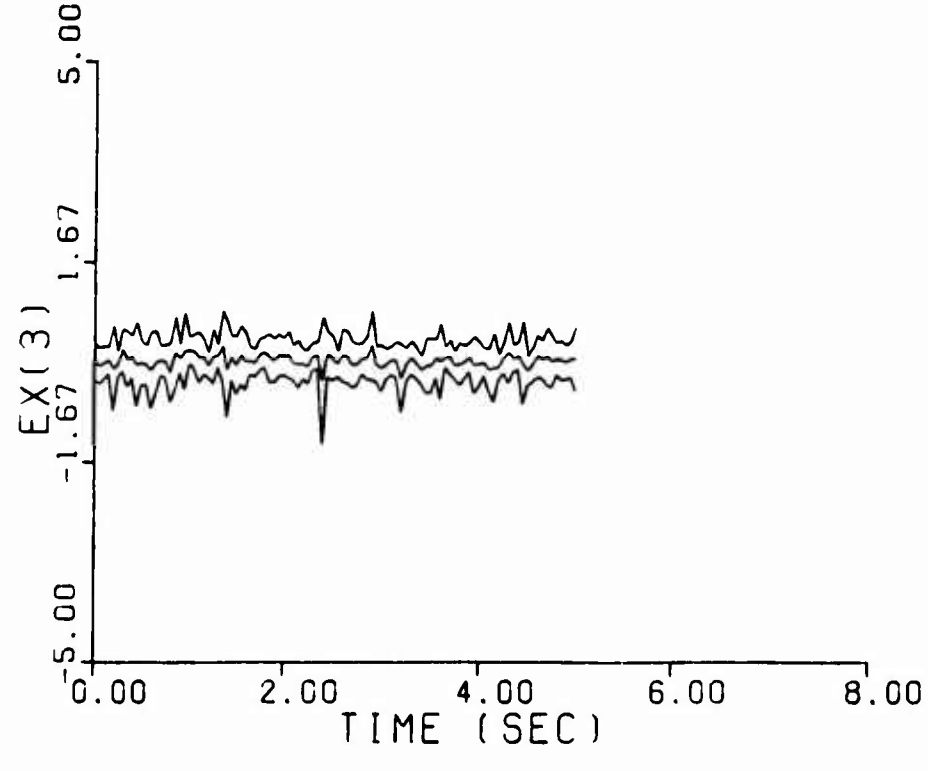

Fig. G-4--Continued

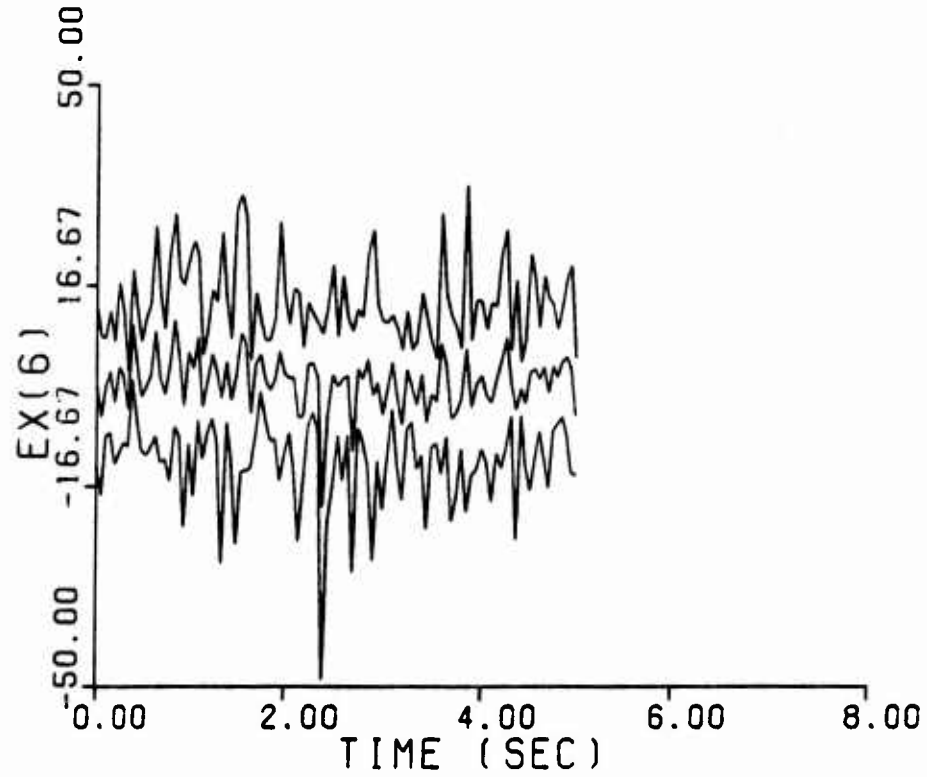

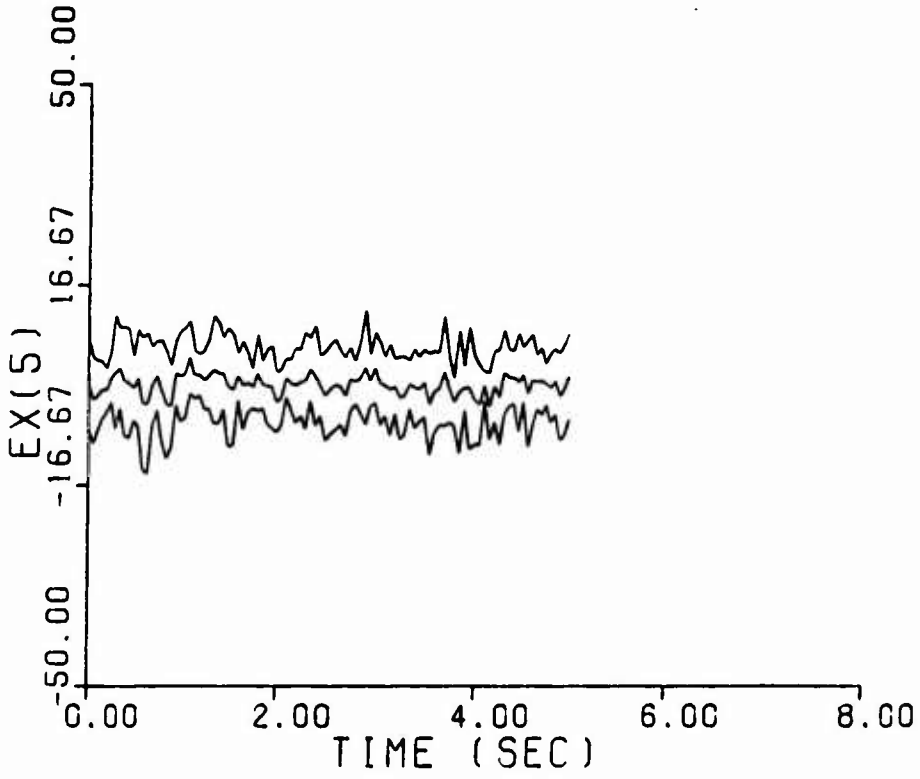

Fig. G-4--Continued

Appendix H: Controller Performance

This appendix contains plots reflecting control using a fixed bank at a discretization of 1 and centered at parameter point (5,5). A dither signal of magnitude = 500 is applied for 1 second beginning at t = 0. At t = 0, control is applied. Plot H-1 provides a comparison for the case where no control is applied at t = 1.0. The control gains are based on the parameter vector at point (5,5).

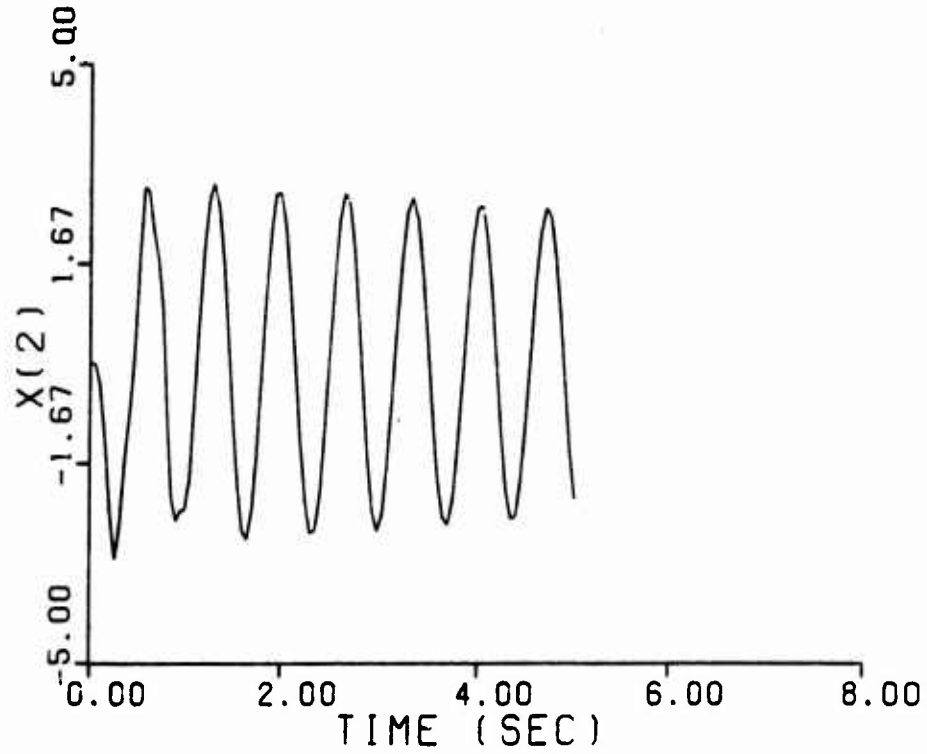

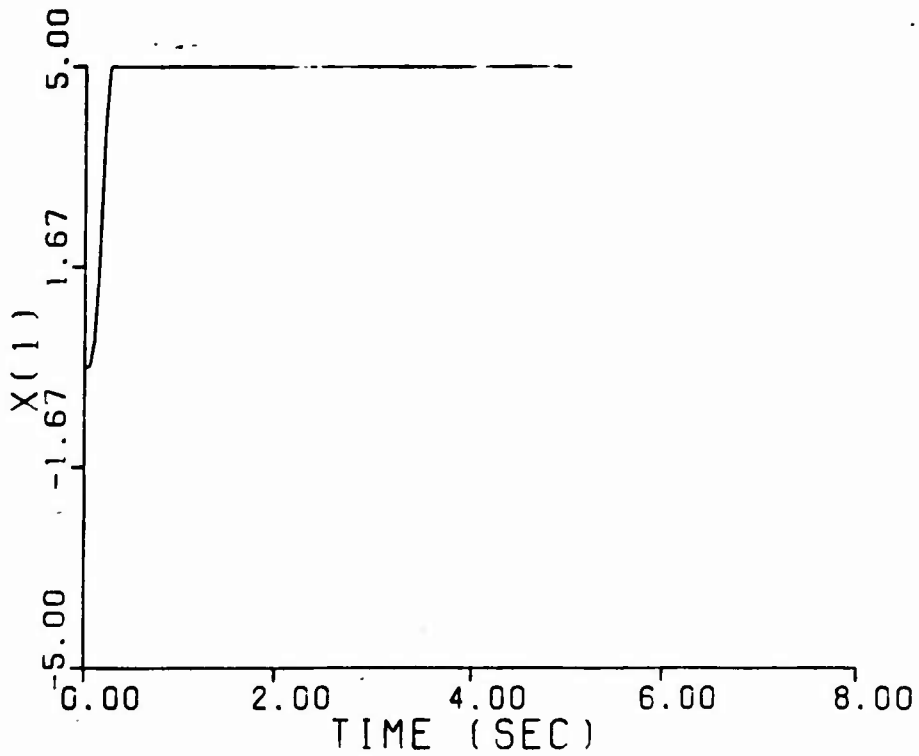

Fig. H-1. No Control, Truth = 5,5

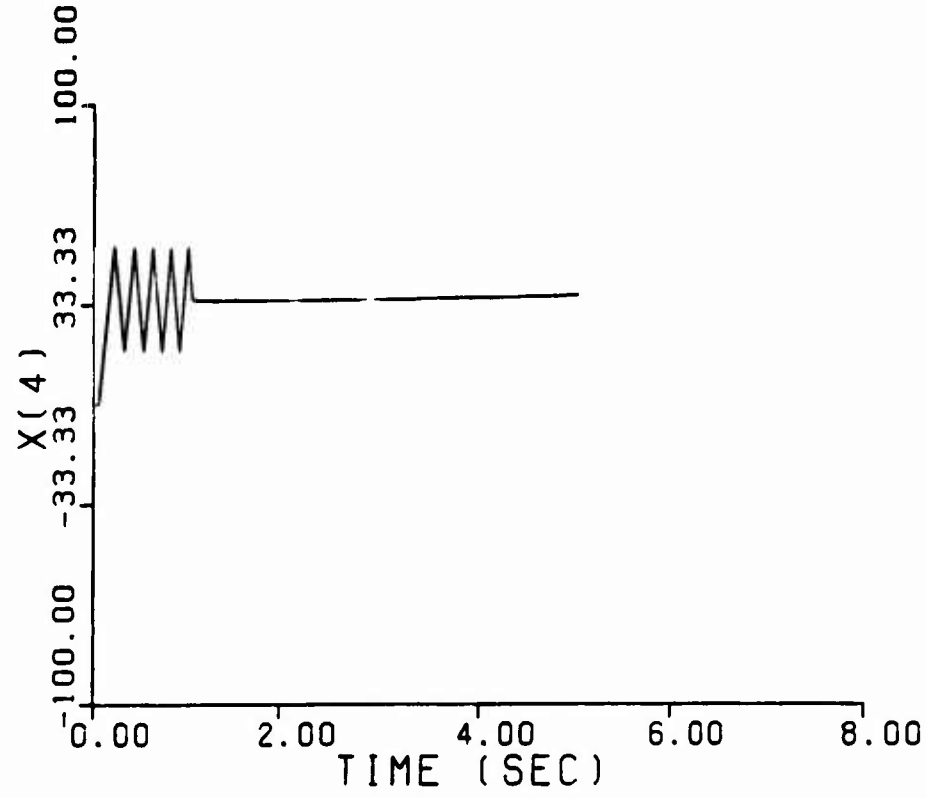

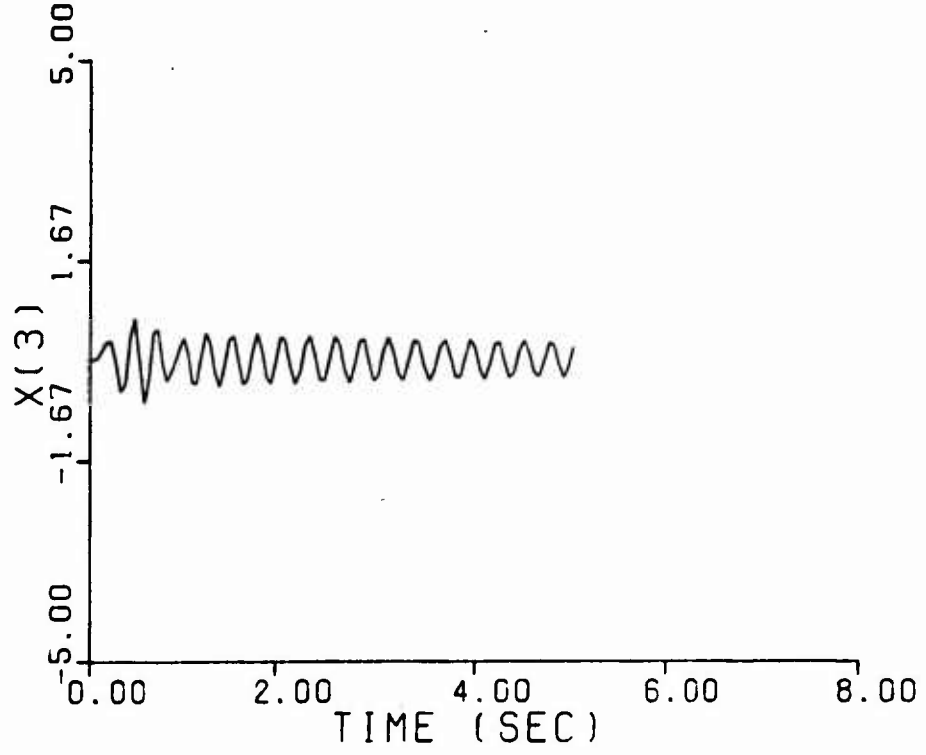

Fig. H-1--Continued

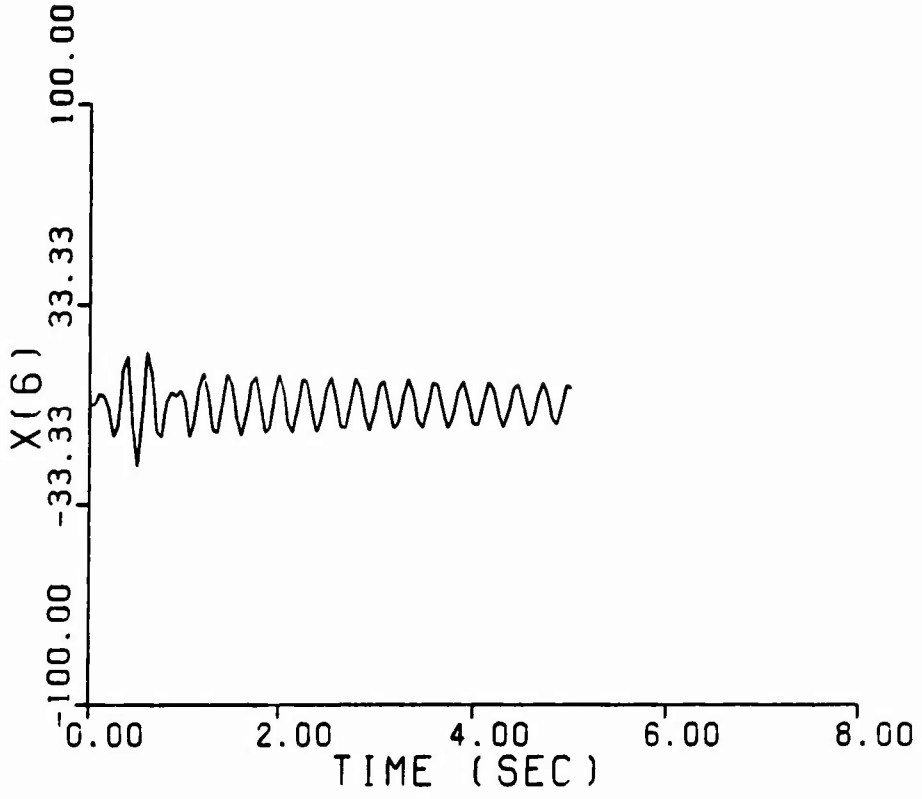

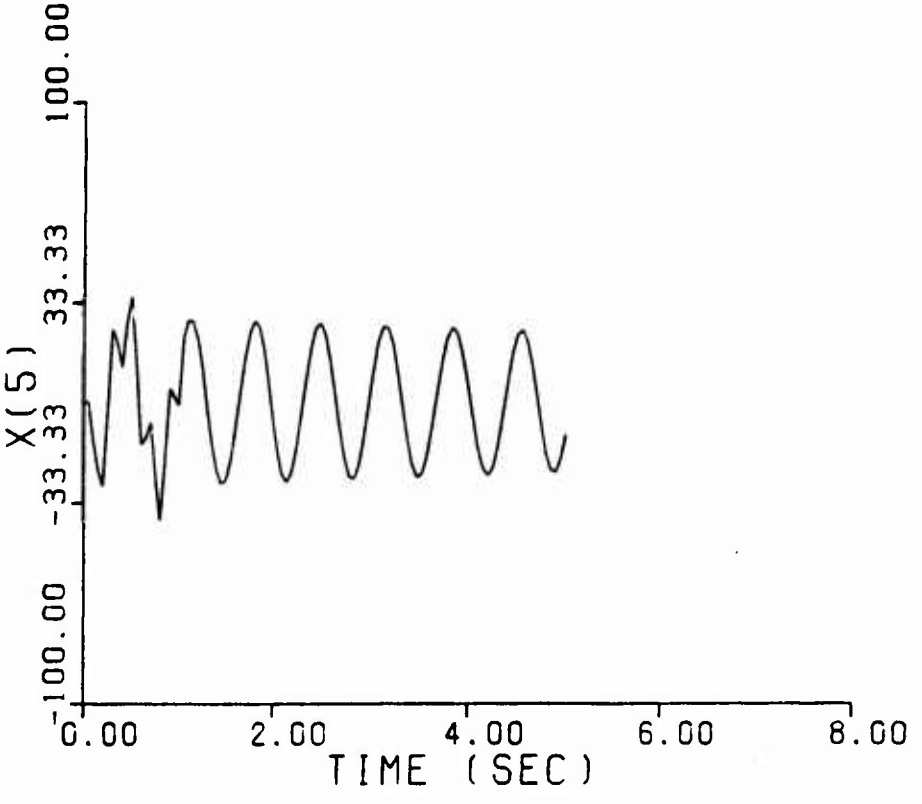

Fig. H-1--Continued

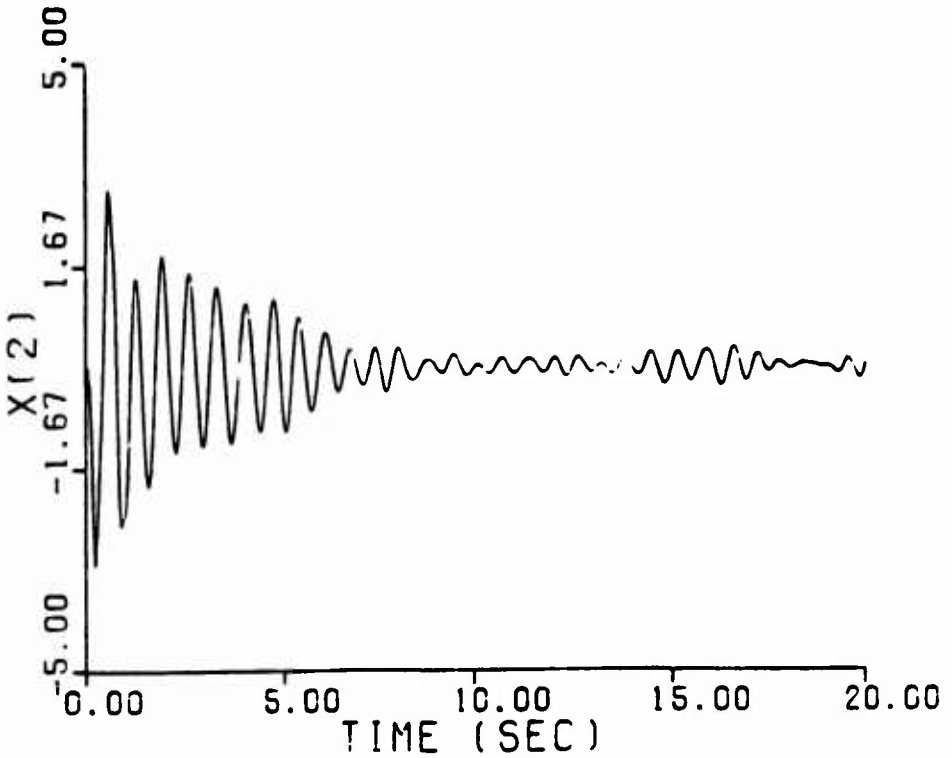

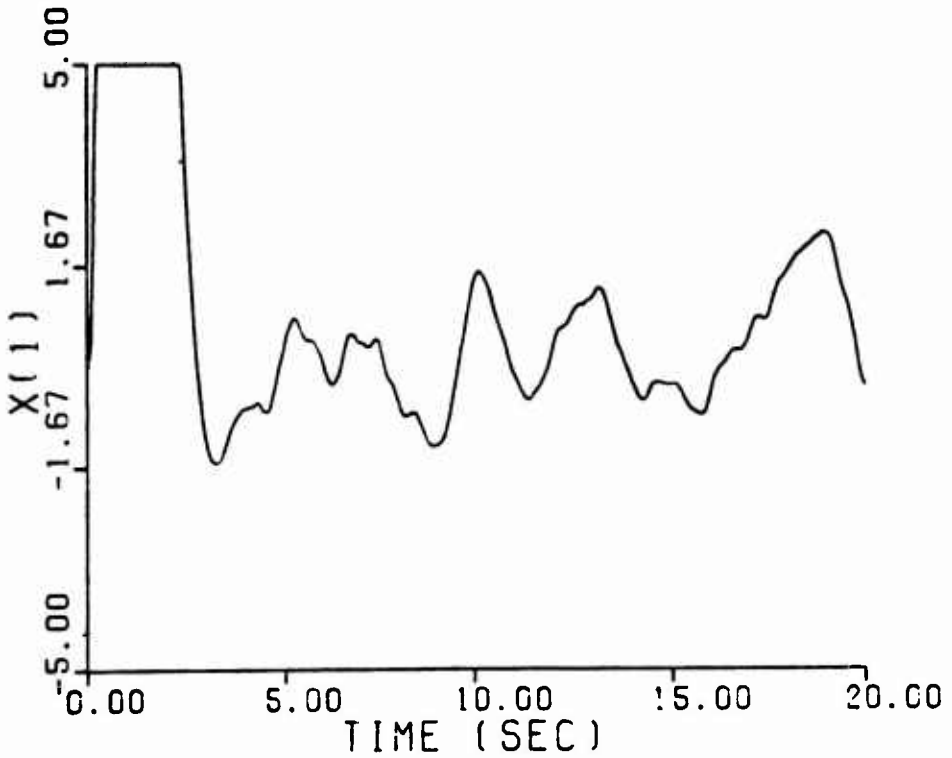

Fig. H-2. Truth = 5,5

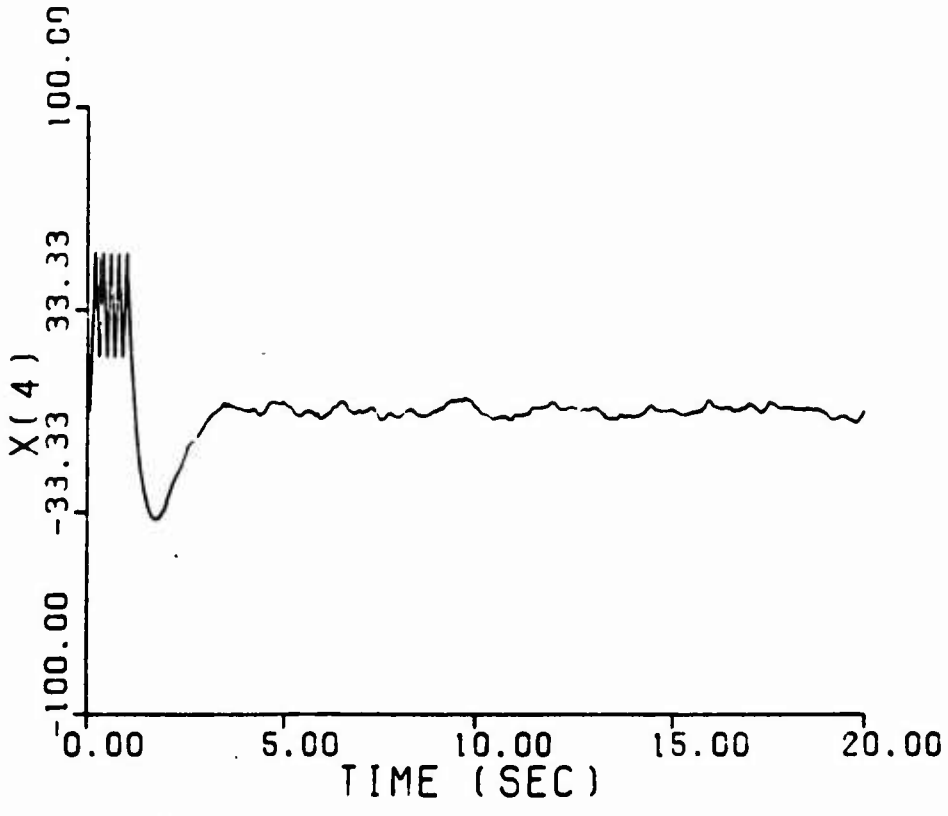

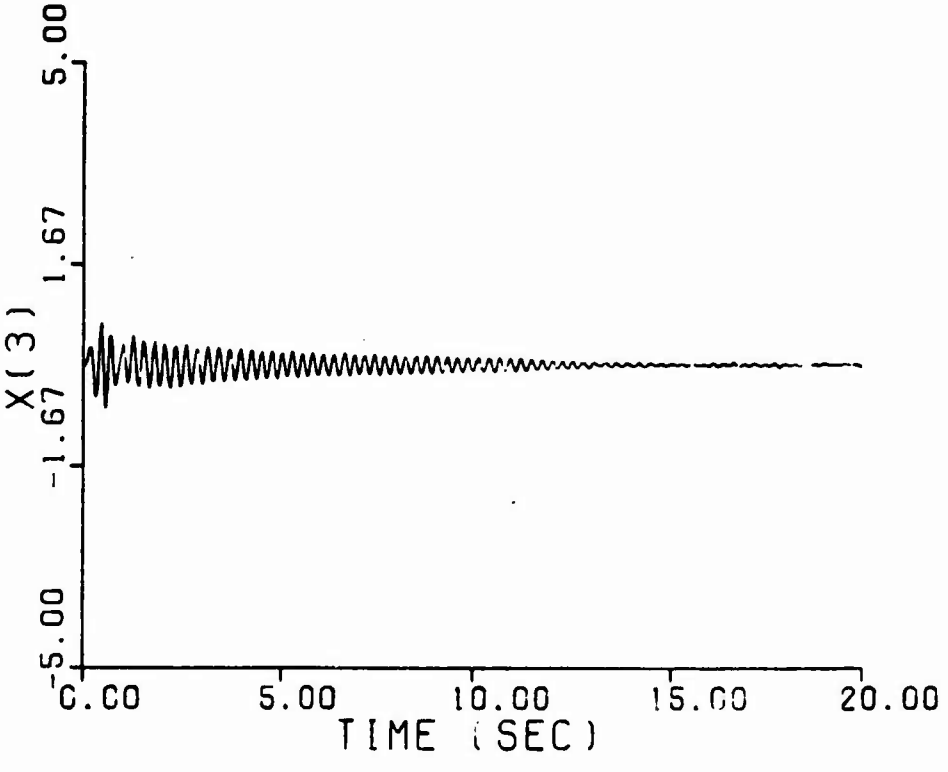

Fig. H-2--Continued

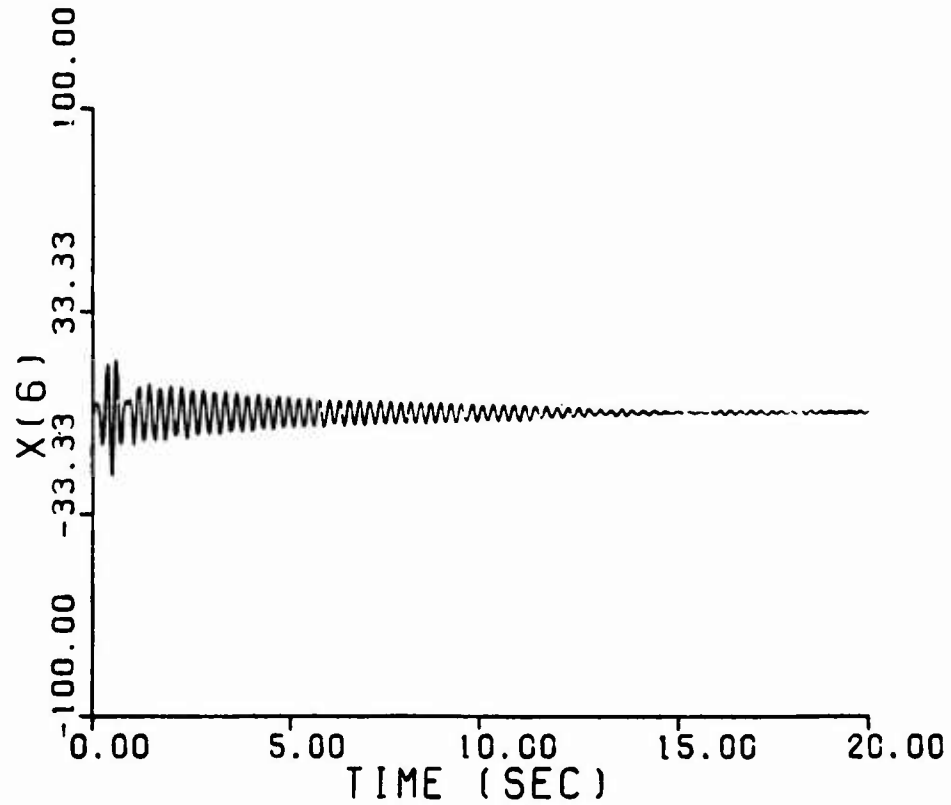

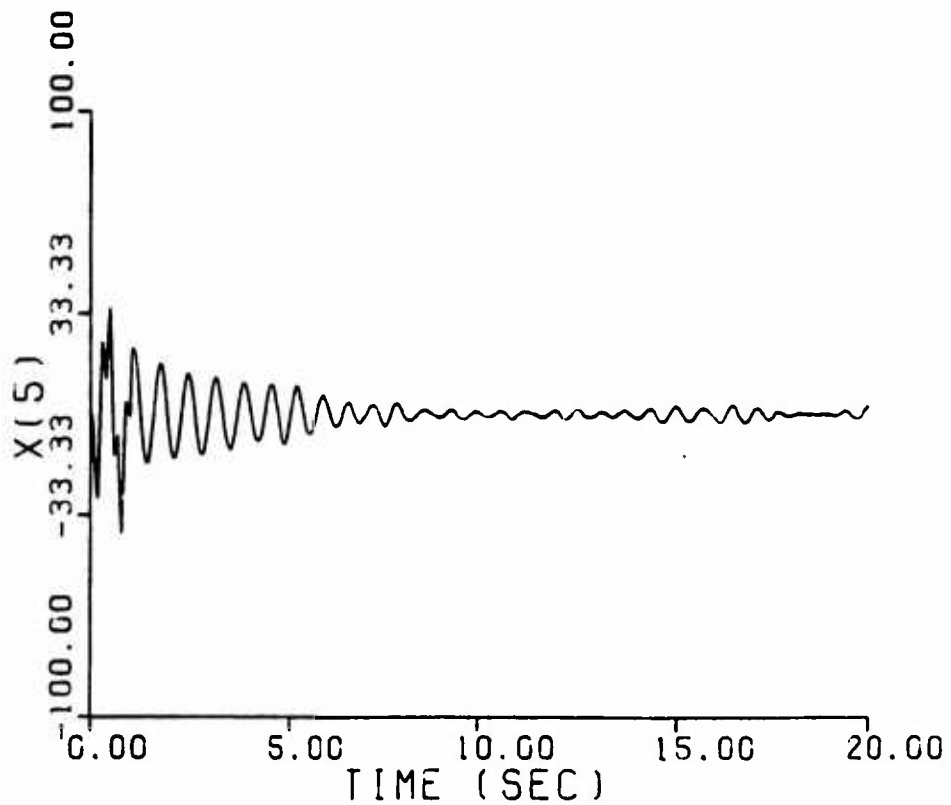

Fig. H-2--Continued

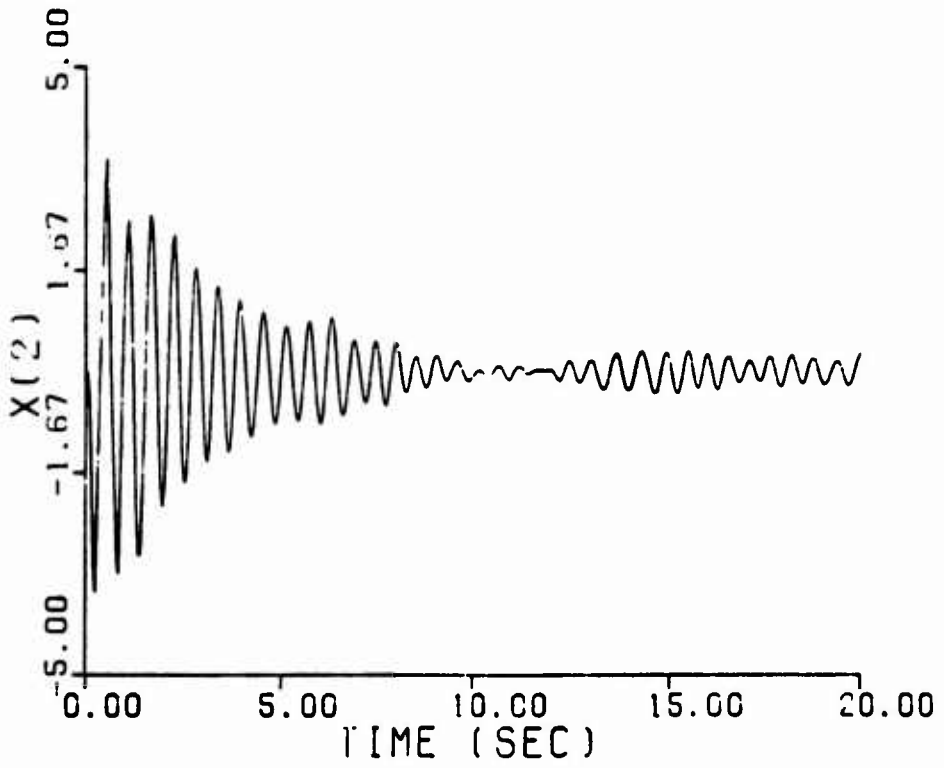

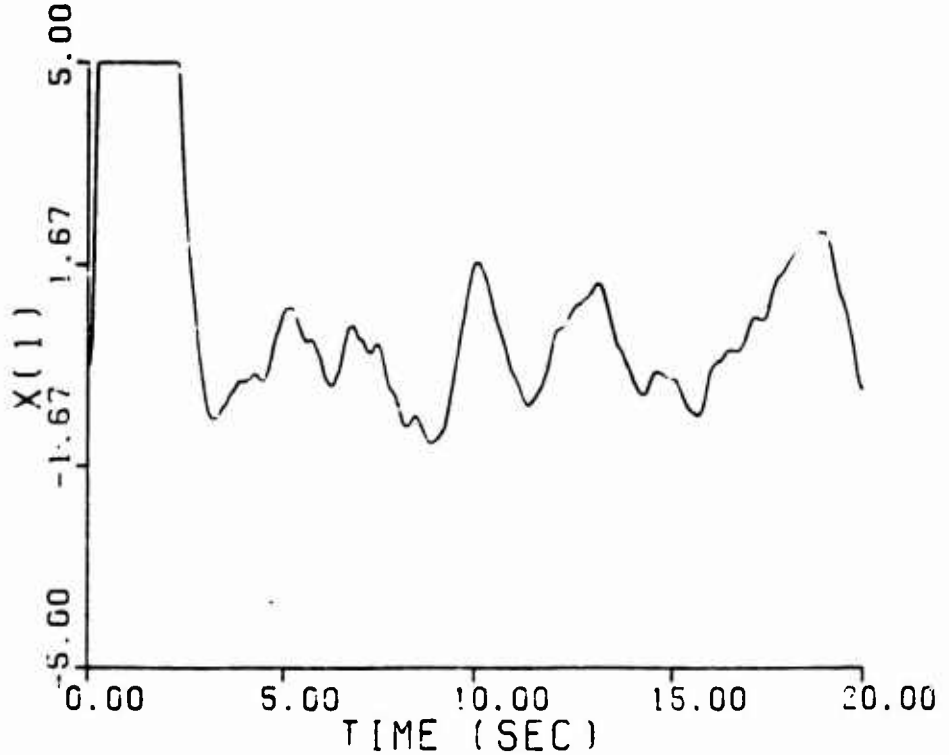

Fig. H-3. Truth = 3,7

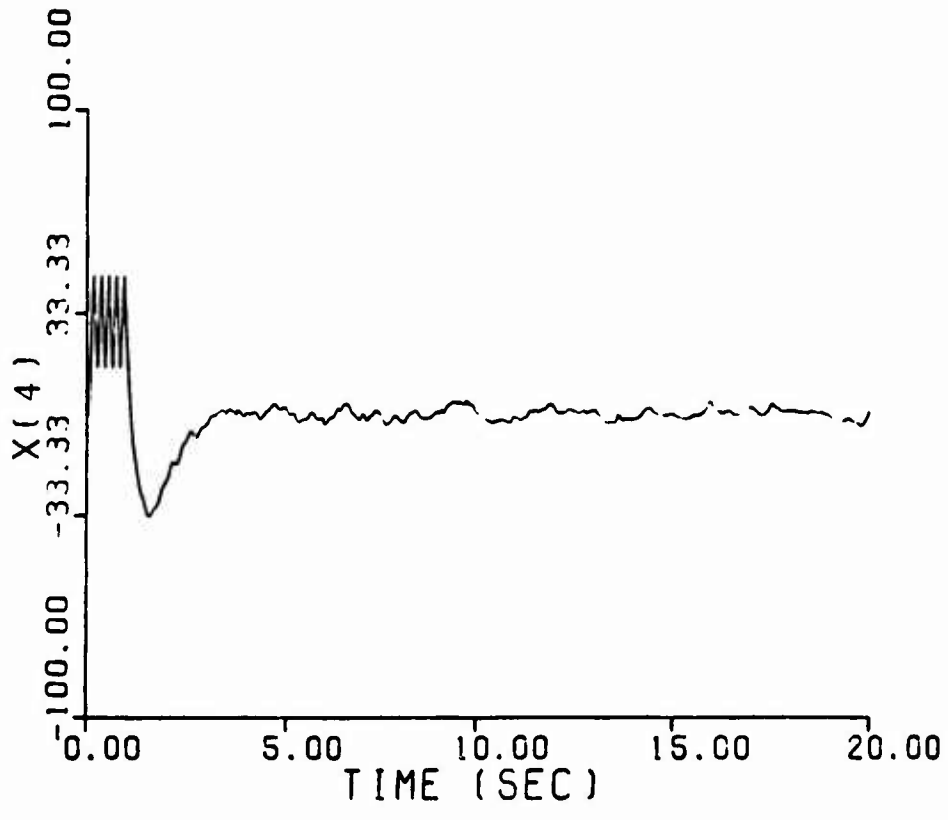

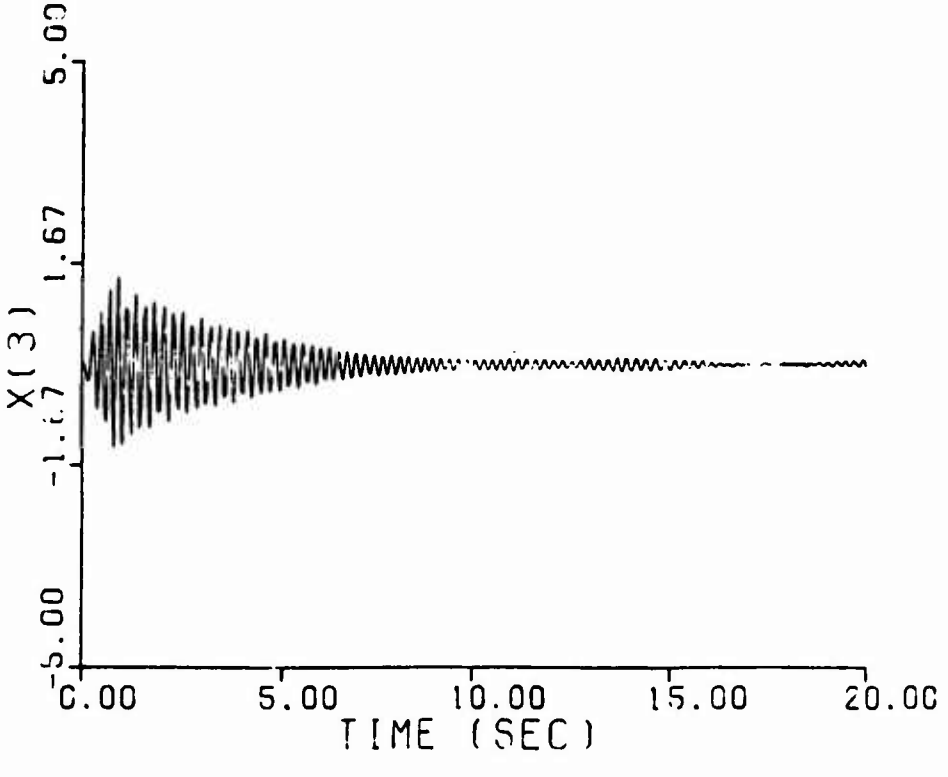

Fig. H-3--Continued

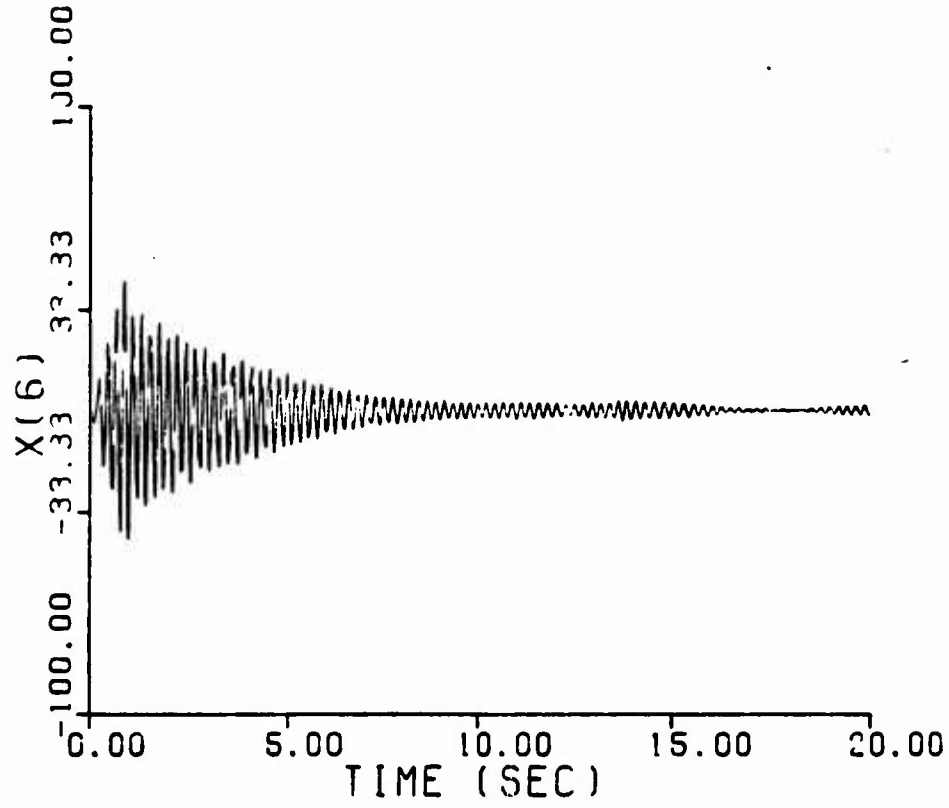

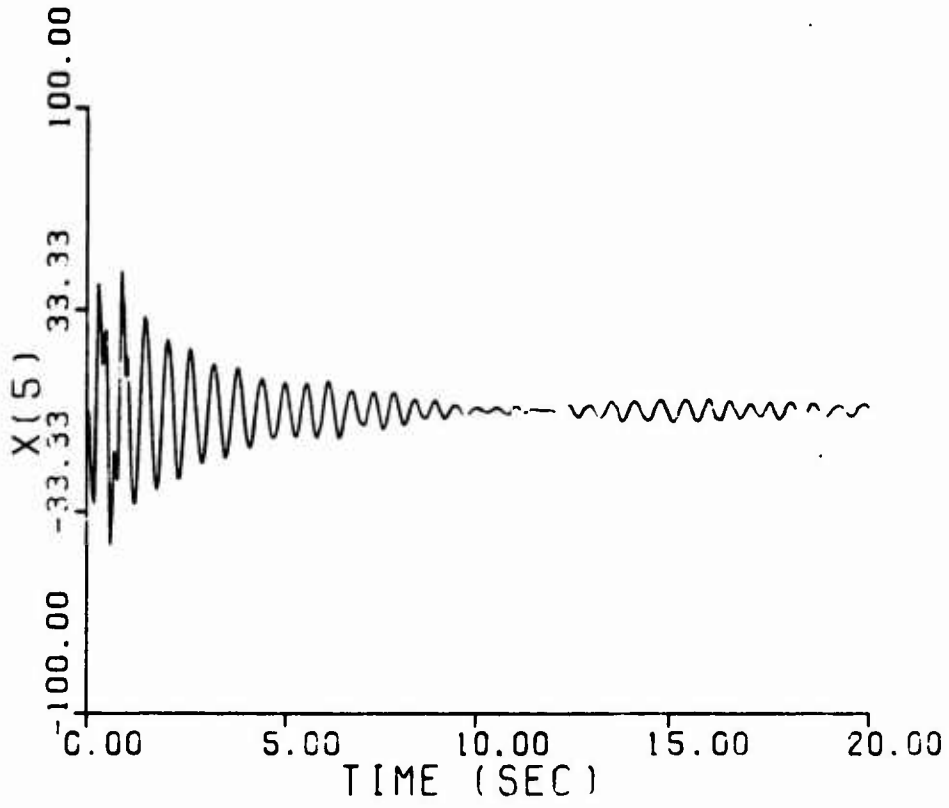

Fig. H-3--Continued

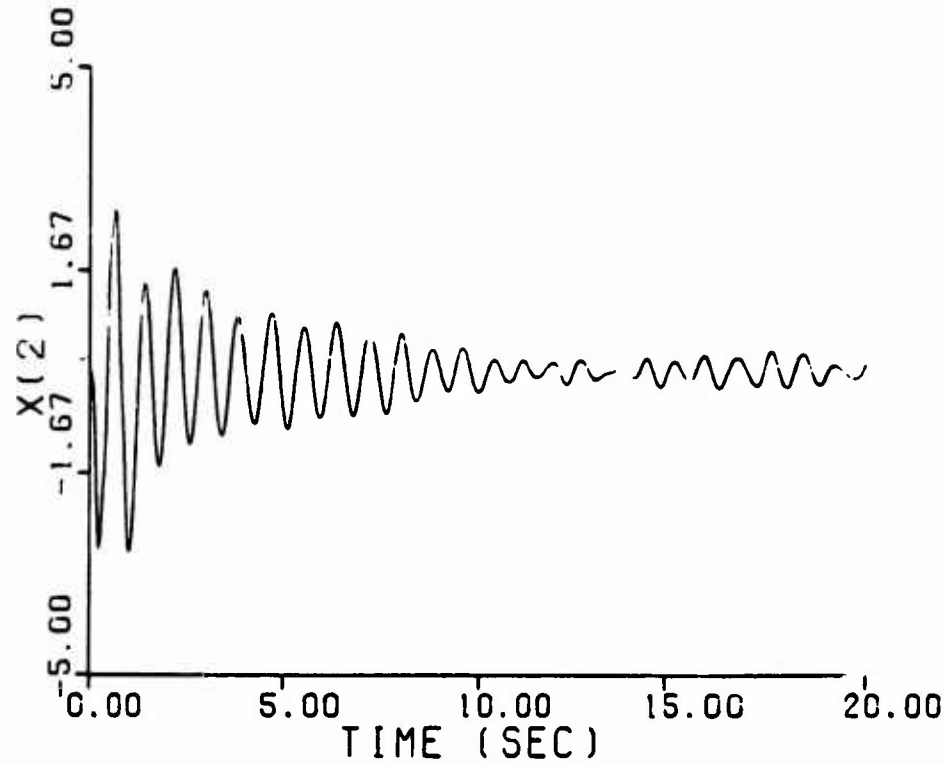

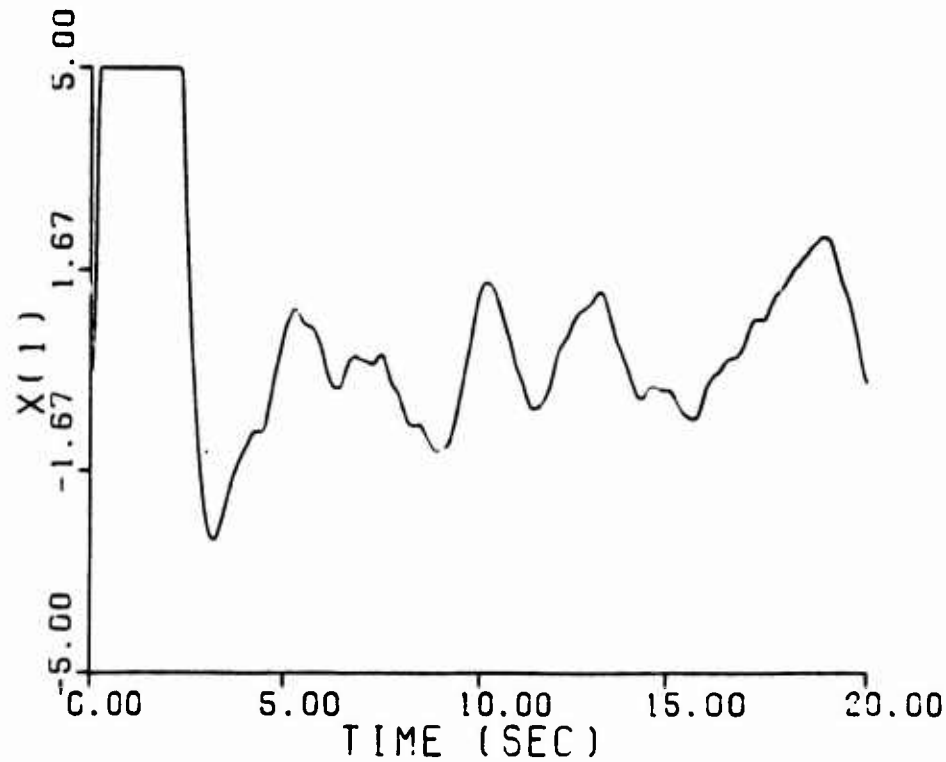

Fig. H-4. Truth = 7,3

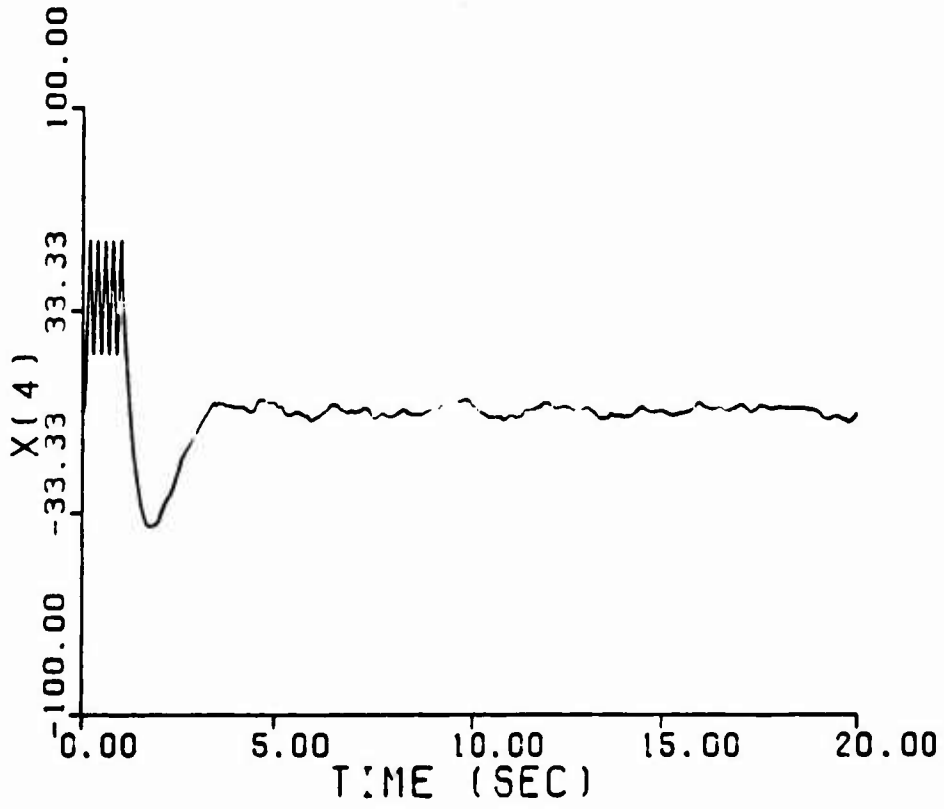

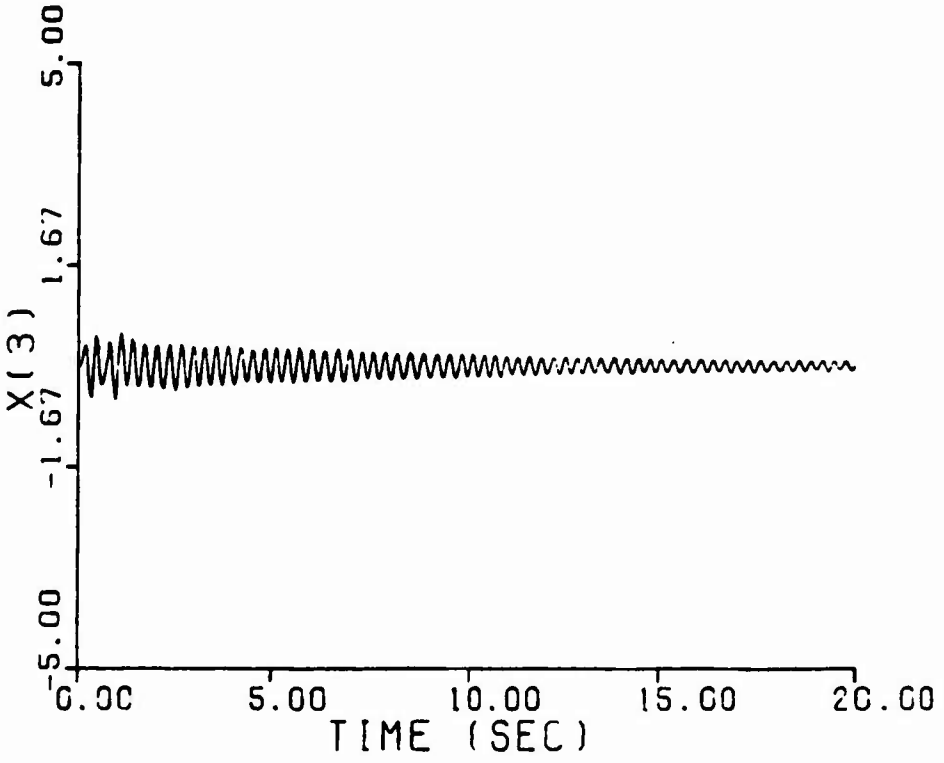

Fig. H-4--Continued

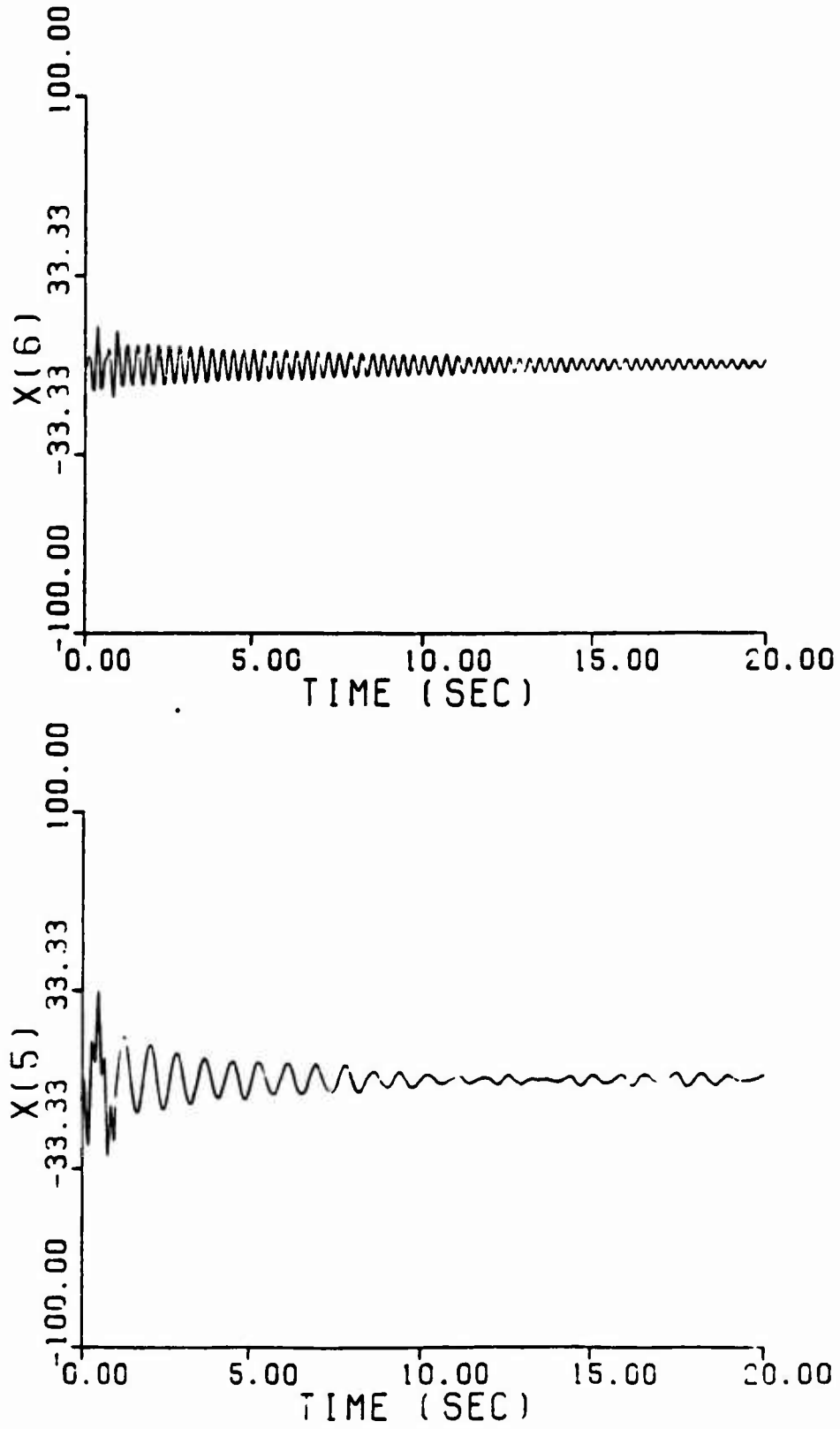

Fig. H-4--Continued

Bibliography

1. Chang, C. B. and M. Athans. "State Estimation for Discrete Systems with Switching Parameters," IEEE Transactions on Aerospace and Electronic Systems, 14 (3): 418-424 (May 1978).

2. Dasgupta, S. and L. C. Westphal. "Convergence of Partitioned Adaptive Filters for Systems with Unknown Biases," IEEE Transactions on Automatic Control, 28: 614-615 (May 1983).

3. Filios, Paul G. Moving-Bank Multiple Model Adaptive Algorithms Applied to Flexible Spacecraft Control. MS thesis, GE/ENG/85D-14. School of Engineering, Air Force Institute of Technology (AU), Wright-Patterson AFB OH, December 1984.

4. Fry, C. M. and A. P. Sage. "On Hierarchical Structure Adaption and Systems Identification," International Journal of Control, 20: 433-452 (1979).

5. Hawkes, Richard M. and John B. Moore. "Performance Bounds for Adaptive Estimation," Proceedings of the IEEE, 64: 1143-1150 (August 1976).

6. Hentz, K. P. Feasibility Analysis of Moving Bank Multiple Model Adaptive Estimation and Control Algorithms. MS thesis, GE/ENG/84D-32. School of Engineering, Air Force Institute of Technology (AU), Wright-Patterson AFB OH, December 1984.

7. Hilbern, C. G., Jr. and Demetrios G. Lainoitis. "Optimal Estimation in the Presence of Unknown Parameters," IEEE Transactions on Systems Science and Cybernetics, 5: 38-43 (January 1969).

8. Kailath, Thomas. Linear Systems. Englewood Cliffs NJ: Prentice-Hall, Inc., 1980.

9. Kokotovic, P. V., R. E. O'Malley, Jr., and P. Sannuti. "Singular Perturbations and Order Reduction in Control Theory--An Overview," Automatica, 12: 123-132 (1976).

10. Kokotovic, P. V. and R. A. Yackel. "Singular Perturbation of Linear Regulators: Basic Theorems," IEEE Transactions on Automatic Control, 17: 29-37 (1972).

11. Korn, J. and L. Beean. Application of Multiple Model Adaptive Estimation to Maneuver Detection and Estimation. Contract DAAK10-82-C-0020. Alphatech, Inc., Burlington MA, June 1981 (AD-B075 921).

12. Lainiotis, Demetrios G. "Optimal Adaptive Estimation: Structure and Parameter Adaptation," IEEE Transactions on Automatic Control, 16: 160-170 (April 1971).

13. -----. "Partitioning: A Unifying Framework for Adaptive Systems, I: Estimation," Proceedings of the IEEE, 64: 1126-1143 (August 1976).

14. Lamb, P. R. and L. C. Westphal. "Simplex-directed Partitioned Adaptive Filters," International Journal of Control, 30: 617-627 (1979).

15. Loving, P. A. Bayesian vs MAP Multiple Model Adaptive Estimation for Field of View Expansion in Tracking Airborne Targets. MS thesis, GE/ENG/85M-1. School of Engineering, Air Force Institute of Technology (AU), Wright-Patterson AFB OH, March 1985 (AD-A155 466).

16. Lynch, P. J. and Siva S. Banda. "Active Control for Vibration Damping," Damping: 1986 Proceedings, Technical Report. Flight Dynamics Laboratory AFWAL/FIGC, Wright-Patterson AFB OH, 1986 (AFWAL-TR-86-3509).

17. Magill, D. T. "Optimal Adaptive Estimation of Sample Stochastic Processes," IEEE Transactions on Automatic Control, 10(5): 434-439 (October 1965).

18. Maybeck, P. S. and K. P. Hentz. "Investigation of Moving Bank Multiple Model Adaptive Estimation and Control Algorithms," Proceedings of the 24th IEEE Conference on Decision and Control, Ft. Lauderdale FL, December 1985.

19. Maybeck, Peter S. Stochastic Models, Estimation, and Control, Volume 1. New York: Academic Press, 1979.

20. -----. Stochastic Models, Estimation, and Control, Volume 2. New York: Academic Press, 1982.

21. -----. Stochastic Models, Estimation, and Control, Volume 3. New York: Academic Press, 1983.

22. -----. Discussion concerning Moving-Bank Multiple Model Adaptive Estimator, March-September 1986.

23. Meer, D. E. "Multiple Model Adaptive Estimation for Space-Time Point Process Observations. PhD dissertation. School of Engineering, Air Force Institute of Technology (AU), Wright-Patterson AFB OH, September 1982.

24. Meer, D. E. and P. S. Maybeck. "Multiple Model Adaptive Estimation for Space-Time Point Process Observations," Proceedings of the IEEE Conference on Decision and Control, Las Vegas NV, December 1984.

25. Meirovitch, Leonard. Analytical Methods in Vibrations. New York: The Macmillan Company, 1967.

26. Moose, R. L. and P. P. Wang. "An Adaptive Estimator with Learning for a Plant Containing Semi-Markov Switching Parameters," IEEE Transactions on Systems Science and Cybernetics, 277-281, May 1973.

27. Netzer, Alan S. Characteristics of Bayesian Multiple Model Adaptive Estimation for Tracking Airborne Targets. MS thesis, GAE/ENG/85D-2. School of Engineering, Air Force Institute of Technology (AU), Wright-Patterson AFB OH, December 1985 (AD-A163 830).

28. Tang, Wang, and Gregory L. Mealy. "Application of Multiple Model Estimation Techniques to a Recursive Terrain Height Correlation System," IEEE Transactions on Automatic Control, 28: 315-323 (March 1983).

29. Turn, J. D. and H. M. Chun. "Optimal Distributed Control of a Flexible Spacecraft During a Large-Angle Rotational Maneuver," Proceedings of the Third VPI&SU/AIAA Symposium, 471-485, Blacksburg VA, June 1981.

30. Venkayya, V. B. and V. A. Tischler. "Frequency Control and Its Effects on the Dynamic Response of Flexible Structures," AIAA Journal, 23(11): 1768-1774 (November 1985).

31. -----. 'Analyze'--Analysis of Aerospace Structures with Membrane Elements. Technical Report. Analysis and Optimization Branch, Structural Mechanics Division, Air Force Flight Dynamics Laboratory, Air Force Wright Aeronautical Laboratories, Air Force Systems Command, Wright-Patterson AFB OH, December 1978 (AFFDL-TR-78-170).

32. Willner, Dieter. Observation and Control of Partially Unknown Systems. PhD dissertation. Electronic Systems Laboratory, Electrical Engineering Department, Massachusetts Institute of Technology, Cambridge MA, May 1973 (ESL-R-496).

33. Yip, Pak T. "Multiple Model Adaptive Filter for Tank Fire Control and Its Microprocessor Implementation," Transactions of the Conference of Army Mathematicians. Bethesda MD, 1982 (AD-P001 033).

Vita

2nd Lieutenant Drew A. Karnick was born [redacted] He graduated from high school with Salutatorian honors in [redacted] in 1981. He attended Rose-Hulman Institute of Technology, Terre Haute, Indiana and graduated cum laude in May, 1985 with a Bachelor of Science in Electrical Engineering and was commissioned through ROTC in the USAF. Upon graduation, he was assigned to the Air Force Institute of Techology.

[redacted]

UNCLASSIFIED

SECURITY CLASSIFICATION OF THIS PAGE

REPORT DOCUMENTATION PAGE

Form Approved OMB No. 0704-0188

1a. REPORT SECURITY CLASSIFICATION UNCLASSIFIED	1b. RESTRICTIVE MARKINGS
2a. SECURITY CLASSIFICATION AUTHORITY	3. DISTRIBUTION/AVAILABILITY OF REPORT Approved for public release; distribution unlimited.
2b. DECLASSIFICATION/DOWNGRADING SCHEDULE	
4. PERFORMING ORGANIZATION REPORT NUMBER(S) AFIT/GE/ENG/86D-41	5. MONITORING ORGANIZATION REPORT NUMBER(S)
6a. NAME OF PERFORMING ORGANIZATION School of Engineering 6b. OFFICE SYMBOL (If applicable) AFIT/ENG	7a. NAME OF MONITORING ORGANIZATION
6c. ADDRESS (City, State, and ZIP Code) Air Force Institute of Technology Wright-Patterson AFB, Ohio 45433	7b. ADDRESS (City, State, and ZIP Code)
8a. NAME OF FUNDING/SPONSORING ORGANIZATION 8b. OFFICE SYMBOL (If applicable)	9. PROCUREMENT INSTRUMENT IDENTIFICATION NUMBER
8c. ADDRESS (City, State, and ZIP Code)	10. SOURCE OF FUNDING NUMBERS PROGRAM ELEMENT NO. / PROJECT NO. / TASK NO. / WORK UNIT ACCESSION NO.

11. TITLE (Include Security Classification)
Moving-Bank Multiple Model Adaptive Estimation Applied to Flexible Spacestructure Control

12. PERSONAL AUTHOR(S)
Drew A. Karnick, B.S.E.E., 2d Lt, USAF

13a. TYPE OF REPORT	13b. TIME COVERED	14. DATE OF REPORT (Year, Month, Day)	15. PAGE COUNT
MS Thesis	FROM _____ TO _____	1986 December	212

16. SUPPLEMENTARY NOTATION

17. COSATI CODES			18. SUBJECT TERMS (Continue on reverse if necessary and identify by block number)
FIELD	GROUP	SUB-GROUP	Adaptive Control Systems, Adaptive Filters, Multiple Model Adaptive Estimation, Multiple Model Adaptive Control, Large Flexible Space Structure, Singular Perturbations
09	05		

19. ABSTRACT (Continue on reverse if necessary and identify by block number)

Thesis Chairman: Peter S. Maybeck
Professor of Electrical Engineering

Approved for public release: IAW AFR 190-1.
LYNN E. WOLAVER
Dean for Research and Professional Development
Air Force Institute of Technology (AFIT)
Wright-Patterson AFB OH 45433
5 March 87

20. DISTRIBUTION/AVAILABILITY OF ABSTRACT	21. ABSTRACT SECURITY CLASSIFICATION
☒ UNCLASSIFIED/UNLIMITED ☐ SAME AS RPT. ☐ DTIC USERS	UNCLASSIFIED
22a. NAME OF RESPONSIBLE INDIVIDUAL Peter S. Maybeck, Prof. of Elec. Eng.	22b. TELEPHONE (Include Area Code) (513) 255-2057
	22c. OFFICE SYMBOL AFIT/ENG

DD Form 1473, JUN 86 — Previous editions are obsolete. — SECURITY CLASSIFICATION OF THIS PAGE
UNCLASSIFIED

Block 18--Continued

Partitioning, Kalman Filter.

This investigation focuses on the use of moving-bank multiple model adaptive estimation and control (MMAE). Moving bank (MMAE reduces the computational burden of MMAE by implementing only a subset of the Kalman filters (9 filters versus 100 in this research) that are necessary to mathematically describe the system to be estimated/controlled. Important to the development of the moving-bank MMAE are the decision logics governing the selection of the subset of filters. The decision logics cover three situations: initial acquisition of unknown parameter values; tracking unknown parameter values; and reacquisition of the unknown parameters following a "jump" change in these parameter values.

The thesis applies moving-bank MMAE to a rotating two bay truss model of a flexible spacestructure. The rotating two bay truss approximates a space structure that has a hub with appendages extending from the structure. The mass of the hub is large relative to the mass of the appendix. The hub is then rotated to point the appendage in a commanded direction. The mathematical model is developed using finite element analysis, transformed into modal formulation, and reduced using a method referred to as singular perturbations. Multiple models are developed by assuming that variation occurs in the mass and stiffness of the structure. Ambiguity function analysis and Monte Carlo analysis of individual filters are used to determine if the assumed parameter variation warrants the application of adaptive control/estimation techniques.

Results indicate that the assumed parameter variation is sufficient to require adaptive control and that the use of a moving bank may provide increased state estimation performance; however, the increase in performance is due primarily to multiple model adaptive estimation. Similar performance can be obtained from a fixed bank estimator with a discretization that covers the range of parameter variation.